UNIVERSITY OF THESSALY

SCHOOL OF ENGINEERING

DEPARTMENT OF MECHANICAL ENGINEERING

PROGRAM OF POSTGRADUATE STUDIES

ΚΑΡΑΓΙΑΝΝΗΣ ΣΤΑΥΡΟΣ - ΘΕΟΔΩΡΟΣ

Computer Aided Design of an Injection Molded Center-Gated Disc

Greece, Volos, March 2014

UNIVERSITY OF THESSALY
SCHOOL OF ENGINEERING | DEPARTMENT OF MECHANICAL ENGINEERING

Division of Energy, Industrial Processes & Pollution Abatement Technology

This thesis was approved by the Final Examination Committee:

First examiner: (Advisor)	Papathanasiou Athanasios Asssociate Professor, University of Thessaly, Department of Mechanical Engineering
Second examiner:	Bontozoglou Vasilis Professor, University of Thessaly, Department of Mechanical Engineering
Third examiner:	Andritsos Nikos Professor, University of Thessaly, Department of Mechanical Engineering

Academic year 2013-2014

3rd Semester (Fall)

CONTENTS

1. Introduction

2. Introduction to Autodesk Moldflow Insight (2012)

3. Working in Synergy

4. Process Settings

5. 3D Mesh Conversion

Abstract

The goal of this work is to provide insight into the basics of the CAD of the injection molding of thermoplastics. The process of injection molding and the way the molten plastic flows into the mold will be described, as well as the factors that affect it. The study has been based on Autodesk Moldflow Insight (2012), which is a high-end plastic injection molding computer-aided engineering software.

There was no previous personal experience on molding of thermoplastics. This is the reason that a very simple geometry was chosen to be studied, i.e. the case of a center-gated disk, which is a thin-walled and symmetrical part. All the necessary steps that should be followed in order to run a successful analysis on Autodesk Moldflow Insight are described here in detail. The equations that describe most of the models used by the software are also presented.

Lastly, it must be noted that the center-gated disk is a geometry often used to examine the fiber orientation of a glass-fiber reinforced polymer. However, this is not the main focus of the study. Some of the most important parameters in injection molding will be discussed here, like temperature, pressure and volumetric shrinkage, as well as the accuracy of the acquired results.

166 Pages, 184 Figures, 12 Tables, 38 References

1. Introduction

1.1 Structure of polymers

Plastics are a class of materials that are built from relatively simple units, called monomers, through a chemical polymerization process. This process is illustrated in figure 1.1. Processing polymers into end products mainly involves physical phase change, such as melting and solidification (for thermoplastics - TPs) or a chemical curing reaction (for Thermosets- TS). The primary physical difference is that thermoplastics can be re-melted back into a liquid, whereas thermosets always remain in a permanent solid state. Only thermoplastics will be discussed here.

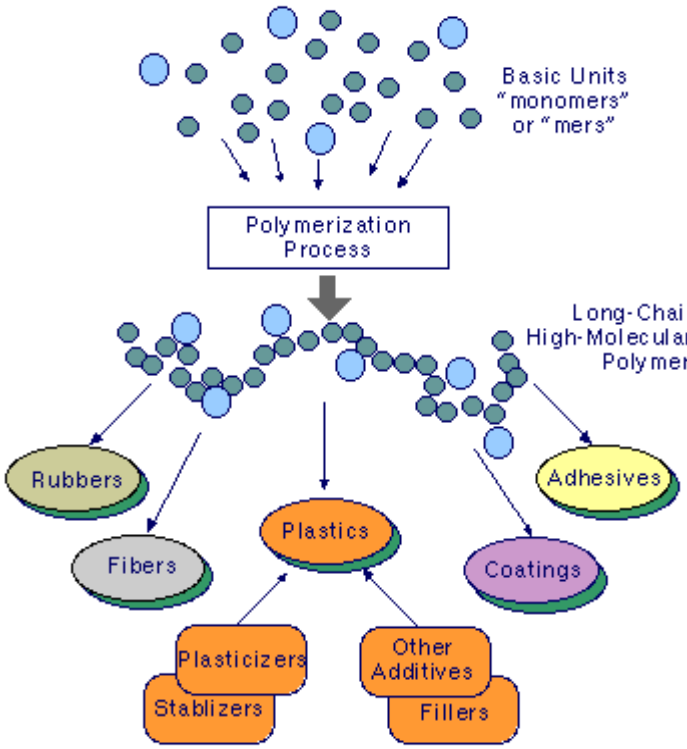

Figure 1.1:

Polymer family, the formation of plastics and the polymerization process. *[1]*

A thermoplastic (TP) is a type of plastic that can be reheated, reshaped, and frozen repeatedly. This quality makes thermoplastics recyclable, too. They have a complex rheology, due to their large molar mass, wide molecular weight distributions, entanglements and interactions between macromolecules and presence of chain branches.

Generally, plastic materials lack stiffness and mechanical strength. This is the reason polymer composites were created. Polymer composites are materials that incorporate certain reinforcing agents into a polymer matrix, to add desirable properties. Low aspect ratio materials, such as single crystal/whisker, and flake-type fillers of clay, talc, and mica, impart increased stiffness. On the other hand, larger aspect ratio reinforcements, such as fibers or filaments of glass, carbon-graphite, aramid/organic, and boron, substantially raise both the tensile strength and the stiffness.

For example, a common way to improve the mechanical properties of a plastic material is to add glass fibers. Glass fibers improve the structural properties, like strength and stiffness and reduce the shrinkage of the part, too. Of course, the mechanical properties of the glass fiber reinforced plastics can vary depending on the fiber distribution, size, fraction, orientation or fiber-plastic adhesion. Glass fibers are used as reinforcing materials in many sectors, like the automotive and naval industries, sport equipments and airplane industries.

However, when fibers are embedded into a polymer matrix, the composite material becomes heterogeneous and should be considered as an anisotropic material. Glass fibers may also impart some unwanted conditions and properties in the process and in the product, such as poor replication and surface finish and filling problems. This is due to the non-uniform distribution and orientation of the glass fibers.

1.2 Thermoplastics classification based on morphology

TPs are formed by combining into long chains of molecules, or molecules with branches (lateral connections) to form complex molecular shapes. All these forms exist in either two or three dimensions. Because of their geometry (morphology), some of these molecules can come closer together than others. Depending on the polymer chain conformation/molecular structure, TPs can be categorized into semi-crystalline (such as PE, PP and PA), amorphous (such as PMMA, PS, SAN, and ABS) or liquid crystal polymers (LCPs). The microstructure of these plastics and the effects of heating and cooling on them are shown in figure 1.2.

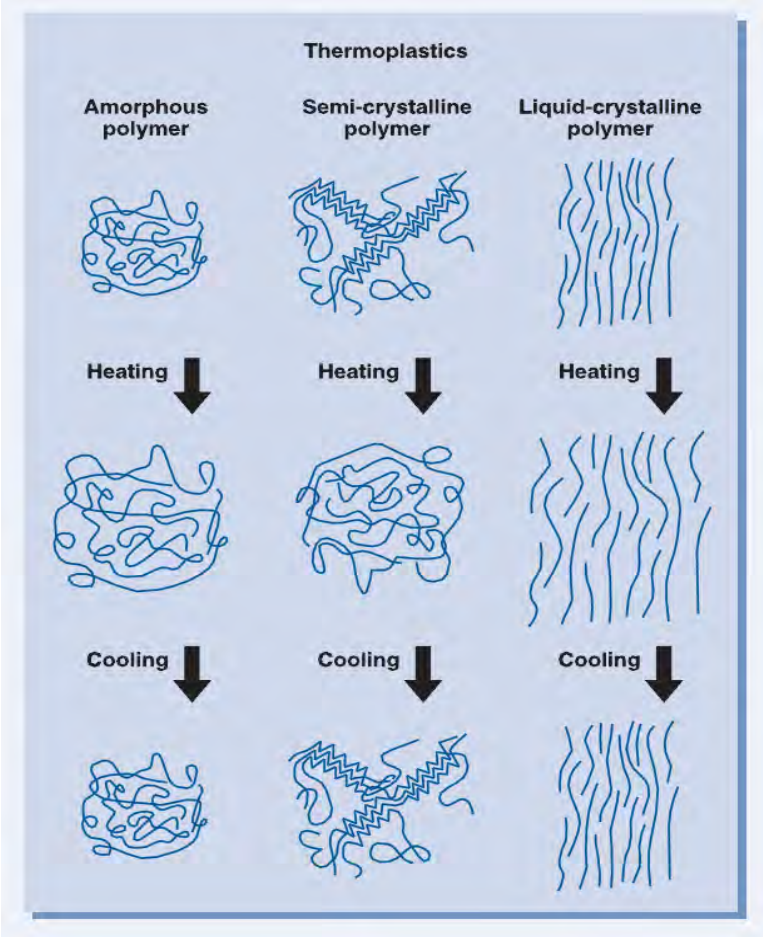

Figure 1.2:

Microstructure of TPs and the effect of heating and cooling, during processing. *(Source: DSM Engineering Plastics, 2005)*

For Newtonian fluids, like water, the viscosity is a temperature dependent constant, regardless of the shear rate. However, most polymer melts are non-Newtonian. This means that their viscosity varies, not only with temperature, but with the shear rate, too. Thus, their viscosity does not remain constant over a given range of shear rates. At lower shear rates the plastic is Newtonian, but as the shear rate increases, the plastic tends to exhibit a non-Newtonian behavior (figure 1.3).

The most common type of (time-independent) non-Newtonian fluid behavior observed is pseudo-plasticity or shear-thinning, characterized by an apparent viscosity which decreases with increasing shear rate. However, most shear-thinning polymer melts and solutions will exhibit Newtonian behavior at extreme shear rates, both low and high. This means that the shear stress – shear rate plots become straight lines and on a linear scale will pass through origin.

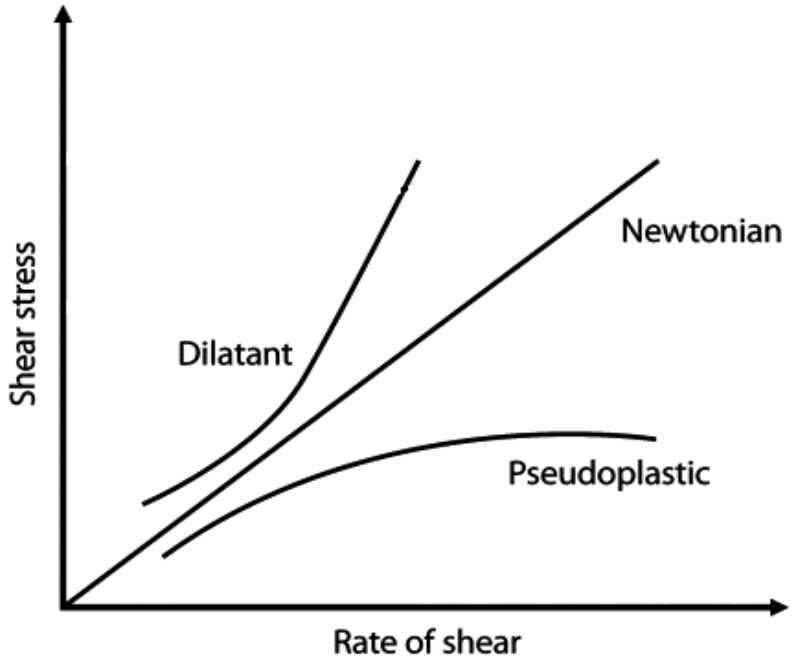

Figure 1.3: Shear stress vs. shear rate diagram. Pseudoplastic (or shear-thinning) fluids have a lower apparent viscosity at higher shear rates. Dilatant (or shear-thickening) fluids increase in apparent viscosity at higher shear rates. Note that: viscosity = (shear stress) / (shear rate). *(Source: Benretem et. al., 2010)*

1.3 Basics of injection molding

Injection molding is the most important process used to manufacture plastic products. TPs are solids at typical use temperatures that are melted or softened by heating, placed into a mould or other shaping device, and then cooled to give the desired shape (Strong, 1996). They can also be reheated and shaped into new parts. Today, more than one third of the TPs are injection molded, and more than half of all polymer-processing equipment is for injection molding. The injection molding process is ideally suited to manufacture mass-produced parts of complex shapes that require precise dimensions. A variety of things can be created through this process, such as electronic housings, containers, bottle caps, automotive interiors, combs and most other plastic products available today.

Injection molding is ideal for producing high volumes of plastic parts, due to the fact that several parts can be produced in each cycle, by using multi-cavity injection molds. Some advantages of an injection molding process are high tolerance precision, repeatability, large material selection, low labor cost, minimal scrap losses and little need to finish parts after molding. Some of the disadvantages include the expensive upfront tooling investment and process limitations.

There are many different types of injection molding machines (IMMs) that permit molding many different products, based on factors such as quantities, sizes, shapes, product performance, or economics. The two most popular kinds of IMMs are the single-stage and the two-stage; there are also molding units with three or more stages. The single-stage IMM is also known as the reciprocating-screw IMM (figure 1.4).

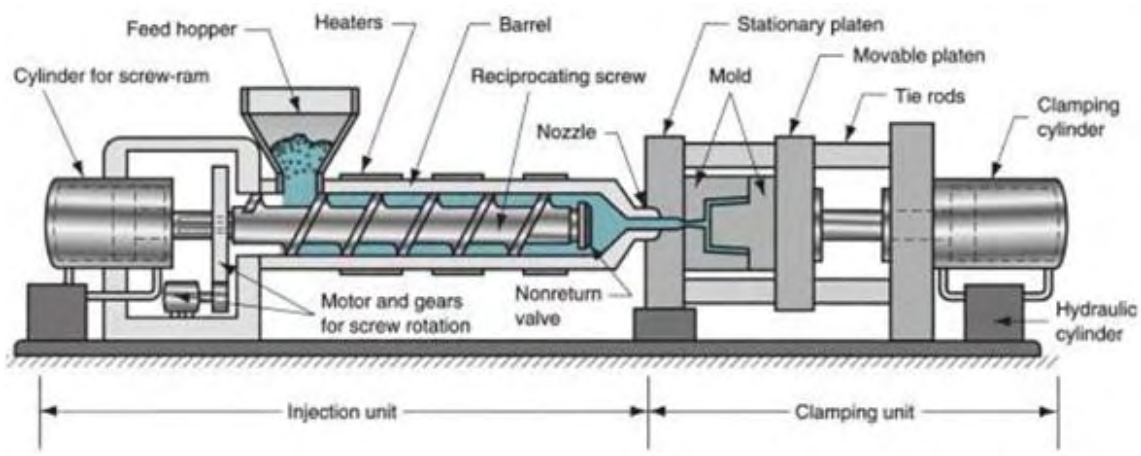

Figure 1.4: A typical reciprocating-screw IMM. *(Source: Groover, 2010)*

An IMM consists of two principal components: (a) the plastic injection unit and (b) the mold clamping unit.

a) The *injection unit* is much like an extruder. It consists of a barrel that is fed from one end by a hopper containing a supply of plastic pellets. A hopper is a large container into which the raw plastic is poured. The hopper has an open bottom, which allows the material to feed into the barrel. Inside the barrel is a screw, whose operation surpasses that of an extruder screw in the following respect: in addition to turning for mixing and heating the polymer, it also acts as a ram which rapidly moves forward to inject molten plastic into the mold. Because of its dual action, it is called a reciprocating screw.

   Variations in melt temperature, melt uniformity and melt output are kept to a minimum, prior to entering the mold. Inside the screw, the material is melted by friction and additional heater bands that surround the reciprocating screw. In other words, heat is supplied by heater bands around the barrel and by the friction that occurs, when plastic is moved by the rotating screw. Therefore, both conduction heating and mechanical friction heating of the plastic occur during screw rotation. The molten plastic is then injected very quickly into the mold through the nozzle, at the end of the barrel, by the buildup of pressure and the forward action of the screw.

This increasing pressure allows the material to be packed and forcibly held into the mold. Once the material has solidified inside the mold, the screw can retract to its former position and fill with more material for the next shot.

Lastly, notice the non-return valve mounted near the tip of the screw (figure 1.4). This will prevent the melt from flowing backward along the screw threads.

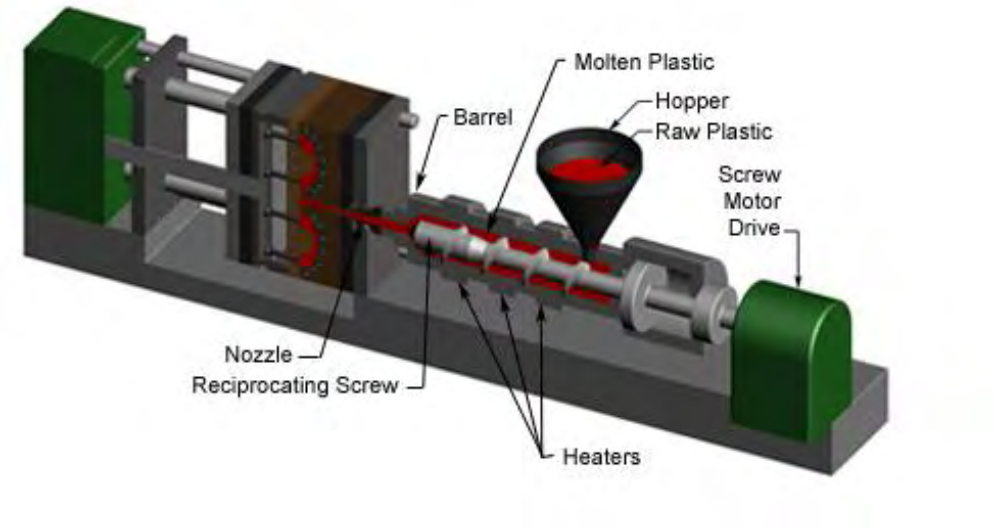

Figure 1.5: The injection unit of an IMM. *[2]*

The screw is usually a simple appearing device, but it accomplishes many different operations at the same time. These include: (1) conveying or feeding solids; (2) compressing, melting, and pressurizing melt; and (3) mixing, melt refinement, and pressure and temperature stabilization. All these operations are accomplished in the following regions of the screw (figure 1.6):

- Feed section: unmelted plastic in the form of pellets or powder enters the beginning of the feed section (back end of the screw). The plastic is carried forward and gravity holds it down to the bottom of the barrel. Imagine it being pushed forward much like snow in front an advancing snowplow. As the resin proceeds further down to the section, a compaction occurs as the pellets are pressed more closely together.

- Compression/Transition section: is where the softening of the plastic occurs; the plastic is transformed into a continuous melt. Most of the melting takes place here. In this zone, polymer changes from compacted pellets with air spaces between, to a melted polymer without voids. Furthermore, material is forced to squeeze into a smaller space and thereby, builds pressure. The greatest pressure buildup along the entire screw length occurs at the end of the transition section.

- Metering section: some final melting takes place here. The plastic is sheared to give the melt its final uniform composition and temperature for delivery to the mold. Frictional heating is accomplished here, as the material is sheared between two surfaces moving in relation to each other, i.e. the barrel inner wall and the root of the screw (figure 1.7).

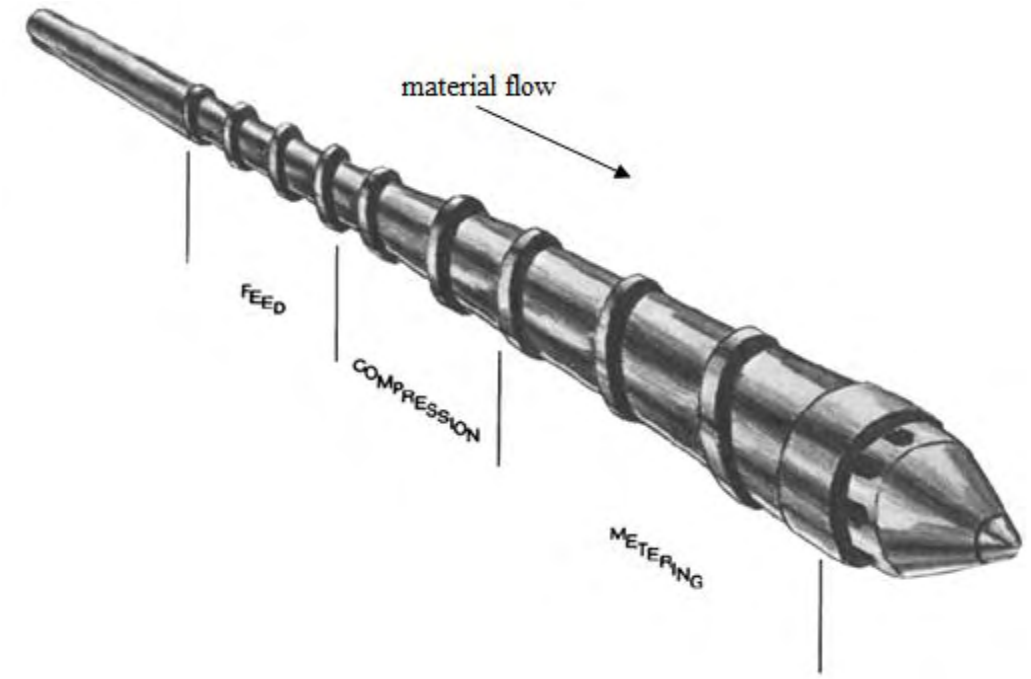

Figure 1.6: Sections of a screw. *(Source: Rosato, 2000)*

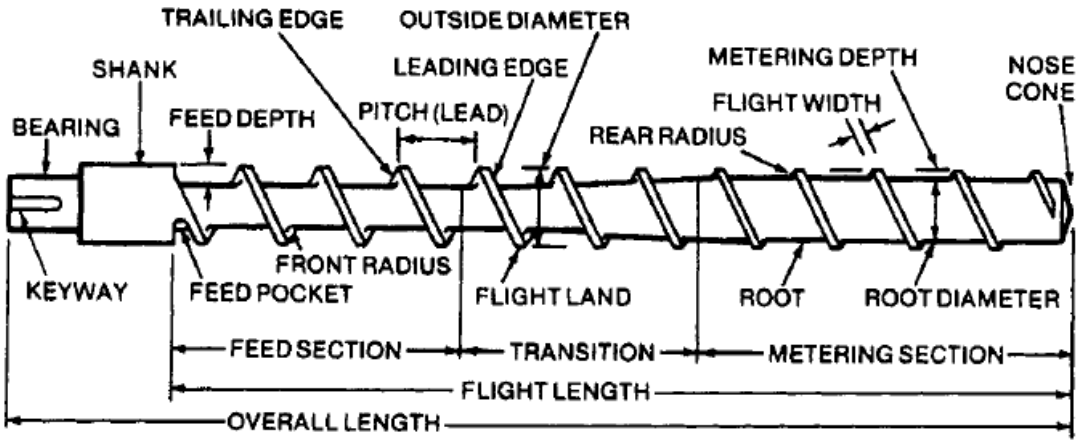

Figure 1.7: General-purpose screw. *(Source: Rosato, 2000)*

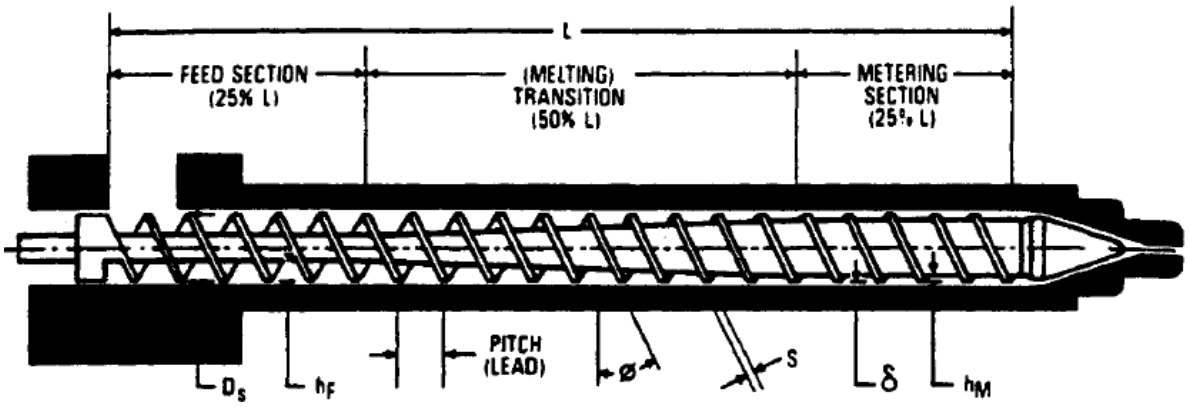

Figure 1.8: A typical metering-type screw with barrel: D_s = nominal screw diameter; φ = helix angle = 17.8°; s = land width = 6.35 mm; h_F = flight depth (feed); h_M = minimum flight depth for metering = 5.6 mm; L = overall length; δ = radial clearance = 0.13 mm; L/D = ratio of length to diameter = 16 to 24; h_F/h_M = compression ratio = 2.0 to 2.2. *(Source: Rosato, 2000)*

b) The *clamping unit* is concerned with the operation of the mold. Its functions are to: (1) hold the two halves of the mold in proper alignment with each other; (2) keep the mold closed during injection, by applying a clamping force sufficient to resist the injection force; and (3) open and close the mold at the appropriate times in the molding cycle.

   Prior to the injection of the molten plastic into the mold, the two halves of the mold must first be securely closed by the clamping unit. When the mold is attached to the IMM, each half is fixed to a large plate, called a platen. The front half of the mold, called the *mold cavity*, is mounted to a stationary platen and aligns with the nozzle of the injection unit. The rear half of the mold, called the *mold core*, is mounted to a movable platen, which slides along the tie bars. A hydraulically powered clamping motor actuates the clamping bars, which in turn push the moveable platen towards the stationary platen and exert sufficient force, so as to keep the mold securely closed, while the material is injected and subsequently cools. After the required cooling time, the mold is then opened by the clamping motor. An ejection system, which is attached to the rear half of the mold, is actuated by the ejector bar and pushes the solidified part out of the open cavity. All the above can be seen in figure 1.9.

Depending on what plastic is being molded, the IMM clamping force can vary from less than 20 tons to thousands of tons. Different plastics require different pressures applied on their melt in the mold cavity, ranging from 15 to 210 MPa. An average IMM uses a range from 100 to 400 tons, but large machines that provide thousands of tons of clamping force, are needed to mold larger products. Lastly, the clamping mechanisms for injection molding can be hydraulic, hydro-mechanical and mechanical.

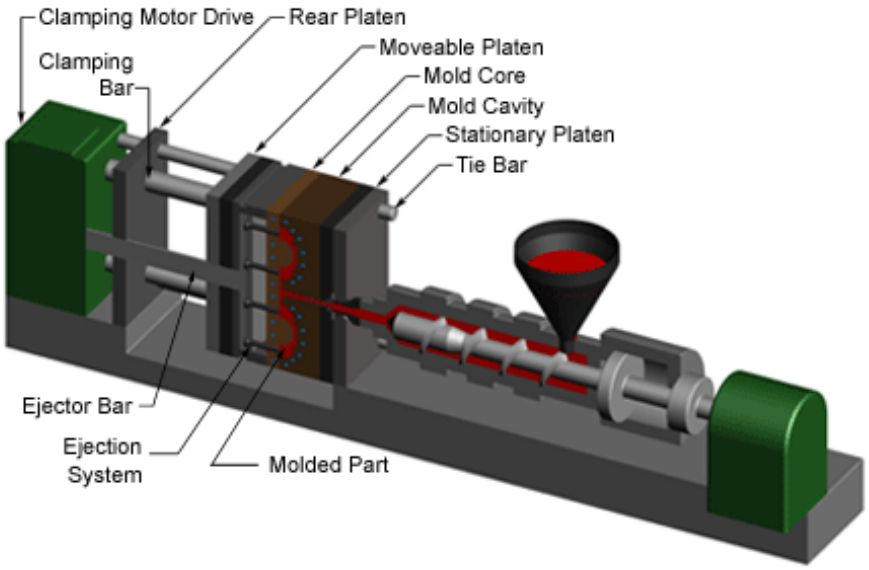

Figure 1.9: The clamping unit of an IMM. *[2]*

All IMMs perform some certain essential functions: (1) *plasticizing:* heating and melting of the plastic in the plasticator; (2) *injection:* injecting from the plasticator under pressure a controlled-volume shot of melt into a closed mold, with solidification of the plastics beginning on the mold's cavity wall; (3) *afterfilling or packing-holding:* maintaining the injected material under pressure for a specified time to prevent back flow of melt and to compensate for the decrease in the volume of melt (shrinkage), during solidification; (4) *cooling:* cooling the TP molded part in the mold until it is sufficiently rigid to be ejected, and (5) *molded-part release:* opening the mold, ejecting the part, and closing the mold so it is ready to start the next cycle with a shot of melt.

These steps can be plotted in a pressure vs. time diagram, as shown in figure 1.10. This is only a general approach.

Note: The injection unit is also called the plasticator.

Note: In most cases, packing and holding are not differentiated and are collectively called the packing or the holding phase.

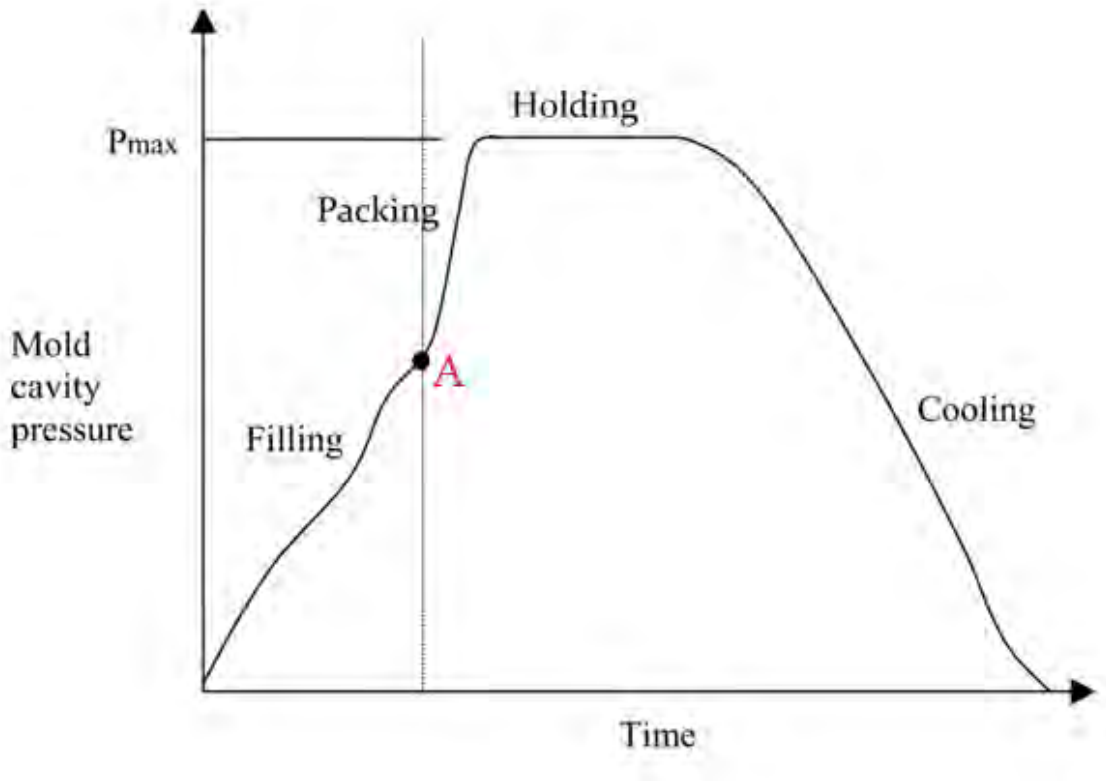

Figure 1.10: Pressure during the molding cycle. In Autodesk Moldflow Insight the packing phase includes both packing time and cooling time. At point A, the cavity has been completely filled.

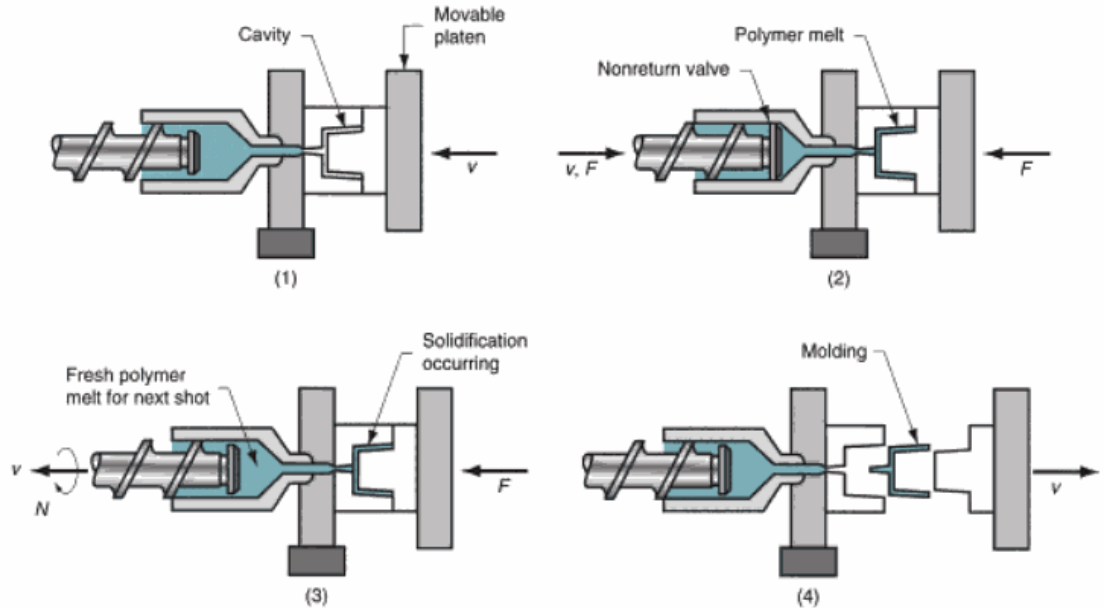

Figure 1.11: An injection molding process. *(Source: Groover, 2010)*

The cycle for injection molding of a thermoplastic polymer proceeds in the following sequence. Let's pick up the action with the mold open and the machine ready to start a new molding (see figure 1.11):

(1) Mold is closed and clamped. (2) A shot of melt, which has been brought to the right temperature and viscosity by heating and by the mechanical working of the screw, is injected under high pressure into the mold cavity. The plastic cools and begins to solidify, when it encounters the cold surface of the mold. Ram pressure is maintained to pack additional melt into the cavity, in order to compensate for contraction during cooling. (3) The screw is rotated and retracted, with the non-return valve open, to permit fresh polymer to flow into the forward portion of the barrel. Meanwhile, the polymer in the mold has completely solidified. (4) The mold is opened, and the part is ejected and removed.

However, the goal of this study is to focus on what happens inside the mold. Till now very few things were discussed about it. However, it is much more difficult and complex than it seems.

The injection molding process uses *molds*, typically made of steel or aluminum, as the custom tooling. The mold determines the part shape and size. When the production run for a part is finished, the mold is usually replaced with a new mold for the next part. There are several types of mold for injection molding. The most common is the two-plate mold and one can be seen in figures 1.12 and 1.13. Generally, molds can contain a single cavity (single-cavity mold) or multiple cavities (multiple-cavity mold), so as to produce more than one part in a single shot.

The surfaces on each side that come together, touch and then get held together by the clamping forces of the IMM are called the "parting line" surfaces of the mold. It is important for the parting line surfaces to line up perfectly, where they meet to form the final shape of the part.

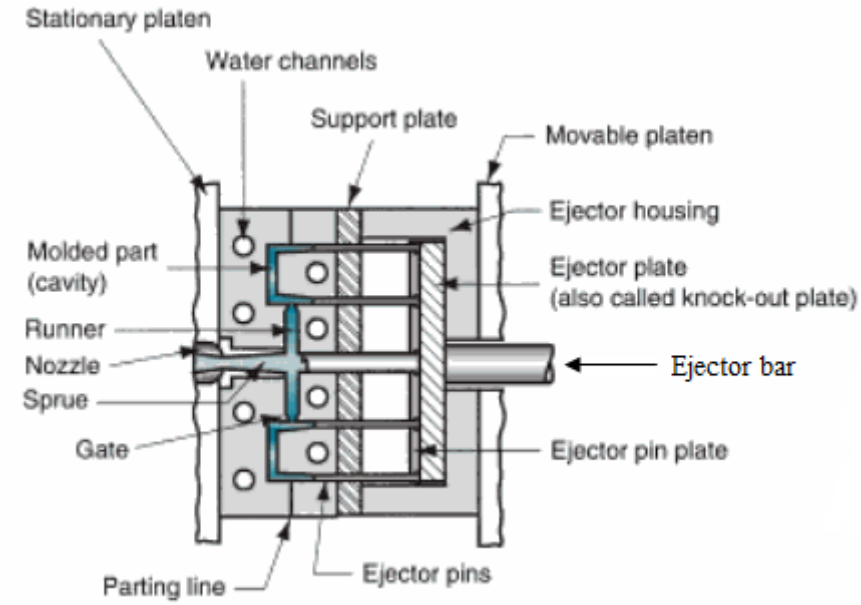

Figure 1.12: A closed two-plate mold. The mold has two cavities to produce two cup-shaped parts (cross-section shown here) with each injection shot. *(Source: Groover, 2010)*

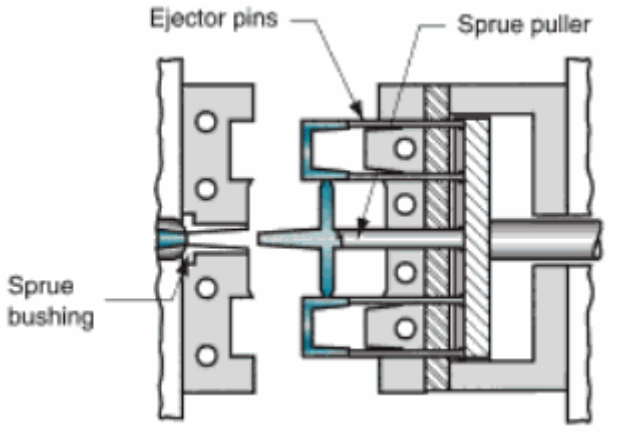

Figure 1.13: An open two-plate mold. *(Source: Groover, 2010)*

In addition to the cavity, there are other features of the mold that serve indispensable functions during the molding cycle. A mold must have a distribution channel, through which the polymer melt flows from the nozzle of the injection barrel into the mold cavity. The distribution channel consists of (1) a *sprue*, which leads the melt from the plasticator nozzle into the mold; (2) *runners*, which carry the molten plastic from the sprue to the cavity (or cavities) that must be filled; and (3) at the end of each runner, there is a *gate*, which directs and constricts the flow of plastic into the cavity. There can be one or more gates for each cavity in the mold. The dimensioning and the design of the sprue, runner and gate are of great importance, as they make up the "feed system" of the mold.

Furthermore, an ejection system is needed to eject the molded part from the cavity at the end of the molding cycle. When the clamping unit separates the mold halves (figure 1.13), the *ejector bar* actuates the ejection system. The ejector bar pushes the *ejector plate* forward inside, which in turn pushes the *ejector pins* into the molded part. The ejector pins then push the solidified part out of the open mold cavity. As shown in figure 1.12, the ejector pins are built into the moving half of the mold.

A *cooling system* is also required for the mold. This consists of an external pump connected to passageways in the mold, through which water is circulated to cool the molten plastic. Air must be also evacuated from the mold cavity, as the polymer rushes in. Much of the air passes through the small ejector pin clearances in the mold. In addition, narrow *air vents* are often machined into the parting surface; only about 0.03 mm deep and 12 to 25 mm wide, these channels permit air to escape to the outside, but are too small for the viscous polymer melt to flow through.

To sum up, a mold consists of: (1) one or more cavities that determine the part geometry; (2) distribution channels through which the polymer melt flows to the cavities; (3) an ejection system for part removal; (4) a cooling system; and (5) vents to permit evacuation of air from the cavities.

Note: With a single-cavity mold, usually no runner is used, so melt goes from the sprue to the gate (Rosato, 2000).

Apart from the mold design, the molding conditions are also very important. The quality of a molded part is greatly influenced by the conditions under which it is processed. There is an infinite combination of conditions that render acceptable parts, bound by minimum and maximum temperatures and pressures. Figure 1.14 presents the molding diagram with the all the limiting conditions: (1) - Below the bottom curve, the polymer is either a solid or will not flow. As the temperature is lowered, a much higher pressure is needed to deliver the polymer into the cavity; (2) - A very high temperature (above the top curve) can lead to mechanical failure of the part, due to the material's thermal degradation; (3) - If the pressure is too low, a short shot (partly filled cavity) could result or excessive shrinkage/sink marks will appear; (4) - A very high pressure, results in mold flash. Flash occurs when the cavity pressure force exceeds the machine clamping force, leading to melt flow across the mold parting line.

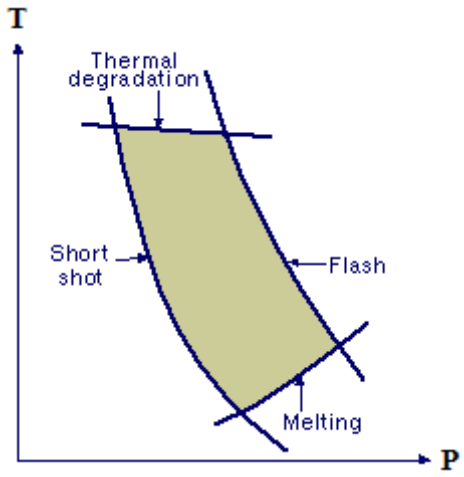

Figure 1.14: Schematic "molding area" diagram that can be determined for a given polymer and mold cavity. Within this area the polymer is moldable. *(Source: Tadmore & Gogos, 1979)*

1.4 Polymer flow behavior in injection molding

Flow technology is concerned with the behavior of plastics during the mold filling process. A plastic part's properties depend on how the part is molded. Two parts having identical dimensions and made from the same material, but molded under different conditions will have different stress and shrinkage levels and will behave differently in the field, meaning that they are in practice two different parts. The way the plastic flows into the mold is of paramount importance in determining the quality of the part. The process of filling the mold can be distinctly analyzed with the ability to predict pressure, temperature and stress.

1.4.1 How plastic fills a mold

It has been found that there are three distinct processing phases in injection molding: (a) filling phase; (b) packing phase and (c) cooling phase.

A) The filling phase:

During the filling phase, plastic is pushed into the cavity, until the cavity is just filled. As plastic flows into the cavity, the plastic in contact with the cold mold wall quickly freezes. This creates a frozen layer of plastic between the mold and the molten plastic. At the interface between the static frozen layer and the flowing melt, the polymer molecules are stretched out in the direction of flow. This alignment and stretching is called *orientation*.

Note: The boundary between the advancing melt and still-empty portion of the cavity is called the melt/flow front. This melt front is like a stretching membrane of polymer, like a balloon or bubble (Rosato, 2000).

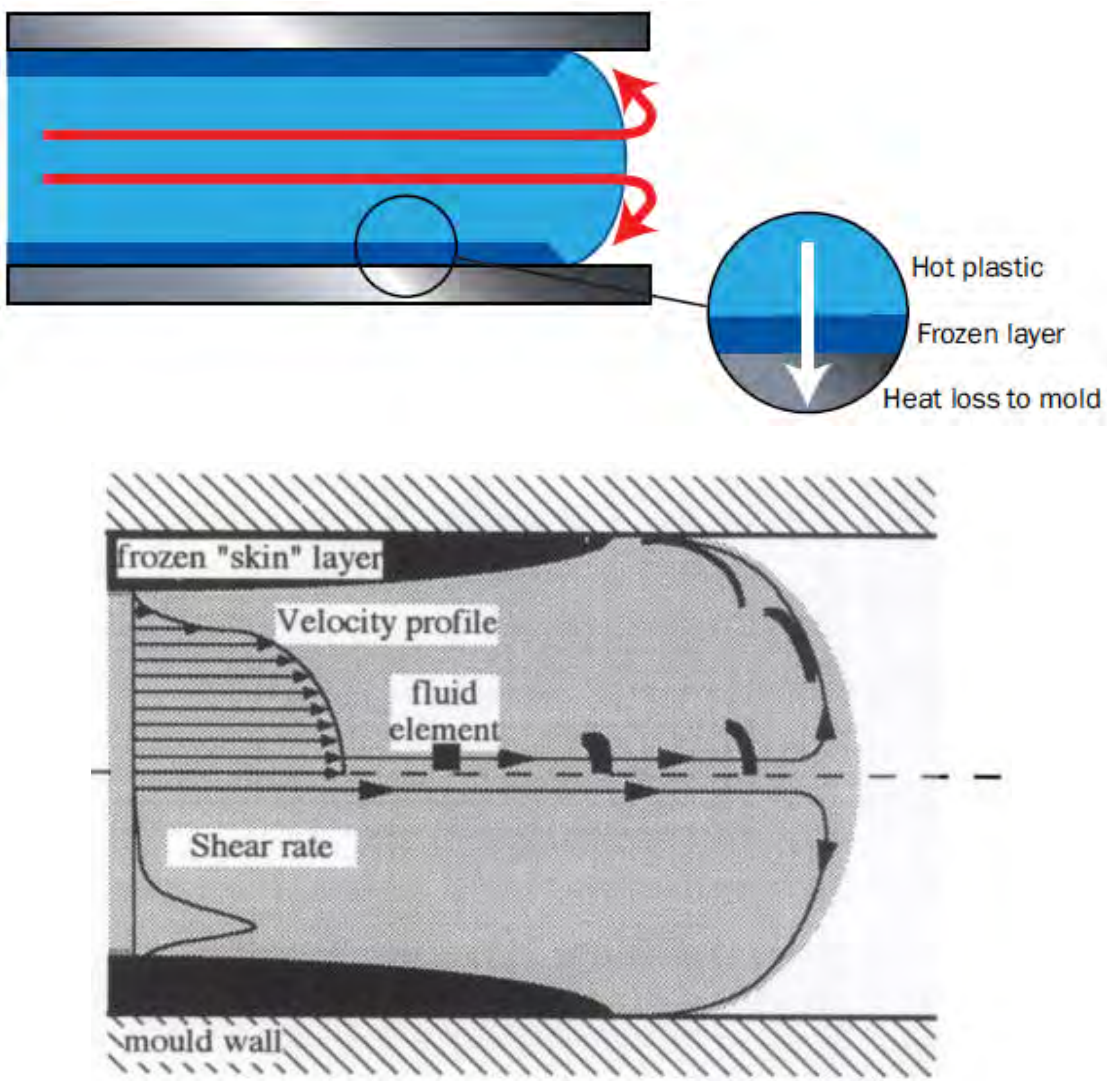

Figure 1.15: (a) Fountain flow and heat transfer. The red arrows show the flow direction of the molten plastic. The dark blue layers show the layers of frozen plastic against the mold walls. The white arrow indicates the direction of heat flow from the polymer melt into the mold walls. *(Source: Shoemaker J., 2006)*; (b) Schematic representation of the fountain flow effect near the melt front, showing the velocity and shear rate profiles, and the deformation of a cubic element of melt, as it approaches the flow front. *(Source: Tadmor Z., 1974)*

Figure 1.15(a) shows how the flow front expands, as material from behind is pushed forward. This "outward" or "diverging" flow is called *fountain flow*. The edges of the flowing layer freeze as they come into contact with the mold wall, in a near-perpendicular direction.

The frozen layer gains heat as more molten plastic flows through the cavity, and loses heat to the mold.

Notice that the term '*fountain flow*' was mentioned earlier. This term is used to describe the local flow occurring a short distance (no larger than 3 x the thickness of the cavity) behind the advancing melt front. A characteristic feature of the flow in the cavity is the fact that the molten material at the core moves faster than the (slower moving) advancing flow front. This material, therefore, approaches the flow front. Since mass must be conserved, when it approaches the flow front, this material has to diverge outward in a fountain like motion, which stretches the polymeric molecules and deposits them at this elongated state on the mold walls, where they freeze. Macroscopically, this motion resembles a rolling of the melt front on the cavity walls.

The flow pattern, described above, is caused by the no-slip condition between the melt and the mould walls, which forces material outwards from the centre of the flow towards the cold mould surfaces, where frozen skin layers form. Further melt flow into the cavity occurs between these layers. As the cubic fluid element approaches the flow front, it experiences elongational deformation, before being deposited on the cold walls, where it freezes to form part of the (frozen) skin layer (figure 1.15(b)). This rapid solidification results in the skin layers of an injection moulding retaining a high degree of elongational orientation, whereas further away from the wall molecular relaxation can occur. Therefore, the "skin" (or "surface") zone has solidified with little or no relaxation and is composed of highly oriented molecules, due to the elongational strains imposed by the fountain flow effect (Wilkinson & Ryan, 1998).

B) <u>The packing phase</u>:

The packing phase begins after the cavity has just been filled. During this phase, further pressure is applied to the material in an attempt to pack more material into the cavity. This is intended to produce a reduced and more uniform shrinkage, with reduced component warpage.

When the material has filled the mold cavity and the packing phase has begun, material flow is driven by the *variation of density* (ρ) across the part. If one region of a part is less densely packed than an adjacent region, polymer will flow into the less dense region, until equilibrium is reached. This flow will be affected by the compressibility and thermal expansion of the melt in a similar way to which the flow is affected by these factors in the filling phase.

The pvT (pressure, volume, temperature) characteristics of a polymer provide the necessary information to calculate parameters such as density variations with pressure and temperature, compressibility, and thermal expansion data. When combined with the material viscosity data, an accurate simulation of the material flow during the packing phase is possible.

In practice, due to the limitations of pressure and available unfrozen flow channel, it is impossible to pack enough material into the mold to fully compensate for shrinkage. The uncompensated shrinkage must be allowed for by making the cavity bigger than the desired part size.

C) The cooling phase:

Although the cooling of the plastic occurs from the commencement of the filling phase, the cooling phase is the time from the end of packing to the opening of the mold clamps. This phase is the extra time that is required to cool the part sufficiently for *ejection*. This does not mean that all sections of the part or runner system have to be completely frozen.

The material at the center of the part reaches its transition temperature and becomes solid, during cooling time. The rate and uniformity at which the part is cooled, affects the finished molding quality and production costs.

1.4.2 Cross-sectional flow and molecular orientation

During filling, there is a significant variation in molecular orientation, shear stress and shear rate distributions trough the cross-section of a part. As plastic flows, it is subject to *shear stress*. Shear stress is force over an area. This shear stress and the associated shear rate will orient the material, i.e. cause the molecules to align themselves in the flow direction. The shear stress varies from a maximum at the outside, dropping off to zero at the center. Shear rate is zero at the outer edge (solid interface), where the plastic is frozen, *rises to a maximum just inwards of the frozen layer* or *near the walls* and then drops towards the center, as shown in figure 1.16.

Let's consider the orientation from the mold surface towards the center. It has been already mentioned that the orientation in the surface skin is related to steady elongational flow in the advancing front. The fluid particles, which will hit the cold wall, will immediately solidify, thus freezing in the orientation induced by the elongational flow they have experienced. The magnitude of this orientation, as pointed out earlier, depends on the rate of elongation. Therefore, an increase in injection speed and a decrease in cavity thickness will result in an increase in orientation.

In other words, a layer of uniformly oriented molecules is placed on the cold surface, by the advancing front. The fluid contacting the cold surface solidifies instantaneously; thus, the maximum orientation induced in the front is retained in it. The source of the "skin" layer is the central region of the flow, where shear rates are very low; therefore, it can be assumed that there is no prior deformation history of this layer except the elongational flow in the front.

The "fountain flow" effect keeps the bulk of the melt from freezing to the walls, but the outer layers will freeze as soon as they make contact. However, further back from the flow front, some ends of the layers just below are attached to the frozen layer and are still moving with the melt front. In this zone, often called "sub-surface" or "shear zone", orientation is caused by the shearing of one polymer layer over another. Shear flow, just as elongational flow, induces molecular orientation.

Therefore, another band of high orientation just under the surface is created, due to the very high shear rates that exist there.

The closer to the center – the more the shear rate and shear stress drops. Since in this area the rate of cooling is also slower, this allows more time for the level of orientation to relax. Therefore, in the "core" region, any orientation that occurs has time to relax back to an unoriented morphology. This is why a little or no molecular orientation is observed in that region.

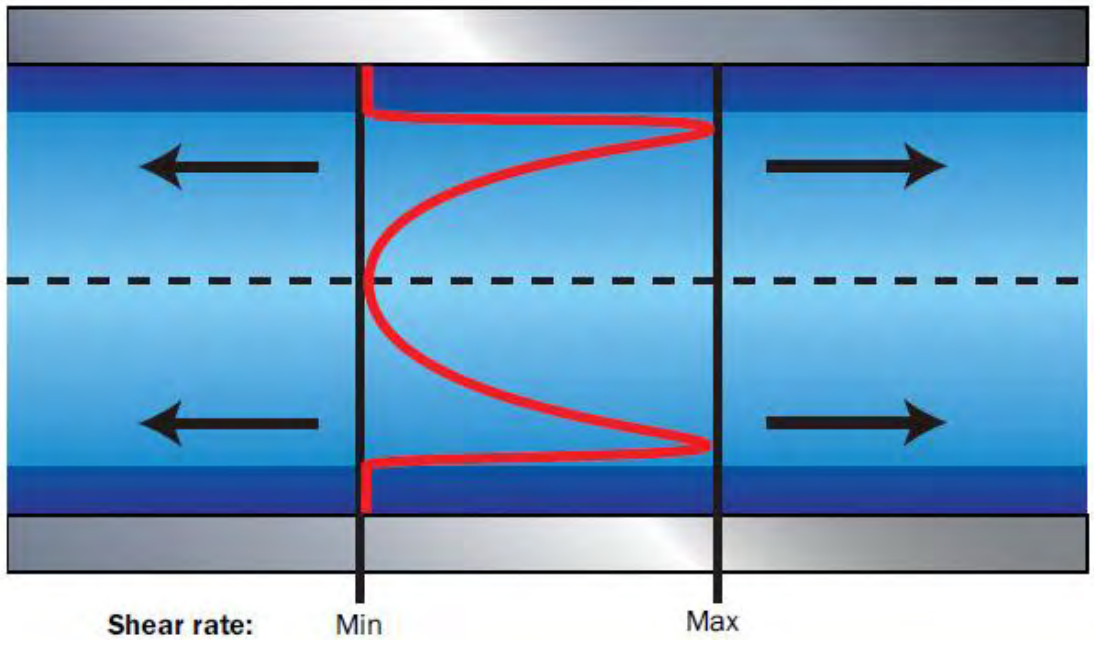

Figure 1.16: Shear rate distribution. Near the walls, where the shear rate is highest, molecules tend to align faster in the flow direction than those near the center-plane, where shear rate is low. *(Source: Shoemaker J., 2006)*

Normally, oriented material will shrink more than non-oriented material. When the melt closest to the mold solidifies, the molecules keep their orientation in the flow direction, as well as their molecular elongation. Hence, this layer has a tendency to shrink in the direction of orientation. On the other hand, the molecules near the center of the melt are insulated from the cold walls, and this allows them to relax. Thus, they are given more time to recover from the oriented state. As a result, they will have less frozen-in orientation. The highly oriented layer ends up being in tension, while the less-oriented material is in compression. This residual stress pattern is a common cause of part warpage.

If the flow was stopped and the plastic was allowed to cool down very slowly, this orientation would have time to relax, giving a very low level of residual orientation. Slower cooling causes the molecules to take longer to cool, so they become less oriented. On the other hand, if the material were kept under stress and the plastic snap frozen, most of the orientation would be trapped in the frozen plastic (figure 1.17).

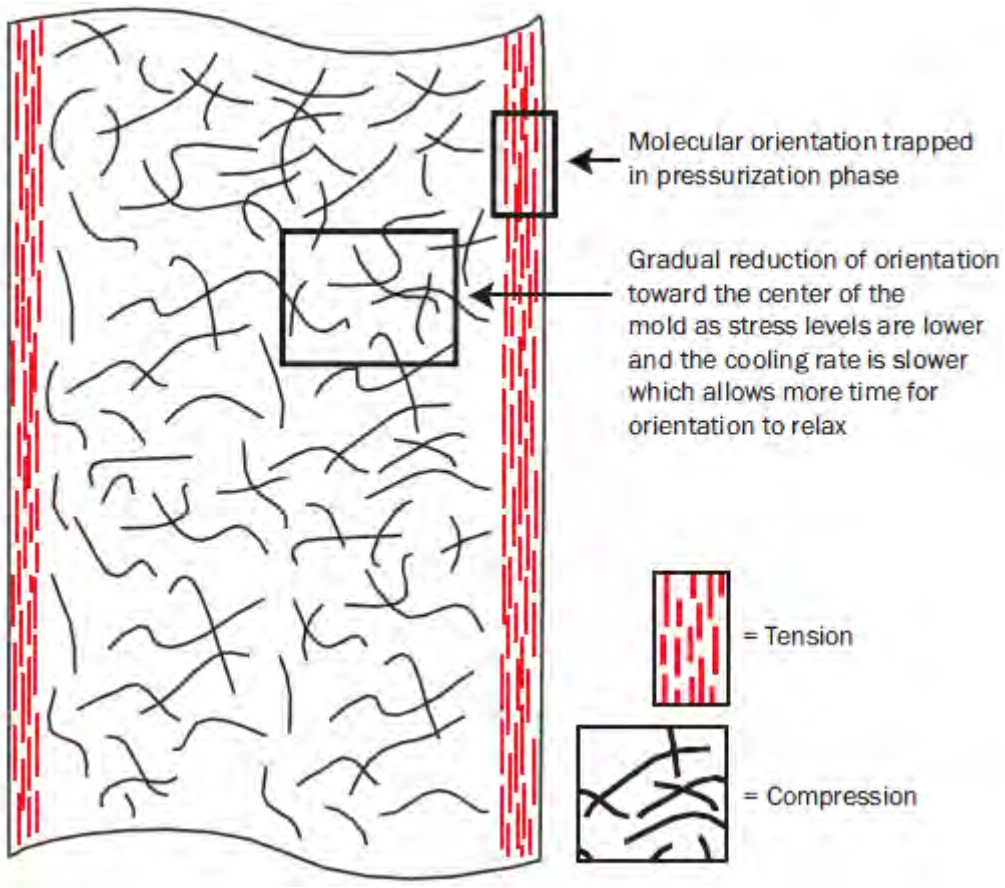

Figure 1.17: Molecular orientation through the thickness of the part. *(Source: Shoemaker J., 2006)*

1.4.3 Frozen layer thickness

During filling, the frozen layer should maintain a constant thickness in areas with continuous flow, because the heat loss to the mold wall is balanced by the hot melt coming from upstream. When the flow stops, the heat loss through the thickness dominates, resulting in a rapid increase in the thickness of the frozen layer. Initially, the frozen layer is very thin, so heat is lost very rapidly. This results in more plastic freezing and the frozen layer getting thicker, cutting down the heat flow.

While the part is filling, the amount of shear heat generated is dependent of the fill rate. The higher the filling speed (shear rate) or the shorter the fill time, the more shear heat will be generated and the thinner the frozen layer will be (figure 1.18). Similarly, higher melt and mold temperatures would reduce the thickness of the frozen layer.

On the other hand, if the injection rate was slow, less heat would be generated by friction along the flow path, with less heat input from the flow. The heat loss would be at the same rate, and with less heat input, the frozen layer would grow in thickness. As the frozen layer gets thicker, the actual flow channel for the plastic gets smaller and therefore, a higher fill pressure is required, for a given flow rate.

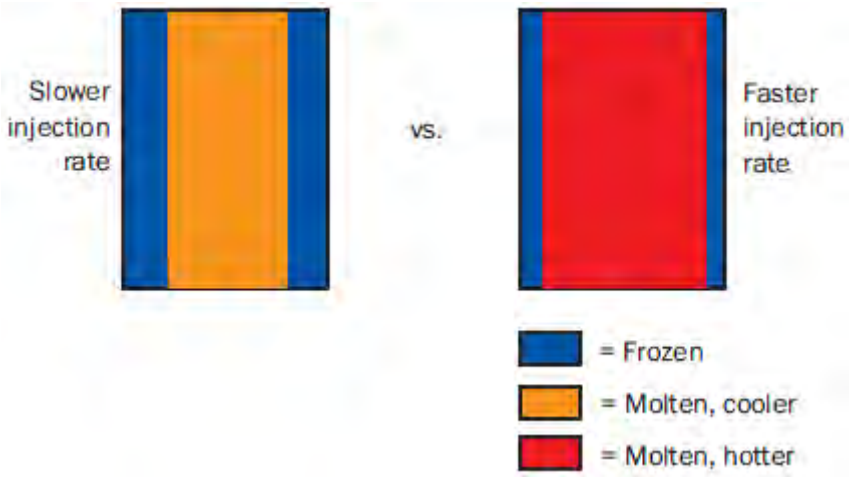

Figure 1.18: Effect of injection rate on the frozen layer thickness. *(Source: Shoemaker J., 2006)*

1.4.4 Molding variations

There are many variables during molding that can influence the final product performance. Of paramount importance, for example, is controlling the fill pattern of the mold, so that parts can be produced reliably and economically. A good fill pattern for a molding is usually one that is unidirectional, thus, giving rise to a unidirectional and consistent molecular orientation in the molded product. This approach helps avoid warpage problems caused by differential orientation.

Compensating flow is unstable. Consider the plate molding (figure 1.19 (a)). One would think that plastic flowing uniformly through the thin diaphragm would top up the thick rim. In practice, the plastic during the compensation phase flows in *rivers* that spread out like a delta, as illustrated in figure 1.19 (b).

There is always some variation in melt temperature coming from the barrel of the injection molding machine. For example, if one part of the melt is slightly hotter than the rest, then the plastic flow in that area will be slightly greater, bringing hotter material into the area and maintaining the temperature. On the other hand, if there is another area that is cooler, the flow will be less, so there will be less heat input, and the plastic will get colder, until it eventually freezes off.

However balanced the initial conditions, this natural instability will result in a river-type flow. This is a very important consideration. The first material to freeze off will shrink early in the cycle. By the time the material in the river flow freezes, the bulk of the material will have already frozen off and shrinkage will have occurred. The rivers will shrink relative to the bulk of the molding, and because they are highly orientated, shrinkage will be very high. The result is high-stress tensile members throughout the molding, a common cause of warpage.

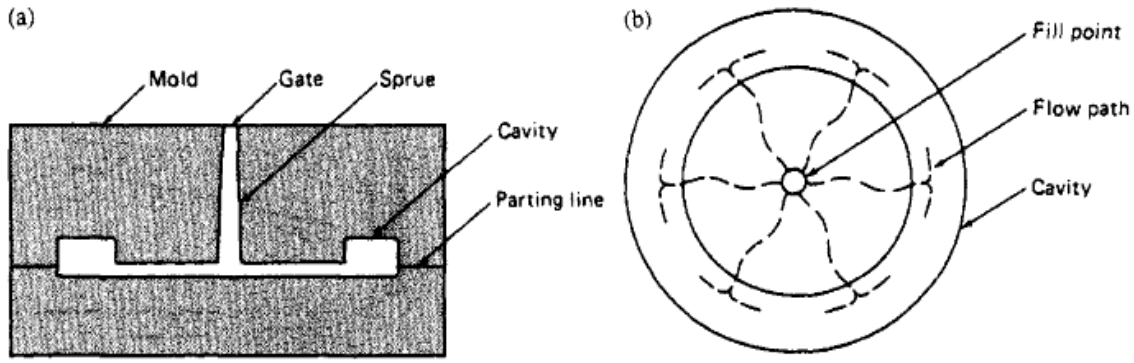

Figure 1.19: Plastic melt does not flow uniformly through the diaphragm of the plate mold (a) in the compensation phase, but spreads in a branching pattern (b). *(Source: Rosato, 2000)*

1.5 Material behavior

Molten thermoplastics (TPs) exhibit *viscoelastic behavior*, which combines flow characteristics of both *viscous liquids* and *elastic solids*. When a viscous liquid flows, the energy that causes the deformation is dissipated and becomes viscous heat. When an elastic solid is deformed, the driving energy is stored. Typical examples are that of the water flow and the deformation of a rubber cube, respectively.

In other words, under certain conditions, molten TPs behave like a liquid and will continuously deform, while shear stress is applied. Upon the stress removal, however, the materials behave somewhat like an elastic solid, with partial recovery of the deformation. This viscoelastic behavior stems from the random-coil configuration of polymer molecules in the molten state, which allows the movement and slippage of molecular chains under the influence of an applied load. However, the entanglement of the polymer molecular chains also makes the system behave like an elastic solid, upon the application and removal of the external load. Namely, on removal of the stress, chains will tend to return to the equilibrium random-coil state and thus, will be a component of stress recovery. The recovery is not instantaneous, because of the entanglements still present in the system.

1.6 Material deformation

In addition to the two types of material flow behavior described above, there are also two types of deformation: *simple shear* and *simple extension* (*elongation*), as shown in figure 1.20 (a) and 1.20 (b). The flow of molten TPs during injection-molding filling is predominantly shear flow (figure 1.22 (c)), where layers of material elements "slide" over each other. The extensional flow, however, becomes significant as the material elements undergo elongation, when the melt passes through areas of abrupt dimensional change (e.g. a gate region), as shown in figure 1.22 (d).

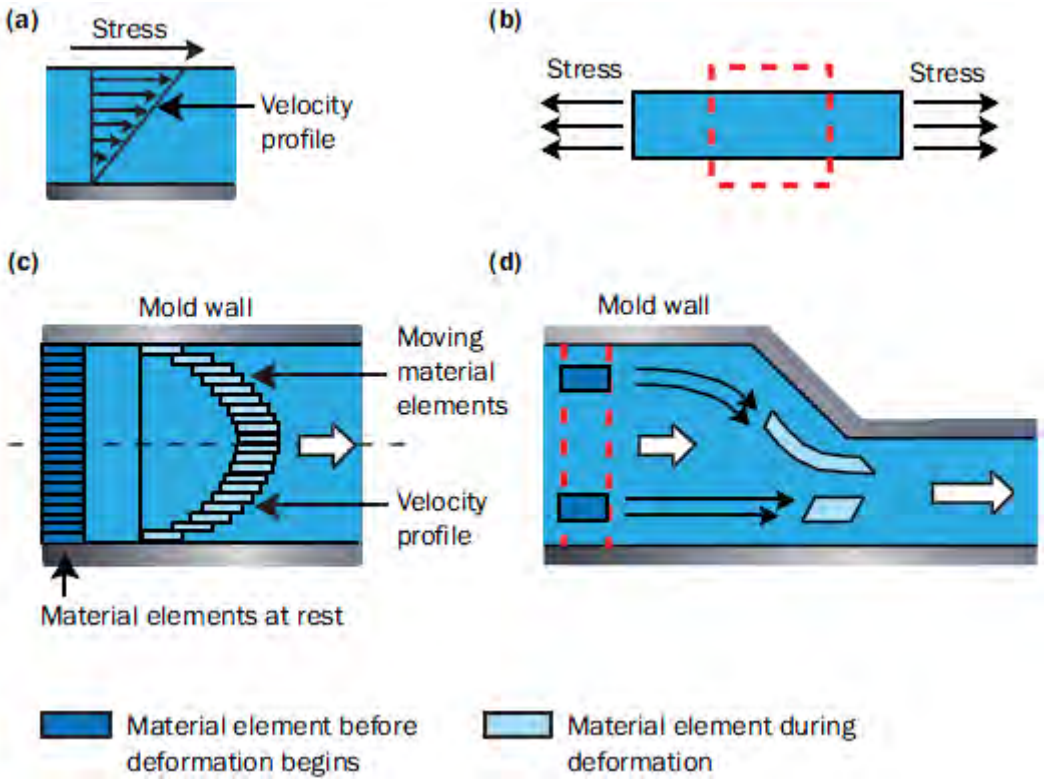

Figure 1.20: (a) Simple shear flow; (b) Simple extensional flow; (c) Shear flow in cavity filling and (d) Extensional flow in cavity filling. *(Source: Shoemaker J., 2006)*

1.7 Material viscosity

Melt shear viscosity is a material's resistance to shear flow. In general, polymer melts are highly viscous because of their long molecular chain structure. The viscosity of a polymer melt can range from 2 to 3000 Pa·s (water 0.1 Pa·s). Viscosity is expressed as the ratio of shear stress (force per unit area) to the shear rate (rate change of shear strain).

Note: When the polymer is deformed, there will be some disentanglement, slippage of chains over each other and molecular alignment in the direction of the applied stress. As a result of the deformation, the resistance exhibited by polymer to flow decreases, due to the evolution of its microstructure (which tends to align in the flow direction). This is often referred to as shear-thinning behavior, which translates to lower viscosity with a high shear rate.

This kind of behavior provides some benefits for processing the polymer melt. For example, if the applied pressure to move water in an open ended pipe is doubled, then the flow rate of water also doubles, because the water does not have shear-thinning behavior. But in a similar situation using a polymer melt, doubling the pressure may increase the melt flow rate from 2 to 15 times, depending on the material. *[3]*

1.8 Shear rate distribution

The faster the adjacent material elements move over each other, the higher the shear rate is. Therefore, for a typical melt flow velocity profile, shown in figure 1.21 (a), the highest shear rate is just inside the frozen layer (or some distance from the wall). The shear rate is zero at the centerline or midplane, because there is no relative material element movement due to flow symmetry, as shown in figure 1.21 (b).

Shear rate is an important flow parameter, because it influences the melt viscosity and the amount of shear (viscous) heating. The typical shear rate experienced by the polymer in the cavity is between 10^2 and 10^4 1/sec. The feed system can see shear rates in excess of 10^5 1/sec.

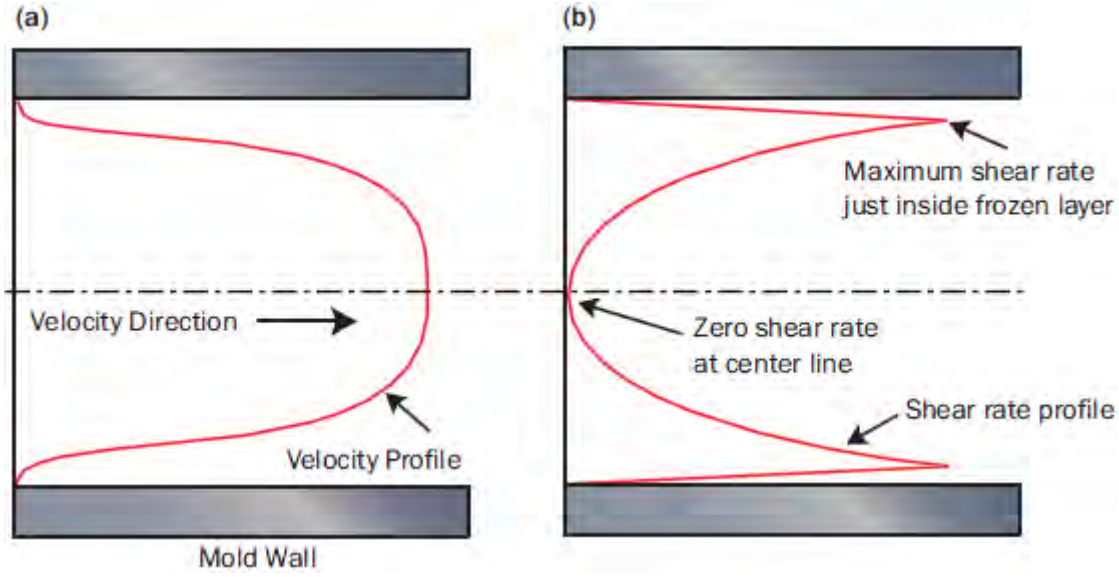

Figure 1.21: (a) Typical velocity profile and (b) The corresponding shear rate distribution in injection molding filling. *(Source: Shoemaker J., 2006)*

1.9 Factors that directly affect the polymer

Since the mobility of polymer molecular chains decreases with decreasing temperature, the flow resistance of polymer melt also greatly depends on the temperature. Through figure 1.22, it is concluded that melt viscosity decreases:

- With increasing shear rate: because of the disentanglement and alignment of the molecules.
- With increasing temperature: because of the enhanced mobility of polymer molecules.
- With decreasing pressure: the lower the pressure – the less viscous the melt becomes.

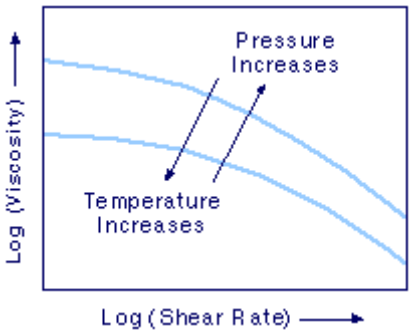

Figure 1.22: The viscosity of a polymer melt depends on the shear rate, pressure and temperature. *[3]*

1.10 Pressure and injection time

The filling phase should be controlled by injection time, i.e. velocity. The part should be filled so that the pressure gradient (pressure drop per unit flow length) is constant during the filling. To maintain a constant pressure gradient, the pressure at the machine nozzle continues to increase as the flow front progresses through the part. Figure 1.23 shows pressure traces for three different injection times.

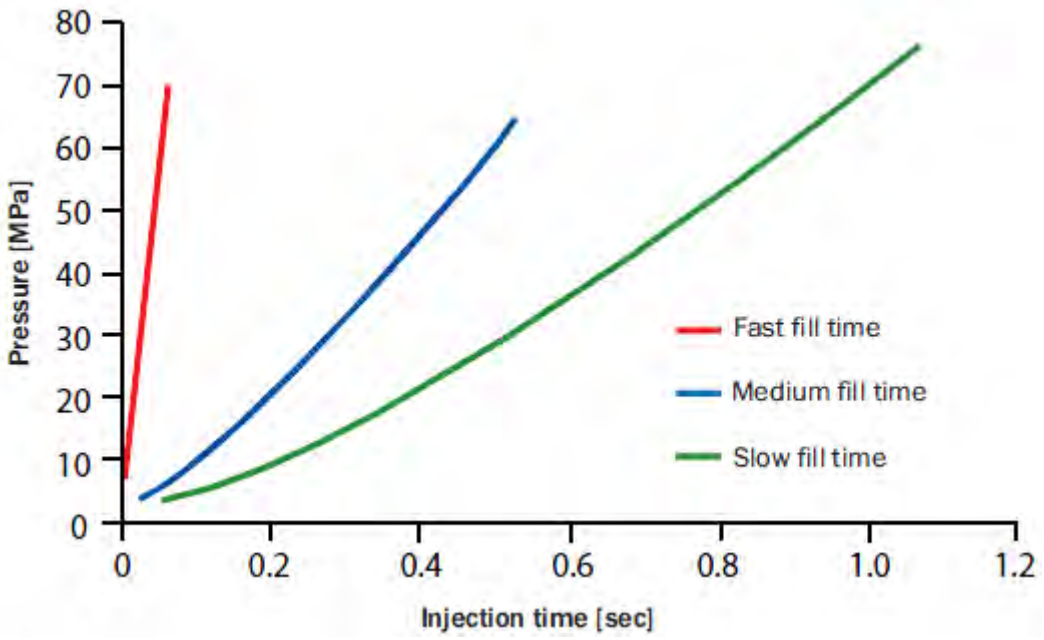

Figure 1.23: Injection time vs. pressure. The pressure gradient (the slope of the lines) is different for each fill time. A faster fill time results in a steeper pressure gradient. However, for each fill time, notice that the rate of change in pressure per unit of time is nearly uniform. *(Source: Shoemaker J., 2006)*

Note: The polymer flow front travels from areas of high pressure to areas of low pressure, analogous to water flowing from higher elevations to lower elevations. During the injection stage, high pressure builds up at the injection nozzle to overcome the flow resistance of the polymer melt.

The pressure decreases along the flow length toward the polymer flow front, where the pressure reaches the atmospheric pressure if the cavity is vented. Broadly speaking, the pressure drop increases with the flow resistance of the melt, which, in turn, is a function of the geometry and melt viscosity. The polymer's viscosity is often defined with a melt flow index (MFI). However, this is not a good measure of the material's behavior during the filling phase. As the flow length increases, the polymer entrance pressure increases to maintain a desirable injection flow rate.

1.11 Factors influencing the injection – pressure requirements

Factor	Variable	Higher injection pressure required	Lower injection pressure required
Part design	Part thickness	Thin part 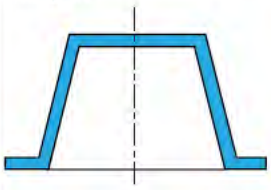	Thick part 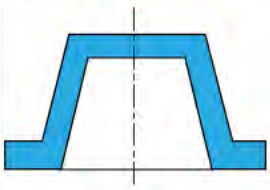
	Part surface area	More wall cooling and drag force 	Less wall cooling and drag force 
	Flow length	Long flow length 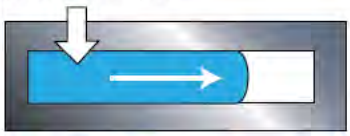	Short flow length 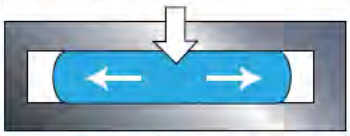

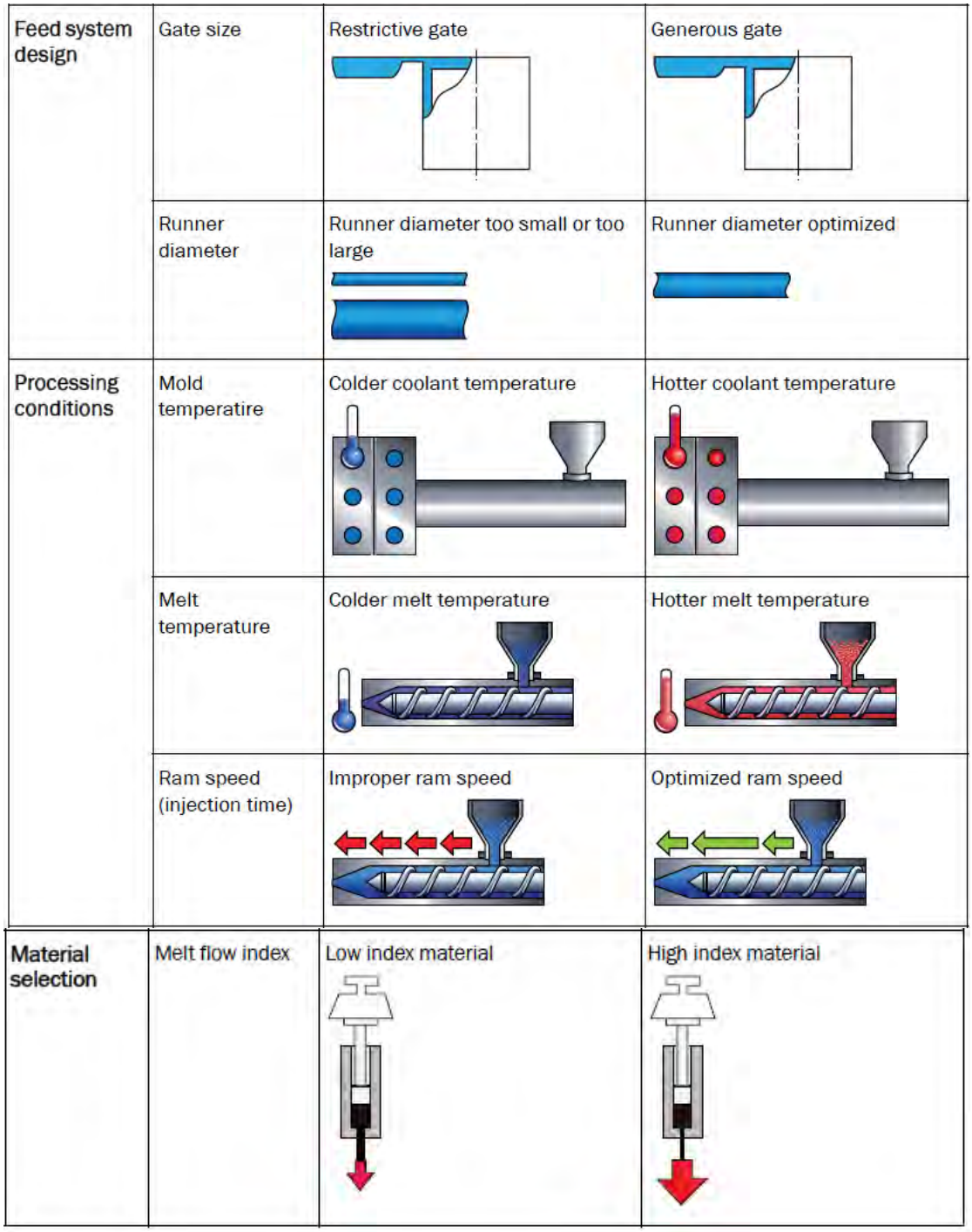

Figure 1.24: An illustration of the design and processing factors that affect the injection pressure. *(Source: Shoemaker J., 2006)*

1.12 Flow models

1.12.1 Filling

All modern mold filling simulation programs for injection molding rely on the General Hele-Shaw (GHS) methodology, so as to compute the filling pattern. The filling of a thin-walled thermoplastic part is a very complex process. This Hele-Shaw approximation is the standard model used in order to simulate polymer injection molding, where flows are assumed to be non-Newtonian and non-isothermal.

The GHS flow model refers to the flow between two plates close together, and hence the width of the gap is assumed to be much smaller than the other dimensions of the flow. This assumption yields that the flow at a given point is mostly influenced by the local geometry and therefore, the velocity in the gap-wise direction is neglected, and the pressure is a function of planar coordinates, only.

The assumptions include the following (see figure 1.25):

- Thin cavity (h<<L)
- Incompressible fluid
- Generalized Newtonian Fluid (GNF) behavior
- Negligible inertia and body forces
- No-slip boundary conditions at the walls
- Flow is symmetric about the midplane (z = 0), with the upper and lower surfaces of the gap at $z = \pm h$
- Pressure does not vary significantly in the z-direction
- Velocity in the z-direction is negligible, compared to the in-plane velocities.

Note: Fluids, for which the rate of shear at any point within the fluid is determined only by the value of the shear stress at that point – at that instant, are variously known as: “time-independent” or “purely viscous” or “inelastic” or “generalized Newtonian fluids” (Nguyen, 2012).

The equations describing the Hele-Shaw polymer melt flow are:

- Continuity equation:

$$\frac{\partial(\rho u)}{\partial x} + \frac{\partial(\rho v)}{\partial y} = 0 \quad (1)$$

- Momentum equation:

$$\frac{\partial p}{\partial x} = \frac{\partial}{\partial z}\left(\eta \frac{\partial u}{\partial z}\right) \text{ and } \frac{\partial p}{\partial y} = \frac{\partial}{\partial z}\left(\eta \frac{\partial v}{\partial z}\right) \quad (2), (3)$$

- Energy equation:

$$\rho_p C_{pp}\left(\frac{\partial T}{\partial t} + u\frac{\partial T}{\partial x} + v\frac{\partial T}{\partial y}\right) = \eta \dot{\gamma}^2 + k_p \frac{\partial^2 T}{\partial z^2} \quad (4)$$

where (x, y, z) are the Cartesian coordinates, (u, v, w) - the velocity components, T – the temperature, p - the pressure, ρ_p - the density of the polymer, C_{pp} - the specific heat of the polymer, k_p - the thermal conductivity of the polymer, η - the viscosity, and $\dot{\gamma}$ is the shear rate. The *thickness direction* is represented by the z-coordinate and no flow will take place in the z-direction. The magnitude of the shear rate is governed by:

$$\dot{\gamma} = \sqrt{(\frac{\partial u}{\partial z})^2 + (\frac{\partial v}{\partial z})^2} \quad (5)$$

The model equations are based upon the following approximations: (i) the flow is inelastic; (ii) the fountain flow phenomena are disregarded; (iii) normal stresses are disregarded; (iv) thermal convection in the gap-wise direction and conduction in the flow direction are disregarded; and (v) the conductivity and heat capacity are constant. The boundary and initial conditions are:

$u = v = 0$ (where the fluid touches a solid boundary in the x-y plane, i.e. at the edges of the mold) (6)

$T = T_w$, at z = ± h (the gap of the cavity is 2h and T_w is a constant wall temperature) (7)

$$\frac{\partial u}{\partial z} = \frac{\partial v}{\partial z} = \frac{\partial T}{\partial z} = 0, \text{ at z = 0} \quad (8)$$

$p = 0$ (at the flow front) (9)

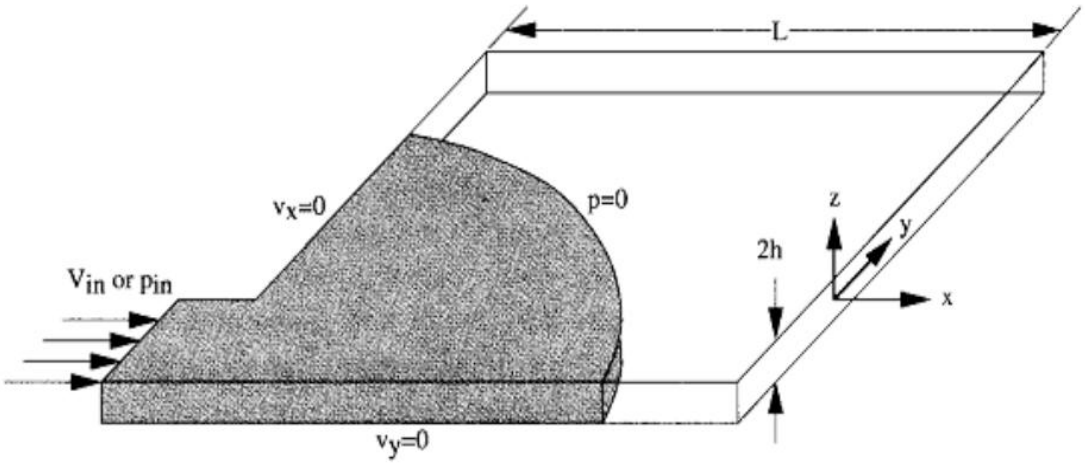

Figure 1.25: A narrow gap geometry example as analyzed by the Hele-Shaw approximation. Note that v_x and v_y will be described as u and v, respectively. At the inlet, there is either a prescribed pressure $p = p_{in}$, or a prescribed normal velocity $V_{in} = -(S / h)\partial p / \partial n$. *(Source: Dantzig & Tucker, 2001)*

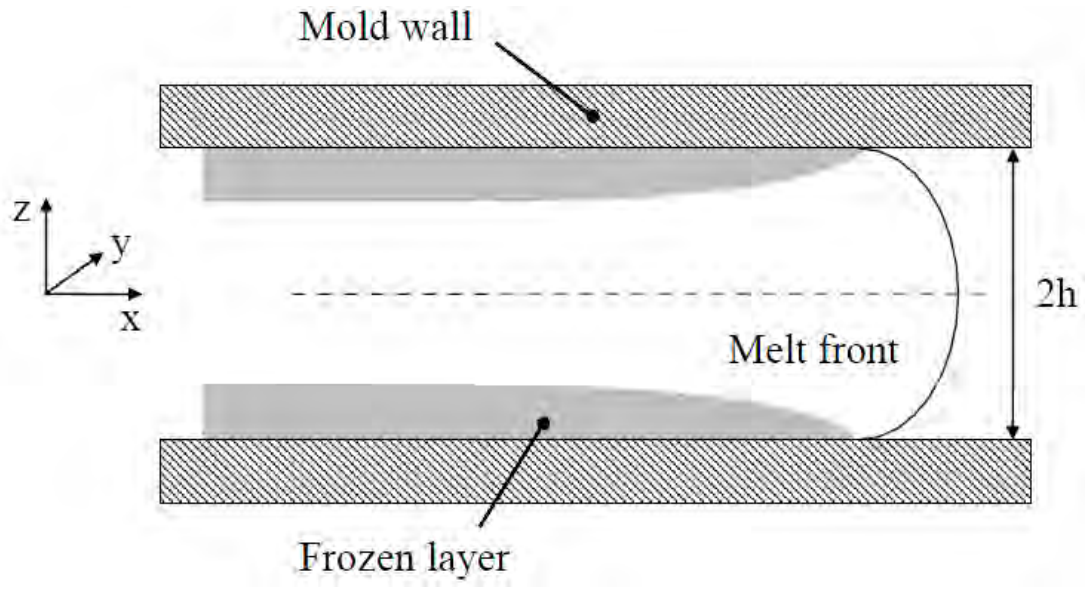

Figure 1.26: Cross-sectional view of the flow front. *(Source: Rännar L.E., 2008)*

Integration of eq. (2) and eq. (3) making use of eq. (9), results in:

$$\eta \frac{\partial u}{\partial z} = \frac{\partial p}{\partial x} z$$
$$\eta \frac{\partial v}{\partial z} = \frac{\partial p}{\partial y} z \quad (10)$$

Integrating once more together with eq. (6) and (7):

$$u = -\frac{\partial p}{\partial x} \int_z^h \frac{z dz}{\eta}$$
$$v = -\frac{\partial p}{\partial y} \int_z^h \frac{z dz}{\eta} \quad (11)$$

Combining eq. (5) with eq. (11) yields:

$$\dot{\gamma} = \frac{z}{\eta} \sqrt{(\frac{\partial p}{\partial x})^2 + (\frac{\partial p}{\partial y})^2} \quad (12)$$

Furthermore, the gap-wise averaged velocities are obtained by integration of eq. (11):

$$\bar{u} = -\frac{S}{h} \frac{\partial P}{\partial x}$$
$$\bar{v} = -\frac{S}{h} \frac{\partial P}{\partial y} \quad (13)$$

where S is called the *flow conductance* or *fluidity* (the ease with which a melt can be forced through a mold):

$$S(x,y)=\int_0^h \frac{z^2}{\eta(x,y,z)}dz \quad (14)$$

where η is the local viscosity and h is half the height of the gap. Substituting eq. (13) into eq. (1) gives:

$$\frac{\partial}{\partial x}(S\frac{\partial p}{\partial x})+\frac{\partial}{\partial y}(S\frac{\partial p}{\partial y})=0 \quad (15)$$

The viscosity η varies across the gap thickness, as well as spatially in the x and y directions. It may also depend on the strain rate and temperature.

Note: The Hele-Shaw flow model is valid distant from the gate and from the active flow front. In these regions, the flow is governed by a boundary layer problem, in which the layer is approximately equal to the thickness of the gap. At the flow front, the flow field is considerably more complex, because of the existence of the fountain flow effect. Moreover, another breakdown of this model occurs when thick sections are considered. Although most injection molded parts are thin in nature, there are some that can have relatively thick regions. Because one of the founding assumptions of this model is the thin section, error increases as the aspect ratio (b/L) of the geometry increases. (Osswald et. al., 2001).

Note: In a general 3-dimensional steady fluid flow problem, one must solve for four dependent variables: u, v, w and p, as functions of three independent variables: x, y and z. However, for highly viscous fluids in a narrow gap, the Hele-Shaw formulation allows to solve one partial differential equation (15), for one independent variable, p, which only depends on x and y (p(x,y)). This is an enormous simplification for modeling the injection mold filling (Dantzig & Tucker, 2001).

The viscosity can be described with different material models, and figure 1.27 plots the viscosity according to three commonly used constitutive models: the Newtonian model (eq.16), the Power Law model (eq.17), and the Cross model (Eq.18).

$$\eta=\eta_0 \quad (16)$$

$$\eta=K\dot{\gamma}^{n-1} \quad (17)$$

$$\eta=\eta_\infty+\frac{\eta_0-\eta_\infty}{1+(C\dot{\gamma})^m} \quad (18)$$

where η_0 is the zero shear viscosity, K is the consistency coefficient, n is called the Power law index, η_∞ is the infinite shear viscosity, m is a parameter called the Cross rate constant/consistency constant and C is a constant related to the material.

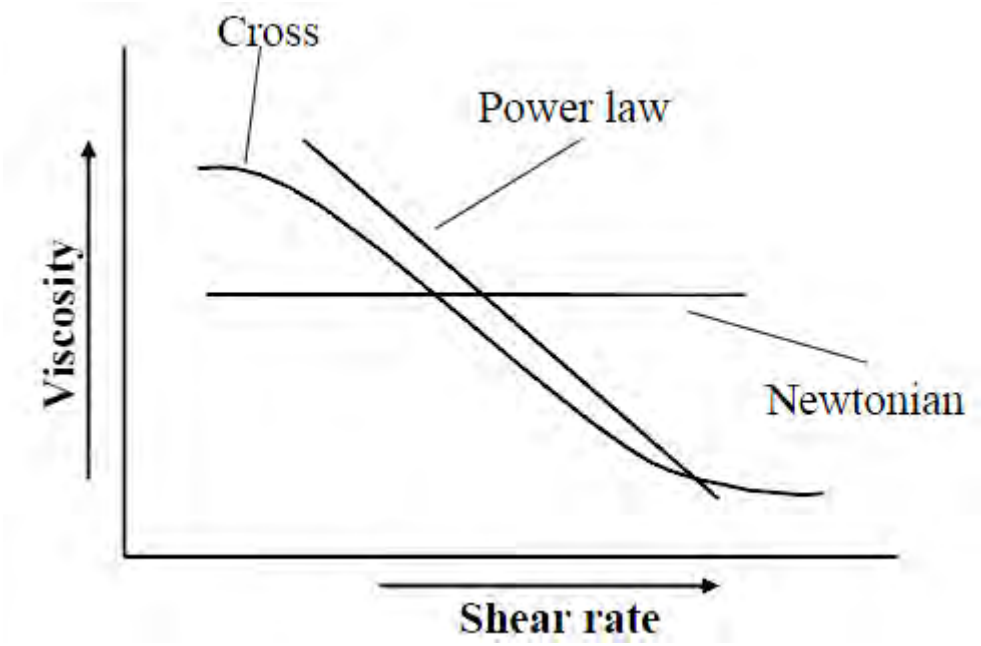

Figure 1.27: The viscosity as a function of the shear rate for three different material models. *(Source: Rännar L.E., 2008)*

1.12.2 Packing

In the packing phase, the mold is filled up by polymer melt. More melt is forced into the mold in order to compensate for the volumetric shrinkage and therefore, a compressible formulation is required to model this behavior. The governing equations for this phase are the same as for the filling phase and consideration is taken to the *compressibility* of the melt, by using a dependency of the specific volume on pressure and temperature (v(T,P)). This is called the pvT relationship, which can be modeled with different complexities.

Commonly used models for the processing of polymers are the Spencer-Gilmore model, which is derived from the ideal gas law by adding a pressure and temperature correction term to the specific volume, and the modified Tait pvT model with 13 parameters. Autodesk Moldflow Insight uses the Tait model (see PVT properties – page 80). This model can predict the abrupt volumetric change for semi-crystalline polymers and it is also suitable for amorphous polymers.

Lastly, it must be noted that the crystallization kinetics has an important effect on the shrinkage and warpage of the final part. The crystallization of a material influences the flow analysis, including changes in the modeling of viscosity, density/specific volume, conductivity, elastic modulus, solidification, the inclusion of latent heat in the energy equation, the orientation effect on shrinkage, etc. The model for crystallization is usually expressed as the rate of crystallization as a function of other terms, such as crystallization rate, temperature, crystallinity, cooling rate, etc.

1.12.3 Cooling

The objective of the mold-cooling analysis is to solve the temperature profile at the cavity surface, using boundary conditions of polymer melt during filling and packing analysis. When the injection molding process is in steady-state, the mold temperature will fluctuate periodically over time during the process, due to the interaction between the hot melt and the cold mold (figure 1.28). In order to reduce the computation time for this transient process, a cycle averaged temperature $\bar{T}$, that is invariant with time, is introduced for the mold, but the transient state is still considered for the polymer.

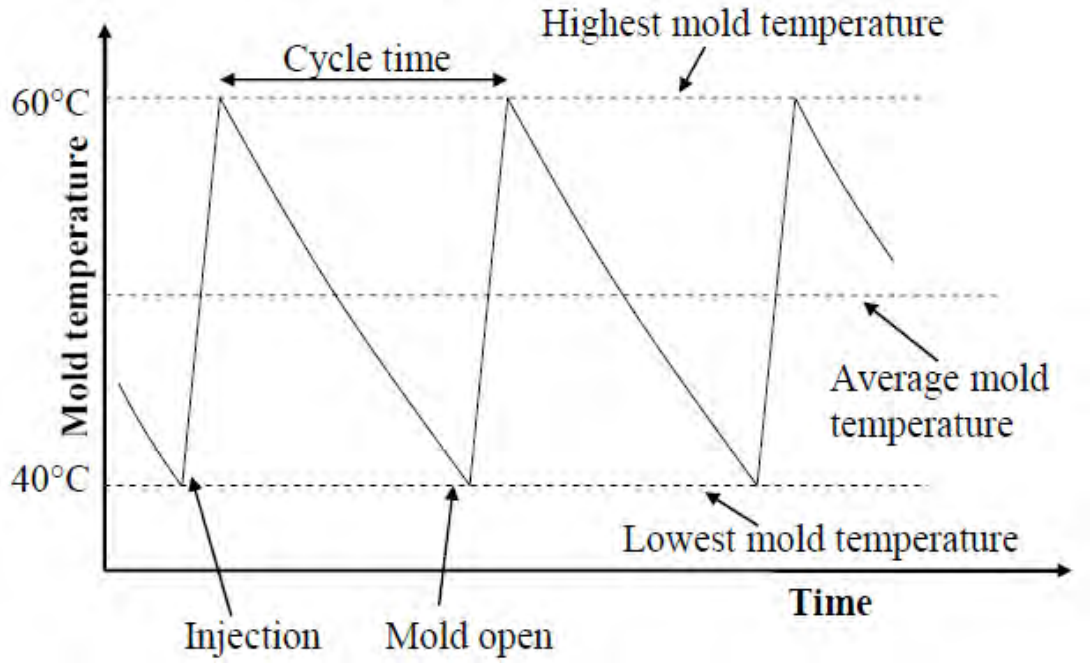

Figure 1.28: Typical mold temperature variations. *(Source: Rännar L.E., 2008)*

The overall heat conduction phenomenon is governed by the energy equation:

$$\rho_m C_{p_m} \frac{\partial T}{\partial t} = k_m \left(\frac{\partial^2 \bar{T}}{\partial x^2} + \frac{\partial^2 \bar{T}}{\partial y^2} + \frac{\partial^2 \bar{T}}{\partial z^2}\right)$$

where ρ_m is the density of the mold, Cp_m is the specific heat of the mold and k_m is the thermal conductivity of the mold. The cooling phase of the process is described by solving a steady-state Laplace equation for the cycle-averaged temperature distribution throughout the mold:

$$k_m \left(\frac{\partial^2 \bar{T}}{\partial x^2} + \frac{\partial^2 \bar{T}}{\partial y^2} + \frac{\partial^2 \bar{T}}{\partial z^2}\right) = 0$$

where $\bar{T}$ is the cycle-average temperature of the mold. The second equation, together with a simplified version of the first equation, where only the gap-wise coordinate is considered, can be both used to predict the mold and part temperature, during cooling.

1.13 Heat transfer models

Injection molding, by nature, is a fully non-isothermal process. This means temperature is non-uniform and that it depends greatly upon time and processing conditions at any stage of the process. Energy in transferred via *conduction* and *convection*, during the molding process.

Most simulation packages assume that the injection temperature is uniform and constant. This is clearly not the case in actual injection molding, where fluctuations in temperature can occur axially along the shot, as well as non-homogeneous temperatures through the thickness of the shot. The uniform injection temperature assumption is clearly not a result of inability of the computer simulation, however, but it has difficulty in measuring the actual injection shot temperature. Therefore, the uniform injection temperature is reasonable, for most calculations (Osswald et. al., 2001).

- Because the material is injected through the gate, the higher shear rates cause an internal heating of the polymer molecules. This heat generation is commonly referred to as *viscous dissipation*. The molecular friction of polymer chains rubbing against one another can cause a rather significant temperature rise in the melt. This effect is readily accounted for by modern simulation techniques.

- Additional heat transfer occurs due to the polymer flow in the form of convection. The fluid motion transfers energy along its flow path and thus convects heat, during mold filling.

- The last major mode of energy transfer, during the injection molding cycle, arises because of conduction. Even though conduction occurs in all directions of the polymer, the thin nature of injection molded parts causes conduction through the thickness direction to dominate. Therefore, simulation programs will typically only consider conduction across the thin gap. This simplification is quite valid, when the low thermal conductivity of polymers is considered. Because the mold wall is much cooler than the hot melt stream, conduction is far greater into the mold than along the flow direction.

Note: Generally, one compounding effect that arises when molding semi-crystalline polymers is the heat of crystallization or fusion. During the process of the crystalline structure formation, a certain amount of energy must be conducted out of the material, before the cooling process can continue.

2. Introduction to Autodesk Moldflow Insight (2012)

What is Autodesk Moldflow Insight ?

Autodesk Moldflow Insight (AMI) is a product suite designed to simulate the plastic injection molding process and its variants, such as gas-assist injection molding, injection-compression, thermosets processing, etc. AMI consists of a single common user interface, called Autodesk Moldflow Synergy and a range of analysis products. Together they provide an insight into the many and varied aspects of plastic injection molding. It is therefore an essential tool for a wide range of users.

What is Autodesk Moldflow Synergy ?

Synergy is the graphical user interface for AMI. It provides a quick, simple method of preparing, running and post-processing an analysis for a model. It also has fast and easy to use wizards for creating multiple cavities, runner systems, cooling circuits, mold boundaries and inserts. Included with Synergy is a material searching capability for the extensive material database, too. Material creation tools exist to import, change/modify and create materials to be used for any AMI analysis. To communicate your results with colleagues, AMI has a report generation facility that creates reports. Anyone can customize the reports to contain any of the results derived from an analysis. The reports can contain images of the parts analyzed, including any of the animated results. One report can contain results from any number of analyses or studies.

2.1 Inside the graphical user interface

Synergy, shown in figure 2.1, is the environment used for pre-process, run and post-process an analysis for all AMI analyses sequences and molding processes.

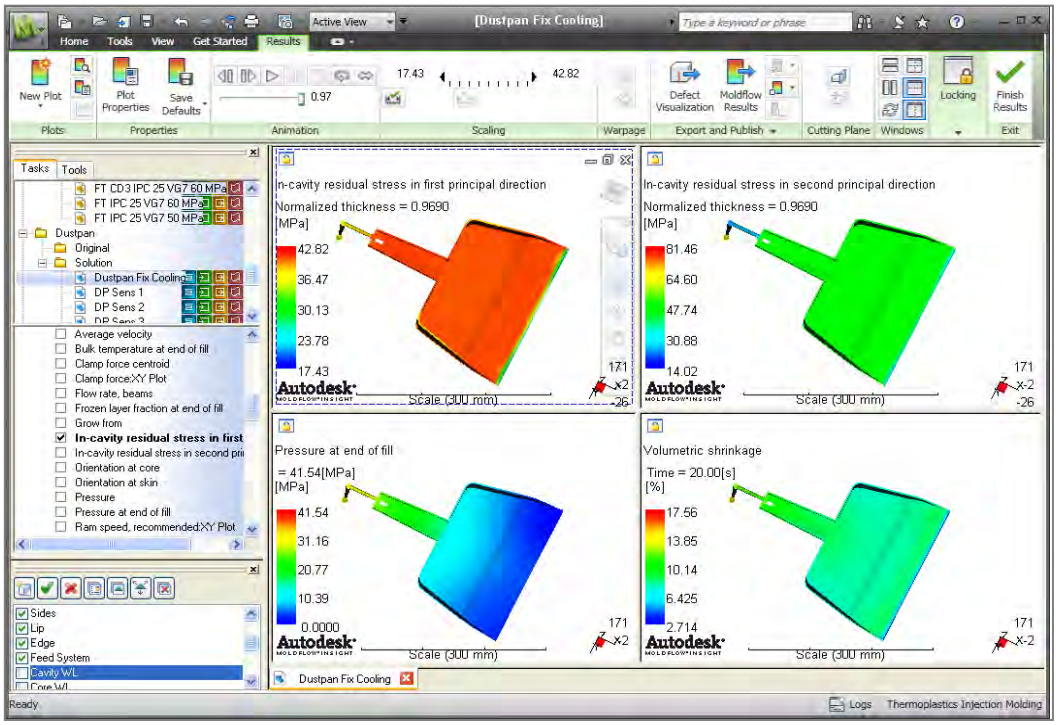

Figure 2.1: Autodesk Moldflow Synergy window.

Within Synergy, you can set up a sequence analysis (such as Cool + Fill + Pack + Warp), run the analysis, view the results and prepare a report. Each section is described in table 2.1.

Table 2.1: Main sections of Autodesk Moldflow Synergy.

Section	Description
Quick Access Toolbar	Provides quick access to the functionality of AMI. Contains group of commands commonly used. This can be customized easily.
Environment tabs	Set of tabs which content depend on what is displayed in the display area and the previous selections. Multiple environment tabs can appear at a given time.
Context menu	Menu accessed with a right click that is context sensitive. Different options appear depending on where the cursor is when the context menu is activated.
Panels	Area on the side of the screen that contains panels used for project, study, and layer management plus tools used for geometry creation, mesh diagnostics and mesh cleanup. A notes panel can be opened that has a section for study notes, (stays with the model when copied) and plot notes for each individual result plot.
Display	This is the area of Synergy where documents (studies) are opened and models are shown.
Wizards	A wizard is a tool that helps you perform a specific multi-step task.

2.2 Application Menu

The Application Menu can be accessed by pressing the  button on the top left corner of the interface. This menu expands and looks like that in figure 2.2. This menu provides access to specific file related commands, such as: new, open/close, save, export, print and study properties. You can access the application options from this menu as well.

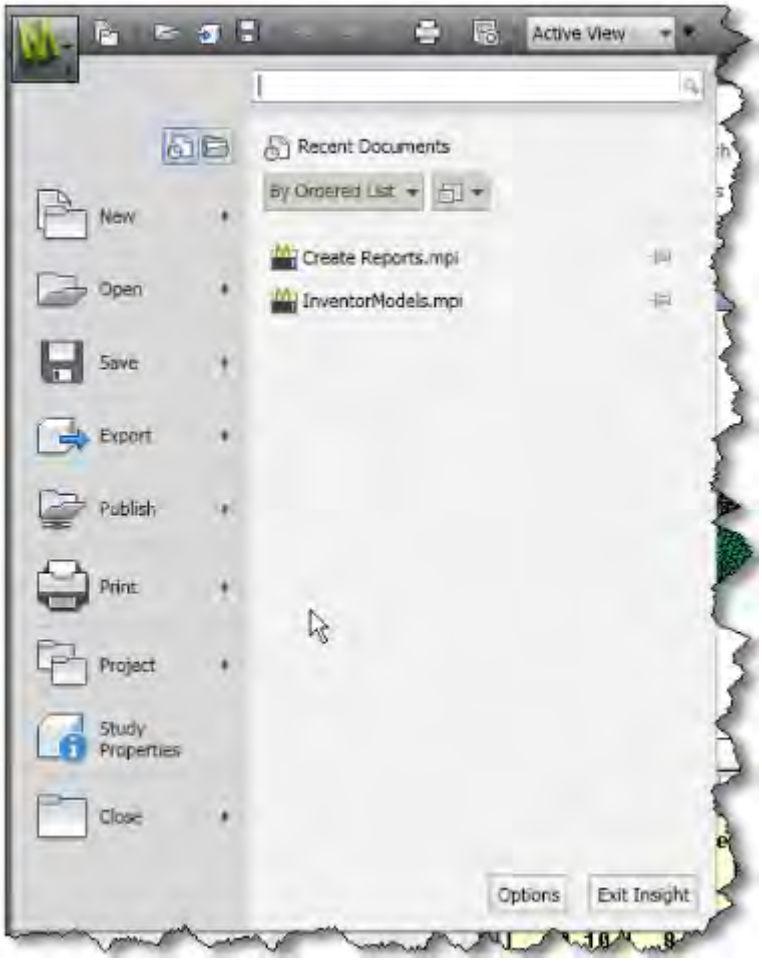

Figure 2.2: Application Menu.

2.3 Quick Access Toolbar

The Quick Access Toolbar, shown in figure 2.3, located at the top of the Autodesk Moldflow Synergy window contains the most commonly used commands available in Synergy.

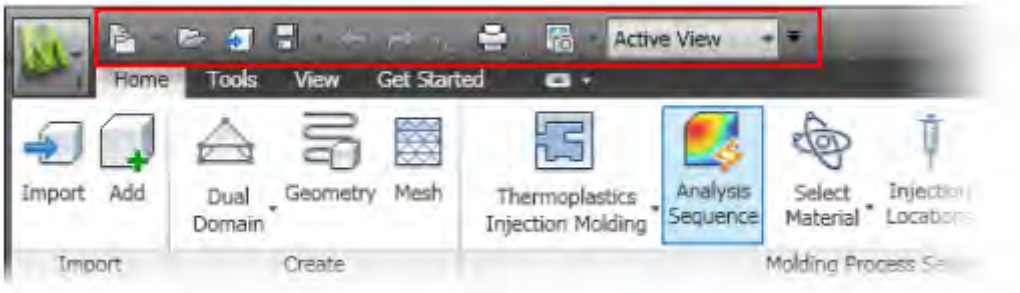

Figure 2.3: Quick Access Toolbar.

2.4 Environment Tabs

The Environment tabs change depending on what is currently shown in the display area and the previous selections. Figure 2.4 shows the Get Started environment tab that you see when opening Autodesk Moldflow Synergy for the first time.

Figure 2.4: Environment tab - Get Started tab.

Multiple environment tabs can appear as a result of a selection. Once you are done with the tasks accessible through such environment tab, just select finish/exit to return to the previous parent tab. Examples of such environment tabs are shown in the following images.

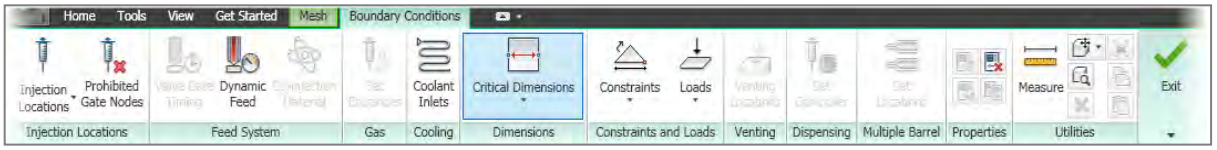

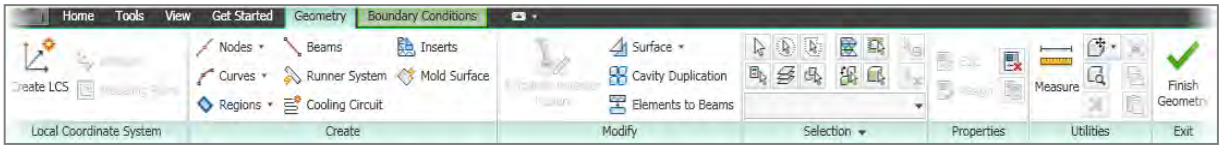

One can change the display of the environment tab at any time. Select any option from the pull-down menu located at the top of the tab, as in figure 2.5.

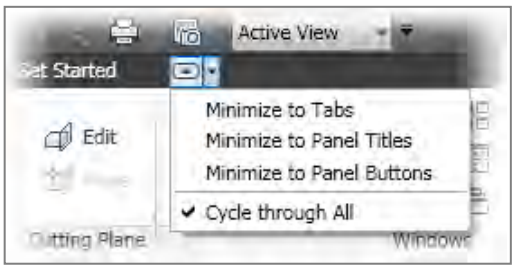

Figure 2.5:

Environment tab display options selection.

Table 2.2: Environment tabs available.

Environment tabs	Function
Get Started	Creating, opening, importing projects and models. Access to monitoring analysis running, access to tutorials, new features documentation and the community.
Home	Importing, adding geometries and meshes. Setting the molding process and analysis sequence, selecting the material, configuring the process settings and all analysis prerequisites necessary for the selected process. Monitoring analysis running, reviewing results and creating reports.
Tools	Creating, importing and editing databases for materials and other properties used in an analysis. The basic commands for the Application Programming Interface (API) are listed here as well.
Geometry (opened from the Home tab)	Creating, duplicating or querying nodes, curves and regions, creating runners, cooling lines, inserts or mold boundary with the aid of Wizards, defining and activating a local coordinate system or modeling plane, and diagnosing surface problems. Tools for selecting entities and properties manipulation.
Mesh (opened from the Home tab)	Creating, refining, diagnosing, and fixing meshes. Tools for selecting entities and properties manipulation.
Boundary conditions (opened from the Home tab)	Adding or modifying boundary conditions to the model such as injection locations, prohibited gate notes, Dynamic Feed, coolant inlets, constraints and loads. Available boundary conditions depend on the molding process selected.
Results (opened from the Home tab)	Setting display options for results, querying results and outputting results to a file. The preferences for the plots properties can be modified from this menu.
Reports (opened from the Home tab)	Creating, editing and viewing reports based on one or more analyses. Notes, images and animations can be created from this tab as well.

2.5 Panels

Creating, editing and validating a geometry or a mesh requires substantial interaction with the part model. So does writing notes about a study or a result. The panel layout provides an uninterrupted access to the part model in the display window and can greatly improve user efficiency and productivity. The Project panel (figure 2.6) displays either the *Tasks* or *Tools* tab.

Figure 2.6: Tasks tab on the Projects panel in Synergy.

2.5.1 Tasks tab

The tasks tab is divided into two sections:

- Project pane.
- Study tasks pane.

A divider bar between the Project pane and the Study tasks pane is movable, so the relative sizes of the two panes can be changed at any time. The Tasks tab is shown in figure 2.6.

a) Project pane

The Project pane is the top level of organization in Synergy. It contains a list of all the studies within a project. A project is equivalent to one "directory" on the hard disk, with a collection of AMI analysis files. Within the Project pane, studies can be organized into virtual "Folders" and any number of folders can be created to organize studies within one project.

For each study in the Project pane, one or more icons may appear to the right of the study name. These icons represent the types of analyses that can be run in AMI and the status of a given analysis. Several icons can be grouped together to form an analysis sequence such as  , which indicates a Cool + Fill + Pack + Warp analysis. Let's assume that a Fill analysis is going to be run. When the analysis is over and all the results are available for the study, the  icon will appear. However, the icon  indicates that the selected analysis is a filling analysis, but has not yet been completed, because it is not filled. If an analysis is aborted, the icon similar to  is shown instead. The red box with the "x" mark indicates that an analysis was started, but not finished and the solver has stopped.

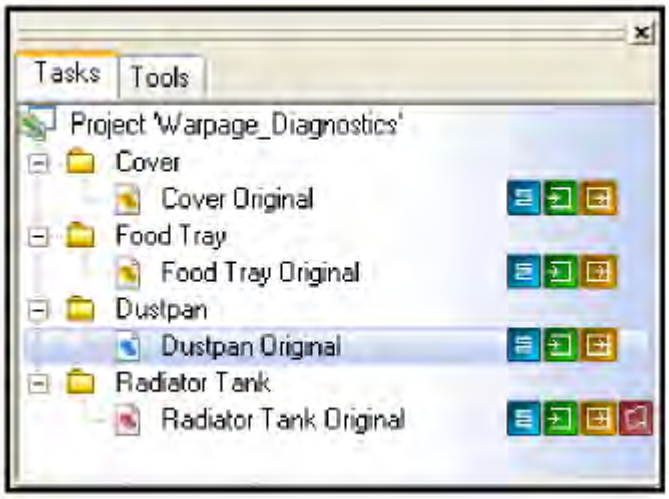

Figure 2.7:

Project Pane.

Studies

Studies are files that contain all the information about a part to run an analysis. The extension is **.sdy*. The study file contains:

- Imported or created geometry.
- Finite element mesh.
- Analysis sequence.
- Material information.
- Injection location(s).
- Process settings.

b) Study tasks pane

The Study Tasks pane displays a list of the basic steps necessary to set up and run an analysis. The information shown in the Study Tasks list always relates to the currently active study. The study tasks pane includes the following icons:

Table 2.3: Study Tasks Icons.

Icon	Name	Description
	Translation model	Indicates the original file format of the geometry.
	Midplane model *	Indicates the model uses midplane mesh technology.
	Dual Domain model *	Indicates the model uses dual domain mesh technology.
	3D model *	Indicates the model uses 3D mesh technology.
	Analysis sequence	Shows the current analysis sequence selected.
	Material	Shows the current material selected and provides access to material searching functions.
	Injection nodes	Sets the injection location on the part. Lists how many injection locations are in the model.
	Circuits	Sets coolant inlet properties and starts the circuit creation wizard. Lists how many cooling inlets are in the model.

	Process setting	Sets all the variables for the analyses selected in the analysis sequence.
	Optimization	Launches a wizard for a design of experiment (DOE) analysis.
	Start analysis	Starts the analysis or opens the job manager with a right click.
	Results	Lists all graphical results.
	Results folders	For each analysis sequence there will be a result folder under which the results are grouped together.
	Task done	Indicates that the task is completed and information is provided so an analysis can be started.

* See ‘Mesh types’ below for more details.

In addition to all the tasks required to set up the study to the point where an analysis can be run, there is also a listing of all results created once an analysis is completed. An example of the Study Tasks list is shown in figure 2.8. In this example, all analysis setup tasks have been completed, an analysis has been run, and results are now ready for viewing.

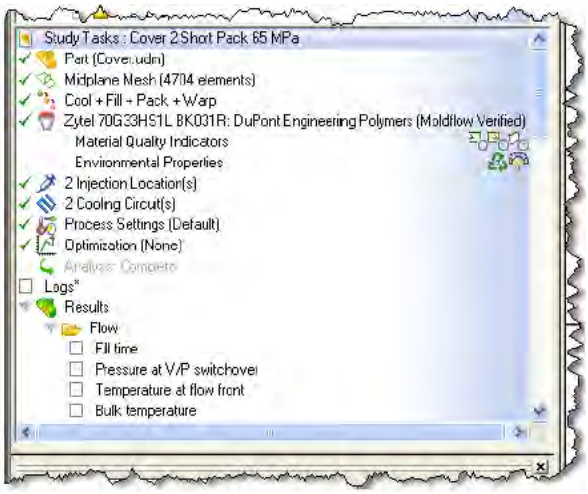

Figure 2.8:

Study tasks list.

Mesh Types

Analyzing a model is a complex operation. Modeling the way molten plastic flows, especially through complex model geometry, is difficult. In order to run an analysis, one must have a meshed model. The mesh is a web that consists of elements, with each element containing a node at every corner. The mesh represents the part shape and provides the basis for the analysis, where molding properties are calculated at every node. The selected mesh type, or analysis technology, determines which molding processes and which analysis sequences are available for selection. The analysis technology types supported by AMI are:

- Midplane model: A *mid-plane* mesh provides the basis for the analysis. This mesh consists of three-node, triangular elements that form a one-dimensional representation of the part shape through its center, or mid-plane. The thickness of the part is represented by a thickness attribute applied to the mesh elements. The thickness of the part is stored in each element. The analysis then incorporates this measurement, by dividing the thickness of the part into thin layers, called *laminaes*. This provides a defined part volume on which calculations can be performed. Midplane analysis technology is appropriate when the part is predominantly thin-walled.

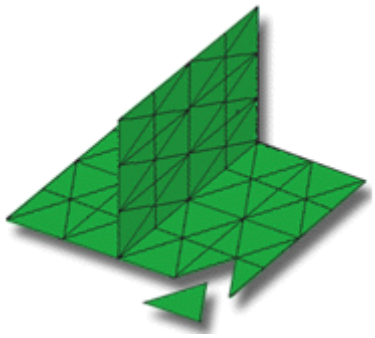

- Dual Domain model: A *surface* mesh provides the basis for the analysis. This mesh consists of three-node, triangular elements that form a one-dimensional representation on each surface of the part. The mesh elements are matched across opposing faces. The thickness of the part is determined by the distance between the opposing faces. The model could be visualized as a hollow body covered with a surface shell. Dual Domain analysis technology is appropriate when the part is predominantly thin-walled.

  When analyzing a part, the volume of the model is represented by thin layers through the thickness of the part (typically 10 or more layers through the thickness, i.e. laminaes). Elements on the opposite faces of the part must be matching so the layers can be built. These matched elements ensure the alignment of the layers through the thickness. These layers enable an accurate representation of thin, cross-sectioned parts, where there is a rapidly changing characteristic profile, for example, temperature, and flow-front velocity.

Note: The number of laminaes (layers) across the thickness defines the number of divisions that the plastic cross-section is broken into.

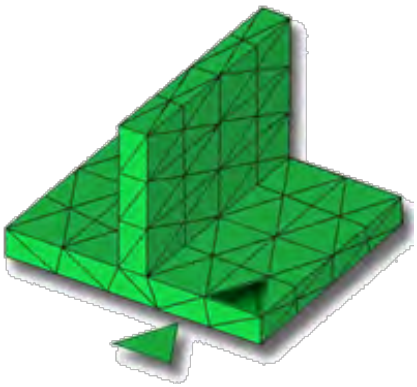

- 3D model: A *volume* mesh provides the basis for the analysis. This mesh consists of solid, four-node, tetrahedral (tetra) elements; each tetra has four triangular faces and six sides. Therefore, a 3D mesh represents the CAD model, by filling the volume of the model with tetras.

  3D meshes work well for parts that are thick/chunky or solid, because tetras give a true 3D representation of the model. A 3D analysis does not make the assumptions that are made for Midplane or Dual Domain analyses. Thus, 3D analyses often require additional computational time to complete. This makes a 3D mesh more appropriate for thick models with complicated shapes, while Midplane and Dual Domain meshes are more applicable for thin-walled, shell-like parts. Furthermore, a tetrahedral mesh does not require a thickness property, as it is true volume-filling mesh. Of course, when a more detailed analysis is needed, such as studying of the fiber orientation of a fiber filled material, then a 3D mesh will be the best choice.

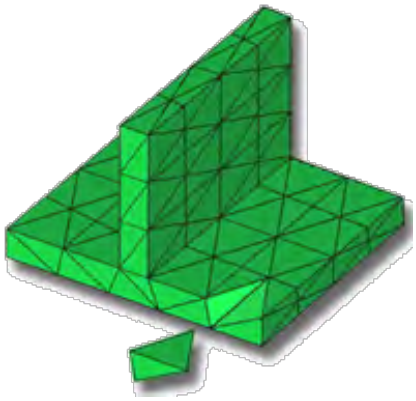

Furthermore, in the project pane, the type of technology used for each model is identified with the icons located to the left of the study name. Midplane is represented with (yellow icon), Dual domain with (blue icon) and 3D with (red icon).

2.5.2 Tools tab

Modeling and meshing tools can be found on the Tools tab in the Project panel. The part model remains visible in the display window without being obscured by tool dialogs, as shown in figure 2.9.

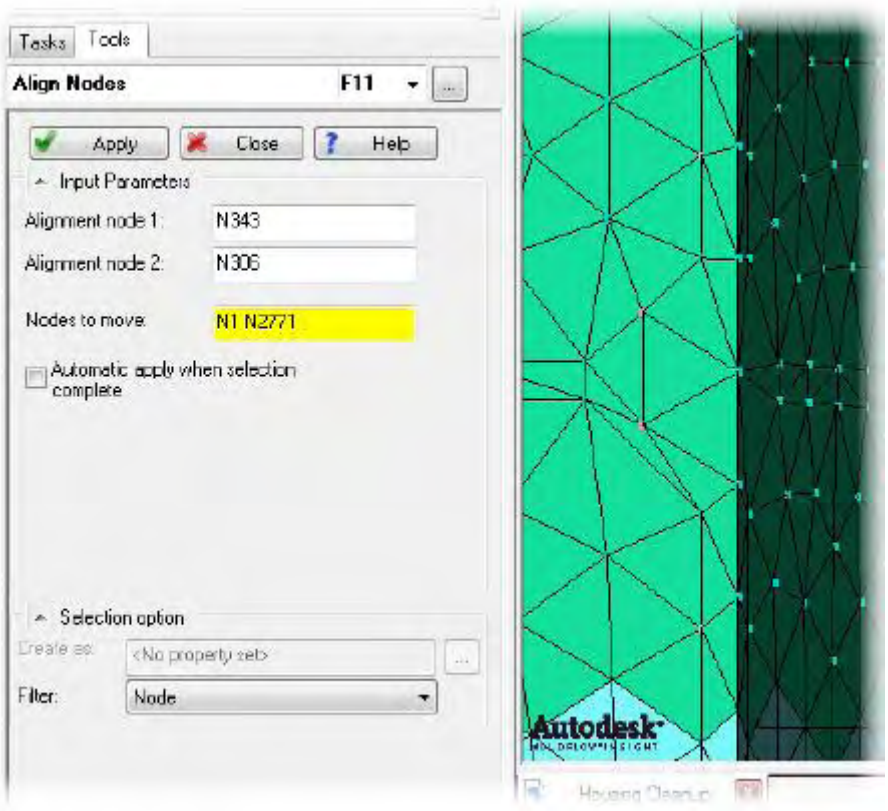

Figure 2.9: Tools tab in the Project panel.

Any of the model creation or mesh editing tools can be accessed easily, once you are in the Geometry or Mesh environment tabs without having to navigate through the Geometry or Mesh environment tabs every time you are in need of a new command.

Layers

Layers is a method of organizing the entities (nodes, elements, regions, etc.) in your model into groups, and then controlling the visibility and display properties of the entities on a per-group basis. The use of layers is very handy when modeling, fixing the mesh or during results visualization. For a model that has been meshed, there will be several default layers, including: Default Layer, New Nodes, and New Triangles. There will also be one or two layers for the imported geometry. Layers can also be organized to represent geometries, such as runners, gates, edge, top, side, etc. The Layers pane is by default, located under the Tasks/tools pane. The layers pane can be a floating dialog. To make the pane float, simple click in the icon area of the pane and drag it of the panel.

In the layers pane shown in figure 2.10, several details can be seen including:

- The bold layer is the active layer. Any new geometry that you create, for example a runner system, will be added to this layer.
- The layers with a tick in the check box  are visible layers. All entities assigned to those layers will be visible on the screen.
- The highlighted layer with the blue background  is the currently selected layer. Most of the layer commands work on the highlighted layer, as illustrated in figure 2.10.

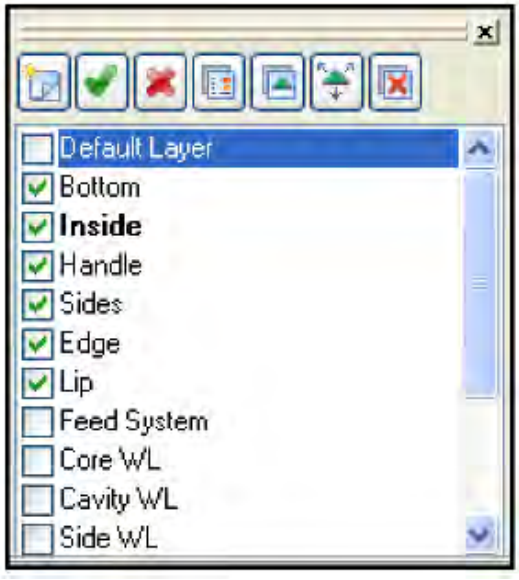

Figure 2.10:

Layers Pane.

A complete list of commands and actions available for layers are shown in table 2.4 below.

Table 2.4: Layer icons.

Icon	*Command*	*Action*
	Create Layer	Creates a new layer. Once created, one may click on the name to change it.
	Delete Layer	Deletes the highlighted layer. If there are any entities on that layer, one will be prompted to delete the entities or to move them to the active layer.
	Activate layer	Makes the highlighter layer active. The layer name becomes bold.
	Layer Display	Allows one to view and edit the color and display methods of entities on the highlighted layer. It also provides the option to hide/show entity labels, for example element or node numbers.
	Assign Layer	Assigns the currently selected entities in the display window to the highlighted layer.
		Adds entities to the highlighted layer by a number of levels. If there is only one

	Expand Layer	element on a layer,  and the expand command is used, all of the elements attached to the single element are added to this layer, as well as all of the nodes on the elements  . The expanded elements can also be moved to a new layer, so there is a layer for the original elements to be expanded and the layer containing the expanded entities.
	Clean Layers	Deletes all layers with no entities on it.

3. Working in Synergy

In this topic the import of a CAD model is going to be examined, as well as the way it can be meshed, the cleanup/repair of the mesh that comes after and how to prepare the model, so that it can be ready for analysis.

3.1 Designing the model

The goal was to study the case of a center-gated disk (thin-walled part), filled with a fiber reinforced material. So the first step was to create a disk with dimensions of: R = radius = 65 mm and h = thickness = 2 mm. This is where the Autodesk Inventor Fusion is helpful. Inventor Fusion is 3D mechanical CAD design software, for creating 3D digital prototypes used in the design, visualization and simulation of products.

Step 1:

Ensure the 'Solid' option from the 'Modeling' tab, on the top left of the screen, is selected. Define the plane on which the model will be designed. This is done through the 'Origin' command on the left. The disk under study will be designed on the XY plane, as shown in figure 3.1 with green color. Remember the plane on which the model was initially created. It will be of great importance later on. Choose the 'Cylinder' option from the 'Solid' tab. Now the only thing missing is the dimensioning of the solid cylinder.

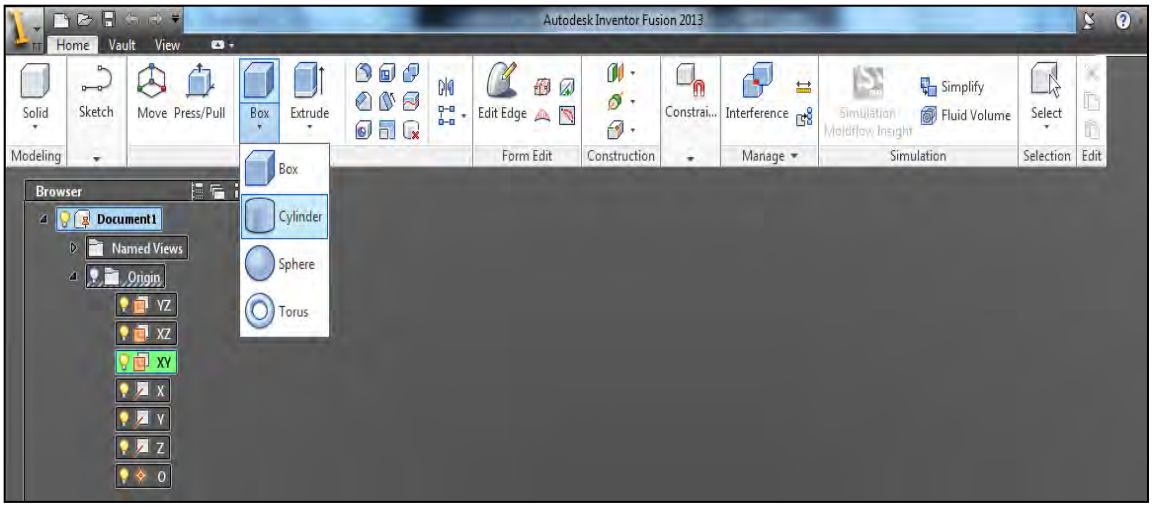

Figure 3.1: Selecting the cylinder option and the design plane.

Step 2:

Move the mouse on the red spot and from there one can specify the radius of the cylinder, as shown in figure 3.2. Type 65 (mm) and then double press 'Enter'. Right after, one should define the height/thickness of the cylinder and that is done through the command 'Extrude', which will appear automatically as a small yellow dart, right after the radius is defined, as shown in figure 3.3. So type 2 (mm) and double press 'Enter' again. The steps described are shown in figures 3.2, 3.3 and 3.4.

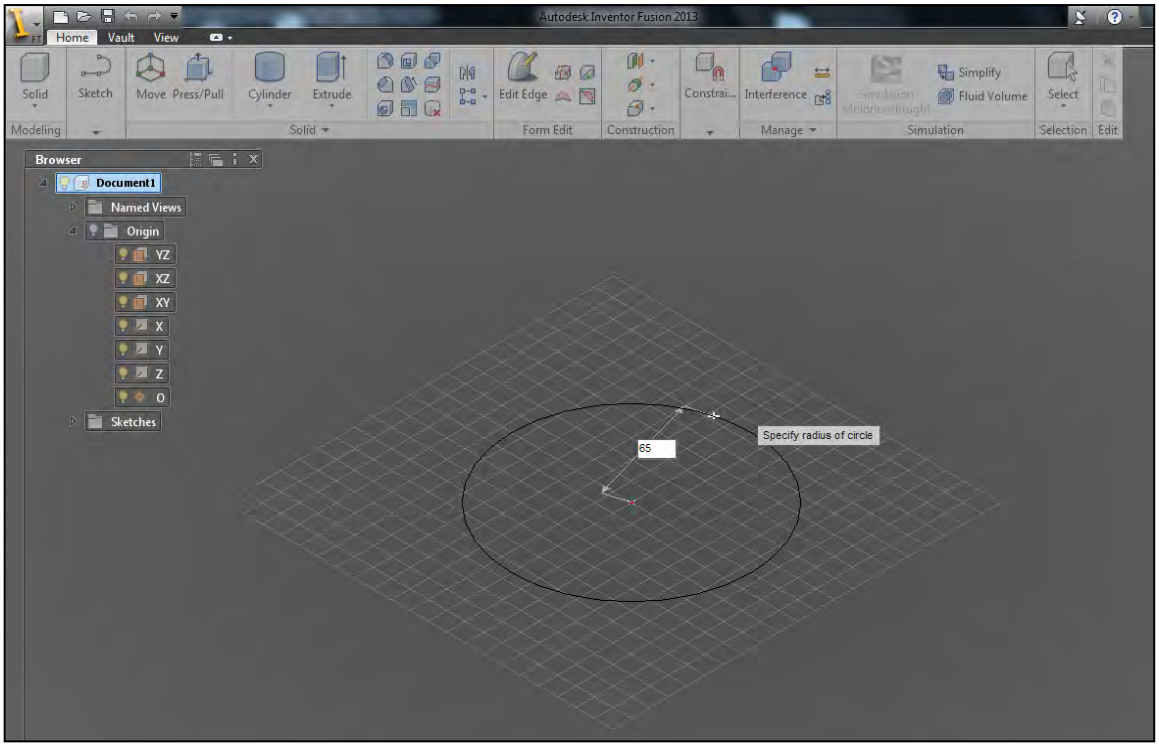

Figure 3.2: Specifying the radius of the circle.

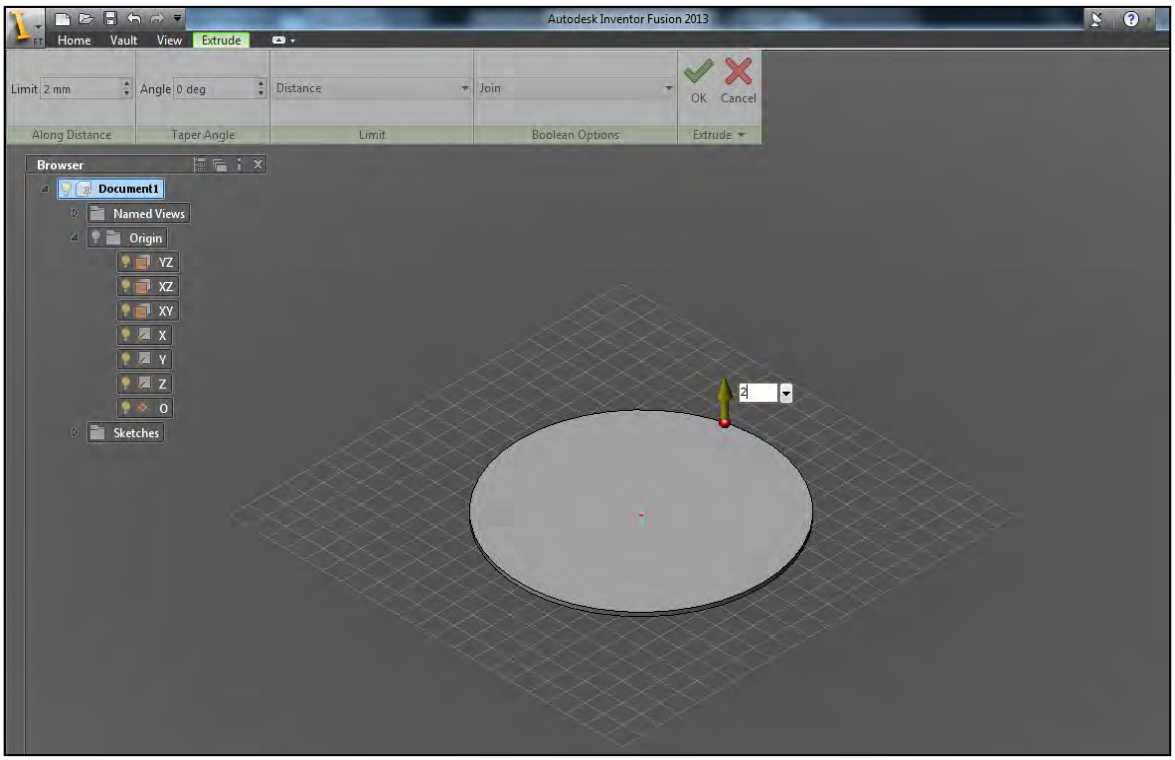

Figure 3.3: Specifying the thickness of the cylinder.

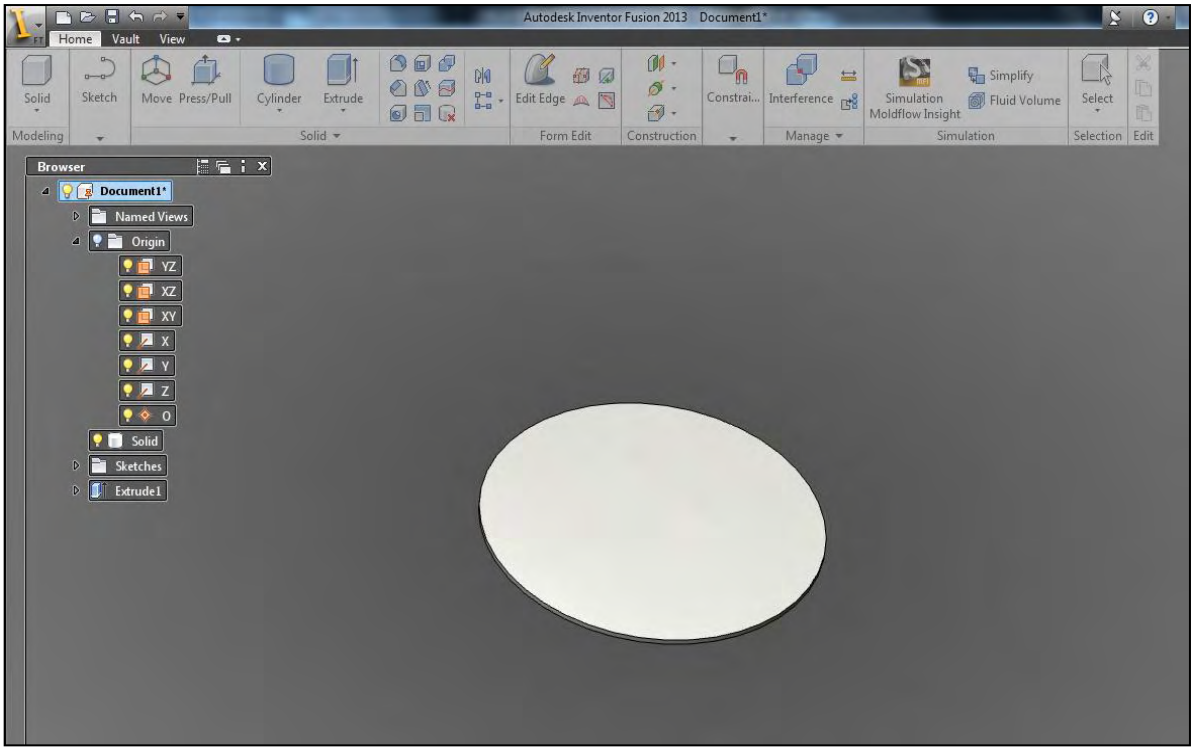

Figure 3.4: Presentation of the final model.

Step 3:

The model is ready for import. Now just save the work and click on the 'Simulation Moldflow Insight' command (figure 3.5). This will automatically create a .sat file (Standard ACIS Text). Save this file in a folder, because this is the file one will need to import in AMI.

Figure 3.5: Sending the file to Autodesk Moldflow.

3.2 Importing the model

Step 1:

Now it is time to open the AMI program. First create a new project with a specific name and save it in a folder. This project can contain lots of studies and every change that is made on the studies, will be saved in this folder. So now import the .sat file, which was created earlier, and the following window dialog will appear.

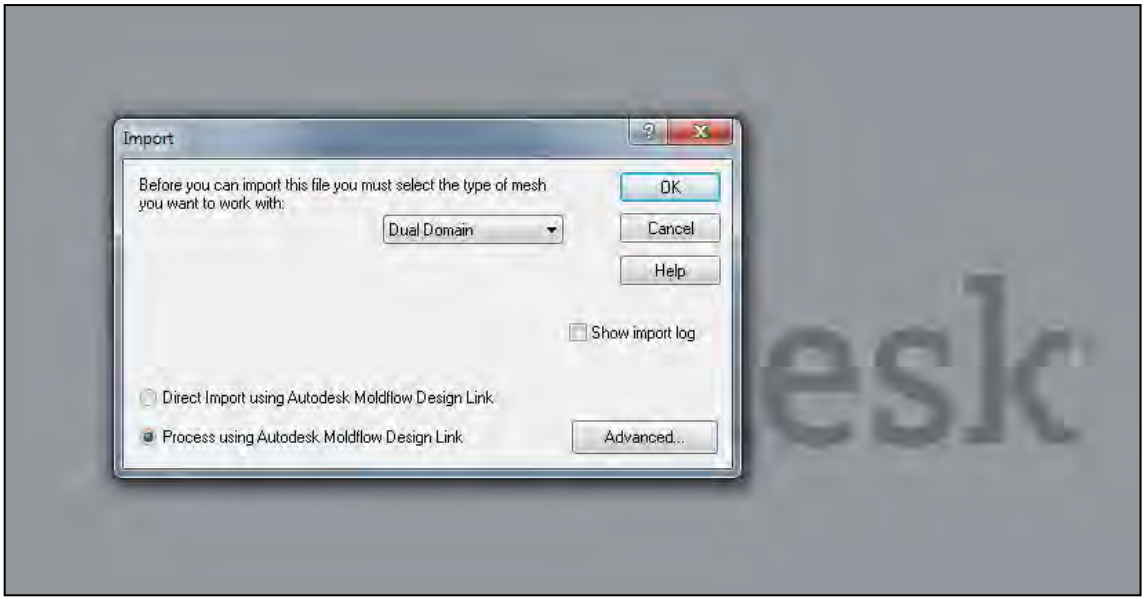

Figure 3.6: The import dialog. Choose the Dual Domain mesh type and the Process using Autodesk Moldflow Design Link option (AMDL).

When importing a solid model, always choose Dual Domain (here) or Midplane. If someone eventually wants to work with a midplane or 3D model, initially import the CAD model as Dual Domain, study the model and clean the mesh up as necessary. After the model is cleaned up, the mesh type can be changed/converted and re-meshed with the new desired format.

Step 2:

Click on the 'Advanced…' option in the lower right corner. AMDL creates a dual domain or 3D mesh directly from the CAD kernel. This results in a better solution that provides better fidelity, better scaling and the ability to handle multi-component models.

- *Global edge length (GEL)*: allows setting the target element edge length when the mesh is generated. This value is the main control for the mesh density of a part. The GEL should be about 2 times or less, the nominal wall thickness for a 3D mesh, and 2 to 5 times the nominal wall thickness for a Dual Domain mesh.

  Because the thickness of the disk is 2 mm, the GEL for this dual domain analysis is set to the minimum (for more elements, therefore better analysis), that is: (2 x h) = 2 x 2 = 4 mm, as shown in figure 3.7.

- *Chord angle*: when tightly curved sections of the model are not meshed adequately, one can increase the mesh densities in these areas by defining a chord angle. This controls how closely the curve of the CAD model is approximated by straight section in the mesh. The smaller the chord angle, the shorter the chord length, the finer the mesh.

When prediction of weld lines is critical or hesitation effects and air traps must be correctly predicted, a finer mesh is preferred over a coarse mesh. In this specific example, the chord angle is set to 41 degrees, as shown in figure 3.7.

- *Mesh on assembly contact faces*: There are 3 different options available here for the meshing of the surfaces of assemblies that come into contact. Here the «Fault Tolerant» option is selected. This helps in repairing any minor errors in the CAD model. Mesh nodes are matched where possible. Some mesh adjustments may be required to match nodes on contact surfaces.

- *Silver removal*: A silver is a small feature that is usually found at CAD surface join boundaries. Silvers can result in small mesh elements with high aspect ratios. It would be better for them to be removed.

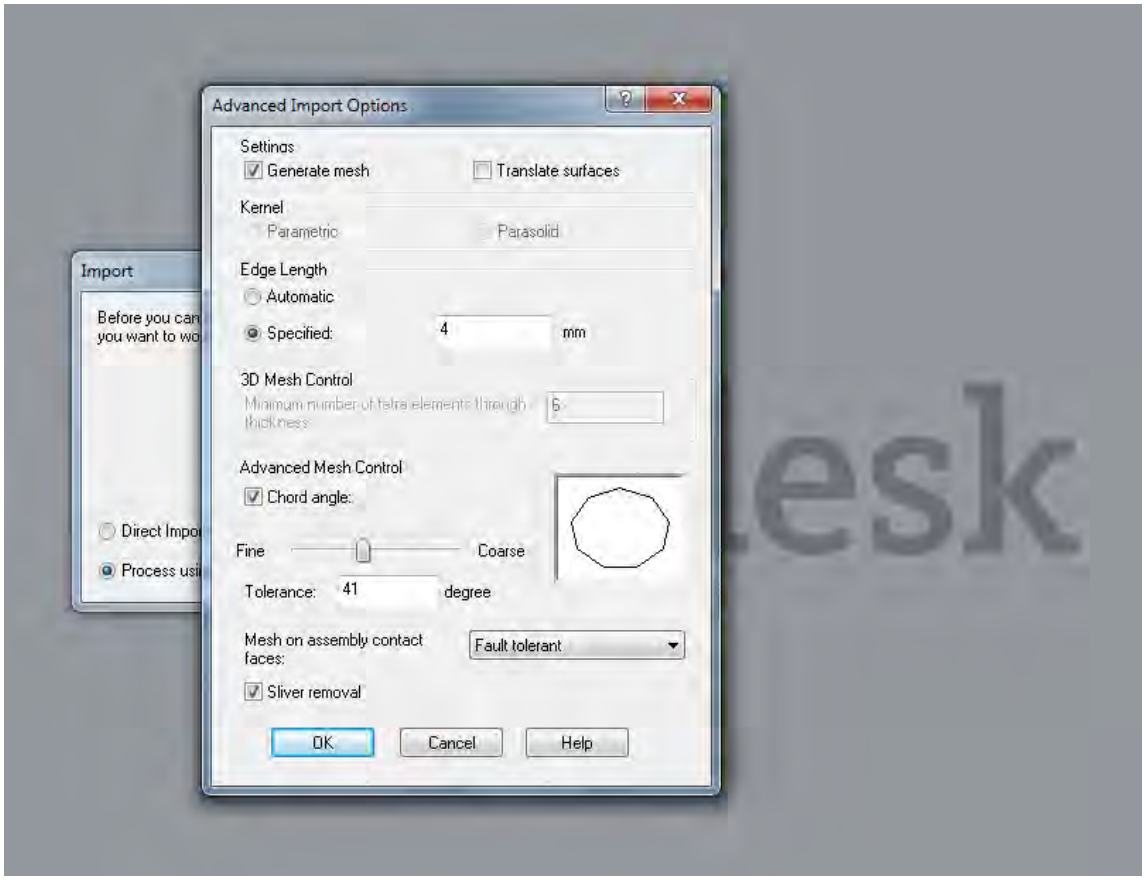

Figure 3.7: Import Options.

Step 3:

Press OK twice. The model will be meshed with the desired values and the final result is shown in figure 3.8. A total of 4772 elements were created.

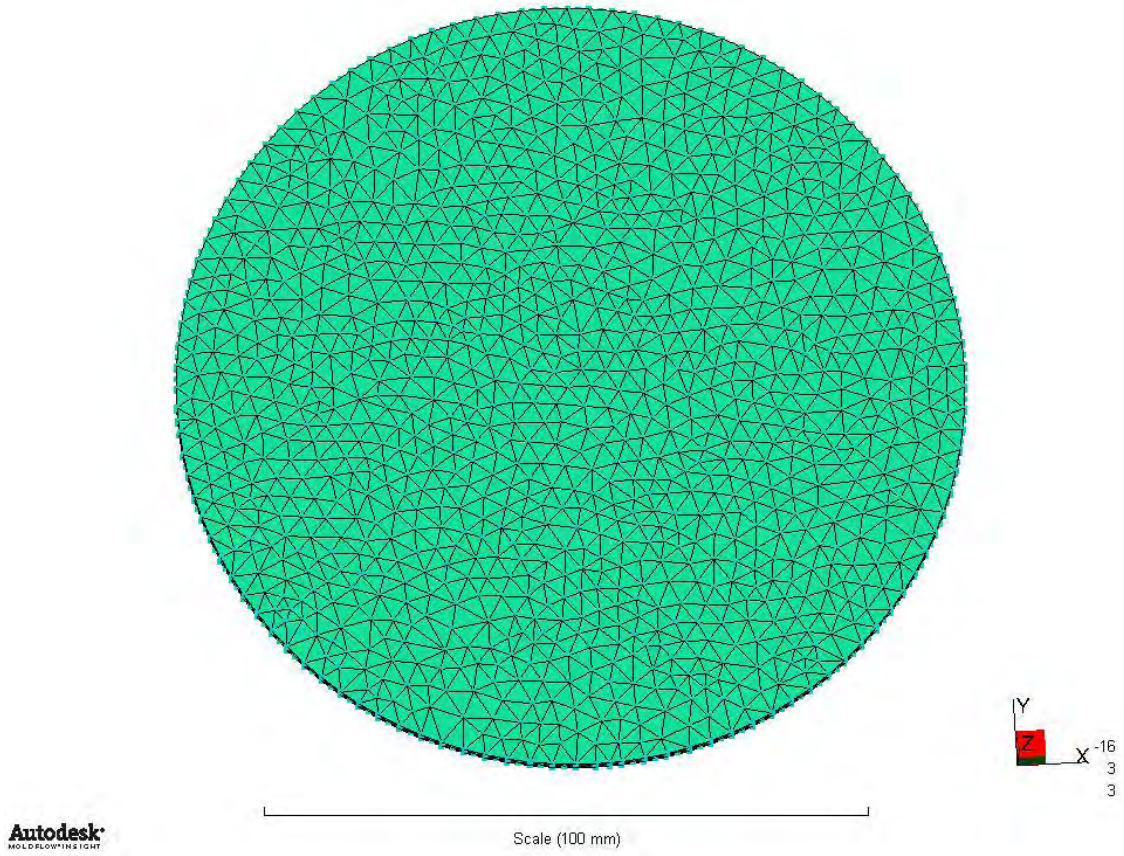

Figure 3.8: Presentation of the disk in the Dual Domain mesh.

3.3 Preparing the model for analysis

This section of course is going to be very extensive, as one should focus on details that will make the final results of the injection molding process more accurate and acceptable.

3.3.1 Assignment of properties

Select the whole part. Right click and choose ‘Properties’. A new window will pop up, like the one in figure 3.9. The first option will select the front and the back side of the disk, while the second option will select the circumference of the disk. Select both properties that appear in this window (holding down CTRL) and click OK.

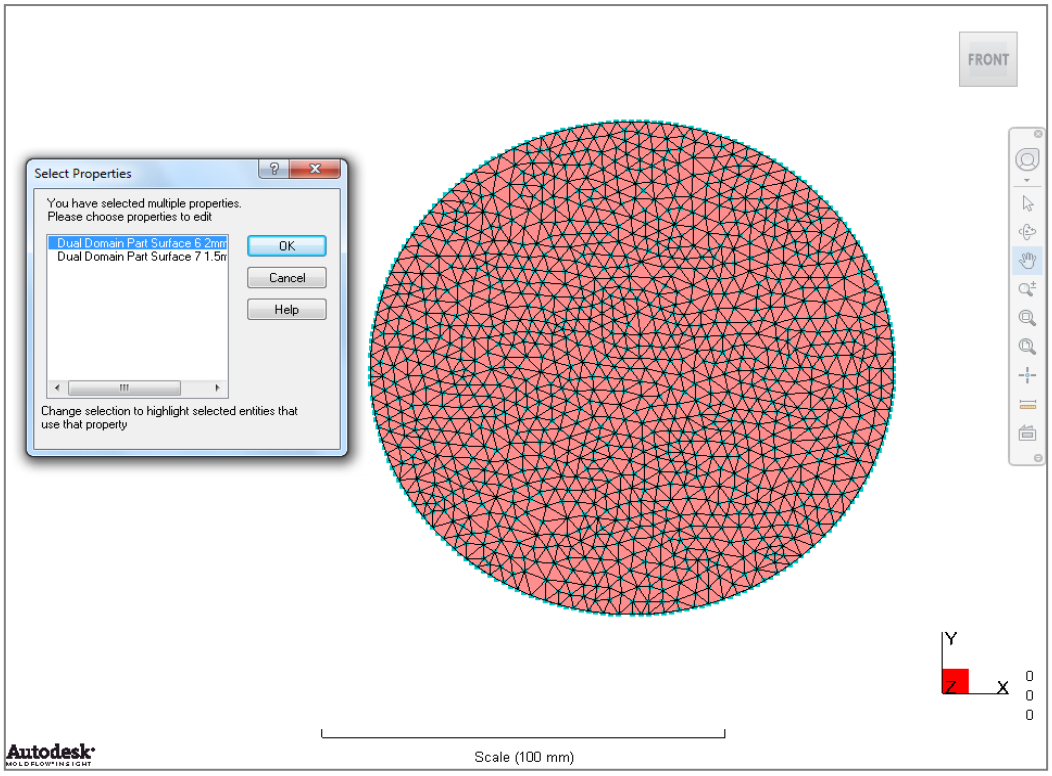

Figure 3.9: Selecting the whole disk's surface.

In the 'Part Surface Properties' tab, one can decide how the thickness in the part will be represented. Here a common value of 2 mm for the whole surface of the part is chosen (uniform thickness), as shown in figure 3.10.

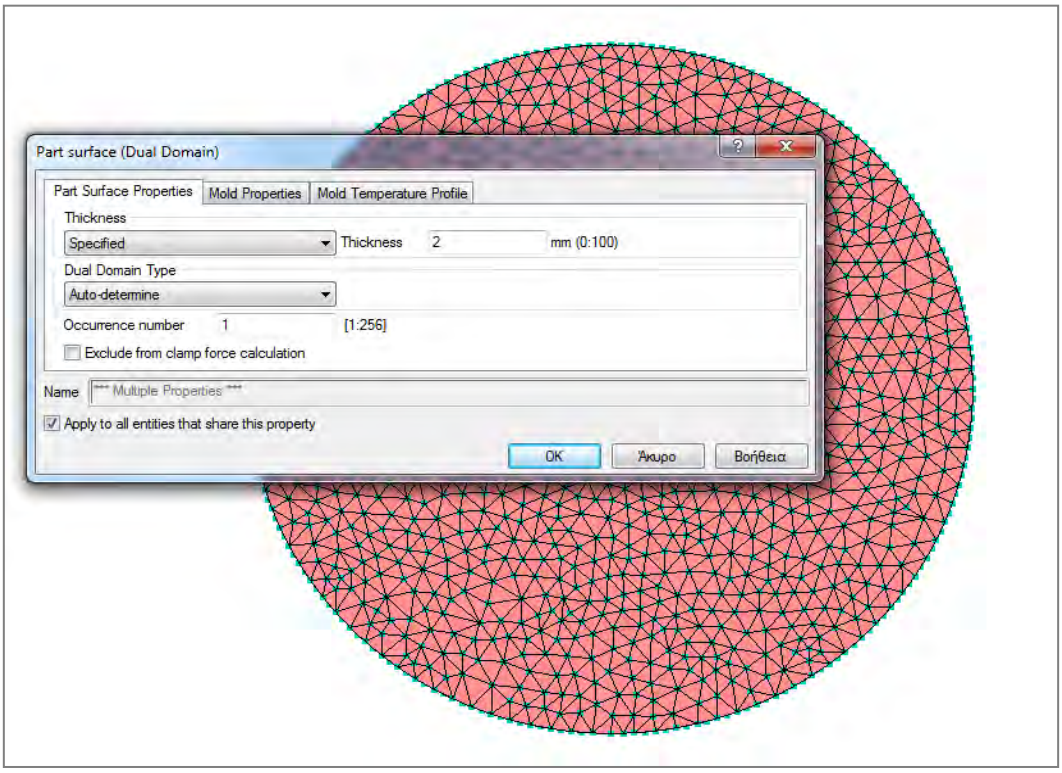

Figure 3.10: Assigning a common thickness for the whole disk.

The ‘Mold Properties’ tab, is used to specify the properties of the mold block in contact with the selected elements or regions of type part surface (dual domain). Here, one can define on which side the cavity and the core will be assigned and specify if a local mold material different from the one used in the process settings, is going to be used. For this study, the top side is chosen as the cavity side and the mold material remains the same (figure 3.12). In figure 3.11, one can see the standard mold and how simply designed it is. Nothing more complex than that is needed to mold a part with a very simple geometry, like a disk.

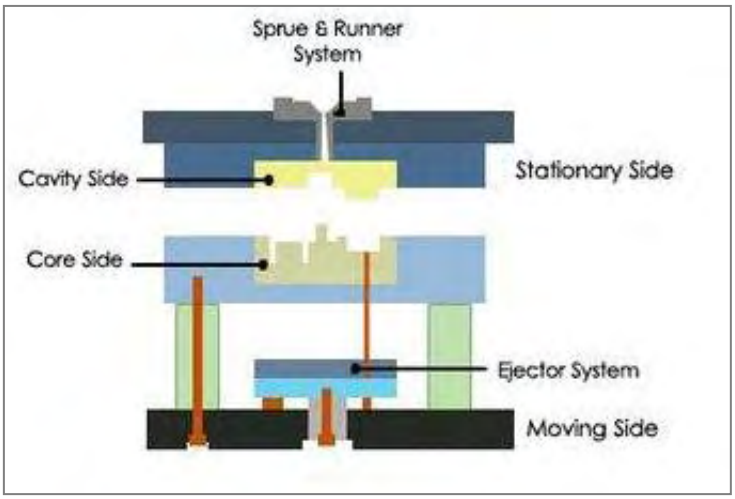

Figure 3.11: A standard mold. The fixed/stationary half is usually called cavity or A-half. The moving half is commonly referred to as core or B-half. The cavity side is the one that “includes” the feed system. *[4]*

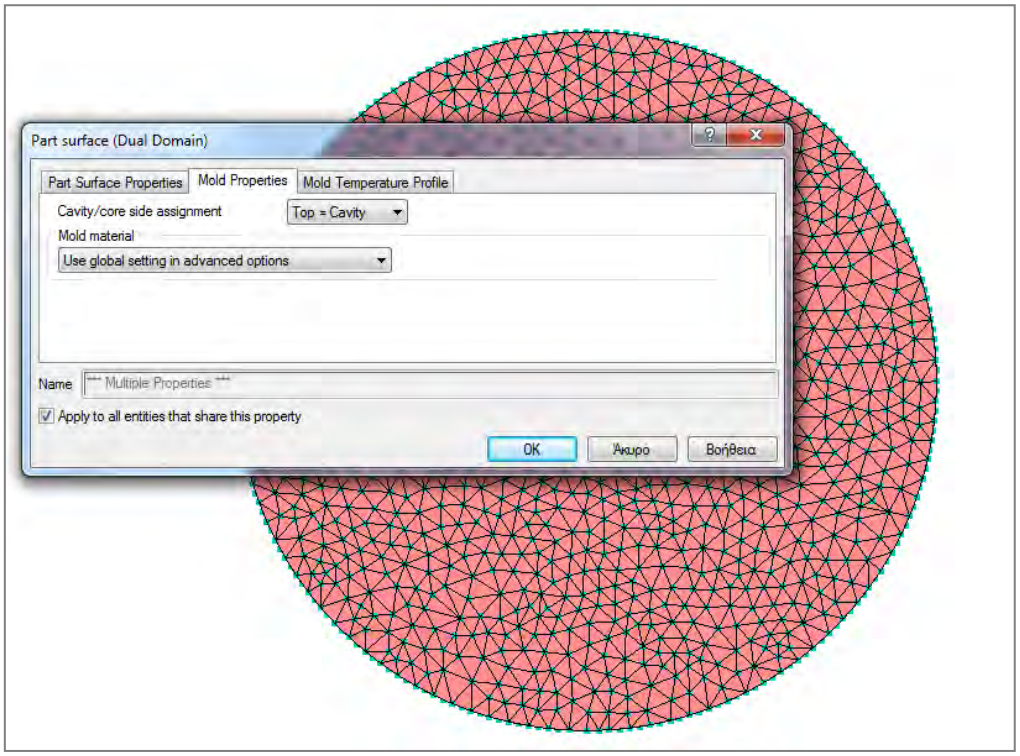

Figure 3.12: Specifying the cavity side and whether the same or a different mold material is going to be used.

The ‘Mold Temperature Profile’ tab, is used in the Fill + Pack analysis. Unlike the conventional injection molding process, in which the mold is maintained at a near-constant temperature, newer techniques utilize a variable mold temperature. The mold is maintained at a hotter temperature during the filling phase, so as to facilitate and achieve smooth surface appearance. During the packing and cooling phases, the mold switches to a much cooler temperature to assist in freezing the part and decreasing the cycle time. The time must be set in ascending order. Keep in mind that temperature profiles cannot be set on hot runner elements. The profile used in the case of the center-gated disk is shown in figure 3.13.

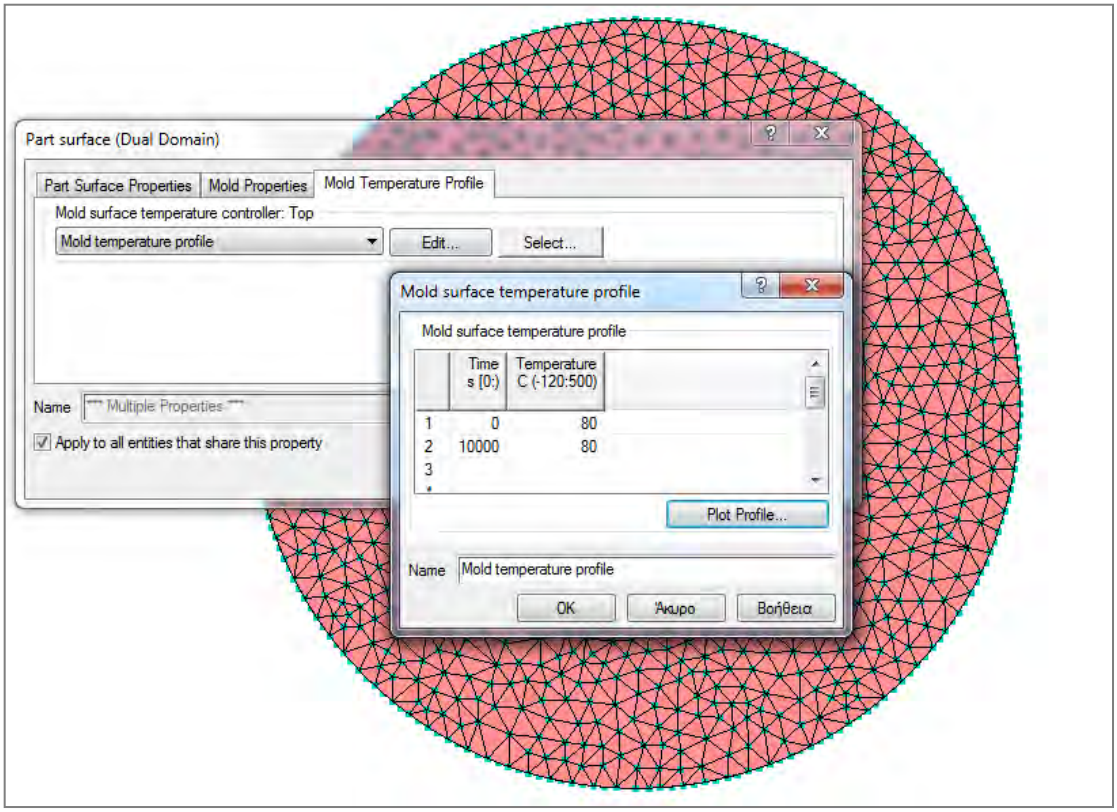

Figure 3.13: Specifying the mold surface temperature profile of the disk, with a constant temperature of 80 °C. This temperature is not randomly selected, as it is the optimum temperature for the material that is going to be chosen later on, recommended by the manufacturer.

3.3.2 Modeling of the feed system

It’s always advisable to rotate and check the model for any inconsistencies. In the case of the disk, the geometry is very simple, so no problems are expected. However, one can examine in detail the resulting mesh for any possible errors/faults, though the ‘Mesh Repair Wizard’ option.

In this topic, the creation of the feeding system is going to be analyzed. Center-gated disk, as the name implies, is a disk gated right in the center. A center-gated part is reasonably well-balanced, but not as good as an end-gated part. The flow front starts out to be radial and then straightens out and becomes linear. A center-gate location is better for round or square parts.

For many cylindrical or symmetrically shaped parts, such as buckets, tubs, helmets, boxes, cups and disk-shaped objects, a direct (or sprue) gate is the most common choice. Before we proceed on with the analysis of the gate design, it would be better to explain what a direct gate is.

Gates can have many different configurations, but they are broadly classified based on the method of gate removal, into manually trimmed and automatically trimmed gates. Manually trimmed gates usually require an operator to separate the parts from the runners, during a secondary operation. The direct gate falls into this type of gates. Manually trimmed gates are used for the following reasons:

- The gate is too large to be sheared from the part as the tool is opened.
- Some shear-sensitive materials, such as PVC, should not be exposed to the high shear rates inherent to the design of automatically trimmed gates.
- Simultaneous flow distribution across a wide front to achieve specific orientation of fibers or molecules often precludes automatic gate trimming.

Sprue gating is different from almost any other type of gating and refers to the cases where there is no traditional runner system or conventional gate. The part is gated directly from the sprue. It is commonly used in single-cavity molds, where the sprue feeds material directly and rapidly into the cavity with minimum pressure drop. With a cold sprue there is no traditional gating. It is generally not considered a good gate design, as the cross-section is larger than the part's wall thickness and it is prone to control the cycle time and over-pack the part. The disadvantage of this gate type is the gate mark left on the part surface, after the sprue is trimmed off. Freeze-off is controlled by the part thickness, rather than determined by the gate thickness. Typically, the part shrinkage near the sprue gate will low; shrinkage in the sprue gate will be higher. This results in high tensile stresses near the gate.

As far as dimensioning is concerned, the starting sprue diameter is controlled by the machine nozzle. The sprue orifice diameter here must be about 1 mm larger than the nozzle exit diameter. Standard sprues can have tapers from 0.5 degrees to 1.5 degrees (1.0 degrees to 3 degrees included angle, see figure 3.14 – on the left), with a common size of about 1.2 degrees taper angle, as shown in figure 3.14 – on the right. Therefore, the sprue's orifice diameter and length will control the diameter of the sprue where it meets the part. Typically, the sprue diameter will be well over double the wall thickness of the part, controlling the molding cycle time.

A small taper angle (a minimum of 1 degree) risks not releasing the sprue from the sprue bushing on ejection. A large taper angle wastes material and extends the cooling time. In most cases the sprue's length should be kept as short as possible, too, enabling rapid mold filling and low pressure losses.

Pressure loss is high in the sprue. This is the only place in a feed system where the channel progresses from a smaller area to a larger. Frequently, smaller orifices are used on long sprue bushings in an effort to reduce the mass. This results in extreme high injection pressure losses, making the part hard to fill (Engelmann & Dealey, 1999). Smaller starting diameters demand much higher clamping forces.

In AMI there are three ways for the dimensioning of a *cold sprue*. One is to give the sprue a non-tapered shape, just by specifying the diameter. Another way is to create a tapered sprue with start and end dimensions.

The third way is to create a tapered sprue again, but this time one should define the start diameter and the tapered angle. When the third way is chosen, one should have a global view of how big the diameter of the sprue, where it meets the part, is going to be.

For example, if a pretty big orifice diameter is used and a common tapered angle is also used, it is certain that mesh problems will appear, such as intersections, between the beam and the triangular elements (dual domain). Of course these can be fixed, but not automatically. A manual repair of the model is required. Sometimes the mesh repair is not an easy job. This is where the following equation helps in the understanding of how big the contact diameter is going to be. The equation is (Engelmann & Dealey, 1999):

$$d_2 = d_1 + L \cdot \tan(\varphi) \quad (1)$$

where: d_2 = the end diameter

d_1 = the start diameter (orifice)

L = the length of the sprue

φ = the included angle (note that in AMI: included angle = 2 x tapered angle).

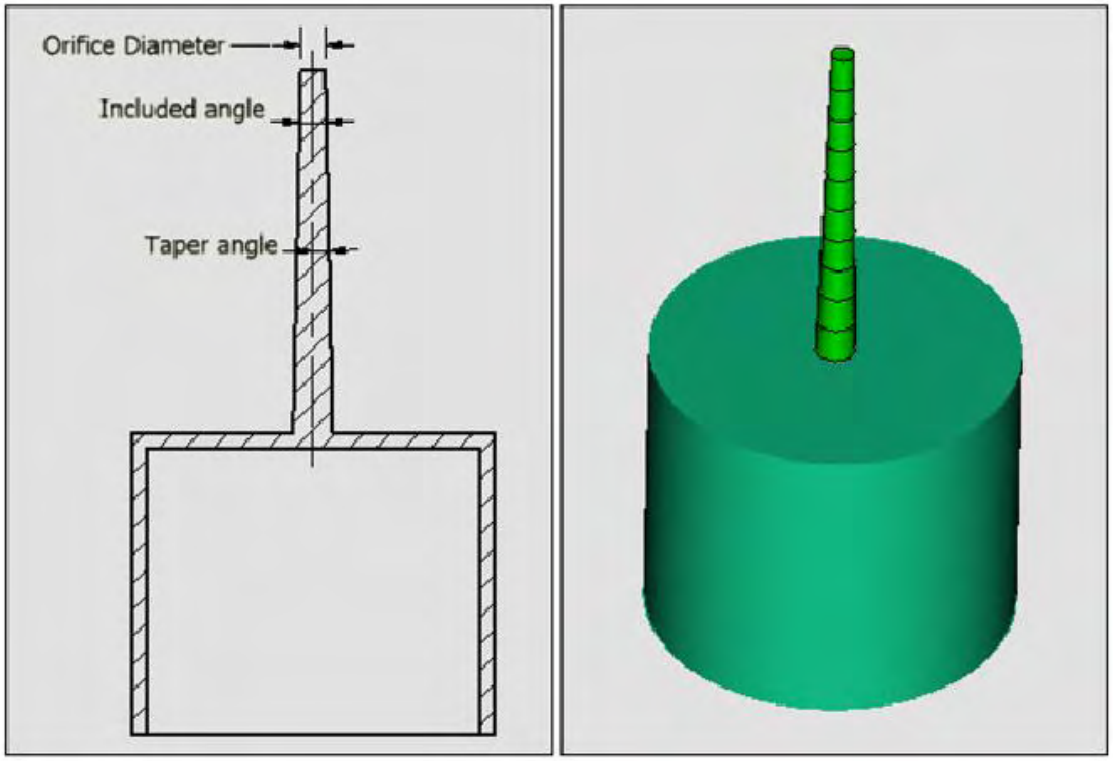

Figure 3.14: A sprue gate can be modeled in AMI with beam or tetrahedral elements.

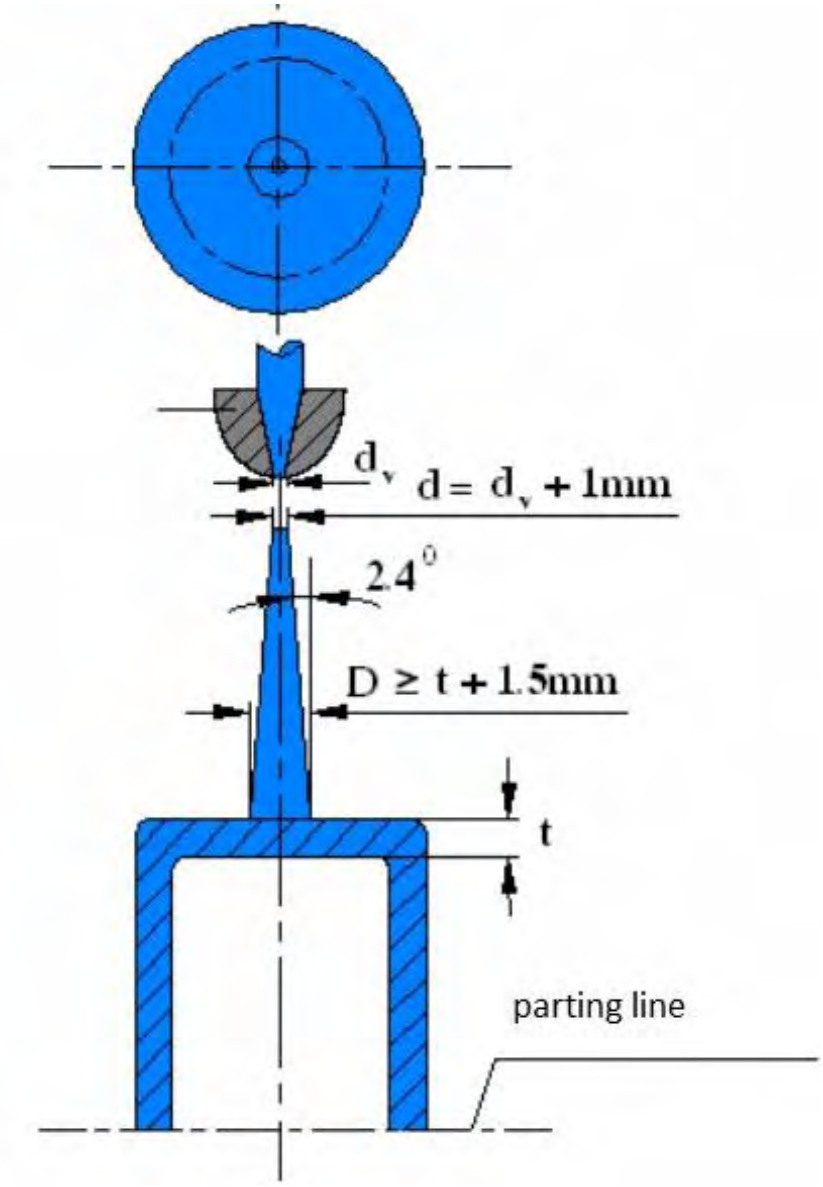

Figure 3.15: Designing principles of a direct gate. Average sprue lengths vary from 2'' to 3'' (51 – 76 mm). *[5]*

So with the role of a sprue gate explained, it is time to move on with its creation. Initially select the front view and zoom all the way in (scale < 10 mm). Open the Geometry tab and go to the 'Create' tab. Select 'Nodes > Node by Coordinate'. Here one can define a new node. In our case, a node right in the center of the part is needed and that is a node with coordinates: (0, 0, 2). Click apply. A small blue node will appear, like the one in figure 3.16.

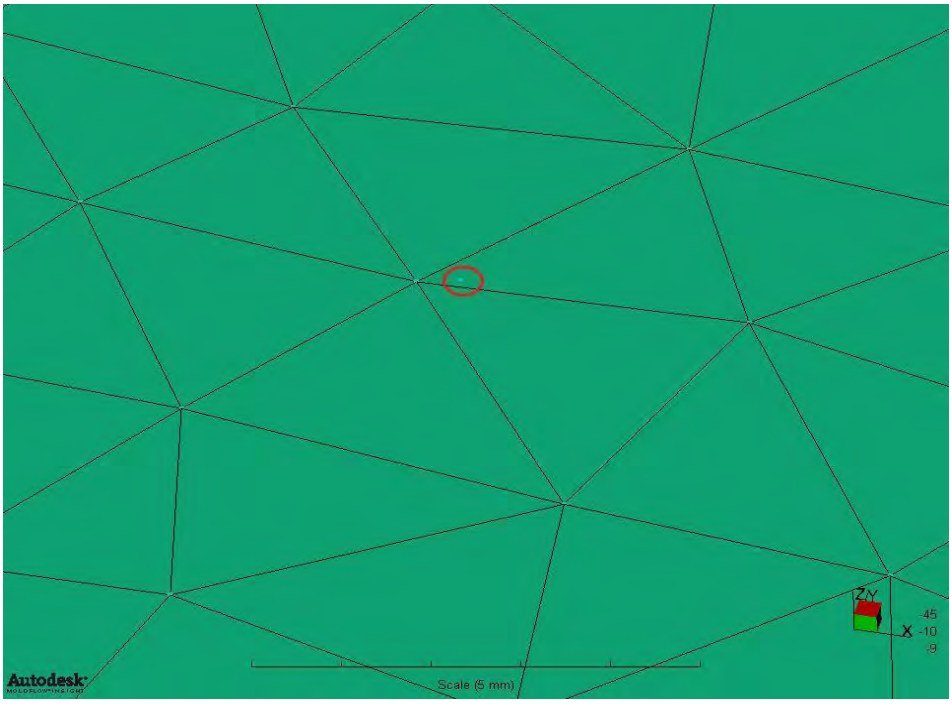

Figure 3.16: Defining the initial (base) coordinate.

The next step is to offset this node. Select 'Nodes > Node by Offset'. Once the new window pops up, in the base coordinates box, select the node that was created right above (this will be the reference node) and in the offset box, type the coordinates: (0, 0, 45). Click apply and then close. This will make a new node, 45 mm higher in the z-direction, as shown in figure 3.17.

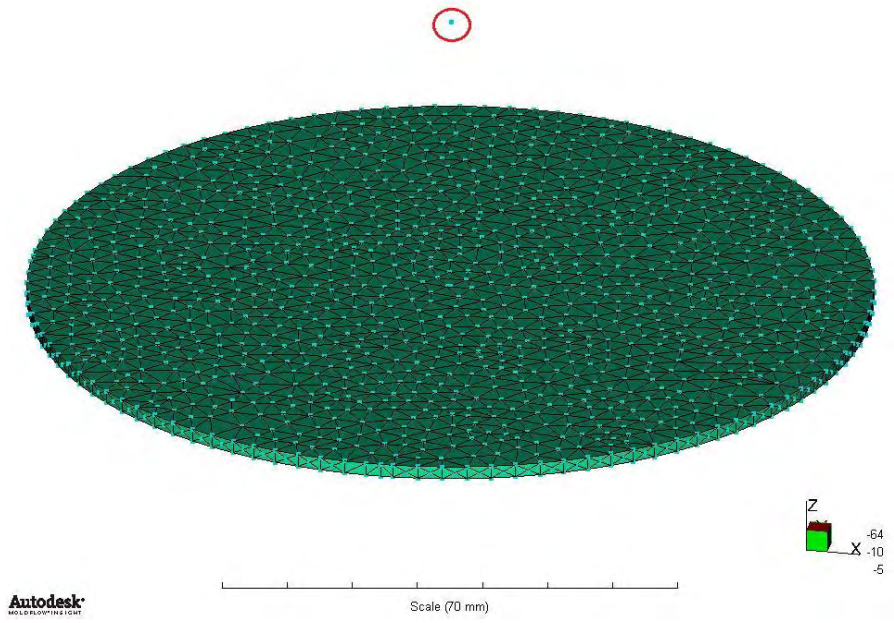

Figure 3.17: Creating the second node. The coordinates of the new node are now: (0, 0, 47).

Now select ‘Curves > Create Line’. A new window pops up. Keep in mind that in the input parameters, the top node (0, 0, 47) should be selected first and the base node (0, 0, 2) should be selected right after. Otherwise, the sprue will be tapered from the bottom to the top.

In the ‘Create as > Modeling entity’ box, create a cold sprue with a start diameter of 3 mm and a tapered angle of 1.1 degrees. Also, in the ‘Mold Properties’ tab, use the same material and in the ‘Mold Temperature Profile’ tab , use the same profile as the one in figure, with a constant temperature of 80 °C. Press OK several times and then click apply and close. A green line will be created, connecting the two nodes. The steps described are shown in figure 3.18.

Note: One is able to understand how big the end diameter is going to be, using equation (1). Therefore:

$$d_2 = d_1 + L \cdot \tan(2.2^o) = 3(mm) + 45(mm) \cdot 0{,}0384 = 3 + 1.729 = 4.73mm$$

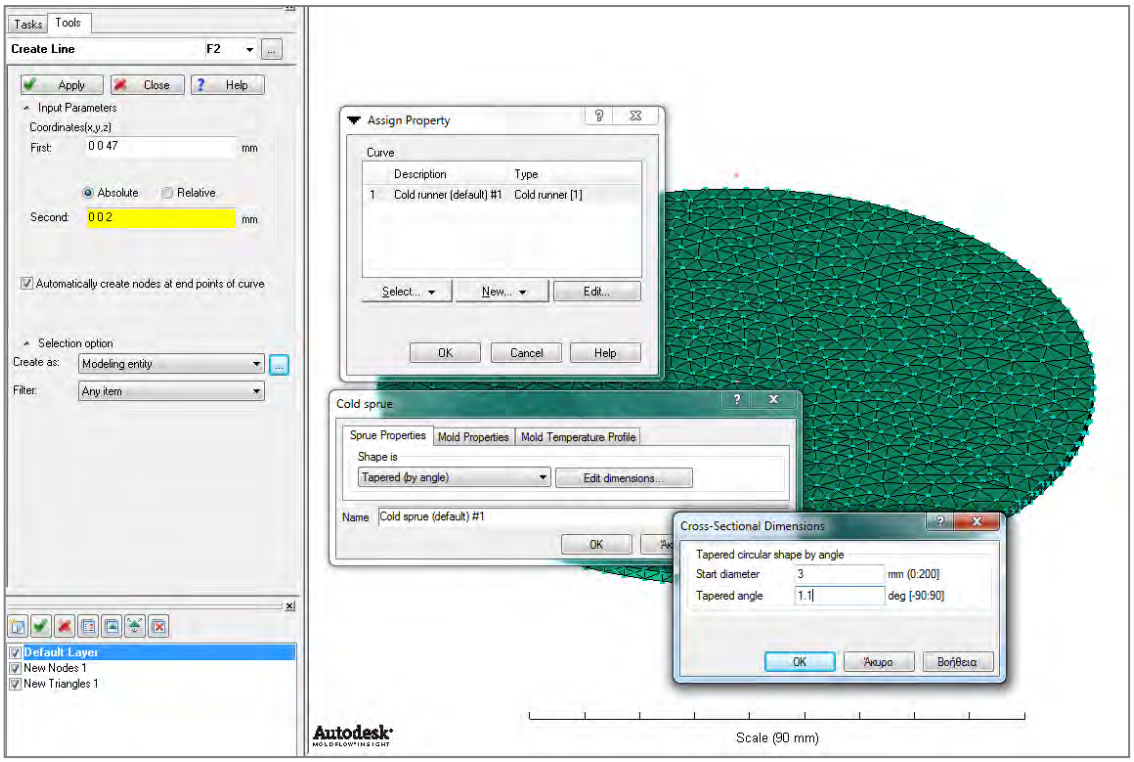

Figure 3.18: Defining the necessary properties of the sprue gate.

The final step is to mesh this green line. Open the ‘Mesh’ tab and select the ‘Generate Mesh’ command. Create a new mesh with a GEL of 4 mm again. Use a merge tolerance of 0.01 mm and a chord height of 0.4 mm. Ensure the match mesh option is checked, as well as the smooth mesh (NURBS Surfaces only) option. Before the ‘Mesh Now’ button is clicked, be sure to have deactivated the ‘Remesh already meshed parts of the model’ option, otherwise the program will create a new mesh all over from the start for the whole part, including the line. The steps are shown in figure 3.19.

- *Merge tolerance*: Sets the minimum distance between nodes that AMI will aim for (0.01 mm here), when it generates your Midplane or Dual Domain mesh. If adjacent nodes are closer together than this distance, nodes will be merged together during mesh creation.

- *Match mesh*: Allows you to align the mesh elements on the two corresponding surfaces of a Dual Domain mesh. A better mesh match increases thickness accuracy and leads to more accurate analysis. Sometimes, activating mesh matching will create thin high aspect ratio elements, called silvers. Although the match ratio will be much higher, there may be some silvers that need to be cleaned up. For dual domain meshes that will be converted to 3D, it would be better to have this option unchecked. For dual domain meshes, match mesh should be checked.

- *Chord height control and chord height*: This check box and text box will ensure that curved features have a mesh on rounded features. Without the chord height control, some surface curves, such as fillets, degrade when meshed.

  Chord height control is effective only with parts that have curved surfaces. Keep the value of the chord height somewhere in the range of 5-25% of the used global edge length. If the value is below approximately 5%, the resulting mesh tends to contain several long and/or thin triangles. If the value exceeds 25%, the chord height control has little effect. For the center-gated disk a 10% of the GEL has been used, that is: (0.1 x 4) (mm) = 0.4 mm.

- *Smooth mesh (NURBS surfaces only)*: this option shifts the position of nodes around to produce a lower average aspect ratio. It should be checked.

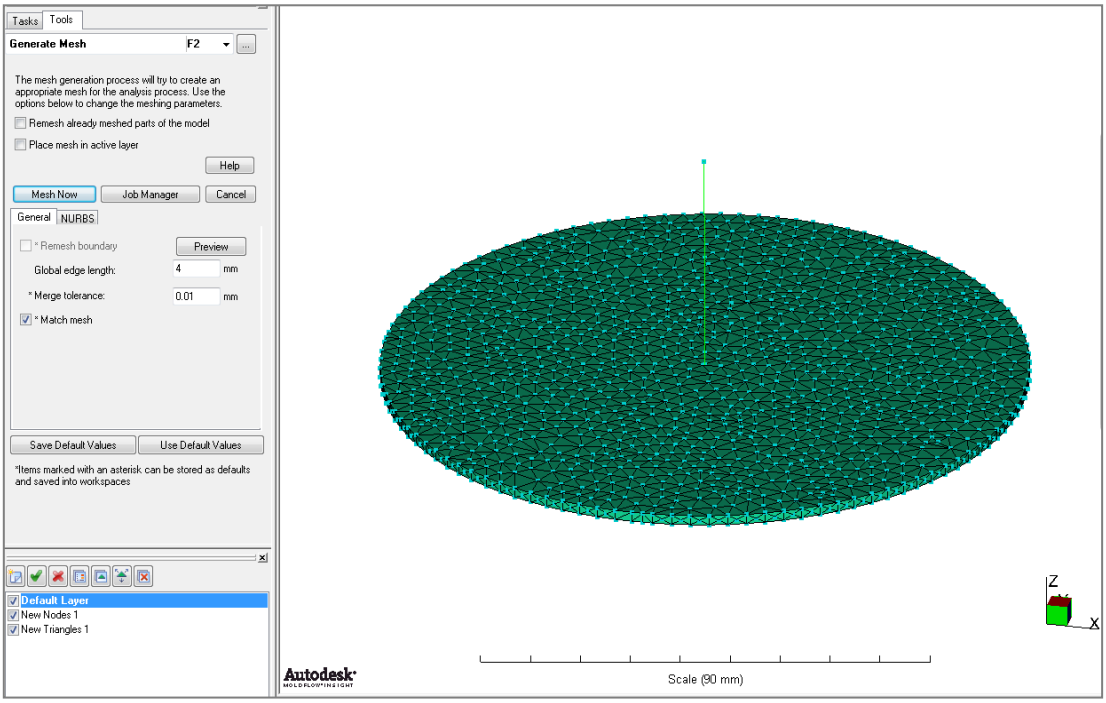

Figure 3.19: Right before the meshing of the sprue gate.

When the desired values have been correctly entered, click ‘Mesh Now’. The result is shown in figure 3.20. Of course, someone can use a smaller GEL for the modeling of the sprue gate. But there is no need to do that in a dual domain analysis. A smaller GEL is going to be used for the whole part, when the conversion to a 3D mesh will be made.

All to do now is check the whole mesh for any errors, such as overlaps, intersections, high aspect ratios, etc. In table 3.1, a summary of all the mesh requirements is shown for the three different mesh types: Midplane, Dual Domain and 3D. In any case, one should check that these requirements are fully satisfied.

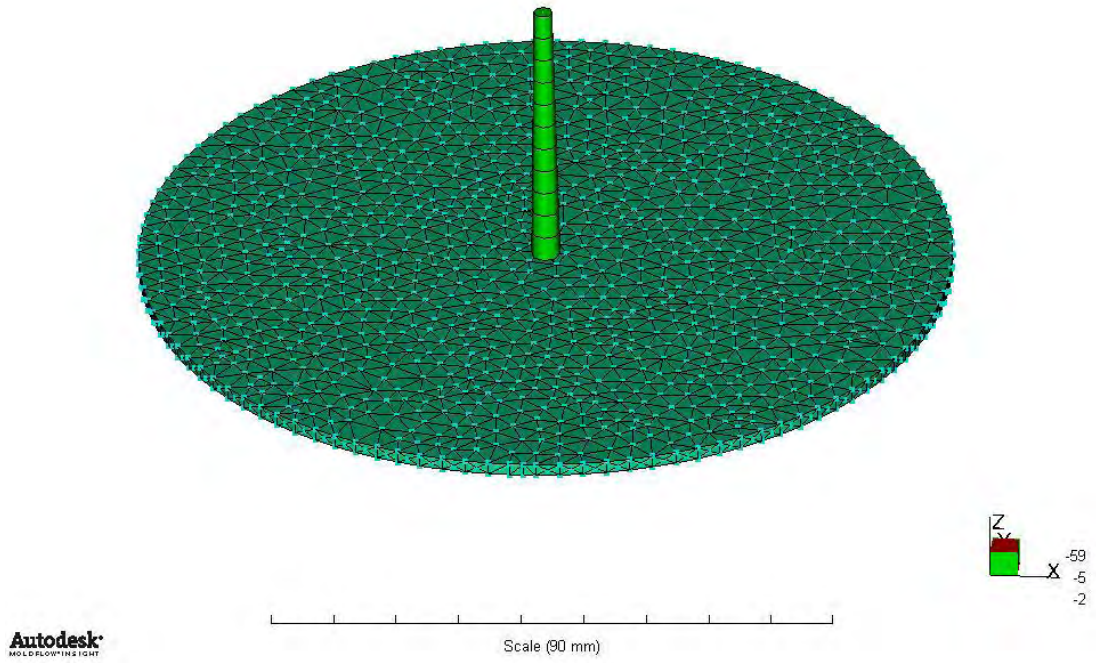

Figure 3.20: The feed system of the part is ready.

3.3.3 Mesh examination

Table 3.1: Summary of mesh requirements for the three mesh types.

Mesh Issue	Dual Domain	3D	Midplane
Free edges	Must NOT have any	Same as dual domain	Can have at boundary of holes and parting line
Non-manifold edge	Must NOT have any	Same as dual domain	Are valid at "T" cross-sections, e.g. ribs
Manifold edge	Only type of edge allowed	Same as dual domain	Most common type of edge
Match ratio	> 85% for flow and > 90% for warpage	Not applicable	Not applicable
Reciprocal Match	> 90% for warpage	Not applicable	Not applicable
Aspect ratio	Average < 3:1 and Maximum < 6:1	< 30:1 on dual domain mesh, before conversion to 3D	Same as dual domain
Connectivity regions	One group for the part	Same as dual domain	Same as dual domain
Element orientation	The top (blue) side of the element pointing outward	Same as dual domain	Consistent mesh orientation
Intersections	Must NOT have any	Same as dual domain	Same as dual domain
Overlapping elements	Must NOT have any	Same as dual domain	Same as dual domain
Zero area elements	Must NOT have any	Same as dual domain	Same as dual domain
Thickness representation	Thicknesses properly modeled	Not applicable	Thickness properly assigned
Inverted tetras	Not applicable	Must NOT have any	Not applicable
Collapsed faces	Not applicable	Must NOT have any	Not applicable
Number of 3D layers	Not applicable	6 layers typically OK, 8 layers for fiber orientation or gas-assist	Not applicable

Internal long edges	Not applicable	< 2.5:1	Not applicable
Extremely large volumes	Not applicable	< 20:1	Not applicable
High aspect ratios	Not applicable	< 50:1	Not applicable
Small angle between faces	Not applicable	> 2 degrees	Not applicable
Large angle between faces	Not applicable	< 177 degrees	Not applicable

Through the 'Mesh Repair Wizard' one should check for any possible errors that might have occurred. Unfortunately, in the case of this center-gated disk, some errors did occur. Specifically 3 intersections were detected. But they can be fixed.

So the first step is to open the 'Mesh' tab and go to 'Mesh Diagnostics > Overlap'. On the left of the AMI interface the 'Overlapping Elements Diagnostic' has been activated. So check the 'Place results in diagnostic layer' option.

This will create a new layer in the layers pane. Click on the 'Show' button and then 'Close'. Figure 3.21 shows the regions that must be fixed.

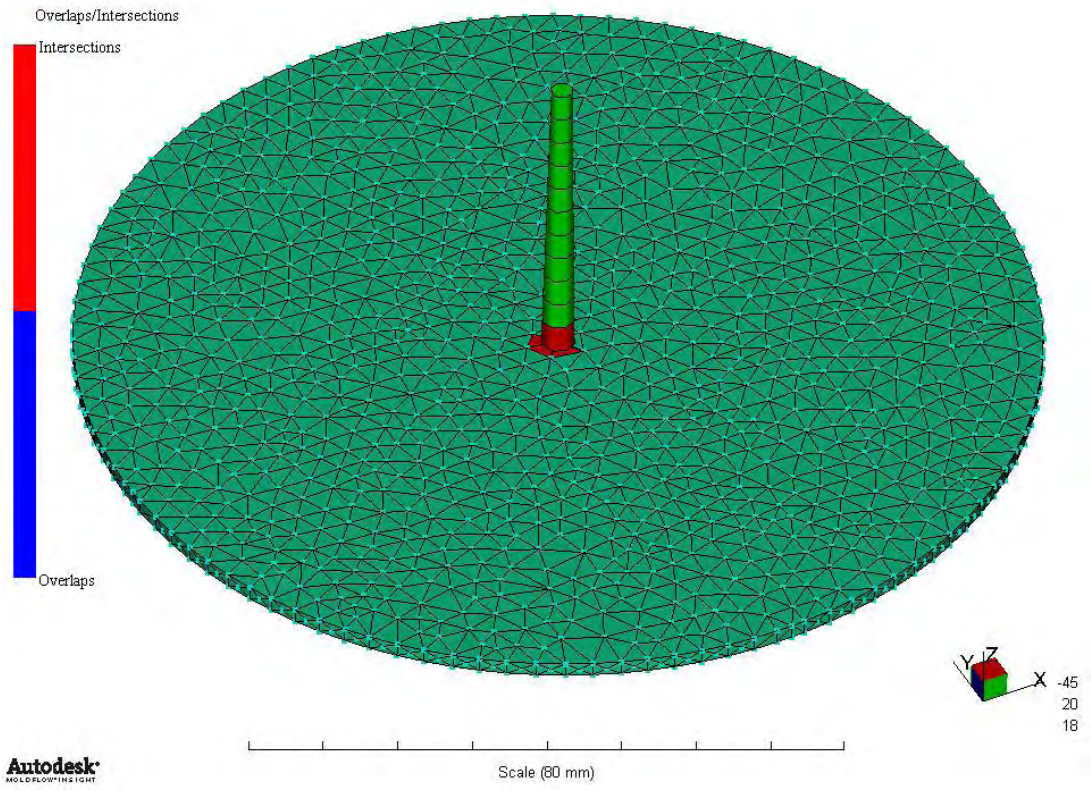

Figure 3.21: Three (3) intersections were detected by the Mesh Repair Wizard.

So now move to the layers pane and right click the ‘Diagnostic results’ option. Select the ‘Hide all other layers’ option and right after click on the ‘Expand Layer’ button. Bring forth the back side of the disk and zoom in (figure 3.22). With the yellow colored circles are pointed out the two nodes that caused the mesh problem. The appearing intersections can easily be fixed, using the ‘Merge Nodes’ command.

So in the new ‘Merge Nodes’ window that appears, choose node 2 (N15634) as the node to merge to and node 1 (N8142) as the node to merge from. Click apply and then close. This will repair the mesh and the final result is shown in figure 3.23.

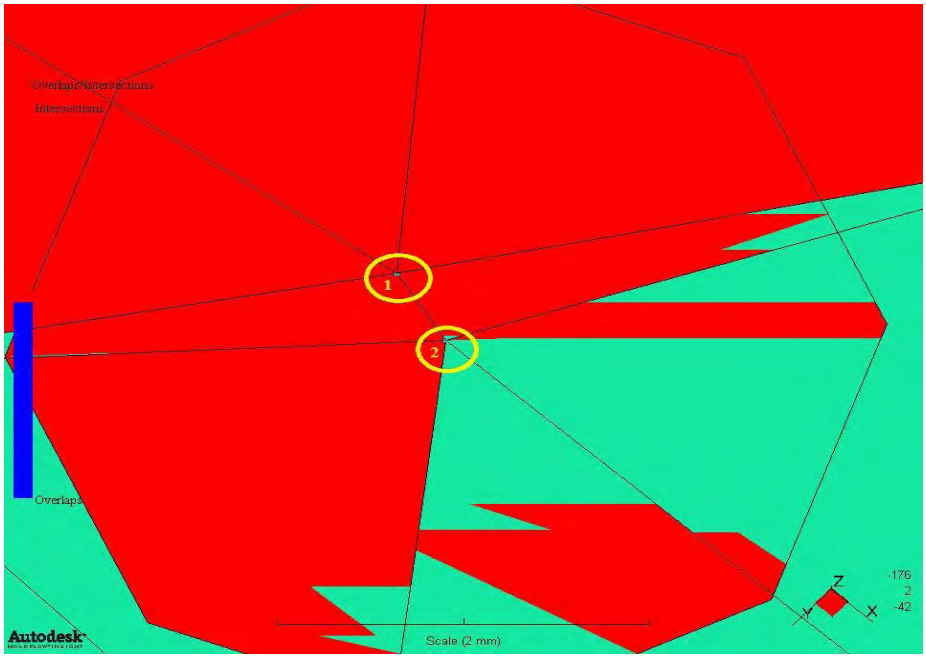

Figure 3.22: Specifying the cause of the mesh problem.

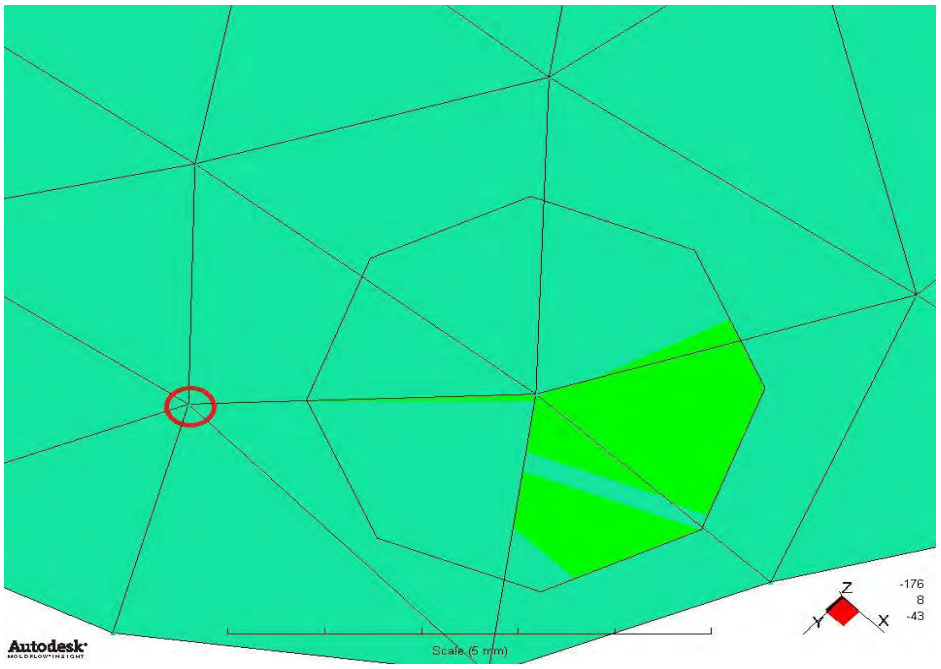

Figure 3.23: Intersections all repaired.

Notice the red colored circle in figure 3.23. The specific node (N8610) needs to be smoothed. With the help of the ‘Smooth Nodes’ option, select this node and click apply. Be sure to have activated the ‘Preserve feature edges’ option. The mesh is now completely fixed, as shown in figure 3.24. In order to make the model appear in its original form again, right click on the ‘Diagnostic results’ option and now select the ‘Show all other layers’ option.

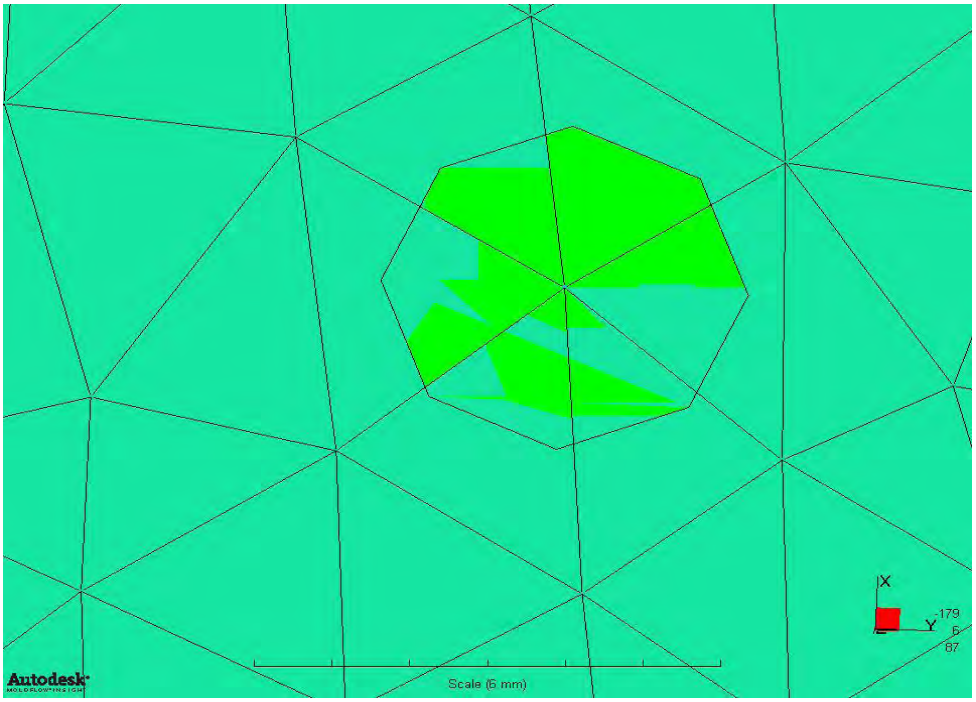

Figure 3.24: Mesh repair is finally ready.

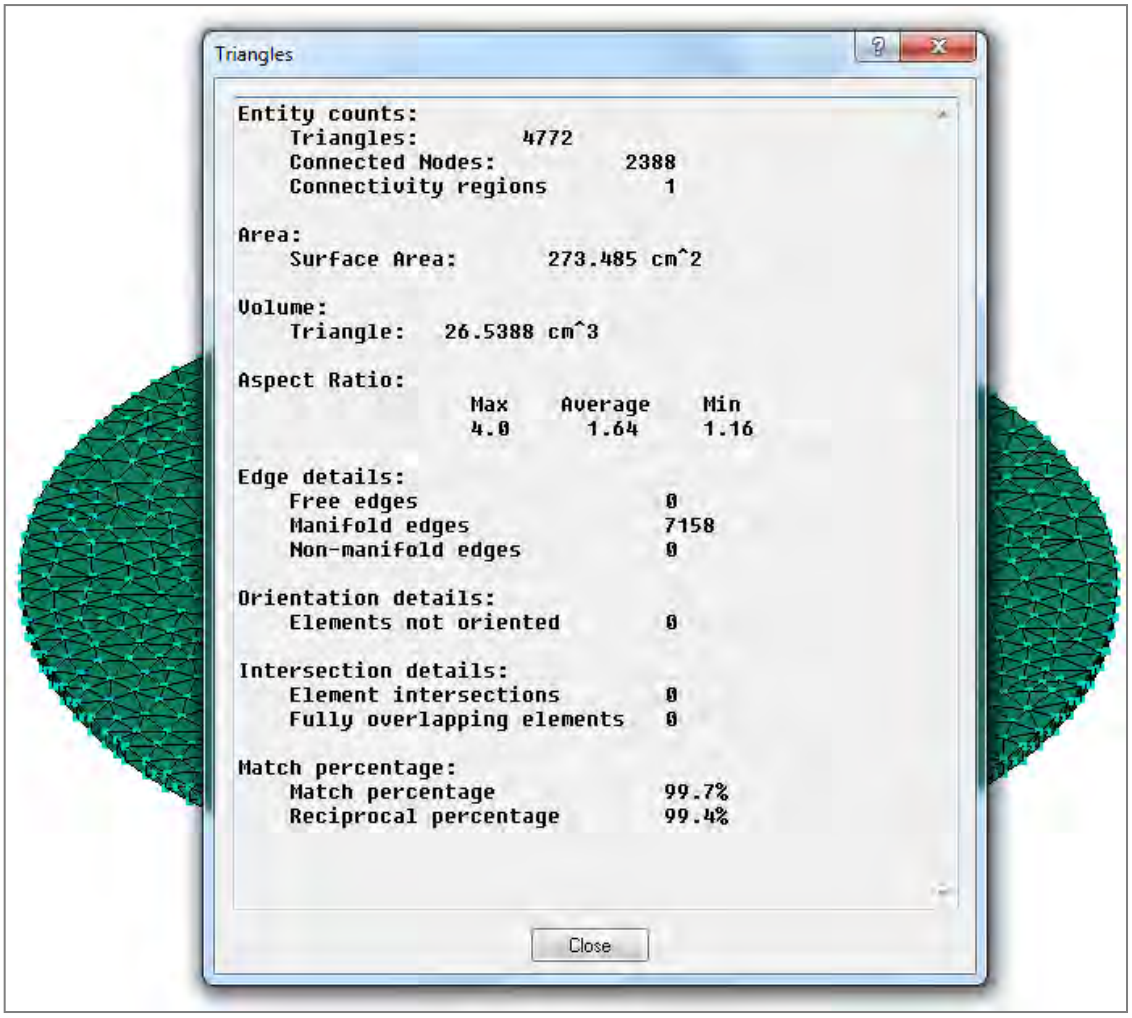

Figure 3.25: Summary report about the current dual domain mesh (using Mesh Statistics). All mesh requirements are more than satisfied, according to table 3.1.

The final step will be completed when the injection location is set. Zoom in on the top of sprue and place an injection location (a yellow cone) on the blue node. This will ensure that the injection location is set right in the middle. An injection location is always necessary, as it specifies the point from which material is going to be fed into the sprue gate, therefore the cavity. Everything is ready now, as shown in figure 3.26. Notice that no ventilation system exists. In order to define one, a pair of cooling circuits must be created. This will prevent the creation of air traps in our part. In this study, a Fill + Pack analysis has been run. So some air traps are expected to appear in the circumference of the disk. However, this is not a crucial problem for the final results. In the next topic, the process settings will be analyzed.

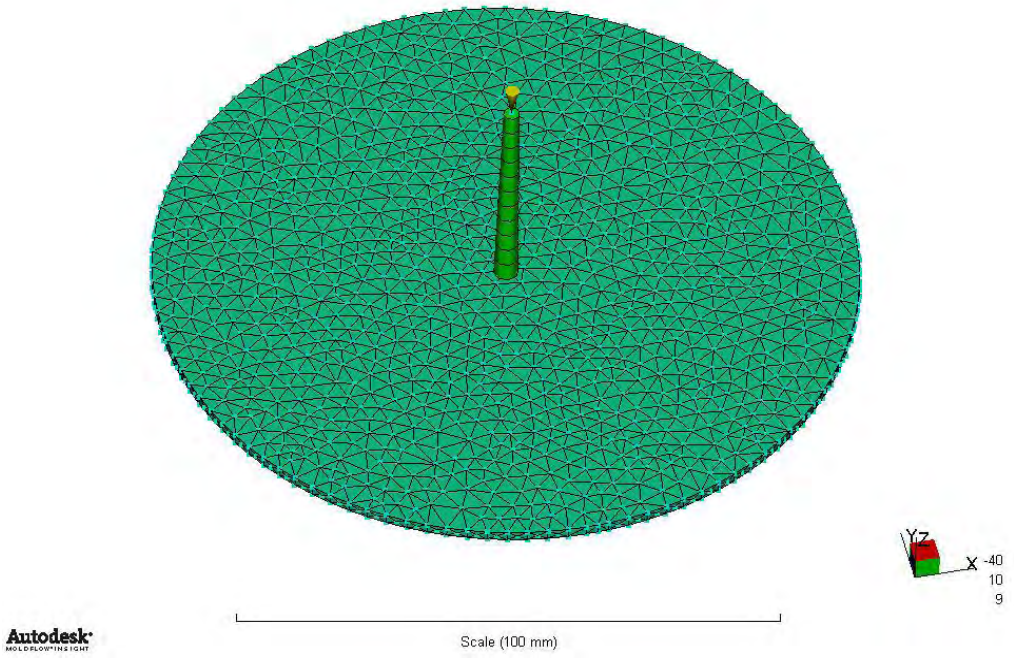

Figure 3.26: Injection location is set. Material will now be injected into the cavity from the top of the sprue. The elements now are 4783 in total (including the 11 beam elements of the sprue gate).

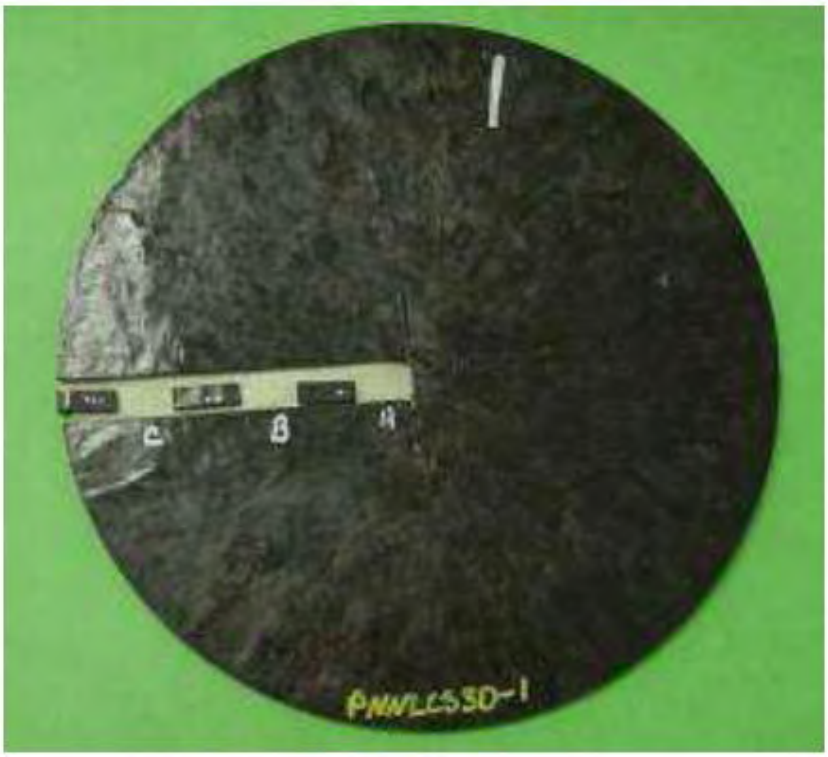

Figure 3.27: A real center-gated disk, with a diameter of 177.8 mm and thickness of 3 mm. *(Source: Kunc et. al., 2007)*

Now let's assume that a complex geometry needs to be studied. In this case a more dense mesh is required. Using a very small global edge length (GEL) when converting from a dual domain to a 3D mesh, won't solve the problem. The number of elements will certainly increase when the 3D mesh is used, however, not to a big extent. In order to achieve a very high number of elements, thus better analysis, but much greater computational time, one should import the model through the AMDL with a rather small GEL. Remember that when the disk was imported, a GEL of 4 mm was used. According to AMI theory, in a Dual Domain analysis the minimum GEL that should be used is two times the part thickness.

But what will happen if the GEL is reduced ? For example, if a GEL of 2 mm or even less is initially used, then the elements in the Dual Domain mesh will be dramatically increased. Therefore, one can imagine how many elements will be created in the 3D mesh. The following figures show the resulting mesh.

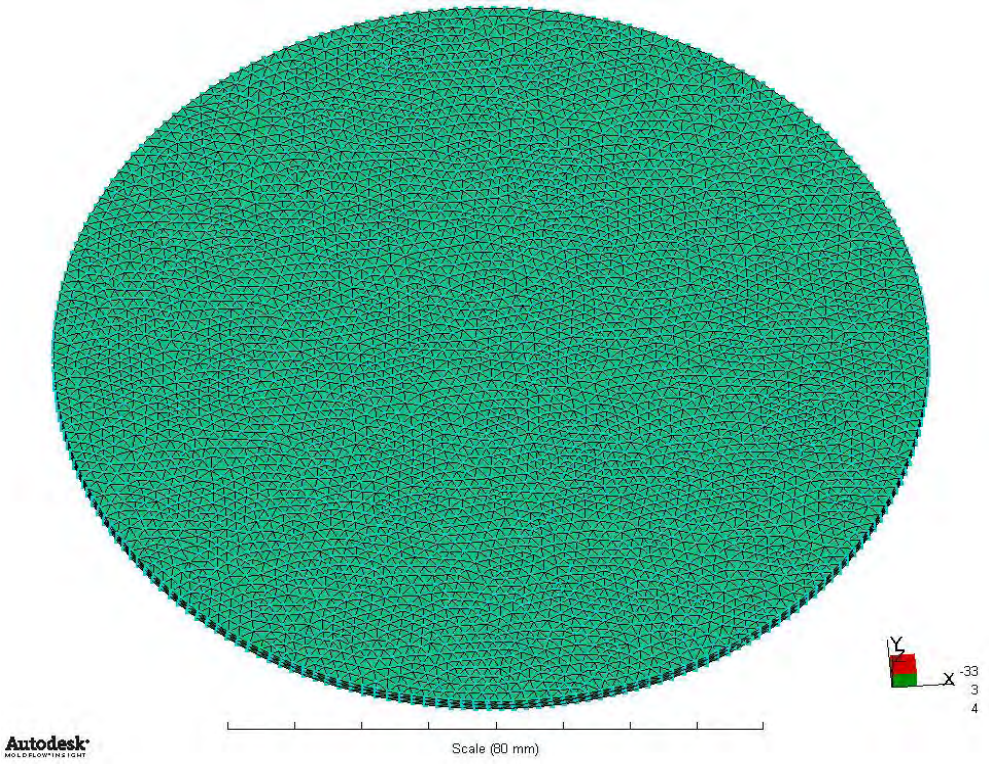

Figure 3.28: Presentation of the disk in a dual domain mesh, using a GEL of 2 mm. A total of 19204 elements were created. Notice how the appearance of the top surface has changed.

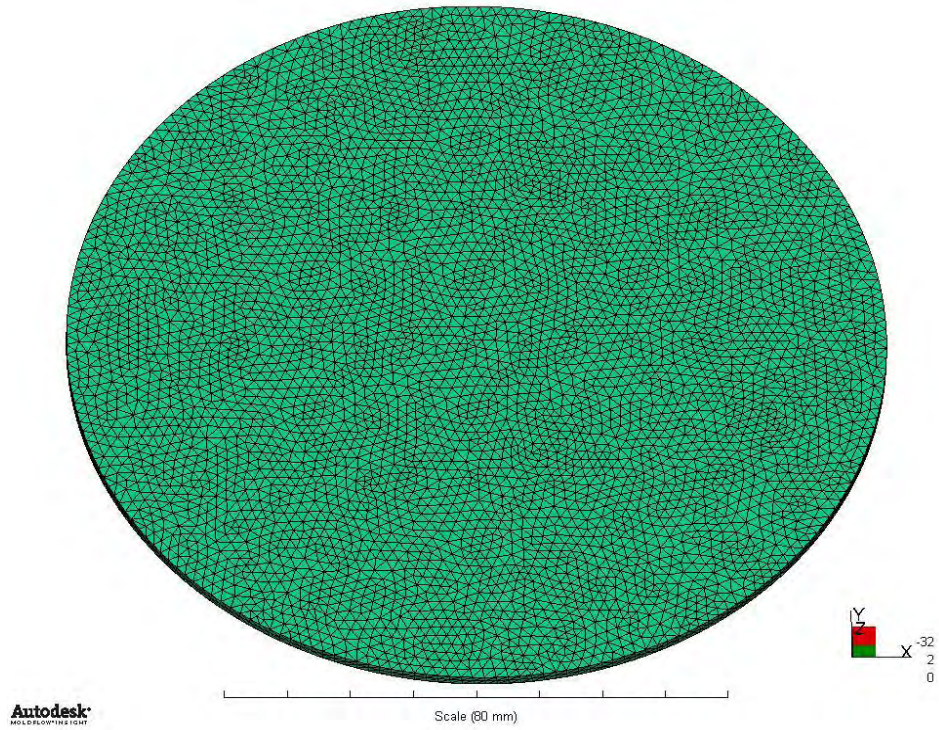

Figure 3.29: Presentation of the disk in a 3D mesh, using a GEL of 2 mm again and 8 layers through thickness (3D conversion will be discussed later). A total of almost 224853 elements were created.

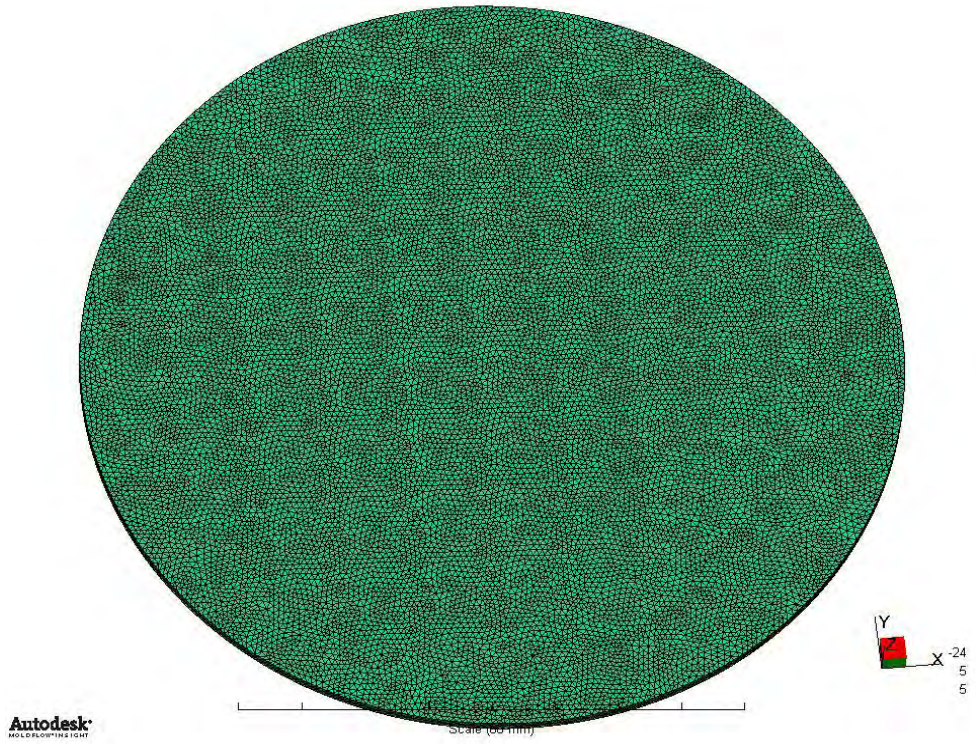

Figure 3.30: Presentation of the disk in a dual domain mesh, using a GEL of 1 mm. A total of about 71888 elements were created. That's too many for a dual domain mesh. Notice how the appearance of the top surface has changed again. The elements are very densely packed.

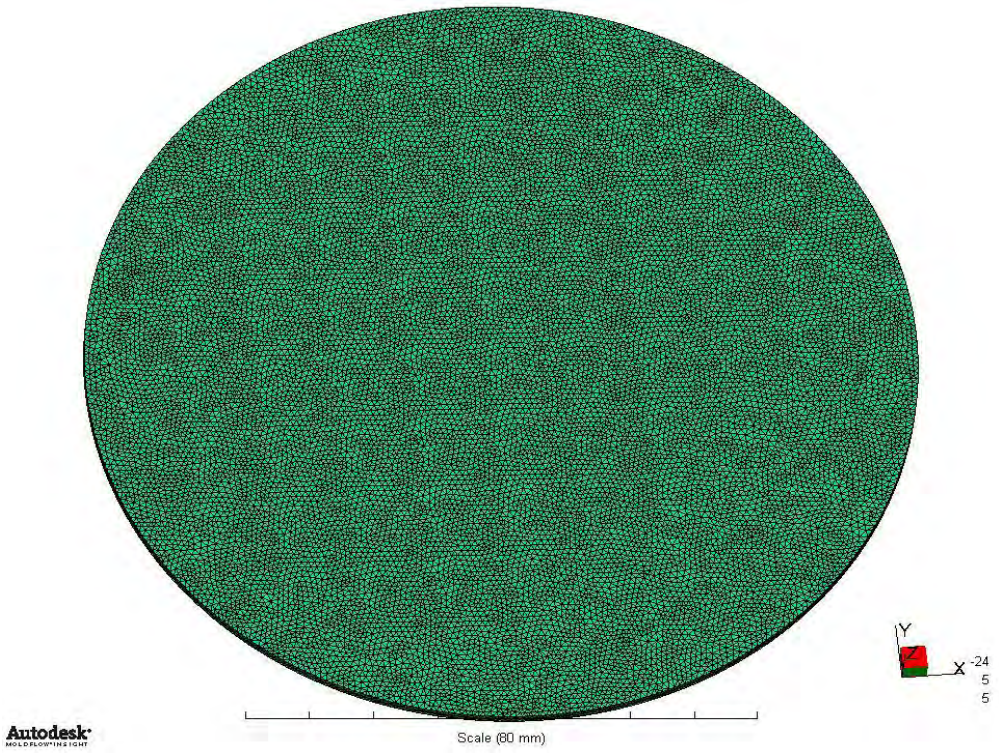

Figure 3.31: Presentation of the disk in a 3D mesh, using a GEL of 1 mm again and 8 layers through thickness (3D conversion will be discussed later). A total of almost 856522 elements were created.

⇒ Although the 3D conversion is discussed much later in detail, it would be useful to point out again that in the original study a GEL of 2 mm (equal to the thickness of the disk) was used, when converting to 3D. The elements created were almost 55000. That's about 4 times less elements, compared to those created when a GEL of 2 mm was used to import the model initially and convert to 3D later (figures 3.28 & 3.29).

⇒ Observing figures 3.28 to 3.31, one can conclude that the elements in a 3D mesh are almost 12 times more than those in a dual domain mesh, using of course the same GEL for the creation of both and 8 layers through thickness (for the 3D conversion). Using even more layers in the thickness direction would increase this ratio dramatically.

4. Process Settings

4.1 Molding Material dialog

First thing to always check is the 'Molding Process Setup' environment tab. The 'Thermoplastics Injection Molding' option should be selected. After this, one can choose the appropriate material for the study. There is an extended material library and with the search button one can find almost any desired material. For the case of this center-gated disk, a 30% short glass fiber (SGF) reinforced polybutylene terephthalate (PBT) has been selected. PBT is a thermoplastic engineering polymer. The material's trade name is *Crastin HR5330HF NC010 (Moldflow Verified)*, from DuPont Engineering Polymers manufacturing company. The material's structure is crystalline.

But why is the phrase '(Moldflow Verified)' included in the material's name? This stands for the fact that the specific polymer has undergone testing by experts. Confidence in simulation results comes from knowing that the material used, will result in accurate analysis predictions. The Autodesk Moldflow Plastics Labs perform multiple injection molding trials and compare analysis predictions with in-mold performance.

Plastic materials are widely used as metal replacement in industrial applications, owing to the advantages of higher strength-to-weight ratio and high corrosion resistance. Glass and carbon fibers are commonly added into plastics to reinforce the mechanical and thermal properties, with negligible change of weight. The addition of fibers introduces anisotropy of the properties in injection-molded parts, mainly due to the preferential orientation of fibers induced by the flow during processing. For example, shearing flow, which is usually dominant during injection-molding processing of a thin part, tends to align fibers in the shearing direction. The part is much stronger and stiffer in the direction along which most fibers are aligned than in the direction crossing the major fiber alignment. In order to determine the properties in injection-molded parts and aid the design of mold and part and the selection of processing conditions, the fiber orientation must be accurately predicted (Wang & Jin, 2010).

If the fibers are randomly oriented, the mechanical and physical properties will be isotropic. If the fibers are aligned in one direction, the composite will be stiffer and stronger in that direction compared with any other direction. The distribution of orientations in a molded part could be quite diverse. One region may have random fiber orientation, while others may have preferred alignment in certain directions.

In the injection molded short fiber composites, a characteristic layer structure is observed, with the fibers oriented in quite different manners according to their location through the thickness, as demonstrated in figure 4.1.

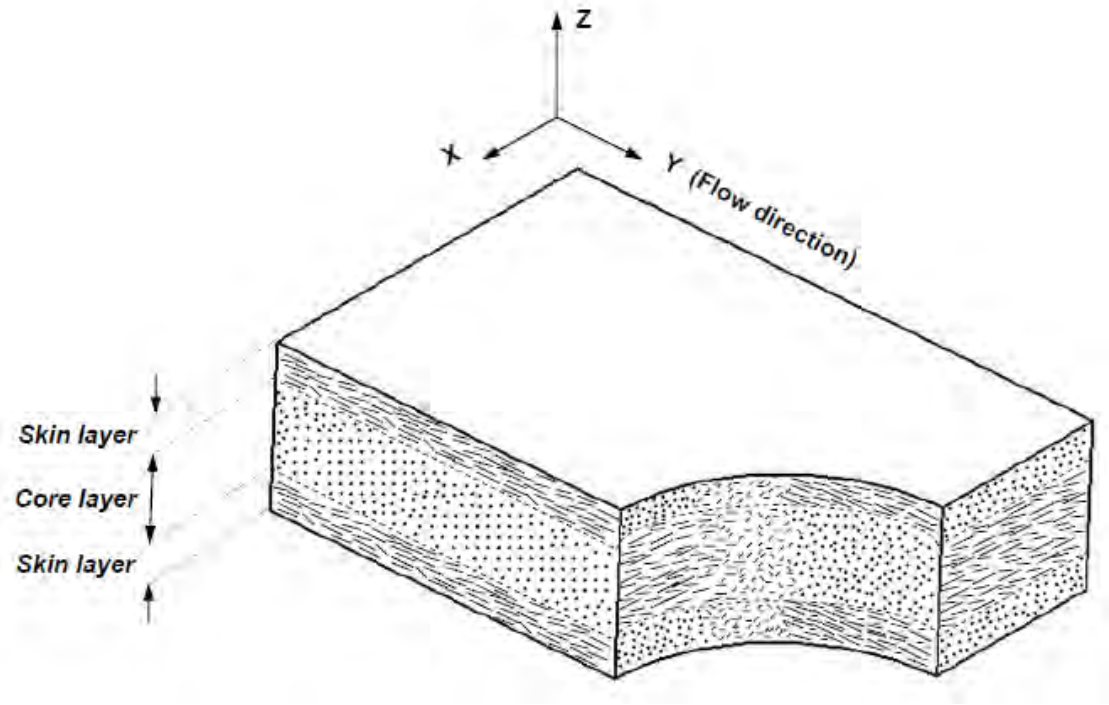

Figure 4.1: Schematic diagram of molding indicating the fiber orientation in the skin and core layers. *(Source: Somjate Patcharaphun, 2006)*

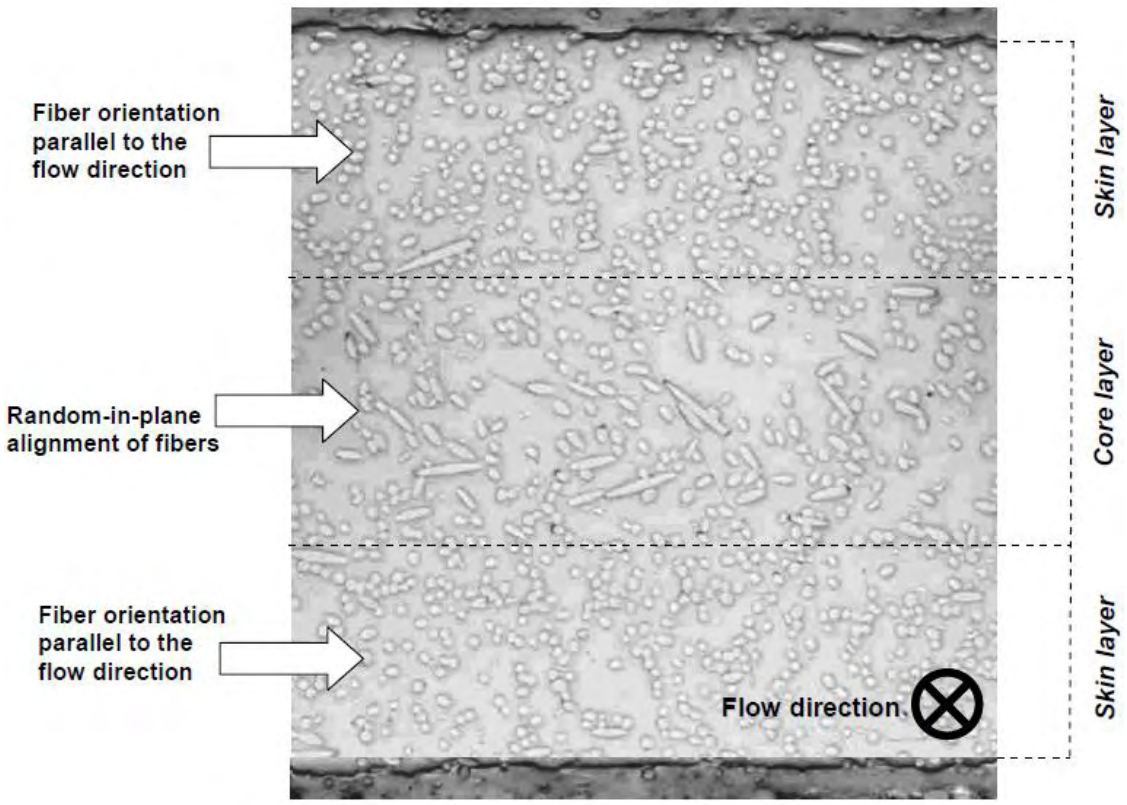

Figure 4.2: Optical photomicrograph showing the fiber orientation pattern across the thickness of a tensile test bar. *(Source: Somjate Patcharaphun, 2006)*

In the skin region, fiber orientation is predominately parallel to the flow direction. This is due to, as the melt fills the mold, there is fountain flow which initially orients the fibers perpendicular to the main flow direction. Fountain flow causes the melt to be deposited on the mold wall with the alignment direction parallel to the mold fill direction. Here, it solidifies rapidly and this alignment is retained in the solid article. Further behind the melt front, shear flow dominates and produces fairly uniform levels of fiber alignment. In contrast, the core of the molding contains fibers mainly aligned perpendicular to the flow direction, due to a slower cooling rate and lower shearing. Moreover, fountain flow does play a role in the development of the fiber orientation distributions, observed in injection molded fiber-reinforced parts (Bay & Tucker, 1992). Its influence, however, is frequently overwhelmed by that of the shear and extensional flows.

Fibers longer than 1 mm are generally considered as long fibers. As described above, a SGF PBT has been selected, i.e. fiber's length is < 1 mm. Usually, the fiber alignment in the flow direction is smaller in long-fiber materials, than in short-fiber materials in injection molded parts (Phelps & Tucker, 2009). The main flow direction, in the case of a center-gated disk, is radial.

Currently, most programs and commercial software, including AMI, use the Folgar-Tucker model (Folgar & Tucker, 1984) to predict the fiber orientation. However, recent experiments, including measurements of fiber orientation in injection-molded parts (O'Gara et al., 2003) as well as measurements of rheology of fiber suspension (Sepehr et al., 2004), indicate that the FT model predicts much quicker fiber orientation change with respect to strain than has been observed, and thus, usually over-predicts the overall fiber alignment.

This is why the reduced strain closure (RSC) model is going to be chosen here. Generally, the RSC model exhibits slower orientation kinetics than the FT model. Again, it must be noted that the goal of this study is not a fiber analysis. The equations behind each model and what they represent will be described later. First, one should look into the properties of the selected material, such as the rheological and thermal properties.

4.1.1. General features

Crastin HR5330HF NC010 is a high flow (HF), moderately toughened and hydrolysis resistant (HR) thermoplastic polyester resin. Some of its features include good chemical resistance, low viscosity, dimensional stability and good processability. It offers excellent balance of properties between terminal pullout and impact resistance.

- *Used for*: automotive applications, engineering parts, connectors, industrial applications/parts, electrical/electronic applications and machine/mechanical parts. Its processing method is through injection molding.

- *Recommended processing*: the melt temperature should be in the range of 240–260 °C and the mold temperature in the range of 30-130 °C, with an optimum temperature of 250 and 80 °C, respectively. The material's ejection temperature is 168 °C**.**

Generally, PBT materials have fast crystallization rates, so the cycle times are typically low.

4.1.2 Mechanical properties

Fiber orientation is one of the major factors that determine the mechanical (elastic) strength as well as the stiffness of a molded part. Theories have been developed to predict the mechanical properties of short fiber composites once the fiber orientation distribution in the parts is known. To calculate the mechanical properties, all the theories follow a two step procedure:

- The properties of a unidirectional short fiber reinforced material are estimated.
- These properties are then averaged across the laminaes according to the fiber orientation distribution density.

The material's mechanical properties are not of concern for this study. That's why the equations that are used for their calculation are not going to be described here. But one should keep in mind that in AMI:

- When matrix properties with materials that have anisotropic matrix data are used, the Mori-Tanaka micro-mechanics model will be chosen by default.
- If the 'Do not use matrix properties' or 'Use 7 matrix properties' option is selected with materials that have isotropic matrix data, the Tandon-Weng mirco-mechanics model will be chosen by default.

Note: Matrix is the polymer without the fibers/filler present. The matrix + fibers/filler make the composite material.

In this study the option 'Use 7 matrix properties' has been selected. Alpha1 defines the thermal expansion coefficient in the flow direction and Alpha2 the thermal expansion coefficient in the transverse direction (figure 4.3). By default, the Tandon-Weng model has been selected for the analysis of the disk.

General Note: In order to modify the properties of a material go to 'Molding Process Setup' tab and from there: 'Advanced Options > Molding Material > Edit'. Everything can be changed from there.

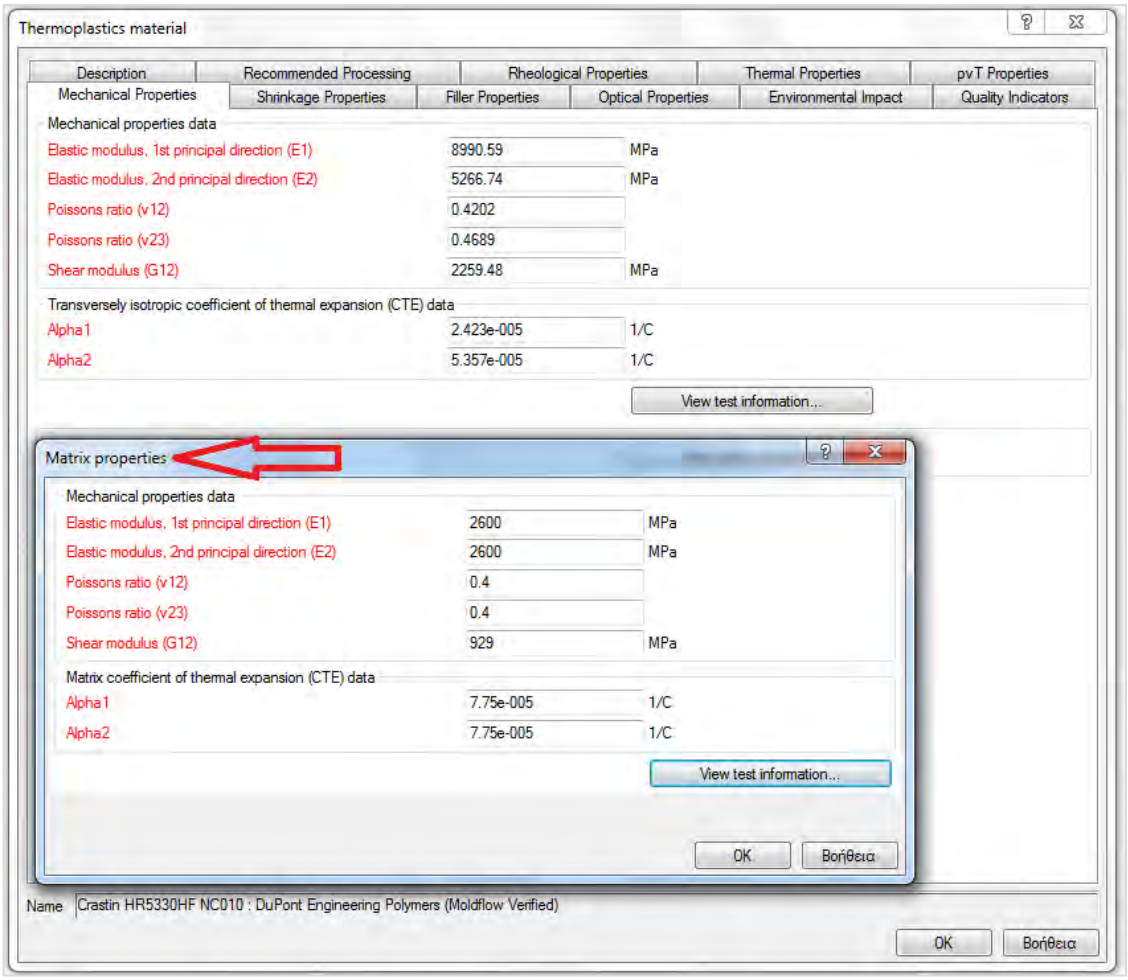

Figure 4.3: Mechanical properties tab. If a property name is shown in red, it indicates that the property has not been tested for this specific material. However, material data from the testing of a comparable generic grade was found to be suitable and has been assigned to this material.

4.1.3 Shrinkage properties

Before the shrinkage prediction method is described, one should first select the appropriate shrinkage model for the flow simulation. And this is very important, as it can improve the shrinkage results to a big extent. As shown in figure 4.4, the 'Corrected residual in-mold stress (CRIMS)' model is selected by default and it must be left as it is. Generally, CRIMS model is selected when shrinkage testing has been performed on the material. This model is more accurate, because it is obtained by correlating actual shrinkage tested values (figure 4.5) with the Fill + Pack analysis predictions.

The 'Uncorrected residual stress' model will be selected when there is no shrinkage data available for the material. The 'Residual strain' model is selected for those materials where the CRIMS model was found inadequate to describe the shrinkage behavior of the material.

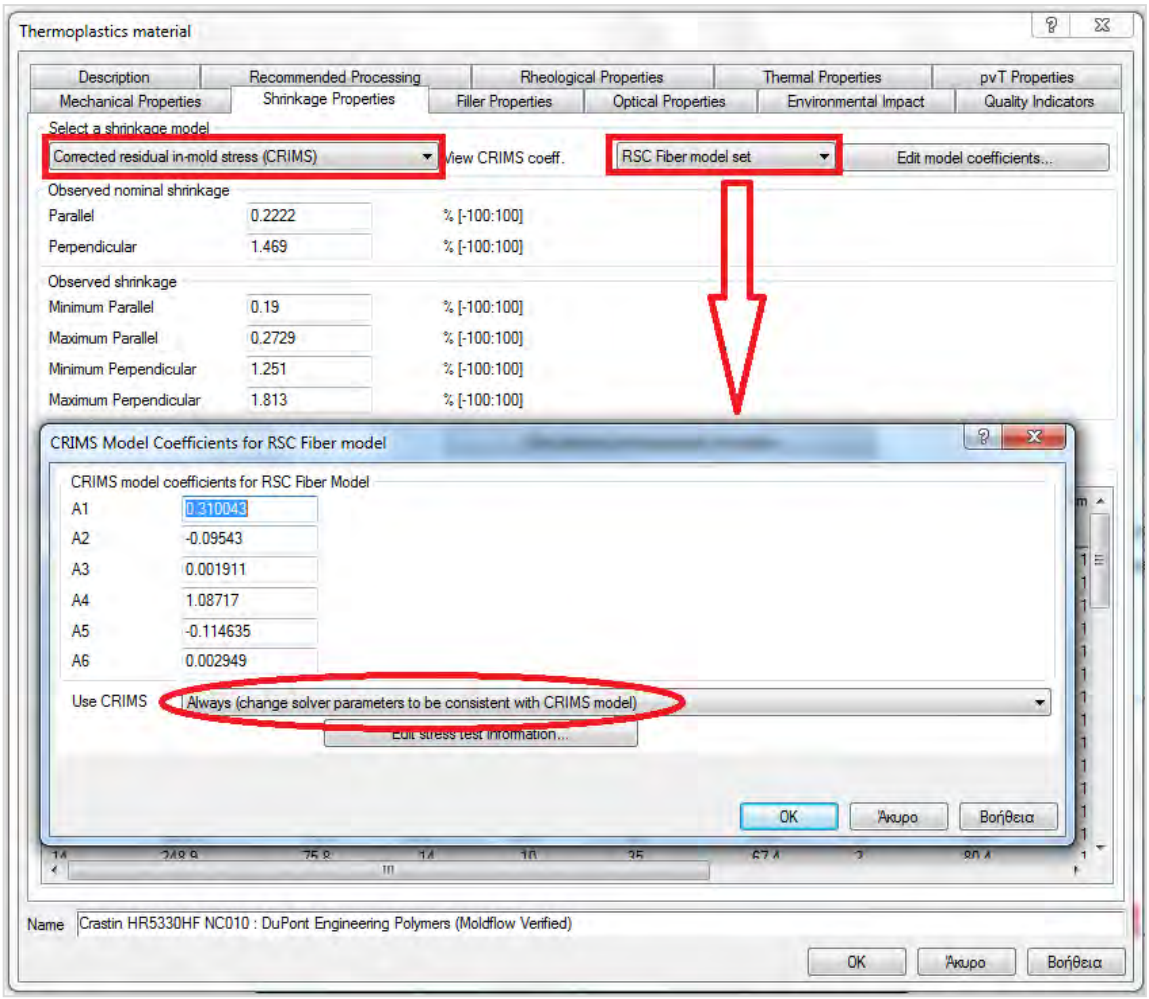

Figure 4.4: Selecting the correct shrinkage model. Notice that the 'RSC Fiber model set' option is also selected. As mentioned above, in this study the RSC fiber orientation model will be chosen.

For the Crastin HR5330HF NC010 material selected for this study, a shrinkage test has been already made, in order to ensure more accurate predictions. The following observed shrinkage data were acquired through the Non-contact metrology (2D) method.

Table 4.1: Shrinkage data for Crastin HR5330HF NC010.

	Observed nominal shrinkage		**Observed shrinkage**
Parallel	0.222 %	*Min. Parallel*	0.190 %
Perpendicular	1.469 %	*Min. Perpendicular*	1.251 %
		Max. Parallel	0.273 %
		Max. perpendicular	1.813 %

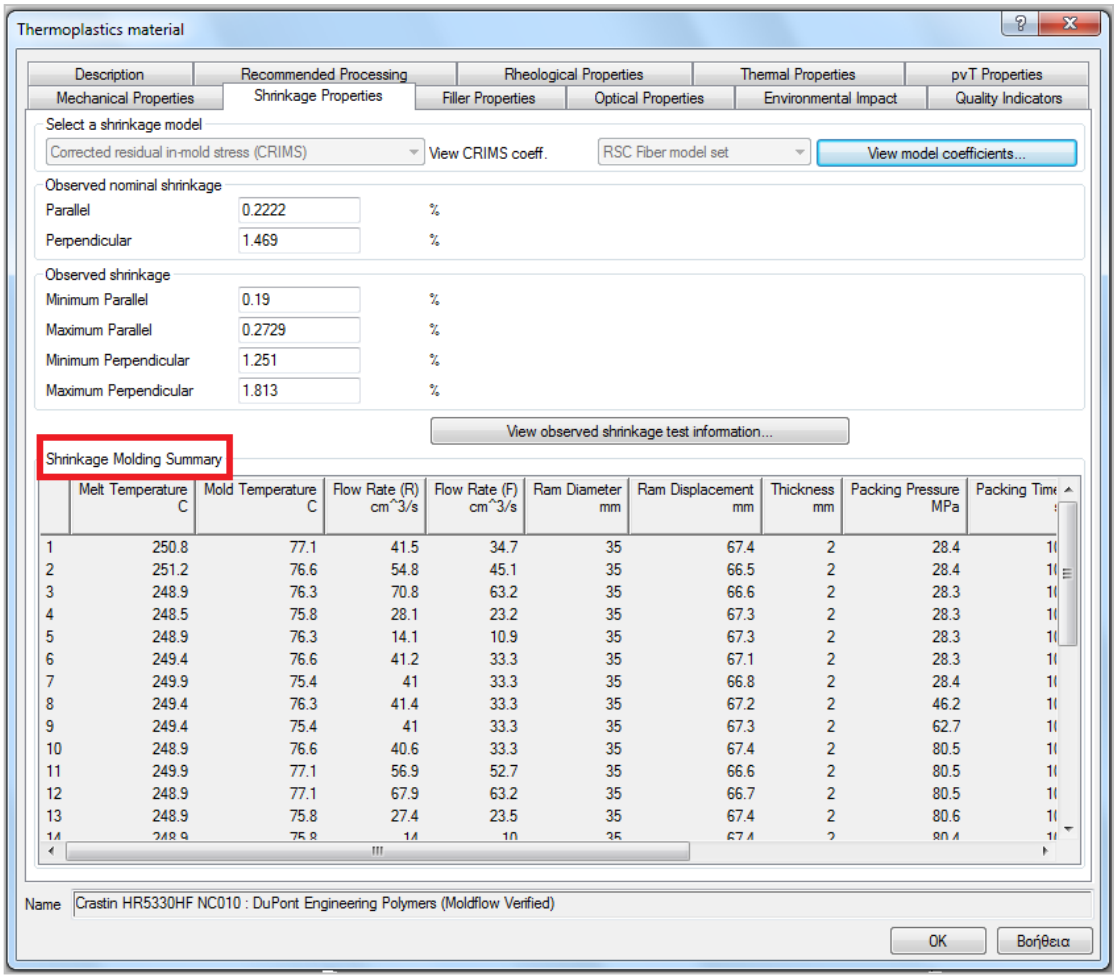

Figure 4.5: The shrinkage molding summary. This table contains the measured in-plane shrinkage, parallel and perpendicular to the flow direction, under a range of different injection molding conditions, such as packing pressure and melt-mold temperature.

For injection molded parts, the part is constrained in the mold. During the solidification of an injection molded part, shrinkage of the solidified layer is prevented by two mechanisms. Once the part is ejected from the mold, these residual stresses will be released in the form of shrinkage deformation. The mechanisms are:

a) Adhesion to the mold walls restrain (at least the outer skin) of the solid layers from moving, and
b) The newly formed solid surface will be kept fixed by the stretching forces of melt pressure.

In-cavity residual stresses (internal stresses) build up during solidification. Due to the nature of constrained quenching, the residual stress distribution is largely determined by the varying pressure history, coupled with the frozen layer growth. Once the part is ejected from the mold, these residual stresses will be released in the form of shrinkage deformation. If the initial strains, which are equivalent to the in-cavity residual stresses, are uniform, the part will shrink uniformly without any warpage and post-mold residual stresses. Warpage is caused by variations in shrinkage throughout the part. Two types of shrinkage variations are considered:

a) Shrinkage variations from region to region (differential shrinkage effect):

For typical thin-walled parts, this form of shrinkage variation can be divided into variations in the thickness direction of molded parts, mainly caused by the differential cooling and variations from surface region to surface region

b) Shrinkage variation in different directions (orientation effect):

The difference between parallel and perpendicular shrinkage and anisotropic material properties, relating to the fiber-orientation distribution, are one of the main causes of part warpage for fiber-filled TPs.

Note: For fiber-filled TPs, reinforcing fibers inhibit shrinkage due to their smaller thermal contraction and higher modulus. Therefore, fiber-filled materials shrink less along the direction in which fibers align (typically the flow direction) compared to the shrinkage in the transverse direction. Thus, the shrinkage in the direction of flow is *lower* than the shrinkage perpendicular to the direction of flow. For the case of a center-gated disk, the direction of flow is radial.

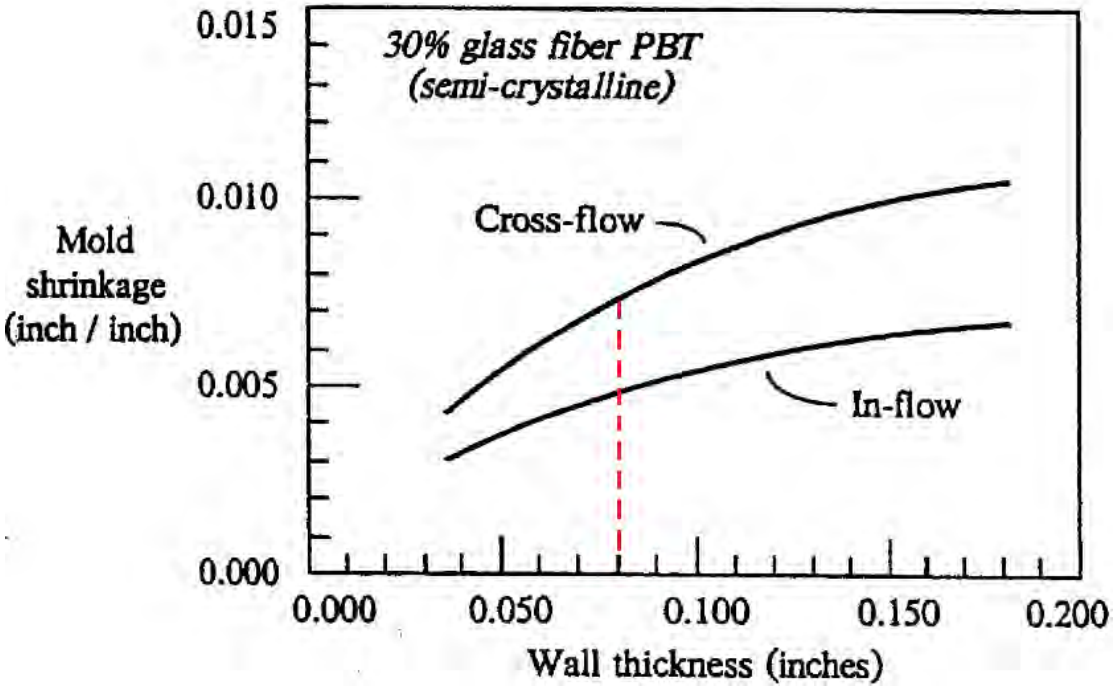

Figure 4.6: The mold shrinkage for a reinforced semi-crystalline polymer, such as a glass-fiber reinforced PBT, varies with direction (flow vs. cross-flow) and with part thickness. (The thickness of the disk is 2 mm or approximately 0.08 inches). *[6]*

The shrinkage of injection molded parts depends on the thermodynamic behavior of the material during processing. For simplicity, a linear elastic behavior in the solidified part and purely viscous behavior in the melt, is assumed.

It is reasonable to approximate the linear shrinkage using the following formulation:

$$\varepsilon_i = \int_{T_r}^{T_o} a_i(T)dT$$

where:

$a_i(T)$ = the linear thermal expansion coefficient (CTE) at temperature T in the i-th principal direction,

T_o = the temperature when the local cavity pressure reached the atmospheric condition (obtained from the flow simulation), and

T_r = the room temperature.

Right below, one can see the CRIMS model coefficients list. As mentioned earlier, many materials in the Moldflow database have been "shrinkage tested". This means that the Moldflow Lab measured parallel and perpendicular shrinkage of moldings molded with different parameters (usually rectangular plates). They also predict shrinkages and some proprietary parameter 'Tau' (frozen shrinkage strain) for all those regimes. After that Moldflow correlates the measured shrinkage with the predicted shrinkage and 'Tau', as:

$$\text{Shrink\_parallel\_exp} = A_1 \cdot \text{Shrink\_parallel\_pred} + A_2 \cdot \text{Tau} + A_3$$

and:

$$\text{Shrink\_perpendicular\_exp} = A_4 \cdot \text{Shrink\_perpendicular\_pred} + A_5 \cdot \text{Tau} + A_6,$$

where "exp" stands for expected and "pred" for predicted.

The $A_1 - A_6$ coefficients are provided with the material database and their values are:

A1	0.310043
A2	-0.09543
A3	0.001911
A4	1.08717
A5	-0.114635
A6	0.002949

Note: The structure of a semi-crystalline material, when in the molten state, is amorphous. However, as it cools, macromolecules tend to organize themselves according to their own nature, i.e. they recover the primary crystalline percentage. In the new reordered areas, the free space among molecules is lower than the amorphous areas: a concrete specific volume reduction ("shrinkage") occurs. So, semi-crystalline polymers shrink more than amorphous ones; typically 0.5-1% vs. 1.5-5% depending upon the particular material, because the crystals formed during cooling, take up less volume than the unoriented (amorphous) molecules that exist during the melted phase. This is the reason why amorphous TPs are less prone to warpage than crystalline resins. While high shrinkage alone does not cause warpage, it increases the probability that warpage will occur.

Furthermore, semi-crystalline materials have a sharp melting point, i.e. they transition from solid to liquid very quickly over a short/narrow temperature range. This becomes clear by observing figure 4.8. On the other hand, amorphous materials have a broad softening range.

In addition, when amorphous polymers are cooled, they slowly solidify over a wide range of temperature, as against the semi-crystalline plastics, which change from melt to solid over a quite narrow temperature span.

If some part of the mold cools at a slower rate, that area will have higher crystalline content and, hence, higher shrinkage. Common examples are that of a part with different wall thicknesses.

4.1.4 PVT properties

The modified 2-domain Tait pvT model is used to determine the density of the material (therefore the specific volume), as a function of temperature and pressure. This variation impacts on many aspects of the flow simulation. The 2-domain Tait pvT model is given by the following equation:

$$v(T, p) = v_0(T) \cdot [1 - C \cdot \ln(1 + \frac{p}{B(T)})] + v_t(T, p)$$

where:

v(T,p) = the specific volume at some temperature and pressure,

v_0 = the specific volume at zero gauge pressure,

T = temperature (K),

p = pressure (Pa),

C = universal constant = 0.0894, and

B(T) accounts for the pressure sensitivity of the material and is defined below.

- The upper temperature region ($T > T_t(p)$ – *liquid phase*) is described by:

$$\begin{aligned} v_0 &= b_{1m} + b_{2m} \cdot (T - b_5) \\ B(T) &= b_{3m} \cdot \exp[-b_{4m} \cdot (T - b_5)] \\ v_t(T, p) &= 0 \end{aligned} \qquad (4.1.4.1)$$

- The lower temperature region ($T < T_t(p)$ – *solid phase*) is described by:

$$\begin{aligned} v_0 &= b_{1s} + b_{2s} \cdot (T - b_5) \\ B(T) &= b_{3s} \cdot \exp[-b_{4s} \cdot (T - b_5)] \\ v_t(T, p) &= b_7 \cdot \exp[b_8 \cdot (T - b_5) - b_9 \cdot p] \end{aligned} \qquad (4.1.4.2)$$

where:

$T_t(p) = b_5 + b_6 \cdot p$ = the transition temperature. The transition temperature is the glass transition temperature, T_g, for amorphous polymers and the crystallization (melting) temperature, T_c, for crystalline polymers *[7]*. For the material used in this study, the latter is valid.

The transition temperature is the polymer freeze temperature, at which the melt to solid transition occurs. Thus, T_c is the temperature at which a polymer in the liquid-amorphous state is transformed into a solid-crystalline state.

The "m" subscript denotes the state above $T_t(p)$ and the "s" subscript denotes the state below $T_t(p)$.

The b_i parameters are data-fitted coefficients and describe (Wang J., 2012):

The volumetric transition temperature at zero gauge pressure is denoted by b_5. The linear increase in the transition with pressure is denoted by b_6.

The specific volume obtained by extrapolating the zero-isobar curve to the transition temperature is denoted by b_1. This value is the same for both domains when crossing the glass transition.

However, when the material is semi-crystalline, the transition due to crystallization is accompanied by an abrupt change in specific volume, such that b_{1m} (the melt specific volume at b_5 and zero pressure) is greater than b_{1s}.

The temperature dependence of the specific volume is measured by b_2. The b_{2m} and b_{2s} coefficients denote the bulk thermal-expansion in the liquid and solid states, respectively. Furthermore, b_3 and b_4 characterize $B(T)$ in the solid and melt state. The specific volume becomes more pressure sensitive with increasing temperature, when b_4 is positive. Lastly, the constants b_7, b_8 and b_9 characterize $v_t(T,p)$ in the solid state.

Table 4.2: The 2-domain modified Tait pvT model coefficients used for Crastin HR5330HF NC010 in AMI.

b_5 (K)	505.15
b_6 (K/Pa)	5.45e-008
b_{1m} (m^3/kg)	0.0007766
b_{2m} (m^3/kg-K)	4.244e-007
b_{3m} (Pa)	1.17589e+008
b_{4m} (1/K)	0.001959
b_{1s} (m^3/kg)	0.0007302
b_{2s} (m^3/kg-K)	3.244e-007
b_{3s} (Pa)	1.76442e+008
b_{4s} (1/K)	0.004874
b_7 (m^3/kg)	4.639e-005
b_8 (1/K)	0.06314
b_9 (1/Pa)	5.813e-009

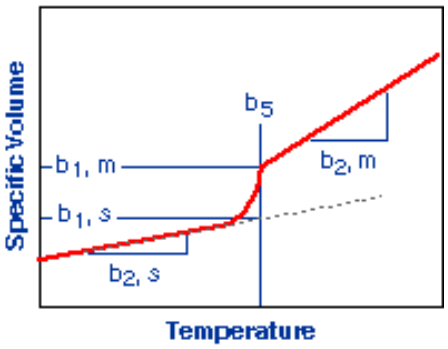

Figure 4.7: Schematic of the pvT diagram for a semi-crystalline polymer. *[7]*

When a crystalline polymer reaches its melting temperature, the cohesion of the crystalline domains is destroyed. Above the melting temperature, the crystalline polymers behave as high viscosity liquids and can generally be processed by injection molding.

The pvT diagram is a condensed presentation of the interrelations of three variables that affect the processing of a polymer: Pressure, Volume and Temperature.

When the temperature of the material is increased, its specific volume also increases, due to thermal expansion. The rate of increase becomes higher at the glass transition temperature, because the molecules have more freedom to move and occupy more space.

This change of slope is observed with both amorphous and crystalline polymers. At higher temperature, the melting of crystalline polymers is marked by a sudden increase of the specific volume, when the well-ordered and rigid crystalline domains become randomly oriented and free to move. Therefore, the specific volume is a signature of the changes of structure of the polymer, as a function of temperature. Also, it should be noted that the pvT behavior of semi-crystalline polymers greatly depend on the rate of cooling. A slow cooling rate will lead to higher degrees of crystallinity and lower specific volumes, than achieved in rapid cooling, typical of the injection molding process.

The melt density (density of material in the melt state) of Crastin HR5330HF NC010 is 1.2751 g/cm^3 and its solid density (density of the material in the solid state of 0 MPa and 25 °C) is 1.5082 g/cm^3.

The pvT diagram for Crastin HR5330HF NC010 is:

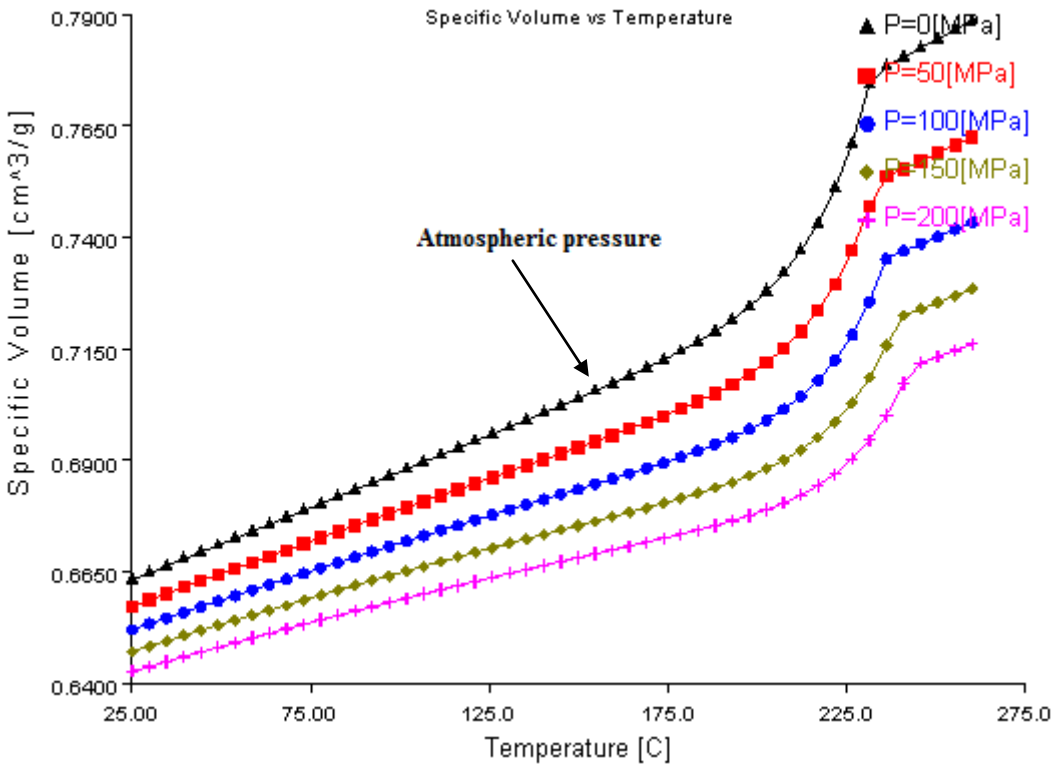

Figure 4.8: Specific volume (cm^3/g) vs. temperature (°C) plotted diagram, for a pressure range of 0 to 200 MPa.

Important note: According to table 4.2, the value of the b_5 coefficient is: b_5 = 505.15 K = 232 °C. This coefficient represents the transition temperature at the P = 0 (MPa) curve of figure 4.8. Therefore, one can understand the importance of this parameter, as it represents the transition from the melt to the solid state.

However, the fact that the melt temperature is at 250 °C and below the 232 °C point, it will turn to solid, is weird enough. Now, as shown in figure 4.13, one can see that another transition temperature exists in AMI (on the rheological properties tab), i.e. $T_{trans.}$ = 201 °C. So which of the two temperatures is used in the calculations ? Let's see:

1. A very simple way to test the effect of those two temperatures is to use them as the melt temperature (T_{melt}). At first, T_{melt} = 220 °C is chosen for analysis. The analysis is running successfully. Now, T_{melt} = 199 °C is also used. Analysis is unable to run. Short shot has been detected. Therefore, one can understand that Moldflow reads the 201 °C as the transition temperature. A short shot has been detected, obviously because the polymer at this temperature is not molten, but solid, at least the most of it.
2. Another way to check, if the 201 °C point is truly the transition temperature, is by observing figure 6.27 (on chapter 6). This figure shows the temperature inside the cavity, near the gate area, at the end of packing/holding (t = 5 sec). According to the logs, at this time point, the frozen volume is 99.9%. Examining the temperature values in that area, shows that temperature is almost everywhere lower than 201 °C; however, there are some regions that are still above 201 °C, i.e. at about 202-205 °C.

This proves that there is still a very small portion of the material that remains melted. Therefore, one concludes that the moment temperature drops below 201 ^{o}C, the material will instantly turn to 100% solid (frozen).

3. The material used in this study (Crastin HR5330HF NC010) belongs to DuPont Corporation. Searching through its properties, in the product information data sheets of DuPont, and more specifically observing its pvT diagram, one can easily tell that: $b_5 \sim 200\ ^{o}$C.

<u>Conclusion</u>: $T_{trans.} = 201\ ^{o}$C.

The stages of an injection molding process can be described using the pvT diagram. Figure 4.9 depicts the pvT diagram of Crastin HR5330HF NC010, for the pressure range of 0 – 50 MPa. This figure is the same with figure 4.8; the main difference is that the b_5 coefficient was changed from 505.15 K (default value) to 474.15 K (201 ^{o}C); reasons were described earlier.

- After the plasticizing stage is over, the material has reached the processing temperature (point A, 250 °C).

- The melt is now injected and compressed into the cavity. The specific volume is decreased to point B (37 MPa, 250 °C).

- The compression (packing) phase is started at point C (50 MPa, ~ 250 °C). During packing, solidification takes place in the mold initially under constant hold pressure. When the solid fraction builds up from the liquid phase, a large difference of volume occurs, which must be compensated by injection of additional liquid resin through the sprue.

- At the end of the holding period (point D, 50 MPa), the material is still in a melted state, i.e. has not yet reached the transition temperature point (201 °C).

- The holding pressure is removed safely. The cooling phase begins and the part cools in the mold. The pressure slowly decreases and temperature drops, until the part reaches its ejection temperature, at point E (0.1 MPa, 168 °C).

- On opening the cavity, the part cools to ambient temperature (point F, 23 °C) and atmospheric pressure, and it is allowed to shrink without constraint. The part shrinks to final dimensions on release from the cavity. The difference between the specific volume of point F and point E (Δv) gives the *final* volumetric shrinkage. The *total* shrinkage is the specific volume difference of point F and point A, i.e. as the polymer cools from its melt temperature to the ambient.

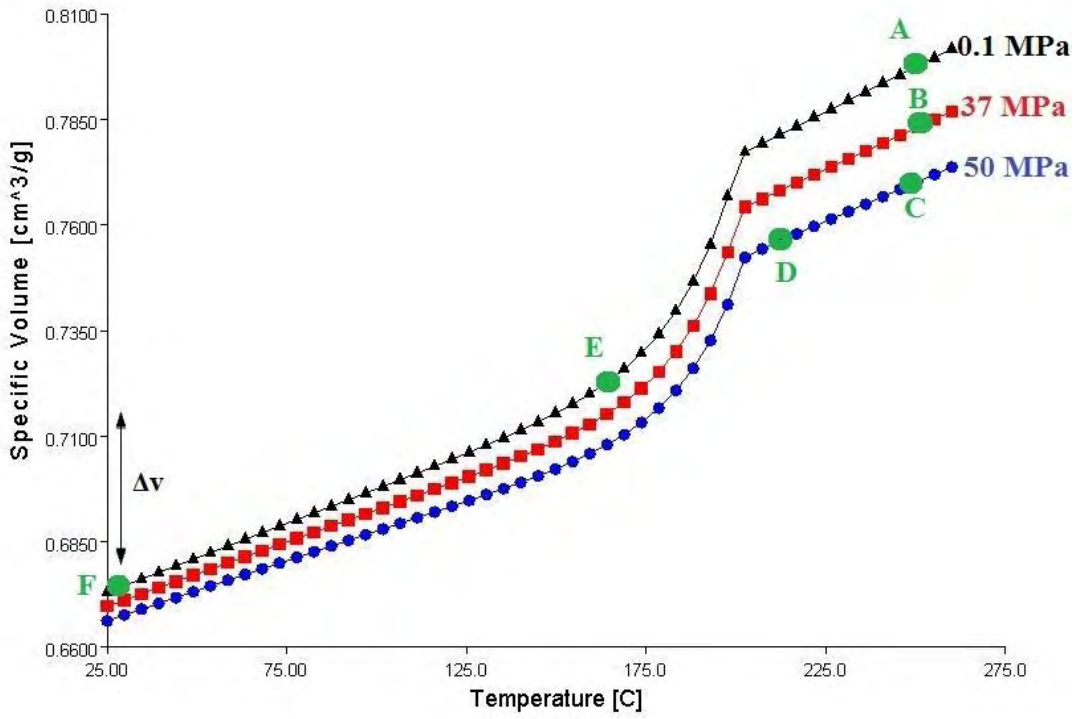

Figure 4.9: pvT diagram for the semi-crystalline Crastin HR5330HF NC010. Points A, B, C, D, E and F (green colored) refer to different steps of the molding process.

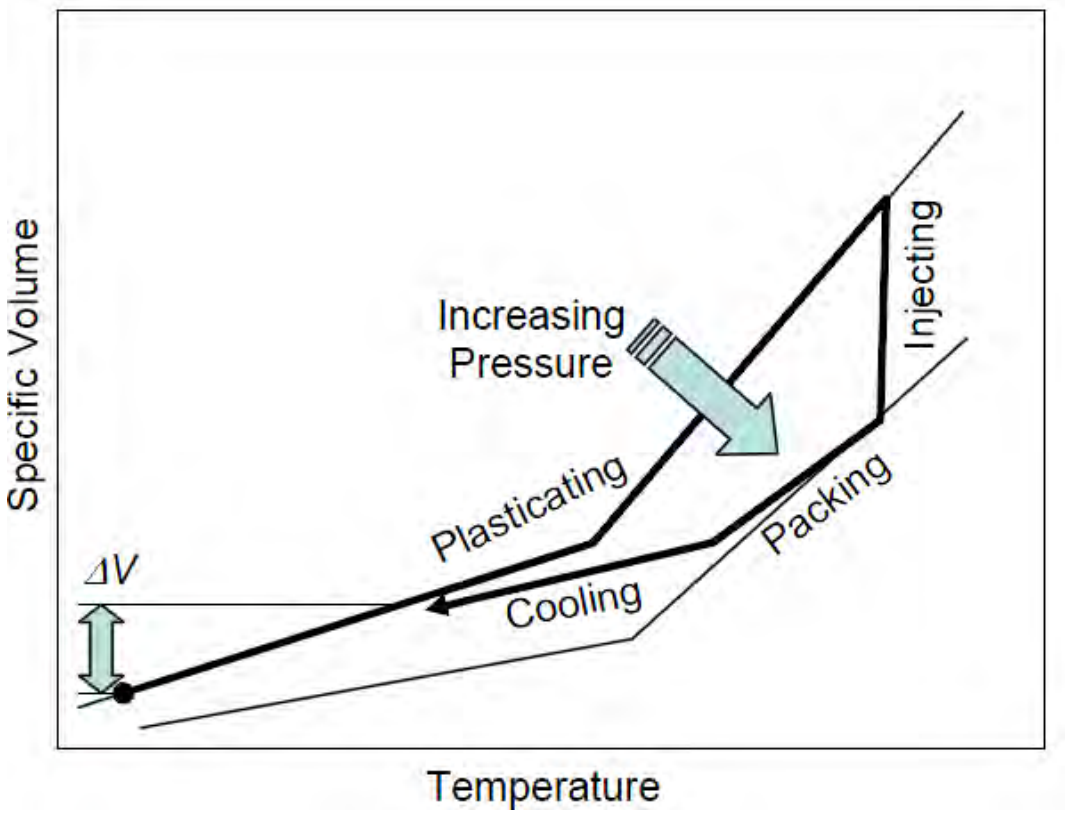

Figure 4.10: Densification of polymer during molding. *(Source: Abbott R. et. al., 2011)*

4.1.5 Rheological properties

In this tab one is able to choose one out of three different viscosity models, which is going to be used in the flow analysis. These are the Cross-WLF viscosity model, the second order viscosity model and the matrix model. The last one can be used only if there are measured data for the specific material. So let's see the equations that describe the first two models:

4.1.5.1 Cross-WLF viscosity model

The *Cross-WLF viscosity model* describes the temperature, shear rate, and pressure dependency of the viscosity. The viscosity model is given by the following equation:

$$\eta = \frac{\eta_0}{1 + \left(\frac{\eta_0 \dot{\gamma}}{\tau^*}\right)^{1-n}}$$

where:

- η is the melt viscosity (Pa-s),
- η_0 is the zero shear viscosity or the 'Newtonian limit', in which the viscosity approaches a constant at very low shear rates,
- $\dot{\gamma}$ is the shear rate (1/s),
- τ^* is the critical stress level at the transition to shear-thinning, determined by curve fitting, and
- n is the power law index in the high shear rate regime, determined by curve fitting.

The zero-shear viscosity is given by the equation:

$$n_0(T, p) = D_1 \cdot \exp[-\frac{A_1(T - T^*)}{A_2 + (T - T^*)}]$$

where:

- T is the temperature (K),
- T^* is a reference temperature, determined by curve fitting of the zero-shear rate viscosity data at various temperatures,
- $A_2 = A_3 + D_3 p$
- p is the pressure (Pa), and
- D_1, A_1, A_3, and D_3 are data-fitted coefficients. D_3 characterizes the linear pressure dependence of T^*(p).

The reference temperature is given by the equation: $T^* = D_2 + D_3 p$, where D_2 is a data-fitted coefficient.

Note: This is the viscosity model that was selected to be used in this study. Melt viscosity determines to a large extent the ability to fill the mold cavity. High viscosity means difficult flow through thin sections and higher injection pressure (DuPont, 2006).

Fitting parameters of the Crastin HR5330HF NC010 material for the Cross-WLF model, as reported by AMI:

n	0.328
τ* (Pa)	157981
D_1 (Pa-s)	5.73855e+009
D_2 (K)	323.15
D_3 (K/Pa)	0
A_1	20.286
A_2 (K)	51.6

The viscosity – shear rate diagram for Crastin HR5330HF NC010 is:

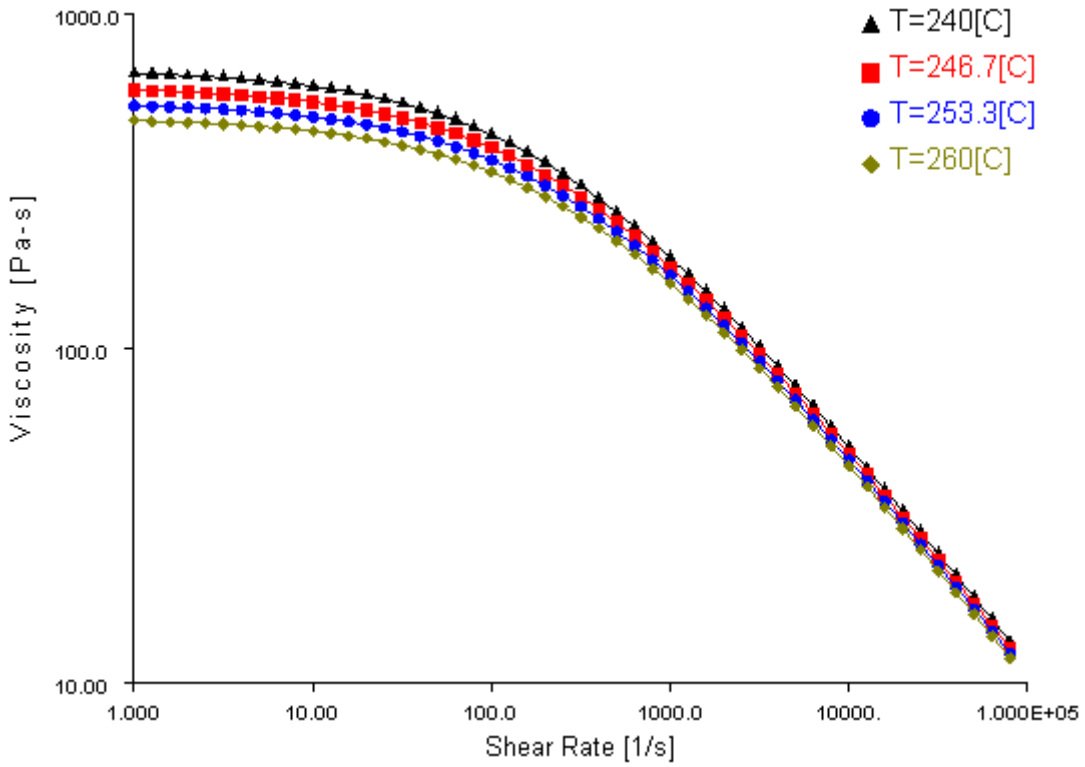

Figure 4.11: Viscosity (Pa-s) vs. shear rate (1/s) plotted diagram, for a temperature range of 240 – 260 °C. Remember that polymer melts are shear-thinning, i.e. the viscosity decreases with increasing shear rates. Many polymers exhibit a Newtonian plateau at low shear rates, a transition region, and then a power law region.

4.1.5.2 Second order viscosity model

The Moldflow *2nd order viscosity model* describes the temperature and shear rate dependence of the viscosity using a quadratic formulation. The viscosity model is given by the following equation:

$$\ln(\eta) = A + B\ln(\dot{\gamma}) + CT + D[\ln(\dot{\gamma})]^2 + E\ln(\dot{\gamma})T + FT^2$$

where:

- η is the viscosity (Pa-s),
- $\dot{\gamma}$ is the shear rate (1/s),
- T is the temperature (°C), and
- and A to F are data-fitted coefficients.

Fitting parameters of the Crastin HR5330HF NC010 material for the 2nd order viscosity model, as reported by AMI:

A	15.717
B	-0.195377
C	-0.0578974
D	-0.0383561
E	0.00117443
F	8.01805e-005
$\dot{\gamma}_{min}$ **(1/s)**	10
$\dot{\gamma}_{max}$ **(1/s)**	1e+006

The viscosity – shear rate diagram for Crastin HR5330HF NC010 is:

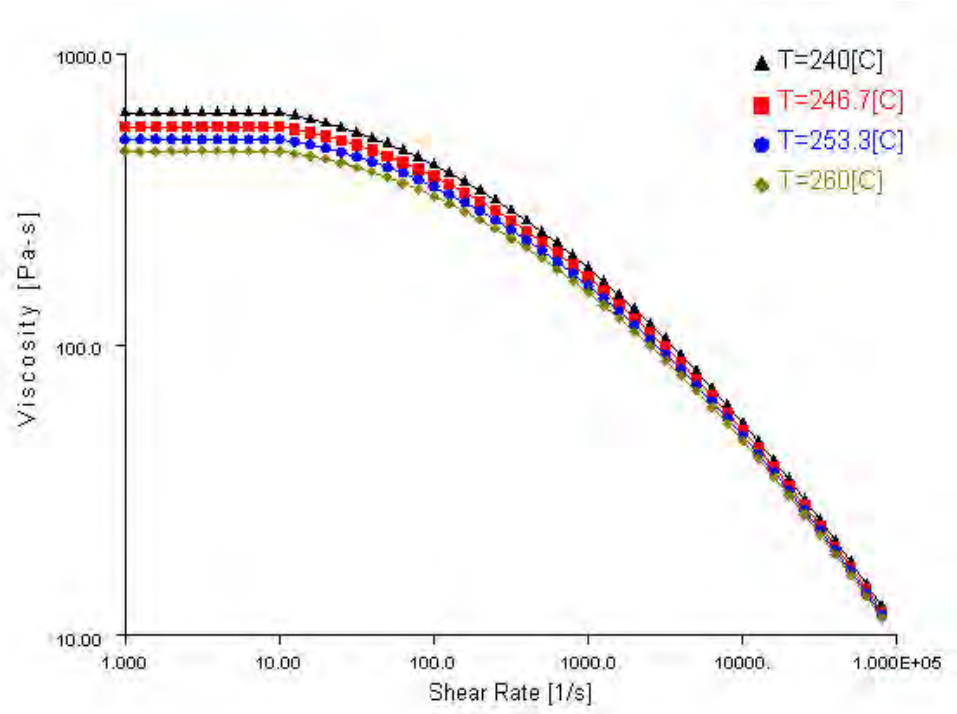

Figure 4.12:

Viscosity (Pa-s) vs. shear rate (1/s) plotted diagram, for a temperature range of 240 – 260 °C.

4.1.5.3 Juncture loss model

A large pressure drop is often observed when the melt passes through contractions in the feed system, such as between the sprue, runners and gates, at the entrance of the die. Typically 85% of the pressure loss occurs at the entrance of the die and 15% at the exit.

Shear viscosity, fluid inertia and extension viscosity also contribute to this juncture loss. The juncture loss model is derived from flow experiments to characterize the pressure drop. The juncture loss model can be used to improve the predictions of pressure and flow balance in the feed system.

The *Juncture loss model* relates the entrance pressure drop, ΔP_e, to the wall shear stress, τ_w, at the contraction.

The overall (measured) pressure drop is defined as:

$$\Delta P_m = \Delta P_e + \Delta P_d + \Delta P_x$$

where:

- ΔP_m is the measured pressure loss,
- ΔP_e is the pressure loss at the entrance junction,
- ΔP_d is the pressure loss through the die, and
- ΔP_x is the pressure loss at the exit junction.

Additional pressure losses are accounted for by relating wall shear stress to pressure drop:

$$\tau_w = \frac{\Delta P - \Delta P_e}{4(\mathrm{L}/\mathrm{D})}$$

where:

- L is the length and
- D is the diameter of the entrance junction.

This can be rewritten as:

$$\Delta P = \Delta P_e + 4\frac{\mathrm{L}}{\mathrm{D}}\tau_w$$

When plotting capillary L/D vs. measured pressure drop, the intercept at $\mathrm{L}/\mathrm{D} = 0$ would be the extra pressure loss and the slope would correspond to $4\tau_w$.

It was found experimentally that the results of the extra pressure losses at various temperatures and shear rates can be collapsed onto a single master curve (for a given generic grade of material), by plotting the extra pressure loss versus the wall shear stress.

The following correlation, originally developed by Munstedt (1978), is used to relate the extra pressure loss to the wall shear stress in the capillary data analysis.

$$\Delta P_e = C_1 {\tau_w}^{C_2}$$

The Bagley correction constants for a material, also known as the juncture loss coefficients, C_1 and C_2, are derived from a series of capillary viscosity experiments with different die lengths. Measurements using different capillary die sizes are made to correct for the juncture losses. The overall pressure drop for each experimental run is simulated using the finite difference simulation and an optimization procedure is used to iterate upon all the WLF model constants, as well as the C_1 and C_2 constants, until the RMS deviation between the predicted and the measured pressure drop is minimized.

A better approach might be to note the range of the coefficients and typical values.

There is a relationship between the coefficients, so as C_1 increases, C_2 decreases. For the Crastin HR5330HF NC010 material the juncture loss method coefficients are:

C_1 = 0.007887 $Pa^{(1-C_2)}$ and C_2 = 1.577.

4.1.5.4 Extension viscosity model

The *Extension viscosity model* describes the dependence of the viscosity on the shear rate, temperature, pressure, and extension rate in a 3D flow. The extension viscosity coefficients are determined by using the shear viscosity model and experimental pressure measurements in convergent flow. The extension viscosity model is given by the following equation:

$$\bar{\eta}(T, p, \dot{\gamma}, \dot{\varepsilon}) = f(\dot{\varepsilon})\eta_S(T, p, \dot{\gamma})$$

where:

- $f(\dot{\varepsilon}) = 1 + \frac{A\dot{\varepsilon}}{B+\dot{\varepsilon}}$
- $\bar{\eta}$ is the unified viscosity (Pa-s),
- η_S is the shear viscosity (Pa-s),
- T is the temperature (K),
- p is the pressure (Pa),
- $\dot{\gamma}$ is the shear rate (1/s),
- $\dot{\varepsilon}$ is the extension rate (1/s), and
- A and B and are data-fitted coefficients.

The coefficient A reflects the importance of extension stresses. The extension stress makes no contribution to the viscosity when the value of B is zero. Valid ranges for A are: min = 0, max = 1e+007, typical = 10. The coefficient B reflects the extension rate of the transition to strong extension stresses. Valid ranges for B are: min = 0, max = 1e+007, typical = 500.

For the Crastin HR5330HF NC010 material the coefficients are:

$$A = 15.5633 \text{ and } B = 23912.7.$$

Note: The extension viscosity model is used only in tetrahedral regions of a 3D Fill+Pack analysis (if this option is selected in the Rheological Properties tab of the Thermoplastics Material dialog). In the case of Midplane and Dual Domain Fill+Pack analysis, as well as for beam elements in a 3D Fill+Pack analysis, pressure loss due to extension stresses are calculated by using the juncture loss model.

In figure 4.13, one can see the rheological properties tab in AMI. The Cross-WLF model is chosen for the analysis, the juncture loss method coefficients are known, as well as the transition temperature ($T_{trans.}$), the Moldflow Viscosity Index (MFI) and the Melt Mass-flow Rate (MFR) values.

- *MFI:* Calculates a single point reference viscosity level (in Pa-s) at the designated temperature and a shear rate of 1000 (1/s). For the material under study the MFI is: VI(250)0169. This means that the material has a viscosity of 169 Pa·s, at a shear rate of 1000 1/sec and T = 250 °C.

- *MFR:* an ISO standard measure which describes how easily a given melt flows. The higher the value the more readily it flows. MFR is identical to the MFI. For the material under study no MFR was given. Probably it wasn't measured. But searching through the properties of Crastin HR5330HF NC010, it was found that:

  Melt volume-flow rate (MVR): 8 cm^3/10 min
  Temperature: 250 °C
  Load: 2.16 kg

  Test Standard:

  ISO 1133

  (Source: CAMPUSplastics)

  In AMI the melt mass-flow rate is needed. But don't forget that the material's melt density is known. This means:

$$MFR = MVR \times \rho_{melt} = 8(cm^3/10\,\text{min}) \times 1.2751(g/cm^3) = 10.2\,g/10\,\text{min}$$

  This is the value that one can see in figure 4.13.

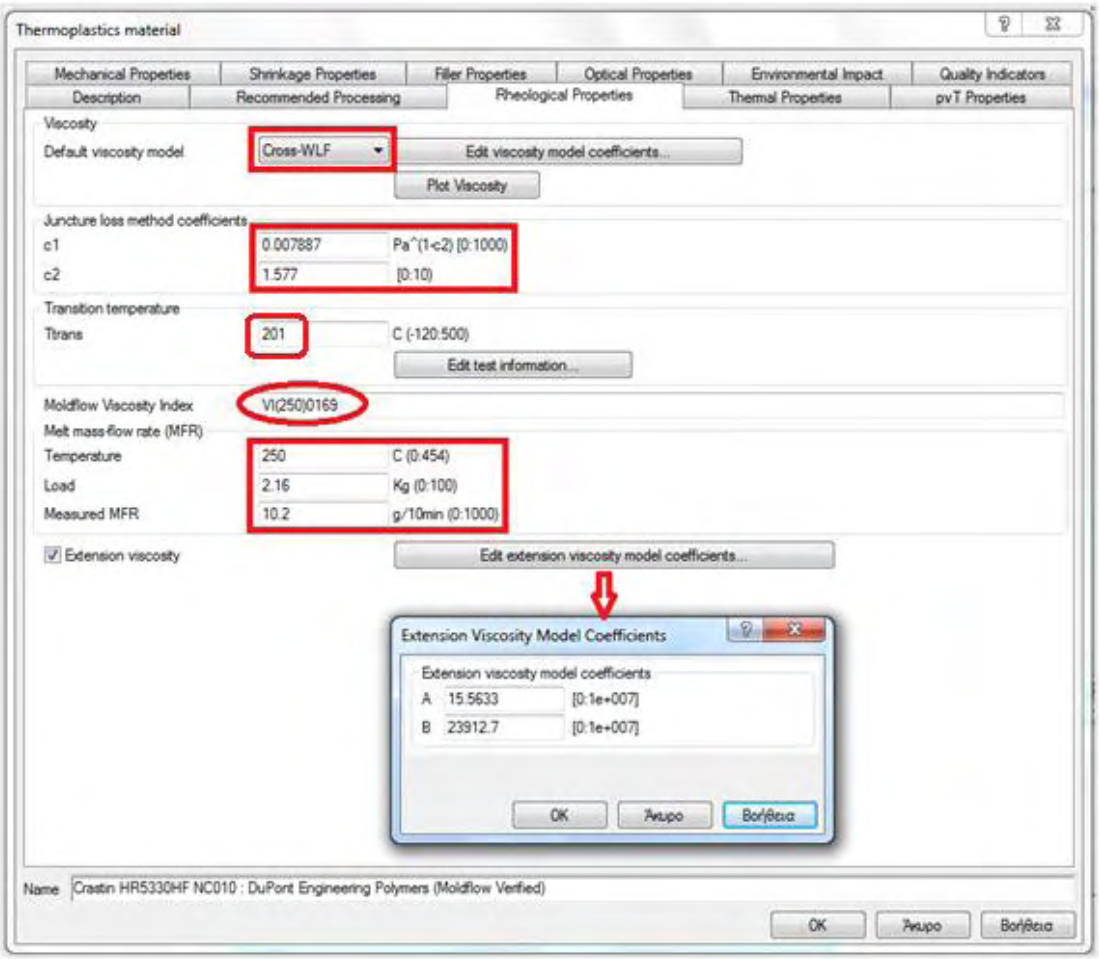

Figure 4.13: Selecting the appropriate viscosity model and adding the MFR information.

4.1.6 Thermal properties

The thermal properties tab of the thermoplastics material dialog is used to specify the thermal properties of a specific thermoplastic. Remember that:

Specific heat (C_p): is the amount of heat required to raise the temperature of a unit mass of material by one degree Centigrade.

Thermal conductivity (k): is the rate of heat transfer by conduction per unit length per degree Celsius.

The behavior of these two properties with the temperature (T), for the semi-crystalline Crastin HR5330HF NC010, is shown in figures 4.14 & 4.15, respectively.

Table 4.3: Specific heat (C_p) over a range of temperatures (T) for Crastin HR5330HF NC010.

T (°C)	**C_p (J/kg-°C)**
51	1213
75	1434
100	1555
120	1633
140	1695
160	1807
168	2201
176	5321
184	2065
190	1729
220	1774
250	1753

The total energy to bring the material up to its molding temperature is given by the area under the curve. Also, because the crystallization process depends on the cooling rate, the crystallization peak shifts to lower temperatures at higher cooling rates. The specific volume of crystalline polymers decreases during crystallization.

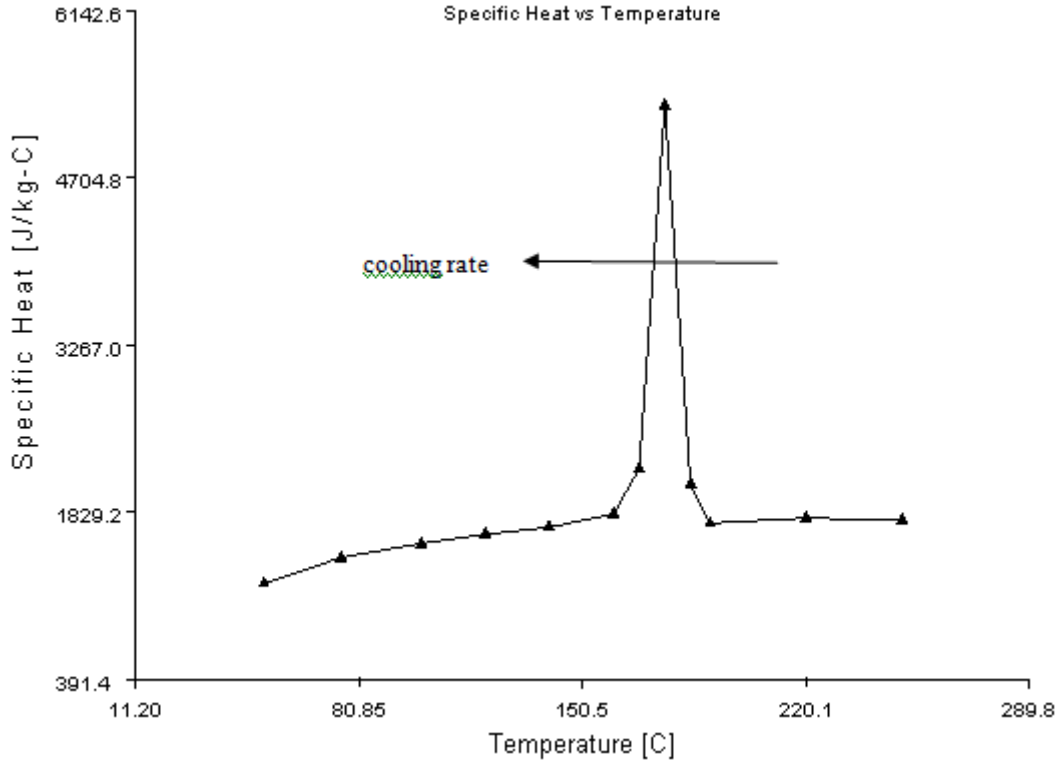

Figure 4.14: Specific heat C_p (J/kg· °C) vs. temperature T (°C). The cooling rate is constant at -0.33 °C/sec (slow cooling rate).

Table 4.4: Thermal conductivity (k) over a range of temperatures (T) for Crastin HR5330HF NC010.

T (°C)	**k (W/m-°C)**
37	0.223
58	0.218
79	0.231
100	0.228
121	0.236
140	0.221
161	0.237
180	0.25
200	0.249
220	0.273
239	0.28
259	0.276

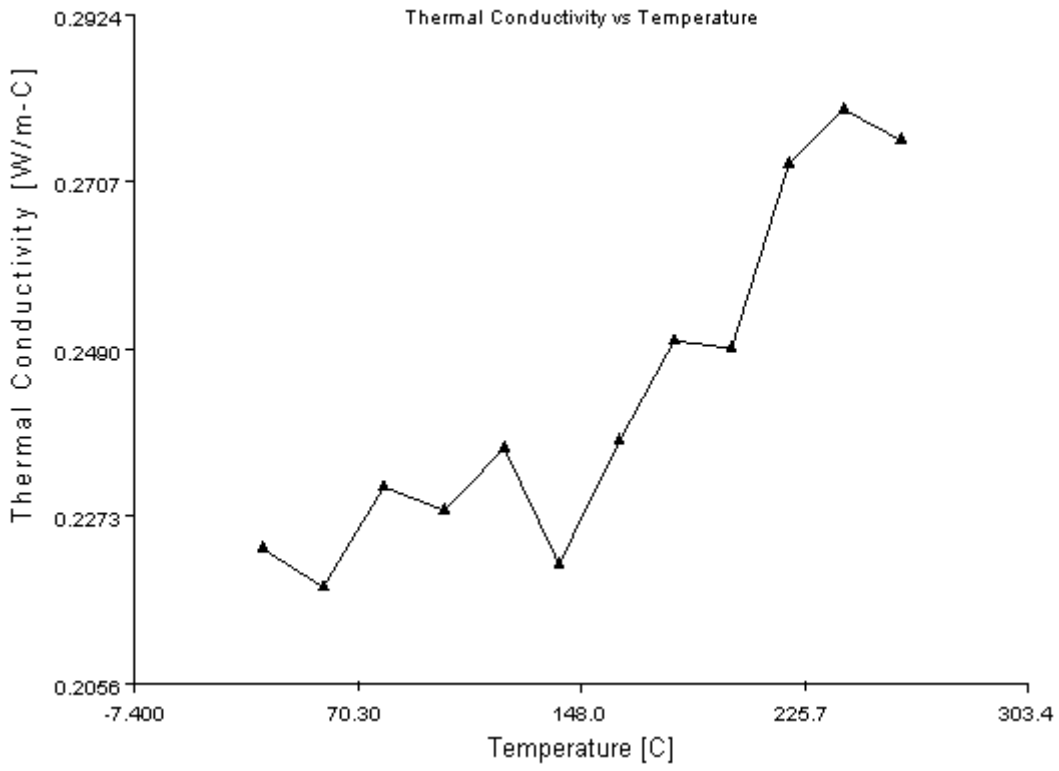

Figure 4.15: Thermal conductivity k (W/m · °C) vs. temperature T (°C).

4.1.7 Filler properties

In this tab one can see the fiber properties of Crastin HR5330HF NC010. In AMI the filler data are common for every short glass fibered material, except those marked in figure. Those must be added manually. All these properties can be changed and become more accurate of course, if a fiber measurement has been previously accomplished. There are different measurement methods, which require an appropriate sample preparation, as well as a variety of special equipment that can be used, such as the optical reflectometer.

Fiber-glass is added to polymer (matrix), when it is necessary to improve their mechanical properties. The reinforcing fiber-glasses may be short or long. Standard fiber-glasses are cylindrical. A typical length of short glass fibers is in the range of 0.2 to 0.5 mm, with an aspect ratio of 10 to 40, and for long glass fibers, 10 to 15 mm. Short fiber reinforced thermoplastics are most commonly used for injection molding.

Crastin HR5330HF NC010 is a 30% w.t. short glass-fibered material. Most commercial composites contain 10% to 50% fibers by weight, which can be regarded as being concentrated suspensions. Considering fibers of diameter (d) and length (L), therefore an aspect ratio (L/d), a fiber concentration by volume or volume fraction (v_f) and a uniform length distribution, a typical concentration classification scale would be:

- Dilute: $v_f < (d/L)^2$
- Semi-concentrated: $(d/L)^2 < v_f < (d/L)$
- Concentrated: $v_f > (d/L)$

The volume fraction of the fibers can be calculated as below:

$$V_g + V_m = V_T$$
$$V_g \cdot \rho_g + V_m \cdot \rho_m = V_T \cdot \rho_T$$

Thus it is:

$$\frac{V_g}{V_T} = v_f = \frac{\rho_T - \rho_m}{\rho_g - \rho_m} = \frac{1.2751 - 1.08}{2.54 - 1.08} = 13.4\% \ ,$$

Where: ρ_T = density of the composite = 1.2751 g/cm^3

ρ_m = density of the matrix = 1.08 g/cm^3

ρ_g = density of the glass-fiber = 2.54 g/cm^3.

Because the matrix density was not known, the value of another unfilled PBT of the same company (DuPont) and same trade name (Crastin) was used.

In a concentrated suspension, the fiber orientation behavior becomes very complex, since both mechanical and hydrodynamic fiber interactions apply. The 30% by weight PBT composite used here, fits into this concentrated regime.

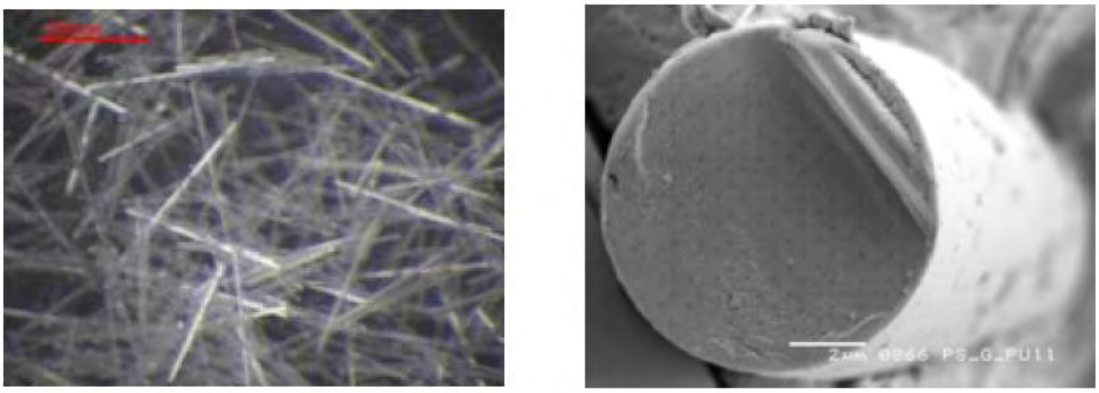

Figure 4.16: Picture of glass fibers (left picture) and a magnified view of one single glass fiber (right picture). *(Source: A. Islam et. al., 2011)*

During the injection molding process fibers are involved in a lot of interaction with machinery. As a result, the initial length of fiber may be reduced dramatically. This is called fiber breakage or fiber attrition. There are softwares that calculate this fiber breakage, but this is not going to be of any concern here. The initial length is assumed as the final fiber length, as no fiber breakage takes place.

Because no measurement has been made for the material used in this study, the values of another similar composite were used. That is the 30% w.t. Valox 420, of Sabic Co. Valox 420 is a short glass fiber reinforced PBT with a crystalline structure, too. From a burn-off process of Valox, the number average fiber length of 949 fibers has been found to be: L = 362.8 ± 5.4 μm and the average measured diameter of 1000 fibers was determined as: d = 12.9 ± 0.05 μm (Vélez-García, 2012). As shown in figure 4.17, for Crastin HR5330HF NC010 a fiber length of 364 μm or 0.364 mm and a diameter of 12.9 μm or 0.0129 mm has been used. This means:

$$\left\{ \begin{array}{l} v_f = 0.134 \\ d / L = 1/28.2 = 0.035 \end{array} \right\} \quad \mathbf{v_f > (d/L)}$$

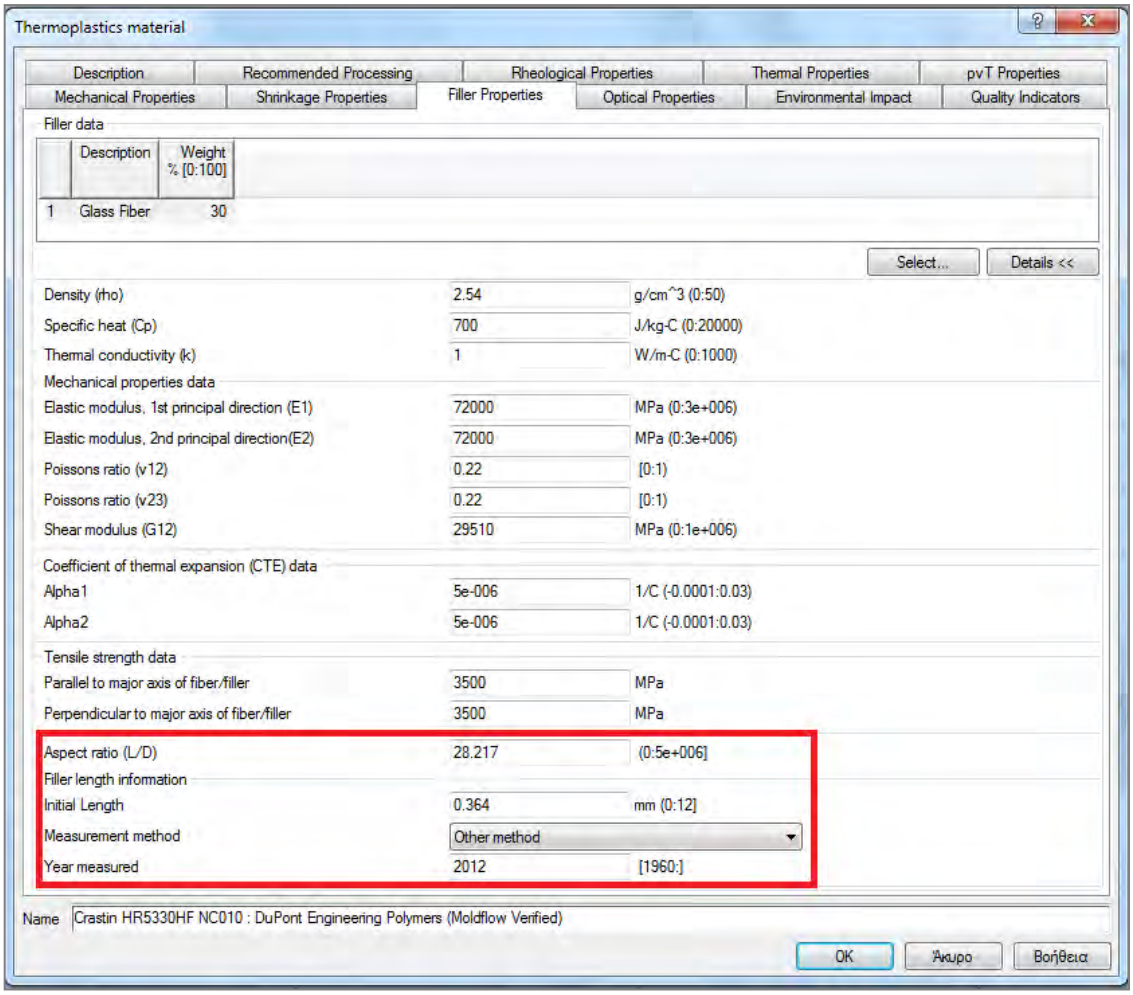

Figure 4.17: The filler data tab in AMI. Properties in the red colored rectangle are those that were added. The rest remained unchanged.

4.2 Process controller dialog

The Process controller dialog is where most control aspects of the processing conditions are specified. Different tabs on this dialog will be visible depending on the molding process and analysis sequence that has been chosen. A Fill + Pack analysis has been run for this study.

Before going into details on how the processing conditions can be modified in AMI, one should understand the importance of the "time" term in injection molding:

Total Cycle Time is the total time required to complete all the stages of an injection molding cycle. In AMI the total cycle time is made up of the following stages:

- *Filling time:* The time required to fill the entire mold with polymer. The injection molding machine controls the velocity (flow rate) of the molten polymer entering the mold, during this stage of the cycle.

- *Packing time:* The stage of the injection molding cycle when pressure is applied to the polymer melt, so as to compress the polymer and force more material into the mold.

  This compensates for the shrinkage that occurs, as the polymer cools from the melt temperature to ambient (room) temperature. From 5 to 25% more material can be added to the mold, during the packing stage. The gate should freeze during the packing time, so as to prevent material from exiting the mold. This time is also known as the *holding time.*

- *Cooling time:* The cooling time is the stage of the injection molding cycle when there is no more pressure being applied to the polymer. The mold is held shut and the polymer continues to cool, until the part can be ejected. The cooling stage is normally the longest part of the molding cycle and can account for up to 80% of the total cycle time. Usually, cooling takes up 40% to 60% of the total cycle time.

- *Mold open time:* The time for which the mold is open before the next molding cycle begins. During this stage, additional heat transfer occurs between the mold and ambient air. Typical mold-open times are 2 to 5 sec. This time includes the following:

  1. Opening the mold,
  2. Ejecting the part
  3. Preparing for the next cycle, such as loading inserts (not always part of the cycle), and
  4. Closing the mold.

Now move to the process controller tab.

4.2.1 Profile/Switch-Over control tab

4.2.1.1 Filling control

In the filling control dialog, one can specify how the filling phase of the analysis will be controlled. There are many options, such as filling control by flow rate, injection time and ram speed profile. In this study, flow rate will control how fast or how slow the material will be injected into the sprue. All simulations were run with a flow rate of 28-29 cm^3/s, so that the cavity would be filled at about 1 sec. Generally, Crastin HR5330HF NC010 requires fast fill rates (PBTs in general solidify fast). Because the center-gated disk is a thin-walled part with rather small dimensions, this injection time is considered medium to fast. For example, an injection time of 0.5 sec would be considered as a fast one. The following equation is an easy way to estimate when the cavity will be completely filled:

$$t_{fill} = \frac{V_{disk}}{\dot{V}}$$

Where: V_{disk} = total volume of the disk = 27.07 (cm^3)

$\dot{V}$ = the volumetric flow rate (cm^3/s).

Ignoring heat transfer, increasing the fill time decreases the required fill pressure.

At the end of filling phase inside the mould, melt is relaxed, i.e. it expands, resulting in filling up of the remaining space in the mould. This causes pressure peak inside the cavity. Fill pressure is a measure of resistance to the flow of melt. Initially, there is no resistance to flow of melt. Resistance increases as the cavity is being filled up. This is seen as pressure rising before switch-over.

4.2.1.2 Velocity/Pressure switch-over

In the velocity/pressure switch-over (V/P) dialog, one can specify the criteria by which the molding machine will switch from velocity control to pressure control. Near the end of the filling stage (before the cavity is completely filled), the process control scheme switches over to pack/hold pressure control. The switch-over is sometimes called velocity to pressure transfer, where velocity refers to injection velocity and pressure to holding pressure.

The switch-over position is the ram position where the filling (injection) stage switches to the post-filling (packing/holding) stage. The cushion distance is the distance from the switch-over position to the farthest position that the end of the screw can reach, as shown in figure 4.18.

Thus, the switch-over position determines the cushion distance. The cushion should contain adequate material for post-filling the part. An insufficient cushion could cause sink marks. The typical cushion distance is about 5 to 10 mm.

Therefore:

- Switching too late can lead to:

a) Mold opening and flashing, due to build up of excessive cavity pressure towards the end of filling (sudden pressure spike),
b) Burn marks as the plastic slams into the end walls of the part, and
c) Damage to molding machine and/or mold as the ram bottoms out.

- Switching too early can lead to:

a) Short shot due to insufficient ram displacement, and
b) Longer cycle times.

In this study a V/P switch-over at 98% volume filled has been set. This means that the process switches from flow-rate control to pack/hold pressure control, exactly when the percentage of the total volume filled exceeds the specified value. Note that the percent of filled volume is the same as the percent of total stroke setting on an injection machine. Typical values are above 95%.

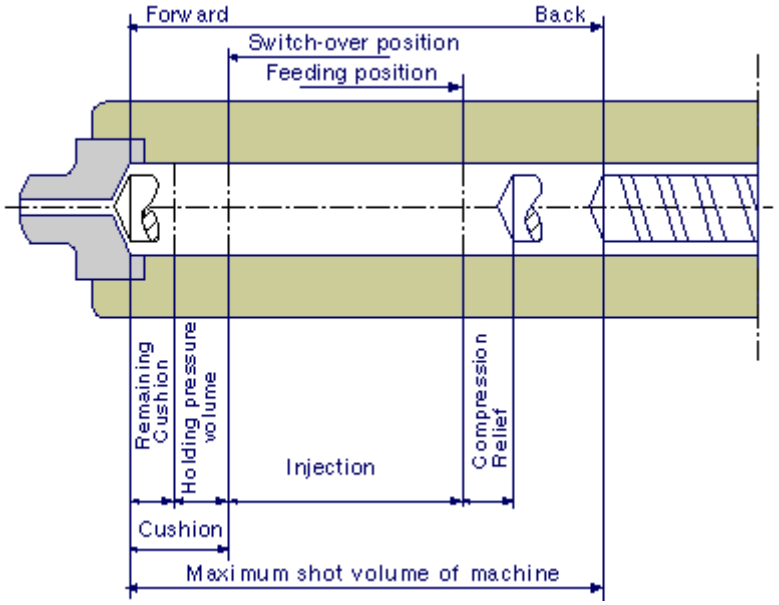

Figure 4.18: Screw positions at various stages. *[8]*

4.2.1.3 Pack/Holding control

Maybe one of the most important procedures in injection molding is the packing time and the packing pressure specification. The efficacy of thermoplastic packing has important effects on warpage, shrinkage, and the incidence of defects, such as sink marks. This is why the description here will be more detailed.

According to DuPont product information data sheet, a typical hold pressure for Crastin HR5330HF NC010 is around 60 MPa and a typical hold pressure time varies from 3 to 4 sec/mm wall thickness. The wall thickness of the disk is 2 mm, so the material's typical holding time is translated to: 6-8 sec. However, this is only a general and theoretical estimation.

In this study, the option 'Packing pressure vs. time' has been selected and the following *constant* packing profile was used:

Duration (sec)	Packing pressure (MPa)
0	50
4	50
0	0

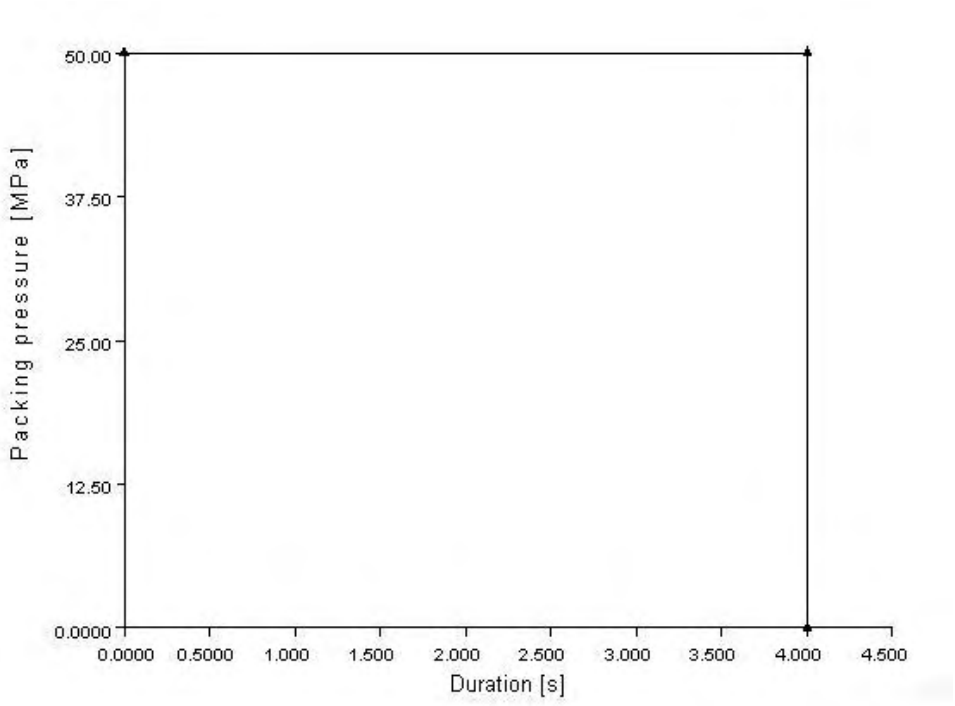

Figure 4.19: The packing pressure (MPa) vs. time (sec) profile that was used in all simulations.

An important aspect of the *packing pressure* is that it cannot be so high, that it exceeds the clamp limit of the injection molding machine. Increasing the packing pressure means increased clamping force. In order to determine the maximum packing pressure that should be used in the analysis, a rough guide is:

$$P_{max} = \frac{F}{A} 100 \times 0.8 MPa$$

where:

- F is the clamp force (tonnes), and
- A is the total projected area of the model (cm²).

The above formula will determine a pressure, assuming a constant gradient across the part, so that 80% of the machine capacity will be used (20% safety factor). This is only a conservative approach, but can be used as a starting point. For the disk it is:

$$P_{\max} = \frac{102(tonnes)}{132.71(cm^2)} \cdot 100 \cdot 0.8 \simeq 61.5 MPa$$

The maximum clamp force of the machine is known and it will be discussed later on. The total projected area of the part has been calculated by AMI automatically (logs dialog).

Generally, one should choose the lowest acceptable holding pressure, as this minimizes the internal stresses in the part and saves material, as well as operating costs. A very high holding pressure can cause excessive residual stresses that could possibly warp the molded part.

Thus, considering the 61.5 MPa as the maximum acceptable packing pressure, simulations were run with pressures below 60 MPa, until the suitable one was eventually found. From the AMI logs, one can read the injection pressure used. In the case of the disk, this pressure was found to be 37 MPa. Thus, the packing pressure was set higher than that, at 50 MPa. A lower pressure could be used, too. However, the 50 MPa pressure was eventually selected, as it gives very satisfying results. It was also noticed that if a packing pressure ≥ 79 MPa is used in the analysis, then the maximum clamp force of the injection molding machine is exceeded.

Generally, a very small packing pressure may cause sink marks. Sink marks are an indentation on the surface of a molded part that usually occur when there is a significant local change in wall thickness. They are mainly caused by thermal contraction (shrinkage) of the melt, during cooling in the mold (figure 4.20). In other words, sinking is caused by the outer skin of plastic solidifying, while the material inside is still molten and viscous. As it cools and solidifies, the material compacts.

The plastic enters the cavity through the gate. As long as the gate is not frozen, the plastic can enter the cavity or leave the cavity. Therefore, the holding pressure must be applied till the gate is frozen. This is where the importance of time factor gets into the picture. If enough time is not given, the following can happen:

A) Enough plastic will not get into the cavity and B) the plastic inside the cavity, which is under high pressure, will come out of the cavity. Thus, it is imperative that the time for which the holding pressure is applied, is enough to freeze the gate of the part.

In order to determine a suitable *packing time*, samples molded with different packing times are weighed and the time after which the weight remains constant is set as the final packing time. As time is increased more and more in the packing phase, material enters the cavity, increasing the weight.

But as soon as the gate is frozen, the plastic cannot continue to enter nor exit the cavity and therefore, the part weight remains constant. This is known as the *gate freeze time or gate seal time*. This is better to be done in a 3D analysis, where one can observe how the part weight changes over time. There is no reason to use a big packing time.

It's best for it to be minimized, so as not to extend the cycle time. The gate's solidification identifies the beginning of the cooling stage, during which most of the material inside the mold solidifies, so that the product shape is consolidated.

Thus, in the 3D simulations (which will be discussed later) all the packing times in the range of 3-8 sec, were used. In all simulations, the packing pressure was kept constant at 50 MPa. The goal was to check after which time the part weight remained constant. The time after which the part weight stopped increasing for the first time was at about 3.5 sec. In other words, this is the gate seal time. Truth is that the packing time was set a bit higher than the gate seal time, to ensure that the gate is frozen during every shot. This will ensure consistency and any small variations will be compensated for.

According to figure 4.21, the ideal packing time seems to be around 3.5 sec. However, packing time was finally set to 4 sec. According to figure 4.22 (using the 'sink marks, index' result), sink marks appear only on the sprue, but not on the disk's surface. For more precision one can use the 'Examine' tool, from the 'Results' tab. Through this option, one can check the exact result values on the surface of the model. Everywhere on the disk this value is zero. If sink marks appear or are found through the 'Examine' tool, then some other parameters should be changed, so as to eliminate them. However, sink marks on the sprue are not considered a problem, because a direct gate is manually trimmed.

The 'sink marks, index' result indicates the likely presence and location of sink marks (and voids) in the part. Keep in mind that sometimes negative values may appear. This means overpacking in some area of the part.

Note: Overpacking occurs when the easiest (shortest/thickest) flow paths fill first. Once this flow path has filled, it will still be under pressure as extra plastic is injected into the cavity to fill the remaining flow paths. This pressure will push more material into the already full flow path, causing it to have a higher density and lower shrinkage than other regions. The overpacked fill path will have frozen under pressure, so stresses will be frozen in.

If the sink marks index is high, then it is possibly because a significant portion of the melt is freezing under zero or low pressure. The larger the volume that freezes under low pressure, the higher the sink marks, index and the greater the likelihood of a sink mark. When the local pressure has decayed to zero, during the packing and cooling stage, the 'sink marks, index' for the part is calculated as follows:

$$S = \frac{(x^+ - x^-)\cdot\rho_\delta(T_{trans}P_{atm}) - \int_{x^-}^{x^+}\rho(z)dz}{2h\cdot\rho_\delta(T_{trans}P_{atm})}$$

where:

$T_{trans.}$ = the transition temperature of the polymer (201 ^{o}C),
x^{+} = the upper interfacial location where the temperature of the polymer is at the b_5 value in the 2-domain Tait pvT model,
x^{-} = the lower interfacial location,
ρ_{δ} = the solid density of the polymer,
P_{atm} = the atmospheric pressure, and
h = the half-gap thickness.

Figure 4.20: Notice the sink marks (a local surface depression, like dimples) on the surface of a part. *[9]*

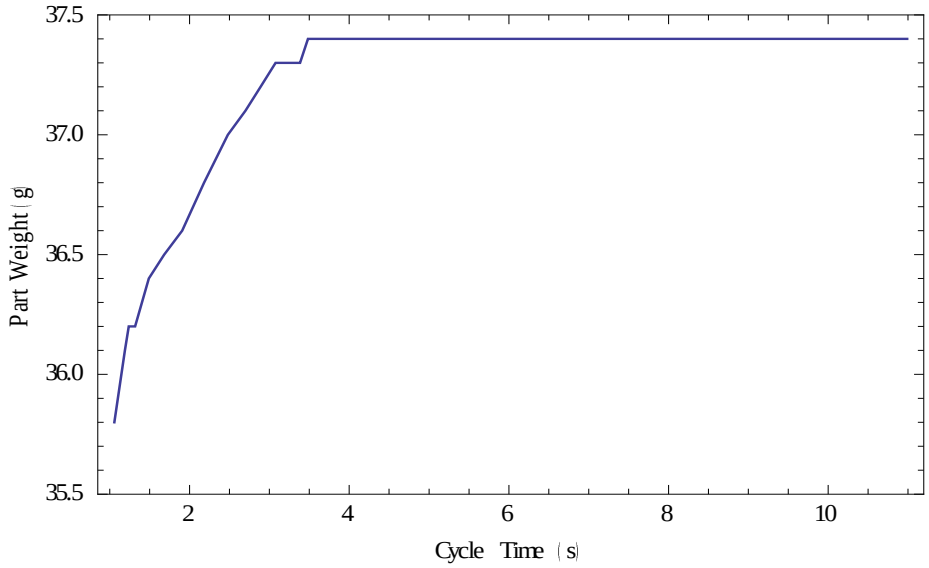

Figure 4.21: The part's weight behavior (g) vs. cycle time (sec), for a packing pressure of 50 MPa and packing time of 4 sec. Notice that the curve starts at 1 sec time. That is right after the disk has been completely filled.

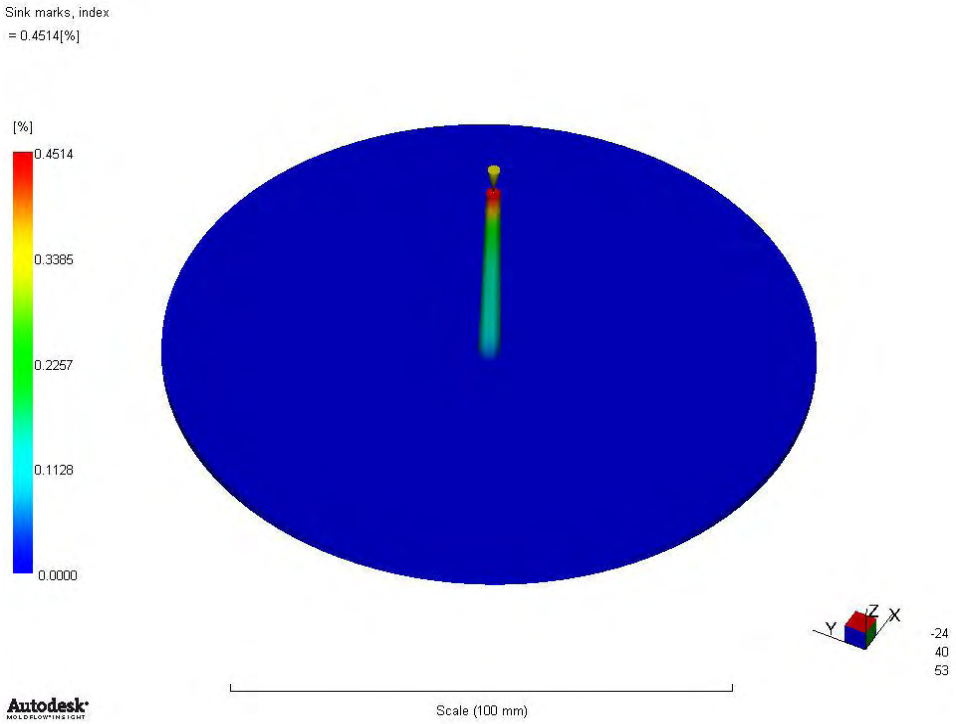

Figure 4.22: Sink marks for a packing time of 4 sec. Packing pressure was held constant at 50 MPa.

As far as shrinkage is concerned, the size and the geometry of the part, as well as the type of material used, will determine the range of shrinkage. Larger parts will normally have a larger acceptable range of shrinkage. Because warpage is caused by a variation in shrinkage, the volumetric shrinkage of a part influences both the potential warpage and dimensional stability of a part. If a part shrinks uniformly (ideal case), it changes in size, but injection molded plastics usually do not shrink uniformly. The amount of warpage is reduced, when the volumetric shrinkage is minimized.

With a typical part, dimensions are smaller and incidences of sink marks and voids near the end of fill are higher. Alternatively, the opposite is true near the gate, where one can expect larger dimensions, and fewer and smaller sink marks and voids, which is due to the amount of packing. Typically, the area around the gate is packed much better than the end of fill. This variation in shrinkage between the end of fill and the gate area can cause warpage. A small distribution in shrinkage across the part causes the properties across the part to become more uniform.

Uniform volumetric shrinkage requires the pressure in the cavity to be controlled. Volumetric shrinkage is a function of the pressure on the plastic when it freezes off; the higher the pressure, the lower the shrinkage. Normally, there is a wide variation in shrinkage across the part, because of the high pressure gradient.

The viscosity of plastic is high, so the resulting pressure gradient prevents the area near the end of fill from having a pressure equal to the pressure around the gate; therefore, the shrinkage at the edge of the part (far from the gate) is normally higher than around the gate.

The amount of shrinkage can be controlled if the pressure is lowered over time, during the packing phase of the cycle. This can be done after areas at the end of fill have frozen off, and while areas closer to the gate are still cooling. The freeze front is moving from the end of fill towards the gate, so the lower pressure near the gate results in shrinkage similar to the shrinkage near the end of fill.

Three figures are shown below. Each one depicts the average volumetric shrinkage (the average value of volumetric shrinkage over the half-gap thickness for 3D models) at the end of cycle, for three different packing pressures. Goal was to check the effect of pressure increase on the shrinkage of the part. The packing time was set at 4 sec for all three figures (4.23, 4.24 & 4.25).

Volumetric shrinkage calculations begin once the cavity is filled, based on the difference between the current pvT state and the reference state:

$$VS(t) = \frac{AD(t)}{D(T_{ambient}, p_{atm})}$$

where:

- *VS* is the volumetric shrinkage,
- *AD* is the average density,
- *D* is the density, and
- the pressure p is zero and temperature T is the specified ambient temperature (23^{o}C here).

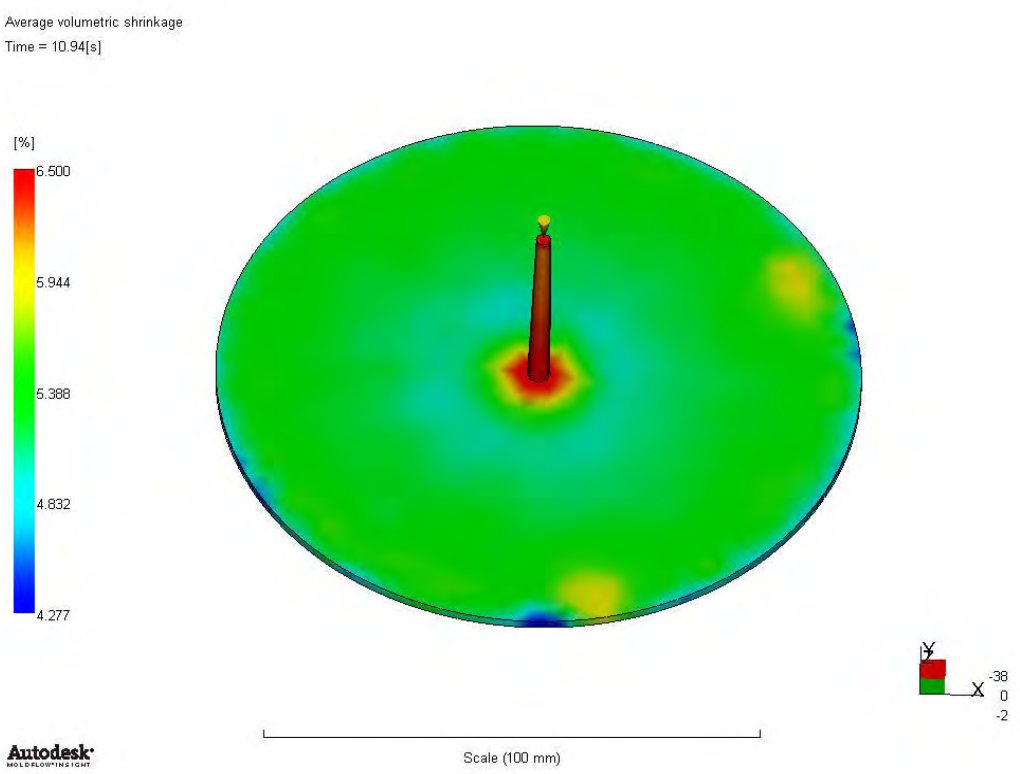

Figure 4.23: Average volumetric shrinkage for $P_{packing}$ = 40 MPa. (Scale range: 4.277 - 6.5%).

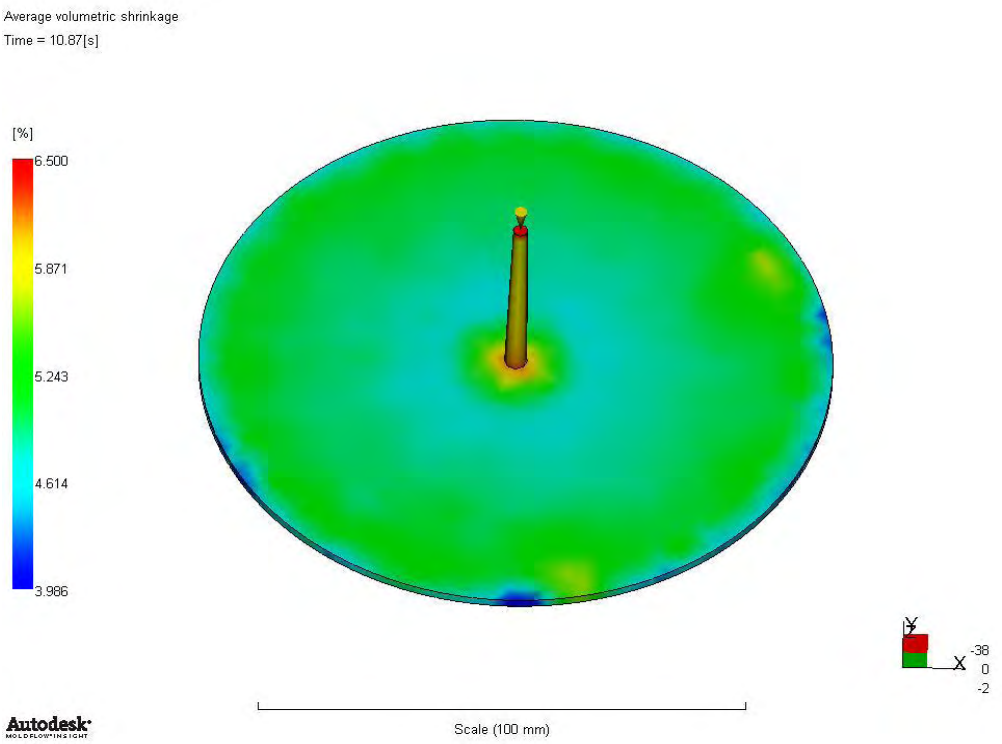

Figure 4.24: Average volumetric shrinkage for $P_{packing}$ = 50 MPa. (Scale range: 3.986 - 6.5%).

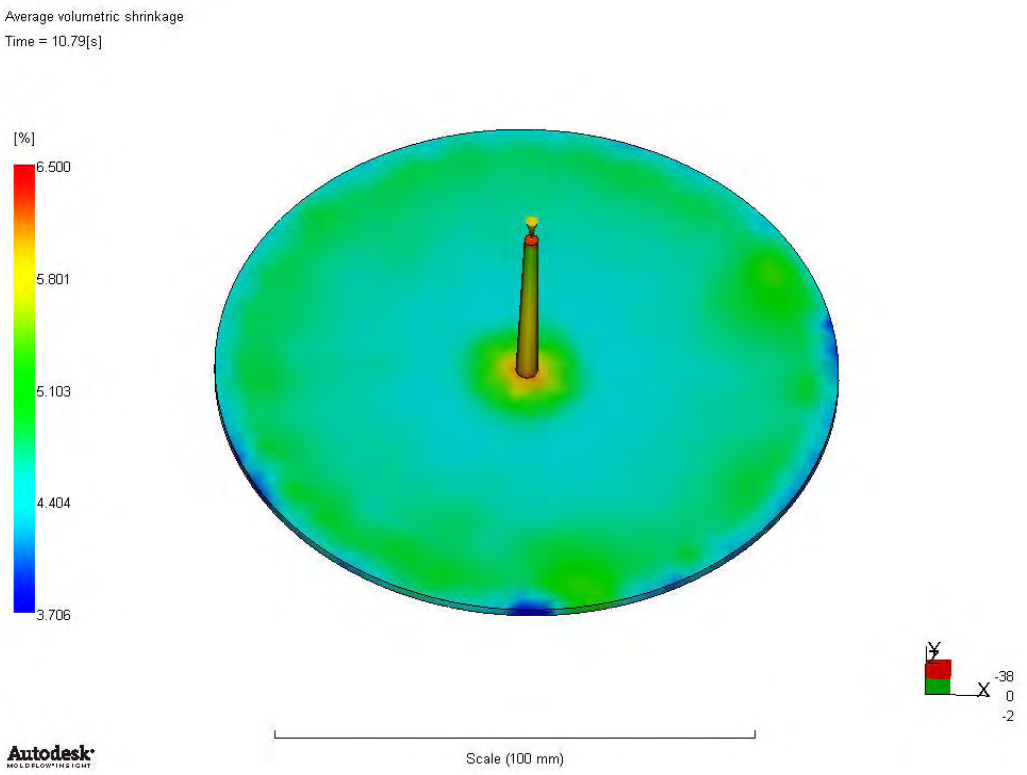

Figure 4.25: Average volumetric shrinkage for $P_{packing}$ = 60 MPa. (Scale range: 3.706 - 6.5%).

It is obvious that as the packing pressure increases, the volumetric shrinkage decreases. In figure 4.23, notice how the green color covers almost the whole top surface of the disk and that the shrinkage close to the base of the sprue is very high (red color). Also, notice that the shrinkage is nearly uniform. Now check how a pressure increase of 10 and 20 MPa, affects the shrinkage in the same regions. The green color seems to become less dominant. In figure 4.25, the green color has almost 'vanished' and blue becomes more visible on the surface of the part. Shrinkage has dropped from about 5.4% down to 4.5%. The only area, at which the shrinkage seems not to have been reduced enough, is that very close to the sprue gate. However, even there it has decreased from 6.5% to 5.8%.

Generally, excessive shrinkage can be caused by a number of factors such as:

- Low injection pressure
- Short pack-hold time or cooling time
- High melt temperature
- High mold temperature
- Low holding pressure

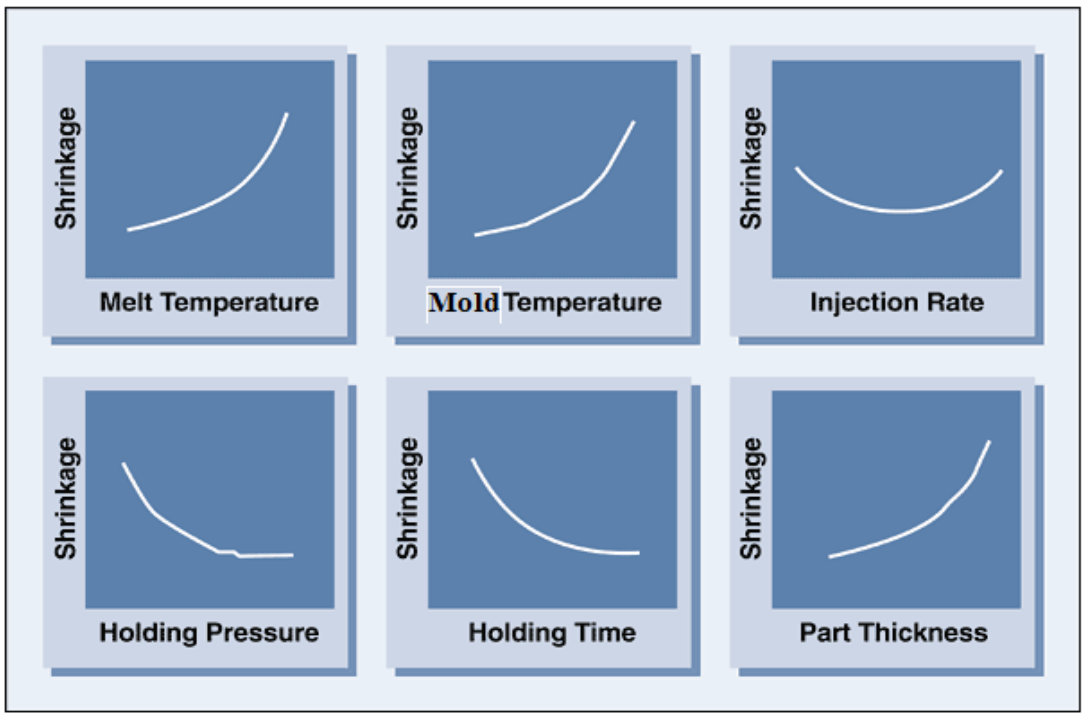

Figure 4.26: Processing and design parameters that affect part shrinkage. *(Source: DSM Engineering Plastics, 2005)*

4.2.2 Temperature control tab

The Temperature Control tab of the Process controller dialog is used to specify default values for temperature control related inputs of a thermoplastics analysis.

Choose the “Uniform” option for the ‘Mold temperature control’ box. This will specify a single mold temperature value for both halves of the mold. Then assign a value of 80 °C and 250 °C in the ‘Mold surface temperature’ and ‘Melt temperature’ box, respectively. This will specify the temperature of the mold at the plastic-metal interface, where the plastic touches the mold and the temperature of the molten plastic, as it starts to flow into the cavity, respectively. At a lower melt temperature, fill pressure is higher on account of higher melt viscosity. Also, one should define the ambient temperature. In this study, a temperature of 23 °C has been selected.

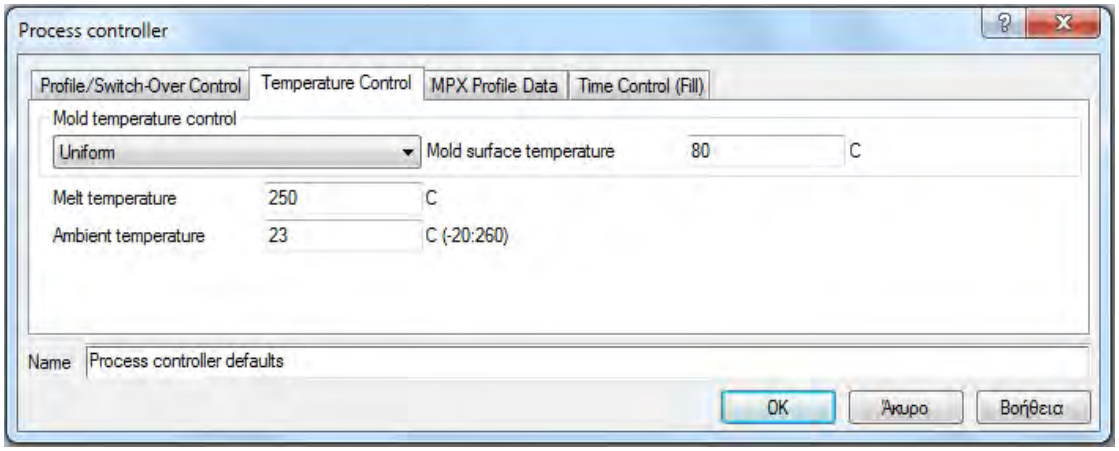

Figure 4.27: The temperature control dialog in AMI.

Note: Remember that the following constant mold surface temperature profile was specified at the very start. This profile will *override* the values set in the process settings dialogs.

Time (sec)	Temperature (°C)
0	80
10000	80

4.2.3 Time control (fill) tab

The Time Control (Fill) tab of the Process controller dialog is used to specify default values for cycle time related inputs of a thermoplastics fill (filling phase only) analysis.

The mold-open time specifies the time takes from the completion of one molding cycle, to the beginning of the next. In this study, it has been set at 4 sec.

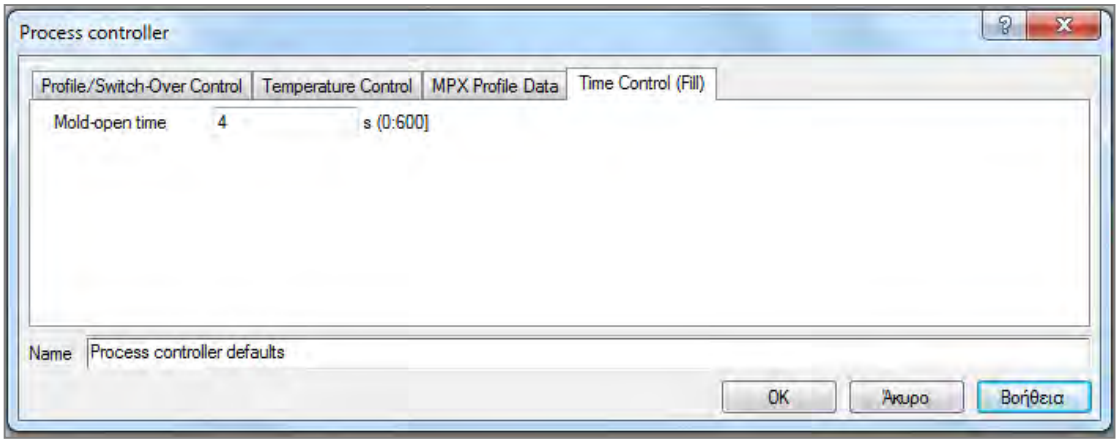

Figure 4.28: The time control dialog in AMI.

4.3 Injection Molding Machine Dialog

Here one can choose the appropriate injection molding machine (IMM) for the analysis. There is a variety of different machines, each one with different capabilities. Some simple criteria, on which the IMM selection should be made, are the following:

a) One of the first things to do is check its clamping force capability (tonnes) and ensure that it satisfies the analysis. An easy and fast way to do so, is by multiplying the maximum pressure in the cavity with the total projected area. In the case of the disk, the projected area (before running the analysis) can be roughly calculated as: $A = \pi \cdot R^2$. So if a packing pressure of 60 MPa is used for example, then the clamping force will approximately be:

$60\ \text{MPa} = 60000\ \text{kPa} = 60000 \cdot 0.102\ \text{ton/m}^2 = 6120\ \text{ton/m}^2$

$1\ \text{ton} = 0.907\ \text{tonne}$

$A_{disk} = 3.14 \cdot (65\ \text{mm})^2 = 13266.5\ \text{mm}^2 = 0.013\ \text{m}^2$

$F_{clamp} = 6120\ (\text{ton/m}^2) \cdot 0{,}013\ (\text{m}^2) = 81.2\ \text{ton or } 73.6\ \text{tonnes}.$

Thus, an IMM with a clamping force higher than about 75 tonnes must be selected.

b) Also, one should check the maximum flow rate of the machine, so as to ensure that both high and low injection times can be achieved. As mentioned earlier, in this study the filling time will be 1 sec. Thus, the selected IMM should be able to provide a volumetric flow rate, such that the specified injection time can be achieved.

c) The maximum shot weight of the injection unit is the amount of plastic that can be injected per shot. Usually, the weight of the molding should not exceed the 70% of the maximum shot weight. The total mass of the disk is approximately 38.1 g.

The molding machine selected for this study has a capability of shooting 3.5 oz (99.2 g). This means that the weight of the part should be less than 69.4 g.

The 112 ton injection molding machine chosen for this study is known as: Cadence 110-310 (Manufacturer: Van Dorn Demag). Figure 4.29 describes the IMM's capabilities.

Note: If one or more of the maximum machine capability constraints are reached in the simulation, the program provides a warning message or adjusts the calculation so these maximum machine capability constraints are not exceeded. In any case, ensure that the option 'Do NOT exceed maximum clamp force' is activated.

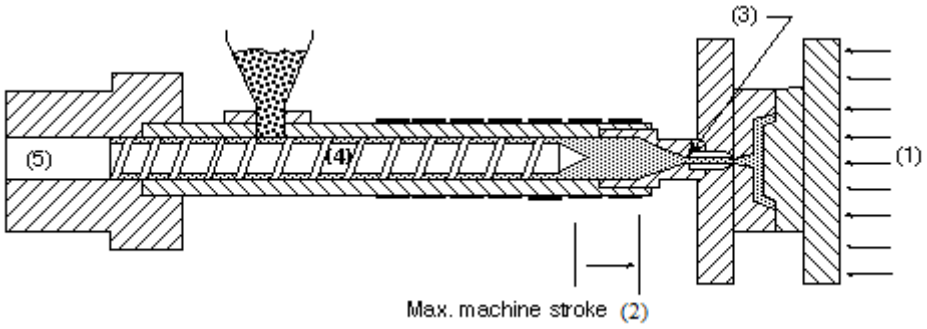

Figure 4.29: Machine capability constraints. *[10]*

(1): Maximum clamp force: approximately 102 tonnes

(2): Maximum injection stroke: 150 mm

(3): Maximum injection pressure: 275 MPa

(4): Maximum injection rate: 175 cm^3/s & Screw diameter: 30 mm

(5) Hydraulic response time: 0.2 sec

General note: The clamp force is the maximum force required to keep the mold closed. The calculated maximum clamp force is a function of the injection pressure and the projected area of the part. The projected area is the area of the model that is projected onto the XY plane. For the clamp force calculations to be correct, the model must be positioned, so that the *clamp force is applied along the +Z axis direction*, as shown in figure 4.30. All solver calculations in AMI are based on the Z direction. This is why it was important remembering the original plane the model was designed on (Inventor Fusion).

The maximum force required to hold the mold closed, is calculated by finding the integral pressure over the projected area of the cavity. That is, the area is divided into small segments, and the pressure is calculated for each of the small segments. The total clamp force is the sum of the products of each of these pressure and area components:

$$F_{clamp} = \sum_{1}^{n} P \cdot A$$

where:

- n= the number of segments into which the total area is divided,
- A= the area of each segment, and
- P= the average pressure at each segment.

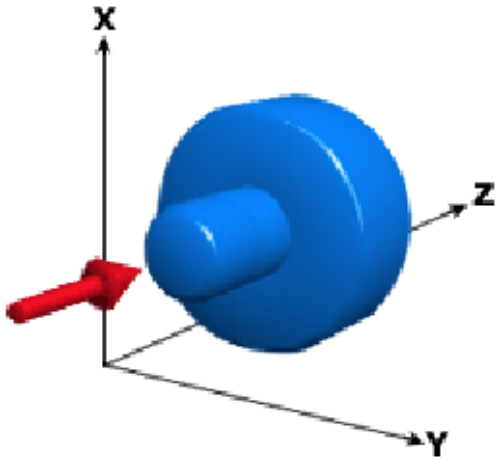

Figure 4.30:

If the model is not oriented so that the clamp force is in the +Z direction, then the model must be rotated so it is.

4.4 Mold Material Dialog

Different characteristics and performances identify steels. As an example, higher hardness of steel improves wear, dent, and scratch resistance and polishability, but lowers machinability and weldability. High sulfur content degrades the stainless qualities and polishability of the steel. Hardness, as a measure of the internal state of stress of the steel, has an adverse effect on weldability, fracture toughness and dimensional stability.

In this study, the *420SS tool steel* has been selected. It is a high-quality stainless steel containing 13% chromium, 0.5% carbon, 1% silicon, 1% manganese and 0.03% sulfur. It offers very good dimensional stability in heat treatment, machinability and polishability. Its characteristics also include high toughness, high nitriding ability and corrosion resistance. The 420SS tool steel is a good choice in the manufacturing of medical, electronic and food processing products that require a combination of both corrosion and wear resistance. It is most commonly used at a hardness of 30 to 35 Rc. It is excellent for large cavities and cores that require a good polished finish and corrosion resistance, too. Its properties are shown in table 4.5.

Table 4.5: Properties of the 420SS tool steel used in AMI.

Mold density (g/cm^3)	7.73
Mold specific heat (J/kg-°C)	462
Mold thermal conductivity (W/m-°C)	25
Elastic modulus (GPa)	200
Poissons ratio	0.29
Mold coefficient of thermal expansion (1/°C)	1.03e-5

4.5 Solver Parameters Dialog

In the thermoplastics injection molding solver parameters (dual domain) dialog are included six tabs in total. There are the Mesh/Boundary, the Intermediate Output, the Convergence, the Fiber Analysis, the Restart and the Core Shift tabs. Only the first four will be of interest here.

4.5.1 Mesh/Boundary tab

The Mesh/Boundary tab is only available for Midplane and Dual Domain analysis types. The Mesh tab is available for the 3D mesh type. The inputs available for edit depend on the molding process that has been selected.

From the 'Number of laminae across thickness' box choose the maximum option (20 laminae). This defines the number of divisions that the plastic cross-section is broken into. The number of laminaes across thickness determines the computational intensity of the analysis. If symmetric thermal boundary conditions exist, the Fill+Pack analysis uses a half-gap calculation and the actual number of laminae used in the calculations is one-half of that specified. In the disk's case, a symmetric thermal boundary condition does exist, so actually 10 laminaes will be used.

From the 'Mold-melt heat transfer coefficient (HTC)' box choose the default values. The HTC option defines the heat transfer at the interface between the melt and the mold wall, which models the associated heat resistance. If the HTC is zero, there is no heat exchange between the melt and the mold walls. If the HTC nears infinity, then there is a perfect thermal contact between the two. In figure 4.31, one can see the values that are going to be used during the analysis. During the filling phase, the HTC is 5000 $W/m^2 \cdot °C$, then during packing it drops to 2500 $W/m^2 \cdot °C$. Finally, during the cooling phase, when the pressure has dropped to zero (the part detaches from the mold wall) the HTC is decreased to 1250 $W/m^2 \cdot °C$.

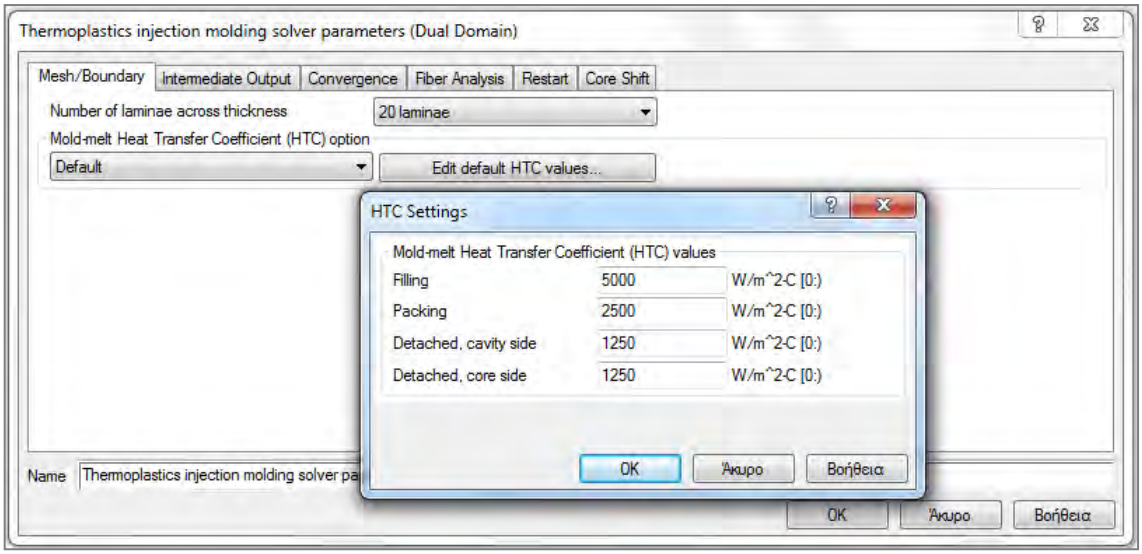

Figure 4.31: The Mesh/Boundary tab in AMI.

4.5.2 Intermediate Output tab

This dialog is used to specify how often intermediate result files will be written.

In the 'Dynamically update results display during analysis' box choose the 'yes' option. This will update the results display every time the solver delivers a new set of intermediate results.

The settings in the 'Filling/packing phase intermediate results' dialog are used to specify the times during the filling phase, or packing phase, at which the solver outputs regular and/or profiled intermediate results. Regular intermediate results are used in the animation of contour results over time and in the display of XY plots of a variable against time. Profiled intermediate results are used in the display or animation of certain results as a function of normalized thickness, that is, through the thickness of the part. In the 'Profiled results' dialog (filling phase), the '20 profiled results' option is selected, as shown in figure 4.32. This will instruct the solver to output a fixed number of sets of intermediate results, at regularly spaced intervals.

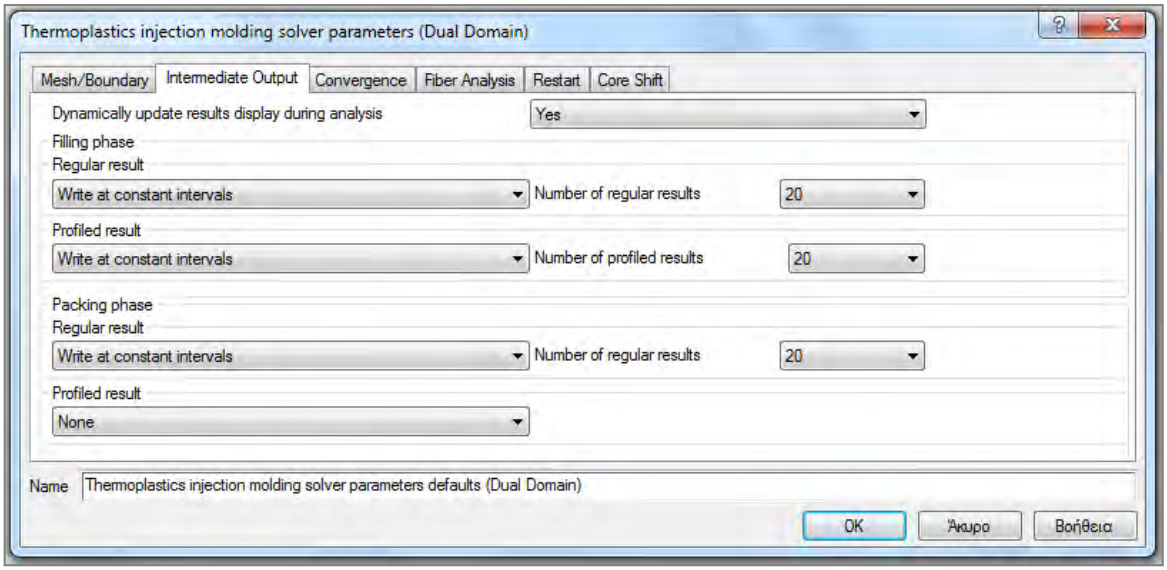

Figure 4.32: The Intermediate Output tab in AMI.

4.5.3 Convergence tab

This tab is used to specify the solver's convergence values.

- *Flow rate - Melt temperature convergence tolerance*: convergence tolerances apply to the % change in a function value from one iteration to the next and are used to identify when a solution has converged. As soon as this % change value falls below the convergence tolerance, the solution has converged. Choose the 'Tight' option for better analysis.

- *Maximum number of flow rate – melt temperature iterations*: specifies the maximum number of iterations that the program will perform in order to solve the flow rate and melt temperature equations. This will continue until either the maximum number of iterations has been surpassed, or the error limit is less than the specified value. Choose the '250 and 400' options, respectively. These are the maximum number of iterations.

- *Nodal growth mechanism*: the nodal growth scheme controls the size of each flow front advancement step taken in a Dual Domain Flow analysis. Choose the 'Single' option. This allows only a single band of elements to fill each time step and will increase the accuracy of the fill pattern prediction.

- *Viscosity treatment at high shear rates*: for certain materials with high temperature or shear sensitivity, extrapolation of viscosity values to high shear rates may introduce instability in the flow calculations. This option relates to a corrective algorithm that eliminates the instability at high shear rates. For the material used in this study, the 'Do not apply' option has been selected.

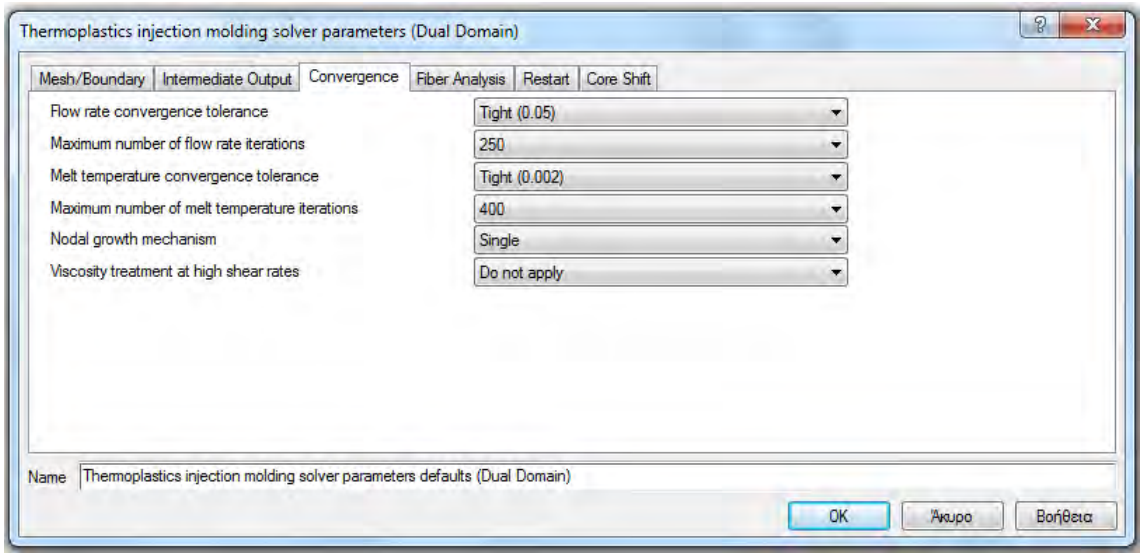

Figure 4.33: The Convergence tab in AMI.

4.5.4 Fiber Analysis tab

This tab is used to specify values for a fiber orientation analysis.

- *Calculate fiber orientation using*: here one can choose the model used by the midplane/dual domain fiber analysis solver to calculate the fiber orientation in the model. As already mentioned, the RSC model (for short fiber-filled materials) is going to be used. One can specify two different parameters here:

  - The coefficient of interaction (Ci): an empirical constant that characterizes the effect of fiber-fiber interaction in concentrated suspensions.

  - Reduced strain closure factor (RSC): a scalar, phenomenological parameter which is used to model slow fiber orientation dynamics (when an option that includes the RSC model is selected to calculate fiber orientation). Again use the default value for now.

AMI will automatically assign values to both the Ci and RSC parameter in a dual domain analysis. Specifically the values 0.0077 and 0.05 were assigned, respectively.

- *Apply fiber inlet condition at*: this option specifies whether the fiber orientation calculation begins at the part gate or at the injection location. For short fiber reinforced materials, the fiber inlet condition is very important and can change the results significantly (when a fiber analysis is studied). One can choose between two options:

  - Gate: the fiber orientation calculation begins at the gate (entrance to the cavity), even if the model includes a runner system.

- Injection location: the fiber orientation calculation begins at the injection location, i.e. the top of the sprue, in the case of a center-gated disk.

- *Fiber inlet condition*: this option specifies the inlet boundary condition of the fiber orientation state. The 'fibers aligned at skin/random at core' and 'fibers aligned at skin/transverse at core' options are available.

  Note that in this study the following combination was used:

Fiber inlet condition at:	Fiber inlet condition:
Injection location	Fibers aligned at skin / transverse at core

- *Edge boundary condition*: this will affect the way that fiber alignment is calculated in elements along the edge of the part. Choose the 'Fibers align along edge' option. For short glass-fiber (SGF) composites, because of the strong influence of radial shear gradients near the center-gated disk mold walls, fibers there tend to be aligned in the flow direction.

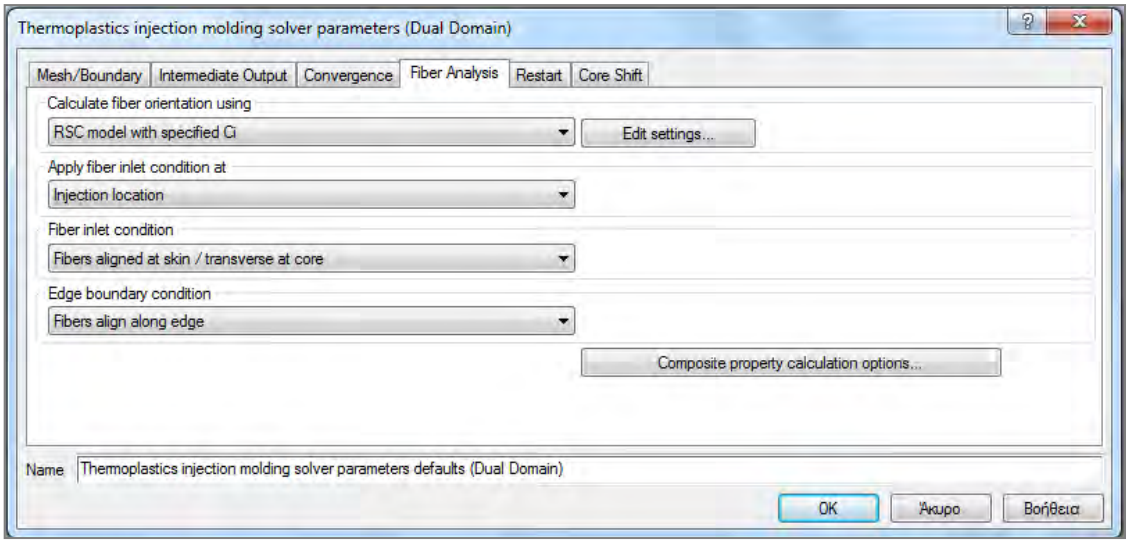

Figure 4.34: The Fiber Analysis tab in AMI.

4.6 Cooling Time Dialog

The plastic starts to cool down as soon as it hits the walls of the mold. Once the holding time is over, the cooling time begins. The mold remains closed till the end of the cooling time. The mold then opens and the part is ejected. Before the mold opens, the part must reach the ejection temperature of the plastic. If the part is ejected before it reaches ejection temperature, the part is too soft and will get deformed during ejection. Excessive cooling time is only a waste of machine time and therefore, profits. Cooling time should also be set such that the part dimensions remain consistent and the process is capable.

Determination of the right cooling time can get complicated. With parts with thick sections, it is difficult to measure the internal temperature in the center of the thickest section. In some parts of the mold, it is difficult to get enough cooling, so cooling times have to be increased to increase the heat transfer. In some cases, the mold temperature can stabilize after as long as a couple hours. Shrinkage can also be influenced by changes in cooling times.

The cooling time option in AMI is directly accessed through the 'Process Settings' dialog. Both in a dual domain and a 3D mesh one can give a specified value of the cooling time or let AMI calculate it automatically. Therefore:

- *Automatic calculation*:

When the automatic calculation is selected, the following window appears:

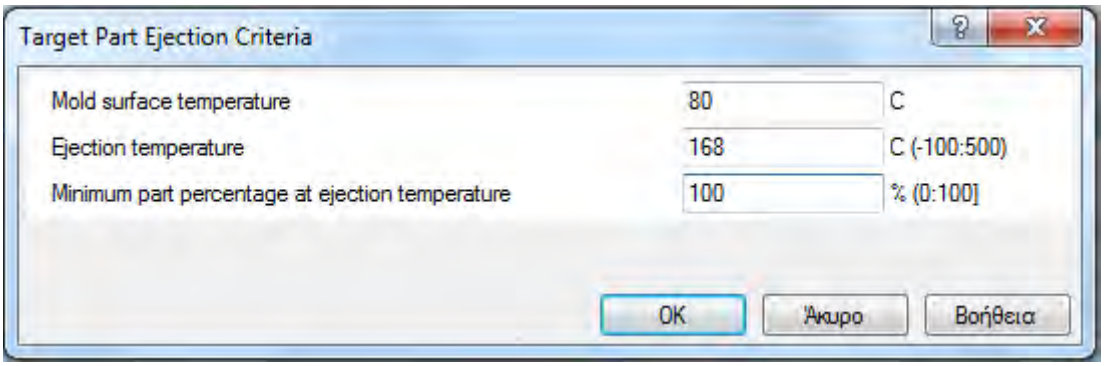

Figure 4.35: The target part ejection criteria window. Analysis will stop, when these criteria are satisfied.

For a Midplane or Dual Domain analysis, the cooling time is determined by the time taken for *each element* to reach at least the specified minimum part percentage frozen at ejection time. A 3D analysis bases the cooling time on the *overall* part volume percentage frozen.

As shown in figure 4.35, the following three parameters must be known for an automatic calculation to be achievable:

a) Mold surface temperature: this temperature cannot be higher than the ejection temperature of the material. In this study, the T_{mold} is constant at 80 °C.
b) Ejection temperature: the temperature at which the material is rigid enough to withstand ejection, without permanent deformation or severe marking from the mold ejector pins. For the material of the study: $T_{eject.}$ = 168 °C.
c) Minimum part percentage at ejection temperature: the program needs to know the minimum part volume that must be frozen, before the part can be ejected (100% here).

For a better automatic cooling time calculation a 3D mesh is required. Having tried the automatic cooling on a dual domain mesh, something seems to go wrong. The program does not calculate the cooling time at all and gives a result of 0 sec. This is the reason why the 3D mesh is preferred (described later).

After the analysis is over, AMI gives a cooling time of 5.9 sec (or approximately 6 sec). Pretty low considering that the packing time is 4 sec. Therefore, the total cycle time is 11 sec (or 15 sec considering the mold-open time) and cooling time takes up 55% of it. But don't forget that the center-gated disk is a thin-walled part with small dimensions and the material used is a PBT. So the cooling time is expected to be rather low.

- *Specified cooling time*:

There are a few equations that one can use in order to calculate the cooling time manually. These are:

a) Short cylinder equation:

$$t_{cool} = \frac{1}{(\frac{23.14}{D^2} + \frac{\pi^2}{L^2}) \cdot a} \ln(2.04 \frac{T_M - T_W}{T_E - T_W}),$$

where:

D = diameter of the disk = 130 mm,

L = length of the disk = thickness of the disk = 2 mm,

a = thermal diffusivity of the polymer melt = $k/\rho \cdot C_p$ = 0.125 mm^2/sec, where ρ is the density of melt,

T_M = maximum (recommended) melt temperature = 260 °C,

T_W = cavity wall temperature (usually the mean temperature) = $1/2 \cdot (T_{W,max} + T_{W,min})$ = $1/2 \cdot (130 + 30)$ = 80 °C, and

T_E = ejection/demoulding temperature = 168 °C.

So it is:

$$t_{cool} = \frac{1}{(\frac{23,14}{130^2} + \frac{3,14^2}{2^2}) \cdot 0,125} \ln(2,04 \cdot \frac{260-80}{168-80}) =$$

$$= \frac{1}{(0,00137 + 2,465) \cdot 0,125} \cdot \ln(2,04 \cdot \frac{180}{88}) = 3,24 \cdot 1,43 = 4.63 \text{sec}$$

b) Plate equation:

$$t_{cool} = \frac{s^2}{\pi^2 \cdot a} \ln\left(\frac{4}{\pi} \frac{T_M - T_W}{T_E - T_W}\right),$$

where:

s = wall thickness = 2 mm.

Notice that this equation is similar to the one above, but because the diameter of the disk D is much greater than its thickness, this means:

$$D >> s \Rightarrow D^2 >> s^2 \Rightarrow \frac{1}{s^2} >> \frac{1}{D^2}$$

Thus, it is:

$$t_{cool} = \frac{2^2}{3{,}14^2 \cdot 0{,}125} \ln\left(\frac{4}{3{,}14} \cdot \frac{260-80}{168-80}\right) = 3{,}25 \cdot 0{,}958 = 3.11\text{sec}$$

c) Rough estimation equation:

$$t_{cool} \sim \frac{s^2}{4a} \sim \frac{4(mm^2)}{4 \cdot 0{,}125(mm^2/s)} \sim 8\text{sec},$$

where "s" is the nominal thickness of the part. As a rule-of-thumb, 1/10 to 1/5 of the estimated cooling time is a good estimate for the fill time. This means that for a cooling time of 8 sec, the filling time should be between 0.8 and 1.6 sec.

Note: As mentioned above, the dual domain analysis does not give a cooling time result. Therefore, in order for all simulations (both in dual domain and 3D) to have the same total cycle time, a *specified cooling time of 6 sec* was used.

Note: If the automatic cooling option is selected, remember that increasing either the T_{mold} or the T_{melt} increases the cooling time, therefore the total cycle time, because it takes longer for the frozen layer to reach the required thickness.

5. 3D Mesh Conversion

5.1 Converting to 3D

After a dual domain analysis is complete, this means the desired values are already set and the no mesh errors exist, then one can duplicate the main dual domain study and convert it to 3D. Do not convert the main study to 3D, but make a copy of it. Both will be needed.

Go to 'Study Tasks' pane and right click on the 'Dual Domain Mesh' option. Select 'Set Mesh Type > 3D'. Right click on the '3D Mesh' option and select 'Generate Mesh'. In the new dialog that pops up, one can see that there are four tabs in total. Let's explain them:

- General tab: Determines what size elements will be created when the part is meshed, that is, the global mesh density.

Like in a dual domain mesh, the global edge length (GEL) and the merge tolerance should be defined. Assign a GEL of 2 mm and a merge tolerance of 0.01 mm. Make sure to have unchecked the 'Match mesh option'. For midplane and dual domain meshes that will be converted to 3D, having this option unchecked will be best, as it may create thin high-aspect ratio elements.

Lastly, check the 'Remesh already meshed parts of the model' option. This will make a new mesh with tetrahedral elements, right from the start.

- NURBS tab: Allows you to match a Dual Domain mesh or smooth a Midplane mesh to assist post-processing, after analyzing the model.

Like in a dual domain mesh, one should define the chord height. Keep the value of the chord height somewhere in the range of 5-25% of the GEL. A 10% of the GEL has been assigned here, i.e. 0.2 mm. Also, ensure the option 'Smooth mesh' is checked.

- Tetra tab: Sets the minimum number of elements and maximum aspect ratio to use when generating a 3D mesh. The options available here are:

- 3D mesher: specifies which meshing technique should be used to generate the tetrahedral mesh.

  Advancing front: this method places nodes on the surface and then places nodes in the interior of the surface being meshed. It creates elements using these nodes. This method allows more control in the placement of the nodes, allows better conformance to the part surface and can implement local density variations more smoothly. It is highly recommended for parts with fillets and other highly curved surfaces.

  Legacy: this meshing method places nodes on the surface, then creates elements using a simple trim and notch strategy. It is recommended for parts which do not have fillets and highly curved surfaces.

Having tested both meshing methods for the case of this center-gated disk, the meshing results are a lot improved with the 'Legacy' option selected. The 'Advancing front' method creates elements with greater aspect ratios and internal long edges, as well as very small angle between faces (lower than 2 degrees). Thus, it is way more difficult for it to be fixed.

- Minimum number of elements through thickness: Sets the minimum number of elements through the thickness that AMI will aim for when it generates the 3D mesh.

  Increasing the number of elements through the thickness increases dramatically the total number of elements, which increases computation time. For a fiber analysis (like here) a minimum of 8 layers must be selected. Experts use 12 layers or more in their studies.

- Tetra aspect ratio control: Allows both automatic ratio control (which produces a mesh with smaller aspect ratios and less elements), and a manual setting for maximum allowed aspect ratio.

  The manual setting uses a more conservative algorithm and is not recommended, unless errors are found using the automatic function. For this study the 'Automatic optimization' option is selected.

  - Tetra advanced tab: moves and distributes nodes in order to reduce the aspect ratio of the generated tetrahedral elements.

  Check the 'Use surface mesh optimization' and 'User surface mesh matching' options. The first one creates a mesh with fewer high aspect ratio elements. The second one specifies that a uniform volume mesh will be created, aligned through the thickness with the elements on the top and bottom of the surface of the dual domain mesh. This will also result in less nodes and elements being created.

  The 'Node biasing through thickness' option allows one to adjust the relative thickness of each element layer in a 3D part. This is achieved by shifting the node layer closer to either the surface or the center of the part. Biasing is the ratio of thickness of an inner layer vs. the outer layer (closer to the surface). A bias > 1 is generally chosen to capture shear rate and shear heating better. Outer layers will be thinner and inner ones will be thicker. Consequently, the node density near the part's surface will be higher than that near the center. A bias < 1 is normally done to capture gas penetration or jetting better. Inner layers will be thinner than outer layers and the node density near the center of the part will be higher than near the surface. In this study the option 'An even distribution without biasing' is selected.

  Lastly, in the 'Mesh smoothing' box choose the 'Smooth all nodes' option. Here one can select how existing nodes should be distributed in order to smooth the mesh. With the 'Smooth all nodes' option activated, interior nodes are moved if doing so can produce elements with a lower aspect ratio.

5.2 3D Mesh Repair Wizard

One of the most important tools in AMI is the mesh repair wizard. After the meshing of the disk a total of 54810 elements were created. With such a high number of elements, some unwanted mesh results may occur. Common mesh problems include high aspect ratios and extremely small or large angle between faces. Most of them can be fixed automatically, just by clicking the command 'Fix' in the mesh repair wizard window. Most of the times, the 3D mesh diagnostics should be checked four and five times. This happens due to the automatic fix. For example, if some elements with extreme angle between faces are traced, then the 'Fix' command will repair most of them. However, this may cause a sudden increase in the aspect ratio of other adjacent elements. Having as a guide table 3.1, the meshing examination begins:

Table 5.1: Mesh results before using the Mesh Repair Wizard.

Inverted Tetras	NO inverted tetras
Collapsed faces	NO collapse on model boundary
Insufficient refinement	Satisfactory mesh refinement
Internal long edges	Max edge length ratio: 1.84
Tetras with large volume	Max volume ratio to average volume: 6.47
Aspect ratio	Min: 1.08 Average: 13.53 Max: 25.39
Small included angles of tetras	Min included angle: 2.223°
Large included angles of tetras	Max included angle: 175.2°

Although the mesh requirements of the table above are all already satisfied, these initial results can be further improved. Emphasis will be given on tetras with extreme angle between faces. Notice that the maximum included angle is 175.2° for now.

At first, the large included angles should be decreased. In the search box of the 'Large included angle of tetras' window, assign a value of 175 degrees. One tetra with very large angle was found. Click on the 'Fix' command. As a result, the new angle between faces has now decreased to 174.9°. A value of 174.5° was assigned after.

Three tetras were found and fixed. The angle dropped to 174.2°, but the aspect ratio increased to 26.7. Goal was to decrease the angle even more, but affecting the aspect ratio to a minimum. Eventually, the maximum angle was decreased to 172.8° and the aspect ratio dropped to 24.8, again. Of course, the angle can be reduced even more. However, one should check how the other parameters will also be affected.

Now move on with the small included angles repair. Notice that the minimum included angle is 2.223° for now. In the search box of the 'Small included angles of tetras' window, assign a value of 2.4°. Three tetras with very small angle were found. Fix them. Assign a value of 2.5°. One element was found. Fix it. Again assign a value of 2.6°. Eight tetras were found. Fix them, too. At this point, the angle changes for the first time, from 2.223° to 2.256°.
Trying to increase the small included angle, values > 3° were assigned at the end. However, the angle did not change. Most of the elements (68) with small included angles cannot be fixed any further. Click close and finish mesh. The model is now ready for analysis.

Table 5.2: Mesh results after using the Mesh Repair Wizard.

Inverted Tetras	NO inverted tetras
Collapsed faces	NO collapse on model boundary
Insufficient refinement	Satisfactory mesh refinement
Internal long edges	Max edge length ratio: 1.84
Tetras with large volume	Max volume ratio to average volume: 6.48
Aspect ratio	Min: 1.08 Average: 13.51 Max: 24.83
Small included angles of tetras	Min included angle: 2.256°
Large included angles of tetras	Max included angle: 172.8°

Furthermore, in order for someone to see the layers that were created through the thickness of the disk, the following steps should be followed:

a) Go to the layers pane.
b) Create a new layer. A new layer was created on the list, named: 'New Layer 12'.
c) Uncheck the 'New layer 12' box.
d) From the navigation wheel choose the 'Select' option and select the model entities that will be examined.
e) After selecting the region of the model that will be examined, on the layers pane select the 'Assign layer' command.
f) Zoom in at the area that was previously selected for examination and one can see the layers through thickness. Remember that 8 layers were created in total. See figure 5.2 for verification.

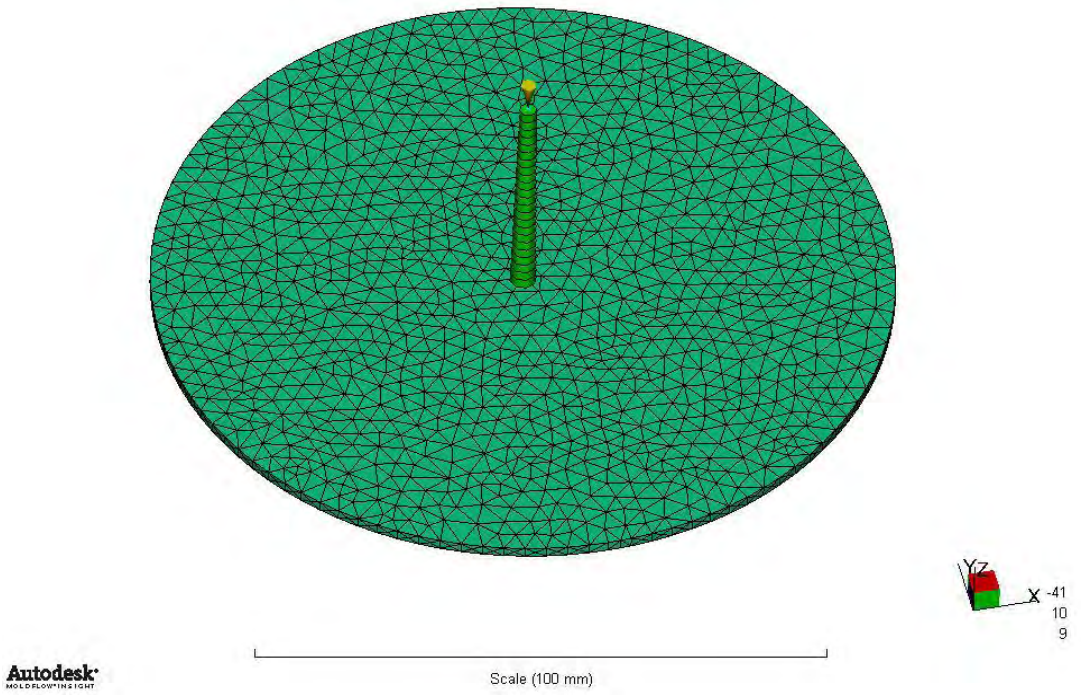

Figure 5.1: Presentation of the 3D meshed disk. Nearly 55000 elements were created.

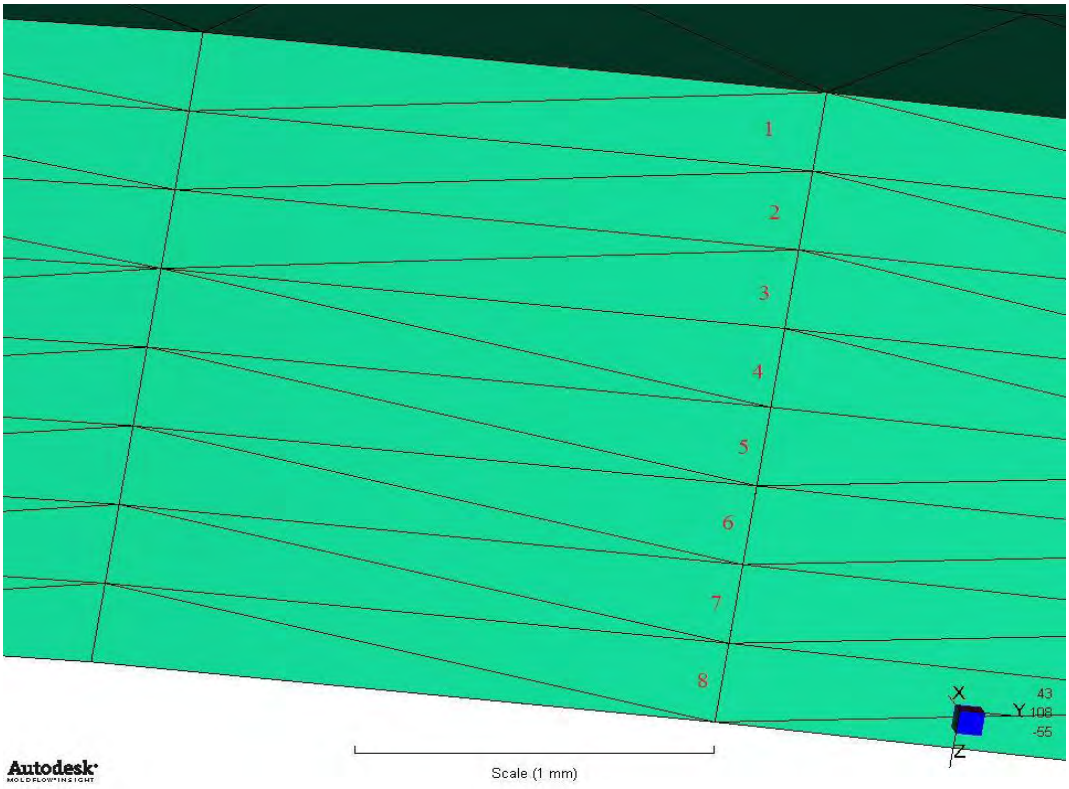

Figure 5.2: Presentation of the 8 layers through the thickness of the 3D meshed disk. Each layer has been numbered.

5.3 Assignment of properties

As in the dual domain mesh, select the whole model and right click. Go to ‘Properties’ and select the ‘Part (3D) (default) #1’ option. This will select the whole part, without the sprue gate.

Go to ‘Part Surface Properties’ tab and in the ‘Local heat transfer coefficients’ box choose the ‘Perfect contact’ option. Also, in the ‘Mold surface temperature’ box select the ‘Profile’ option and use the same temperature profile as in the dual domain mesh, i.e. a constant temperature of 80 °C (see figure 5.3).

Now, select the whole model again and select the ‘Cold sprue (default) #1’ option. This will select only the sprue. Choose the ‘Edit properties of the entire taper section’ option and go to the ‘Mold temperature profile’ tab. Use the same temperature profile again, as described above (see figure 5.4).

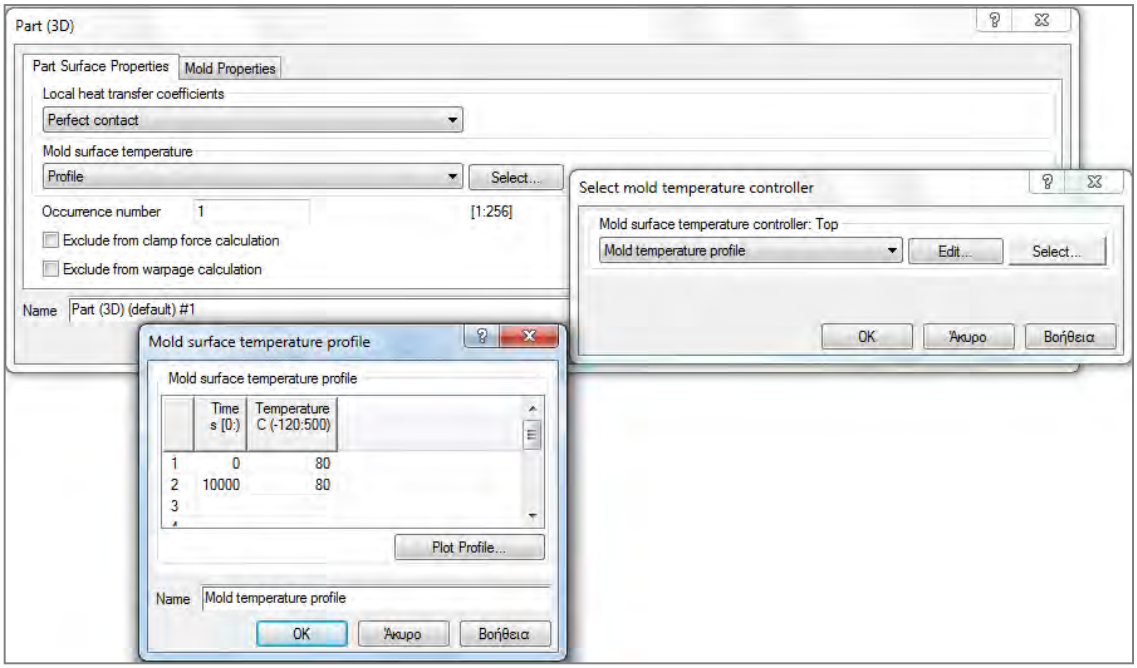

Figure 5.3: Assignment of properties in the 3D part. When the 'Perfect contact' option is selected, then no heat resistance between the part and the mold surface exists. The wall nodes are a fixed thermal boundary for analysis purposes. This option was not available in the dual domain analysis. Of course, one can choose the 'Local HTC' option instead of the 'Perfect contact' or even modify the default values.

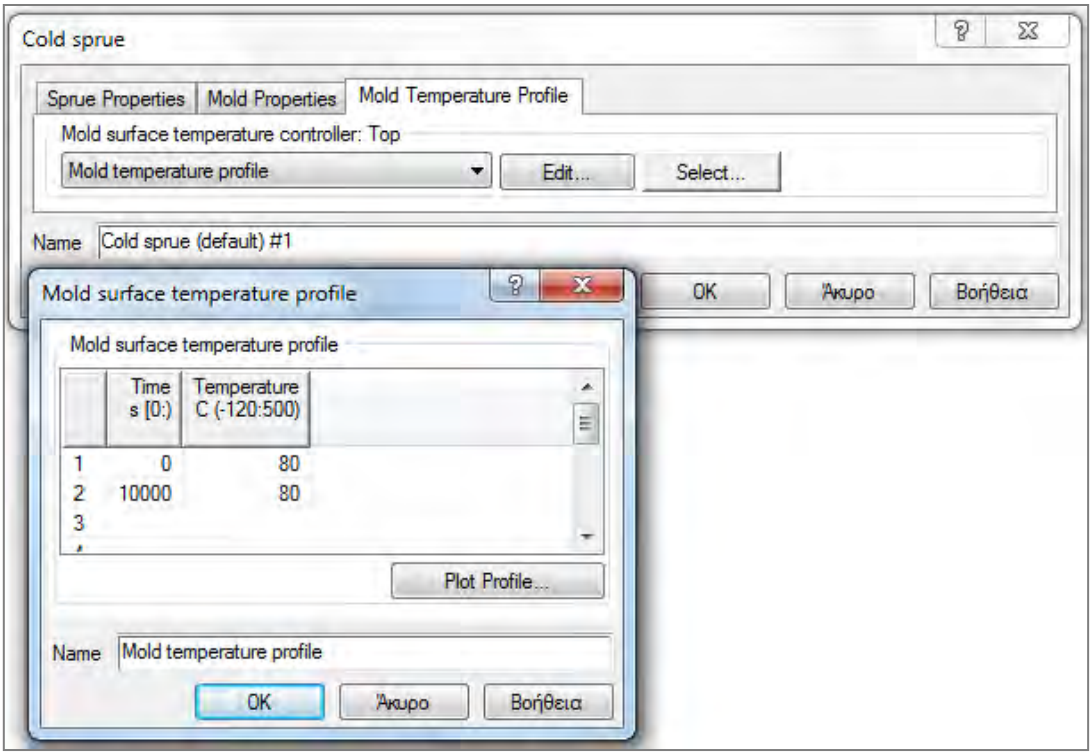

Figure 5.4: Assignment of properties for the cold sprue (3D model).

5.4 3D Solver Parameters Dialog

This dialog contains more tabs than the one in a dual domain analysis. Remember that a Fill+Pack analysis will be carried out here.

Apart from the two tabs that are described below, the other tabs of the 3D solver parameter dialog, affect warpage and cooling analyses, or the modeling of a part insert. For this study, make sure to have chosen the '20 laminates across beam radius' option, in the 'Mesh' tab, for more accurate results.

5.4.1 Fill+Pack Analysis tab

This dialog is used to specify the filling phase, packing phase, gate diameter and general solver parameters for the 3D flow solver used in a Fill+Pack or Flow analysis of a 3D model.

In this study, both inertia and gravity effects were neglected, i.e. the 'Simulate inertia effect' and 'Simulate gravity effect' options were not activated.

Also, the 'Gate contact diameter' option assigns a virtual gate diameter to each injection node, when a modeled gate or runner system is not provided (direct injection). This improves the flow front prediction and provides more accurate pressure results. However, this does not mean that a modeled gate should not be included. The gate contact diameter has no effect when injecting into a beam element or at a gas injection location. In this study, a specified diameter of 3 mm has been used.

Furthermore, one can modify the 'Filling phase' and 'Packing phase' solver parameters dialogs, in order to achieve a more accurate analysis. A maximum 1% volume to fill per time step has been assigned here. This means that in the AMI logs, the filling phase results will be shown for each 1% of the filled cavity volume.

5.4.2 Fiber Analysis tab

Not much to say here. The only available option is which fiber orientation model to be used, during the analysis. As already mentioned, the Reduced Strain Closure (RSC) model will be selected. For someone who would like to see the equations that describe the model, the following should be helpful:

The Folgar-Tucker (FT) orientation equation is the standard model used for fiber orientation calculations. The governing equation is:

$$\frac{Da_{ij}}{Dt} = -\frac{1}{2}\left(\omega_{ik}a_{kj} - a_{ik}\omega_{kj}\right) + \frac{1}{2}\lambda\left(\dot{\gamma}_{ik}a_{kj} + a_{ik}\dot{\gamma}_{kj} - 2a_{ijkl}\dot{\gamma}_{kl}\right) + 2C_I\dot{\gamma}\left(\delta_{ij} - 3a_{ij}\right)$$

where:

- a_{ij} is the fiber orientation tensor,
- $1/2 \cdot w_{ij}$ is the vorticity tensor and $1/2 \cdot \dot{\gamma}_{ij}$ is the deformation rate tensor, and
- C_i is the fiber interaction coefficient, a scalar phenomenological parameter, the value of which is determined by fitting to experimental results. This term is added to the original Jeffery form to account for fiber-fiber interactions.

However, recent experiments and references indicate that the Folgar-Tucker model over-estimates the change rate of the orientation tensor in concentrated suspensions. To capture the slow orientation dynamics and preserve the objectivity, the RSC model has been developed. It also exhibits a similar steady state orientation and provides good agreement with experimental data, too (Wang, 2007).

The RSC model is based on the concept of reducing the growth rates of the eigenvalues of the orientation tensor by a scalar factor, while leaving the rotation rates of the eigenvectors unchanged. Thus the orientation equation is modified to:

$$\frac{Da_{ij}}{Dt} = -\frac{1}{2}\left(\omega_{ik}a_{kj} - a_{ik}\omega_{kj}\right) + \frac{1}{2}\lambda\left(\dot{\gamma}_{ik}a_{kj} + a_{ik}\dot{\gamma}_{kj} - 2\left[a_{ijkl}\dot{\gamma}_{kl} + (1-\kappa)\left(L_{ijkl} - M_{ijmn}a_{mnkl}\right)\right]\dot{\gamma}_{kl}\right) + 2\kappa C_I\dot{\gamma}\left(\delta_{ij} - 3a_{ij}\right)$$

The RSC model differs from the standard FT model only in that:

1. The diffusion term is reduced by the scalar factor κ.
2. The closure term, a_{ijkl}, is replaced by:

$$\left[a_{ijkl} + (1-\kappa)\left(L_{ijkl} - M_{ijmn}a_{mnkl}\right)\right]$$

The fourth-order tensors, L_{ijkl} and M_{ijkl}, are defined as:

$$L_{ijkl} = \sum_{p=1}^{3} \sigma_p e_i^p e_j^p e_k^p e_l^p$$

$$M_{ijkl} = \sum_{p=1}^{3} \sigma_p e_i^p e_j^p e_k^p e_l^p$$

Here, σ_p is the p^{th} eigenvalue of the orientation tensor a_{ij}, and e_i^p is the i^{th} component of the p^{th} eigenvector of the orientation tensor a_{ij}.

The scalar factor κ is a phenomenological parameter, and $\kappa \leq 1$ to model the slow orientation dynamics. The smaller the scalar factor κ, the slower the orientation tensor develops with flow, and the thicker the orientation core layer becomes. When $\kappa = 1$, the RSC model is reduced to the original Folgar-Tucker model.

6. Results

Polymer fill region (3D):

The ‘polymer fill region’ result is generated at the end of filling and shows which elements in the model are filled with polymer melt, at intervals as the cavity fills. Filled elements are shown as green and unfilled elements as transparent. The polymer fill region result is able to show where jetting flow has occurred. This effect is not visible in the ‘fill time’ result, because it can show only one time (the first) that a node fills. Figures 6.1-6.4 show the way the hot polymer fills the cavity at various times, during the filling stage. Note that an even filling pattern exists and that filling is uniform, too.

Note: Jetting occurs when polymer melt is pushed at a high velocity through restrictive areas, such as the nozzle, runner, or gate, into open, thicker areas, without forming contact with the mold walls. The buckled, snake-like jetting stream causes contact points to form between the folds of melt in the jet, creating small-scale "welds". Generally, jetting may result in uneven filling and may lead to air traps inside the part. It can also lead to uneven cooling and increased stress in the part. Jetting leads to part weakness, surface blemishes and a multiplicity of internal defects.

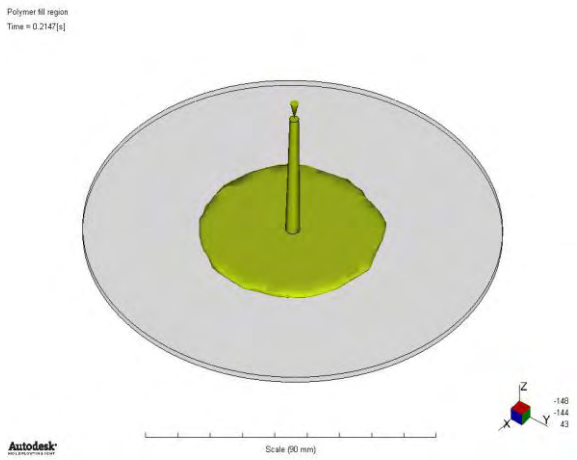

Figure 6.1: Polymer fill region at 0.2 sec.

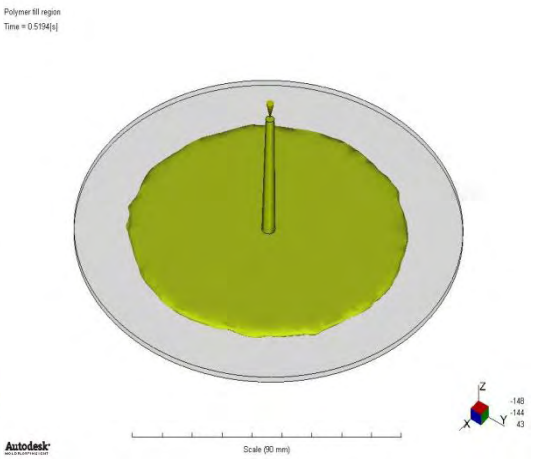

Figure 6.2: Polymer fill region at 0.5 sec.

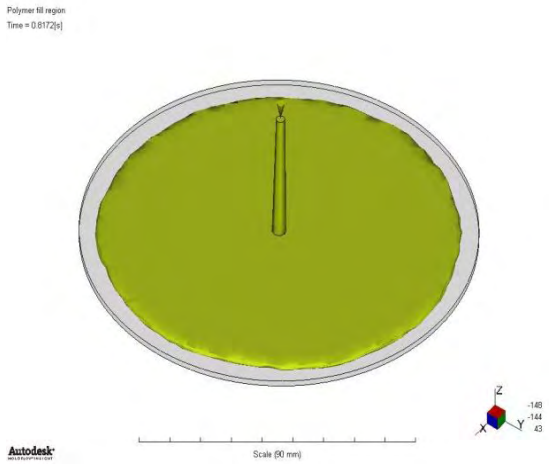

Figure 6.3: Polymer fill region at 0.8 sec.

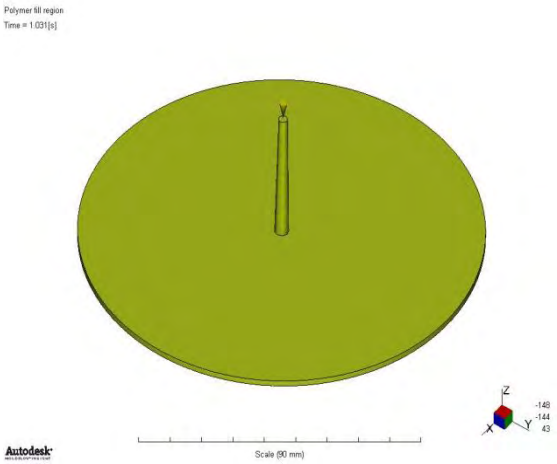

Figure 6.4: Polymer fill region at 1 sec.

Fill time (3D):

The disk (cavity) is completely filled at 1.03 sec. The material is injected from the top of the sprue, with a constant flow rate of 28 cm^3/sec. Thus, it is expected for the regions near the base of the sprue to fill first and for the regions far from the center (edges) to fill last, as shown in figure 6.5

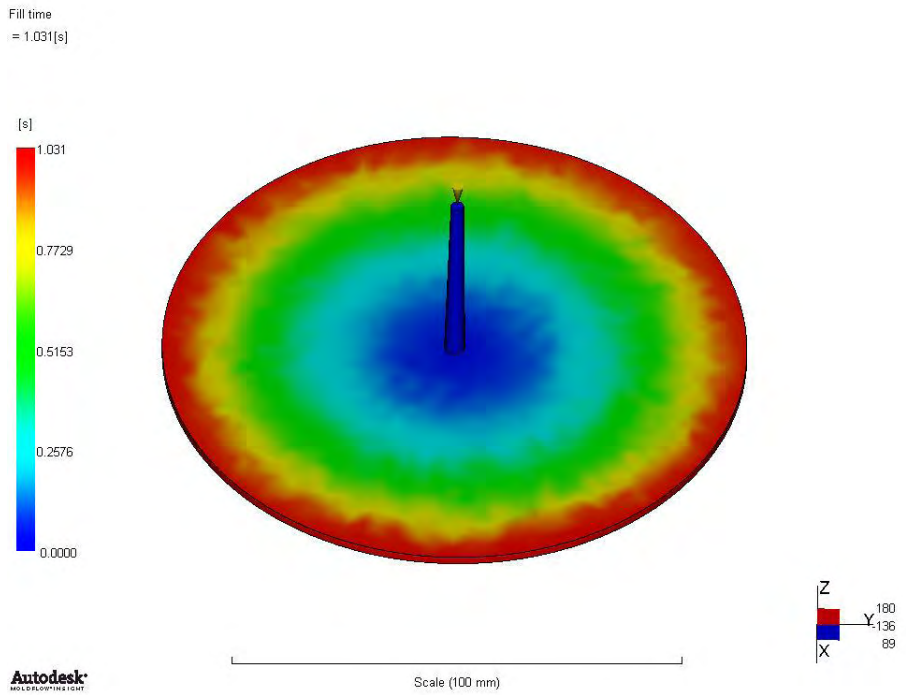

Figure 6.5: Predicted filling times for the disk cavity. (Scale range: 0 – 1.031 sec).

Average velocity (Dual Domain):

The 'average velocity' result shows the gap-averaged magnitude of velocity of the polymer melt, inside the mold cavity, over time. This magnitude of the flow velocity is an average through the thickness, calculated only in the regions where melt still exists; the frozen layers are not included in this calculation.

The average velocity results at four different times of the filling stage are depicted in figures 6.6-6.9. The anticipated unidirectional and uniform flow is observed (radial direction). The flow does not reverse on itself, during the filling phase and no hesitation flow (when the flow slows down or stops along a particular flow path) or weld regions exist.

The highest velocity values are observed inside the sprue. More specifically, higher values will appear on the top of the sprue and lower where it meets the part. This is because material travels from a narrow cross-section to a wider one.

According to reports, for the geometry of a center-gated disk, if the fluid fills the cavity at a constant flow rate, the flow decelerates with increasing radial distance.

As the material exits the sprue and enters the cavity, moving in a uniform fashion in the radial direction, the area available to flow decreases, i.e. Q = A(r)*V(r), with: A(r) = 2*pi*r*h, where h is the thickness of the mold and V(r) the velocity (radial) at position (r). Since the volumetric flow rate (Q) is constant – filling occurs under constant ram displacement – V(r) is inversely proportional to the radial distance (r).

Therefore, a series of plots are also presented (figures 6.10-6.15), depicting the average velocity as a function of distance from the gate, in the radius direction, i.e. V(r). In total, 18 random points were selected across the radius. At t = 0.53 sec (figure 6.10), the melt has almost reached the 40 mm distance. At r = 0, the maximum velocity is observed (113 cm/s) and at a location 4 mm ahead, the velocity has already dropped down to 40 cm/s. Just after mold filling has been completed (figure 6.13), a small extra amount of material flows into the cavity, due to the packing pressure. Moreover, the observed velocity at the injection location is much smaller (7.5 cm/s). As we reach the end of packing (figure 6.15), flow into the cavity becomes zero.

The equations described above apply to an incompressible flow. In our case, that is the filling phase. But does this equation ($V(r) = \frac{Q}{2\pi rh}$) give results that are close to the ones acquired from Moldflow? Let's pick the 0.34 and 0.53 sec time points, where the flow rate is constant and measured at 27.89 cm^3/sec and 27.91 cm^3/sec, respectively. Because the first point selected was for r = 0, the above equation gives an infinite V(r). For this reason, as shown in figures 6.16 and 6.17, the first velocity value on the "blue" curve is around 445 cm/s. The specific value was acquired by using a very small radius distance, i.e. r = 0.5 mm. This was done just to present the velocity difference that exists at r = 0 in a better way.

According to figures 6.16 and 6.17, the velocity values start converging for $r \geq 15$ mm. Before that, the velocity difference is noticeable and the closer to r = 0 – the greater the difference. Indicatively (*equation vs. Moldflow results*):

- *At r = 4 mm*: 54.56 cm/s vs. 39.6 cm/s, at t = 0.34 sec and 54.2 cm/s vs. 39 cm/s, at = 0.53 sec.
- *At r = 7.8 mm*: 28.21 cm/s vs. 23.4 cm/s, at t = 0.34 sec and 28.2 cm/s vs. 22.8 cm/s, at = 0.53 sec.
- *At r = 15 mm*: 14.5 cm/s vs. 13.6 cm/s, at t = 0.34 sec and 14.6 cm/s vs. 13.3 cm/s, at t = 0.53 sec.
- *At r = 19 mm*: 11.6 cm/s vs. 11.3 cm/s, at t = 0.34 sec and 11.7 cm/s vs. 11.1 cm/s, at = 0.53 sec.
- *At r = 28.3 mm*: 7.85 cm/s vs. 8.18 cm/s, at = 0.34 sec and 7.8 cm/s vs. 7.5 cm/s, at t = 0.53 sec.

Possible explanations:

a) Deviation of the velocity profile predicted by Moldflow from the 1-D model assumed by the equation.

b) Deviation from the incompressible flow assumed by the equation.

c) Based on the assumption that a dual-domain analysis probably uses the General Hele-Shaw (GHS) methodology for the cavity filling and considering that the GHS model is valid at some distance from the gate, indeed, this deviation should be expected.

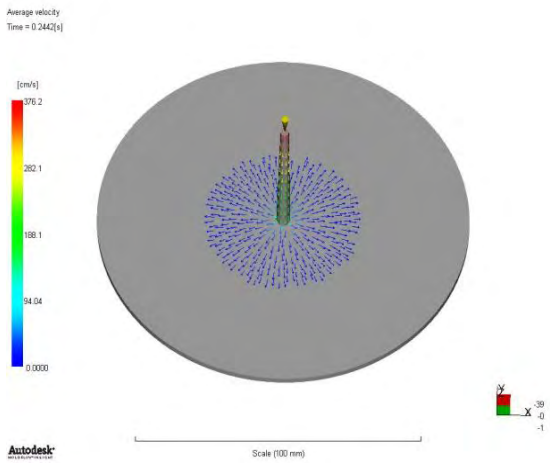

Figure 6.6: Average velocity at 0.24 sec. (Scale range: 0 – 376.2 cm/s).

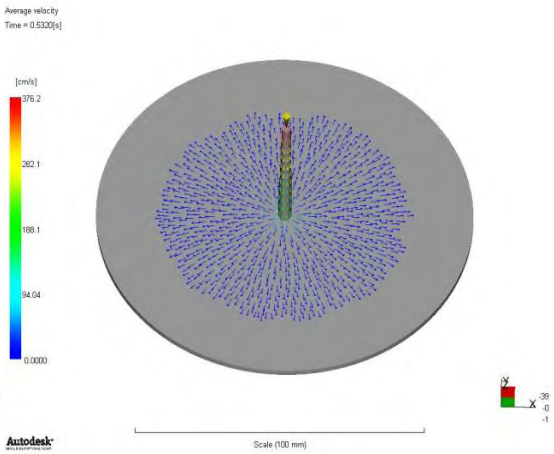

Figure 6.7: Average velocity at 0.53 sec. (Scale range: 0 – 376.2 cm/s).

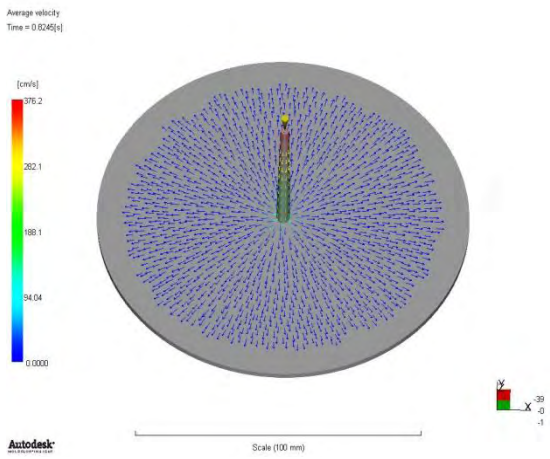

Figure 6.8: Average velocity at 0.82 sec. (Scale range: 0 – 376.2 cm/s).

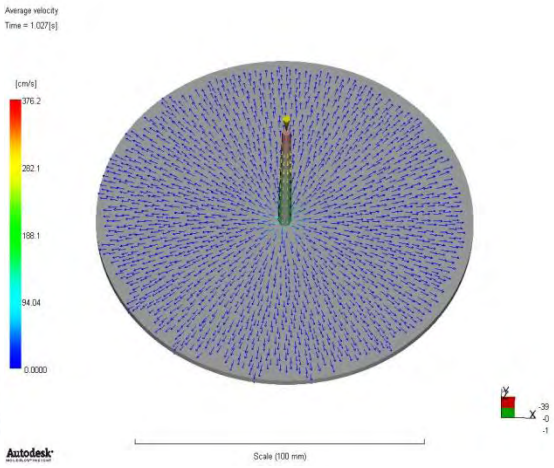

Figure 6.9: Average velocity at 1 sec. (Scale range: 0 – 376.2 cm/s).

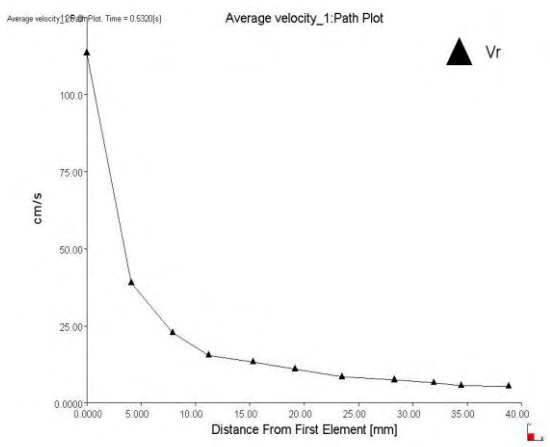

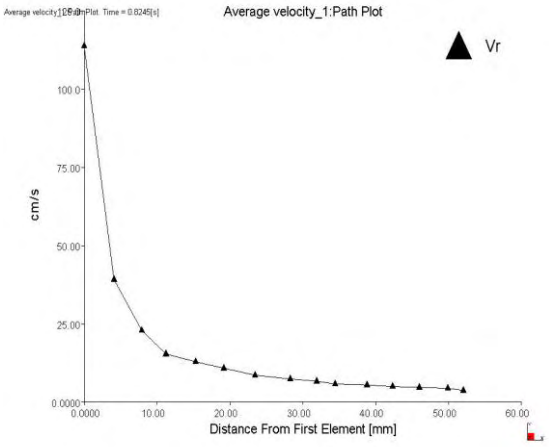

Figure 6.10: Velocity (cm/s) vs. distance from the gate (mm), at t = 0.53 sec (left).
Figure 6.11: Velocity (cm/s) vs. distance from the gate (mm), at t = 0.82 sec (right).

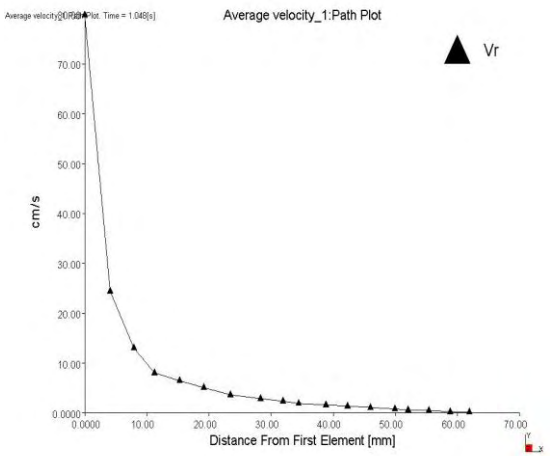

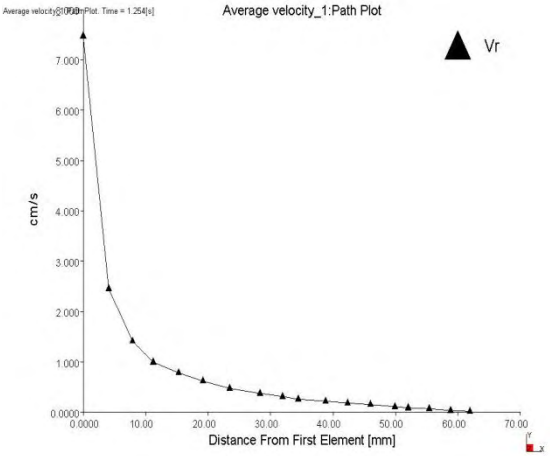

Figure 6.12: Velocity (cm/s) vs. distance from the gate (mm), at end of filling (left).
Figure 6.13: Velocity (cm/s) vs. distance from the gate (mm), at t = 1.25 sec (right).

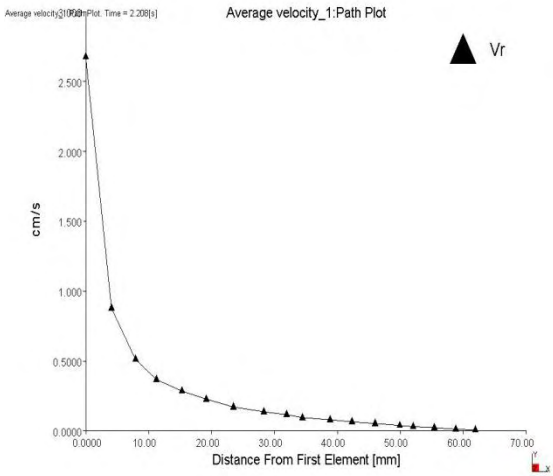

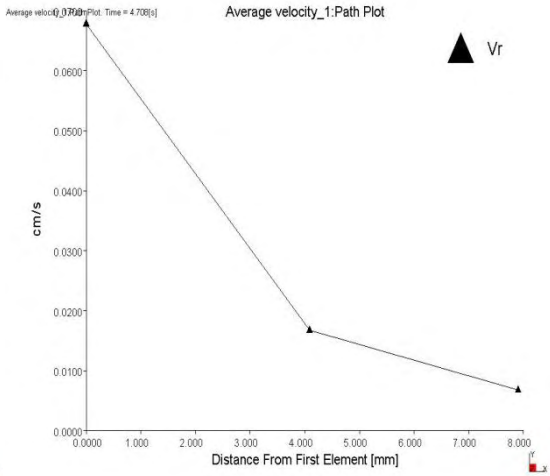

Figure 6.14: Velocity (cm/s) vs. distance from the gate (mm), at t = 2.2 sec (left).
Figure 6.15: Velocity (cm/s) vs. distance from the gate (mm), at t = 4.7 sec (right).

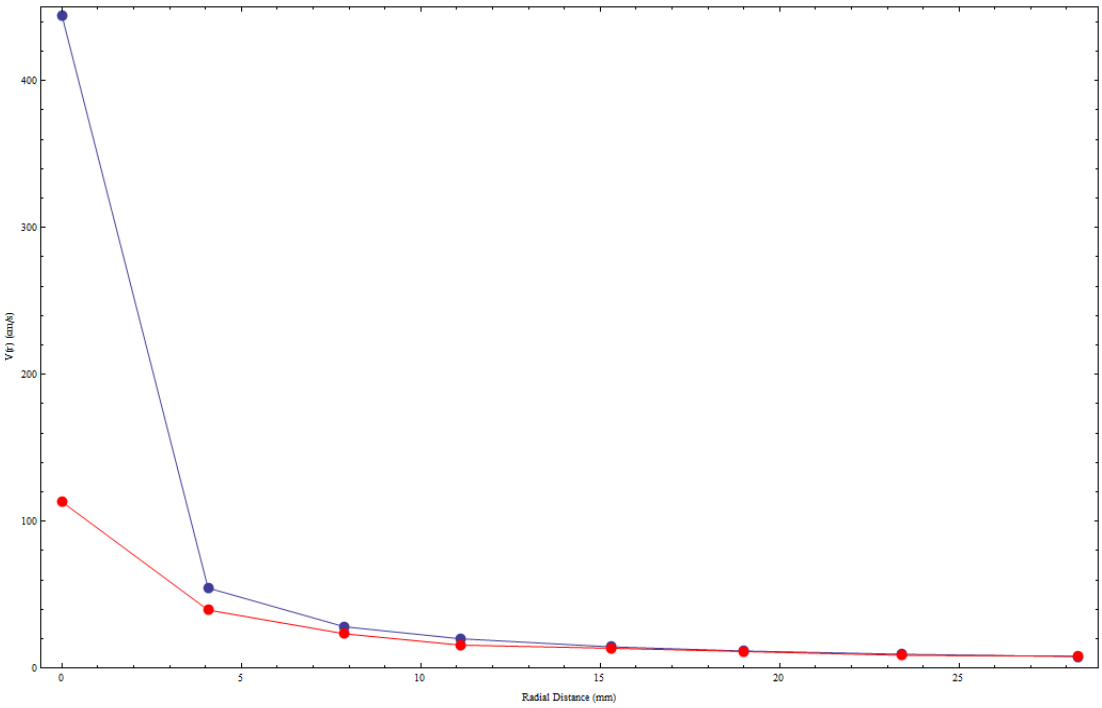

Figure 6.16: Velocity (cm/s) vs. radial distance (mm), at t = 0.34 sec. The "blue" curve depicts the velocity results acquired from the equation and the "red" curve depicts the velocity results given by Moldflow.

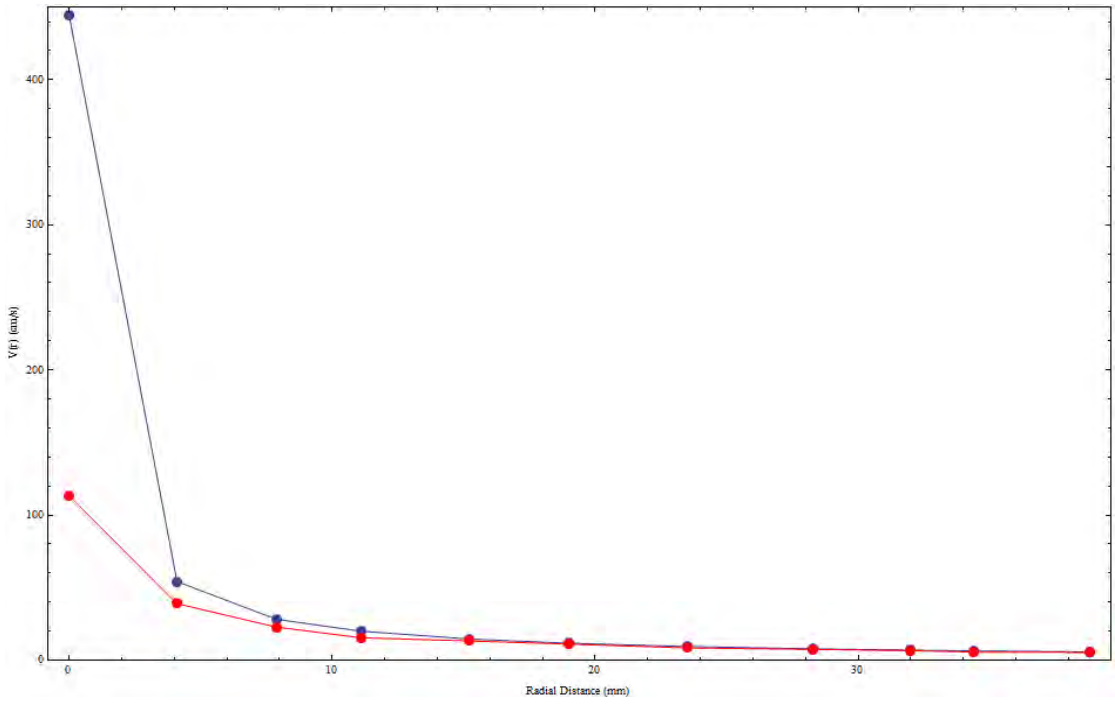

Figure 6.17: Velocity (cm/s) vs. radial distance (mm), at t = 0.53 sec. The "blue" curve depicts the velocity results acquired from the equation and the "red" curve depicts the velocity results given by Moldflow.

Orientation at core & orientation at skin (Dual Domain):

The ‘orientation at skin’ result provides a good indication of how molecules or fibers (when using a fiber-filled material) will be oriented on the outside of the part, showing the average principal alignment direction for the whole local area at the end of filling. The ‘orientation at core’ result provides a good indication of how molecules or fibers will be oriented at the part core, showing the average principal alignment direction for the whole element.

According to reports, in a center-gated disk (CGD) the fibers are transversely aligned at core and flow aligned at skin. The main flow direction in a CGD is radial. Indeed, figures 6.18 and 6.19 verify the theory.

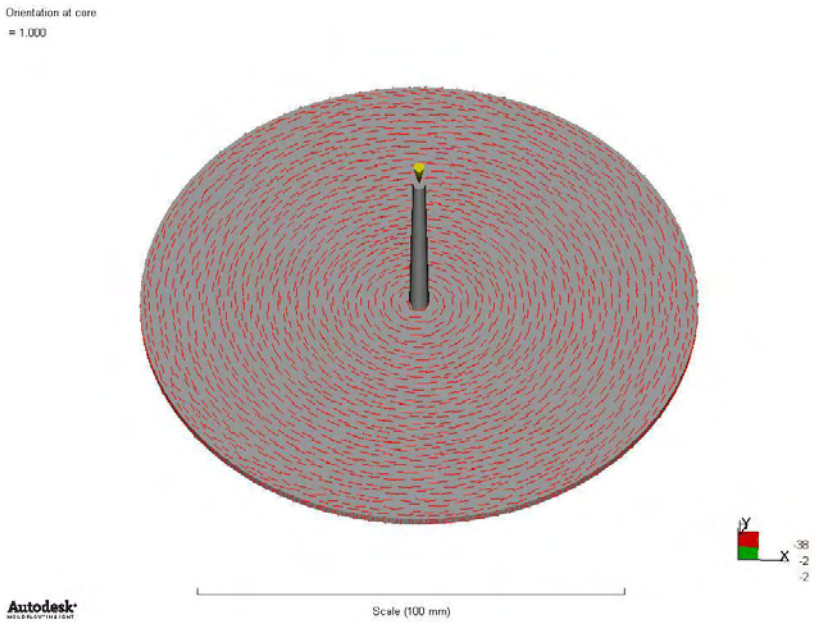

Figure 6.18:

The orientation at core result.

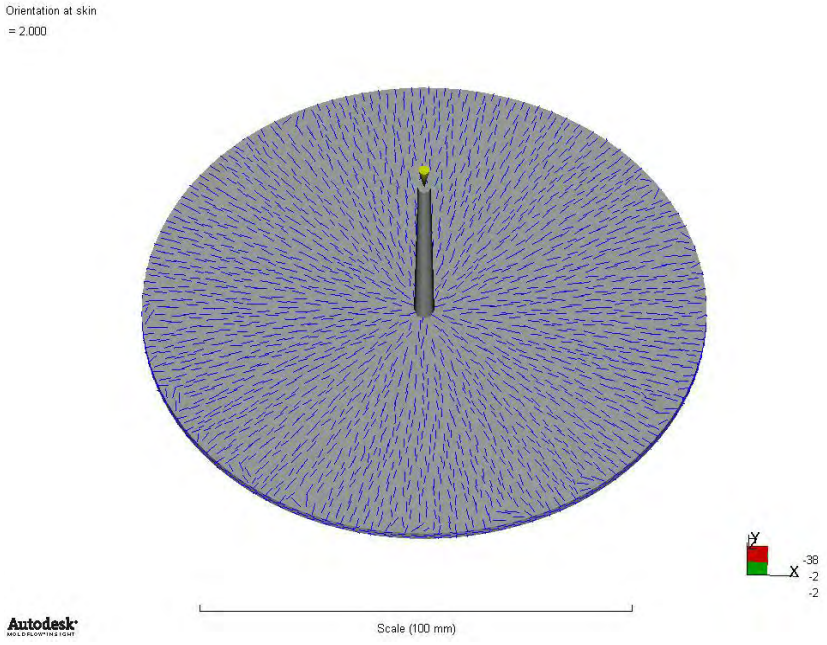

Figure 6.19:

The orientation at skin result.

Pressure at injection location & Clamp force - XY Plot (3D):

The 'pressure at injection location' result ($P_{injection}$) shows the pressure at the injection location at various times, during the filling and packing phases of the analysis. Actually it creates a XY plot of pressure vs. time, according to the results in the logs dialog. This result is very useful for checking whether there are any pressure spikes, which is normally a sign of imbalance.

The 'clamp force' result (F_{clamp}) is a time-series result which shows the force of the mold clamp over time. The clamp force is the resultant value of the pressure distribution over the entire part. It is a history of the force, resultant from filling and packing pressure, which acts to open the mold.

Things should be made clear here. The $P_{injection}$ plot shows the pressure that a user demands to be imposed on the top of the sprue (in the case of the CGD). The F_{clamp} plot will actually show to a user how the system responds to this applied pressure. It's like observing how the cavity pressure develops over time.

In figure 6.20, one can see how the pressure gradually increases during the filling phase. Right after this, the packing phase begins. Initially, it goes up to nearly 40 MPa and for the next 4 sec the pressure remains constant at 50 MPa (end of packing). After the packing phase is over, the pressure is released, reading the IMM for the next cycle.

According to figure 6.21, the clamp force starts increasing and reaches the 27 tonnes at the end of fill (1 sec). Its peak is observed around 1.5 sec (61.6 tonnes). After the 1.68 sec time, clamp force starts dropping, as the frozen volume of the material in the cavity takes up more and more place (> 40%).

For both cases the time axis has been set to end at 6 sec. The reason was that after the 5.2 sec time both clamp force and injection pressure have dropped to 0. Thus, setting the x axis to 6 sec gives a better presentation of the plot. The total cycle time is 11 sec (15 sec if the mold-open time is also considered).

Note: A polymer is considered to be frozen, when the temperature falls below the transition temperature (T_{trans}). For our case: $T_{trans.} = 201\ ^{o}C$.

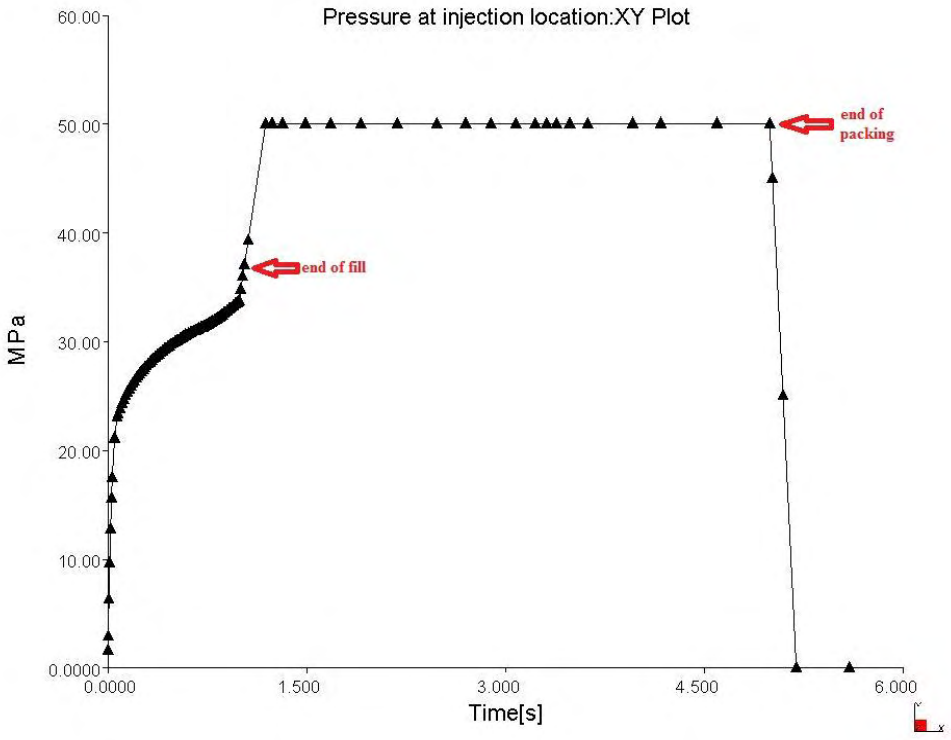

Figure 6.20: Pressure at the injection location (MPa) vs. time (sec).

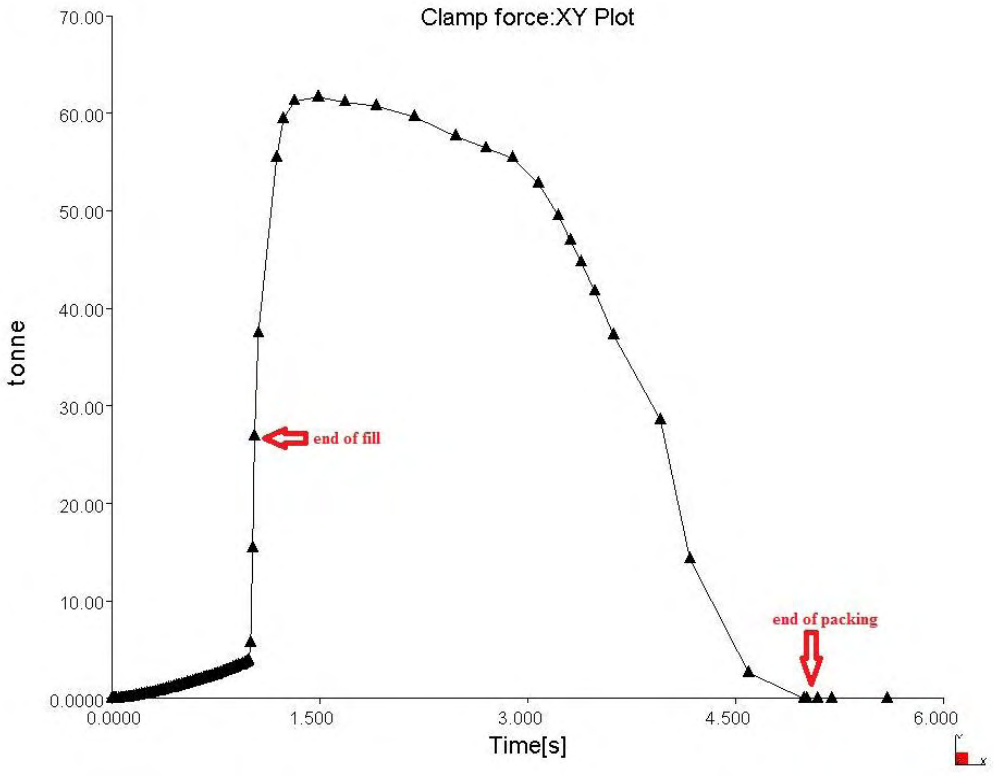

Figure 6.21: Clamping force (tonnes) vs. time (sec).

Remember that figure 6.21 shows the cavity pressure when the 'perfect contact' option has been chosen. In this case, no heat resistance between the part and the mold exists. It's like using an infinite heat transfer coefficient ($h \to \infty$). But in what extent will this result be affected, when the 'Local HTC' option is selected instead ?

Taking into account the default heat transfer coefficients, a slower cooling seems to take place (figure 6.22). Filling pressure requirements are a bit lower in this case, as the frozen volume at the end of fill is 21% vs. 26% (figure 6.21); while during packing the pressure is slightly increased. However, the differences observed are minor. A possible reason could be that these specific values of h are high enough.

On the other hand, using very small heat transfer coefficients (figure 6.23) extends the cycle time to more than 20 sec, because of the very slow cooling that takes place. In effect the cavity in this case is insulated and thus, the material remains in the molten state for a much longer time, and this is reflected in the flat high pressure plateau. Also, notice that the pressure requirements to fill the mold are much lower here and that filling has a linear form. This is expected, as the amount of the material that has solidified at the end of fill is too small (< 2%).

Lastly, using very high local heat transfer coefficients (figure 6.24) almost reminds the 'perfect contact' case.

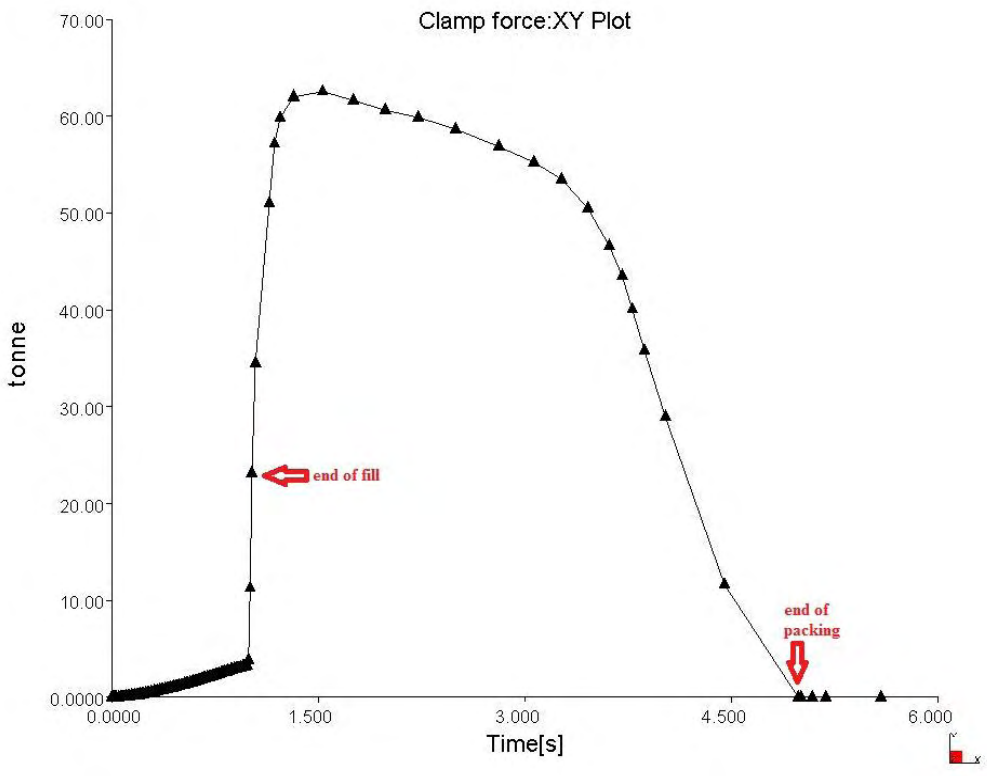

Figure 6.22: Clamping force (tonnes) vs. time (sec), using the default 'HTC' option with: $h_{filling}$ = 5000 W/m$^2 \cdot$ °C, $h_{packing}$ = 2500 W/m$^2 \cdot$ °C and $h_{detached}$ = 1250 W/m$^2 \cdot$ °C.

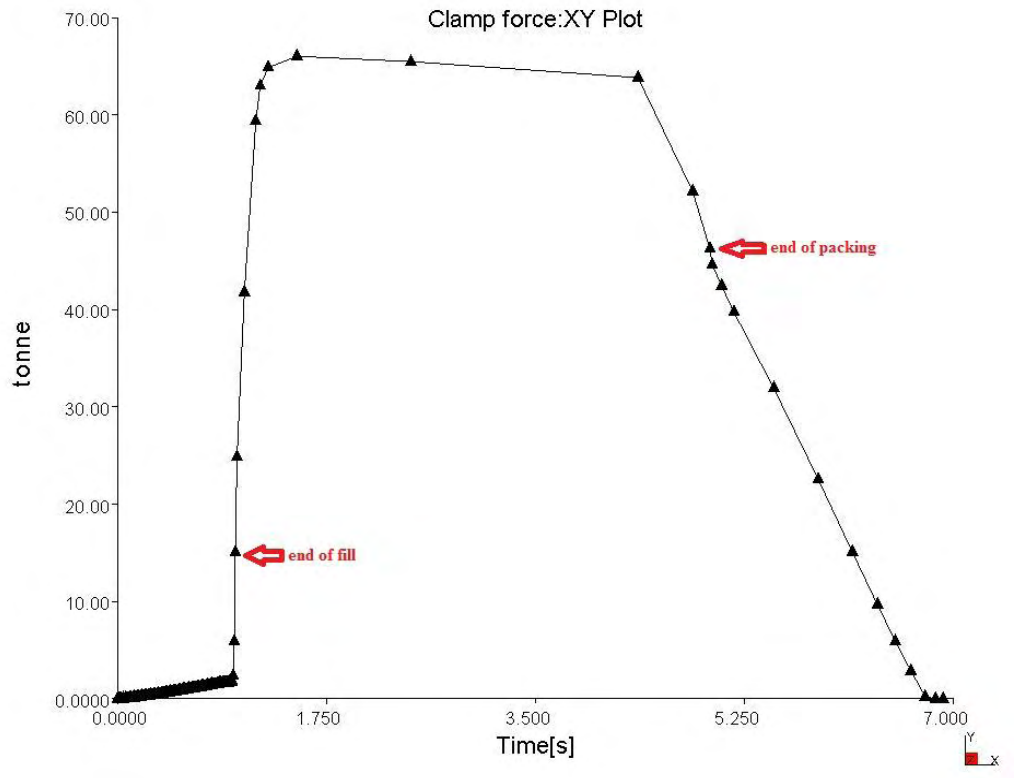

Figure 6.23: Clamping force (tonnes) vs. time (sec), using the 'HTC' option with: $h_{filling}$ = 500 W/m$^2\cdot$°C, $h_{packing}$ = 250 W/m$^2\cdot$°C and $h_{detached}$ = 125 W/m$^2\cdot$°C.

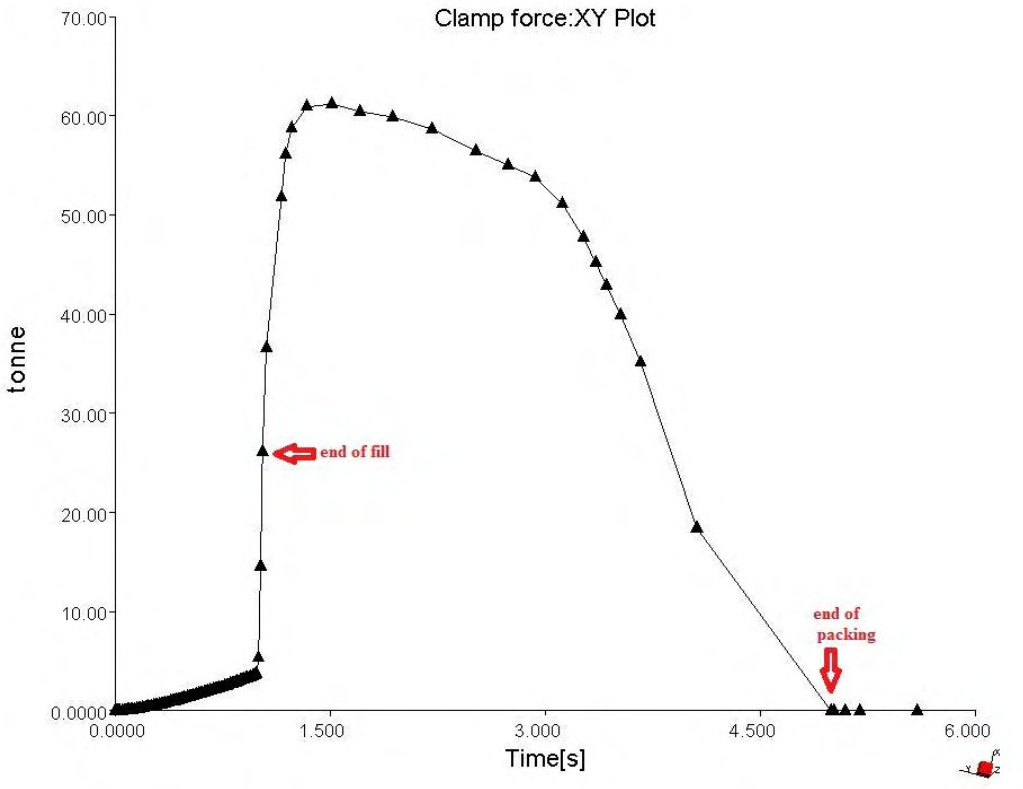

Figure 6.24: Clamping force (tonnes) vs. time (sec), using the 'HTC' option with: $h_{filling}$ = 50000 W/m$^2\cdot$°C, $h_{packing}$ = 25000 W/m$^2\cdot$°C and $h_{detached}$ = 12500 W/m$^2\cdot$°C.

Temperature (3D):

The 'temperature' result shows the temperature of the polymer at nodes, at specified times during the analysis. The following figures show the temperature of the material, through the part thickness, at specified times and for this reason the YZ cutting plane has been selected. The times are: 1 sec (end of filling), 2.5 sec (packing phase), 5 sec (end of packing) and 11 sec (end of cycle).

Figures 6.25-6.28 have something in common. Notice that every time the temperature near the mold walls is much lower than that in the midplane of the cavity. This is because of heat transfer between the hot molten plastic and the cold cavity walls.

At the end of filling (figure 6.25), the temperature in the midplane of the cavity is around 258 °C. The closer to the surface - the smaller the temperature. At t = 2.5 sec, it is obvious that temperature has decreased and the surface solidified layers have grown more. At this point, the frozen volume is almost 60%. Notice how the green color has taken up more space in the cavity (thickness direction). It is also obvious that temperature at the center-plane is still high. At this time point, hot molten material is still injected through the sprue (gate has not frozen yet).

At the end of packing (figure 6.27), the temperature at the midplane has decreased to around 201 °C. The frozen volume is almost 100% and the cavity pressure has dropped to zero. Where the cavity walls touch with the plastic, the material's temperature has become equal to the mold surface temperature (80 °C). Also, notice the growth of the surface solidified layers, compared to the two figures before.

Note: Remember that $T_{trans.}$ = 201 °C. The moment packing phase ends, the frozen volume is at 99.9%. This means that there is still a 0.1% portion in the cavity, where the polymer has not yet turned to solid. Indeed, examining the region under the sprue, gives temperatures both below 201 °C (solid state) and > 201 °C (melt state), i.e. around 202-205 °C.

When the cycle time ends (figure 6.28), both injection and cavity pressure are zero. The frozen layers have taken up most of the cavity space (blue color is dominating) and the temperature at the midplane has dropped down to 150 °C.

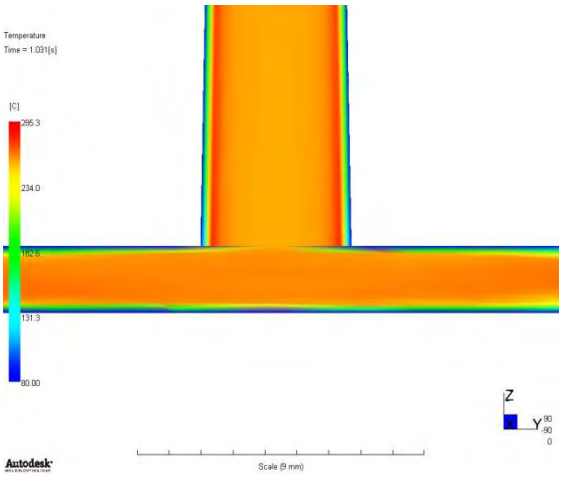

Figure 6.25: Temperature at 1 sec.
(Scale range: 80 – 285.3 ^{o}C).

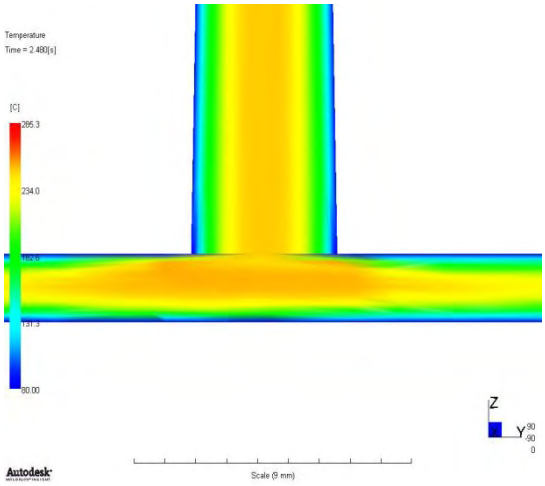

Figure 6.26: Temperature at 2.5 sec.
(Scale range: 80 – 285.3 ^{o}C).

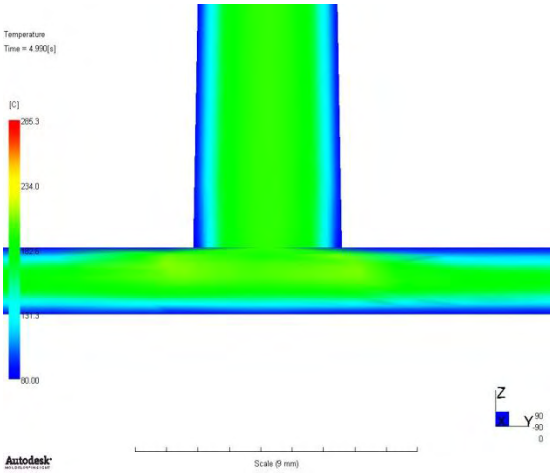

Figure 6.27: Temperature at 5 sec.
(Scale range: 80 – 285.3 ^{o}C).

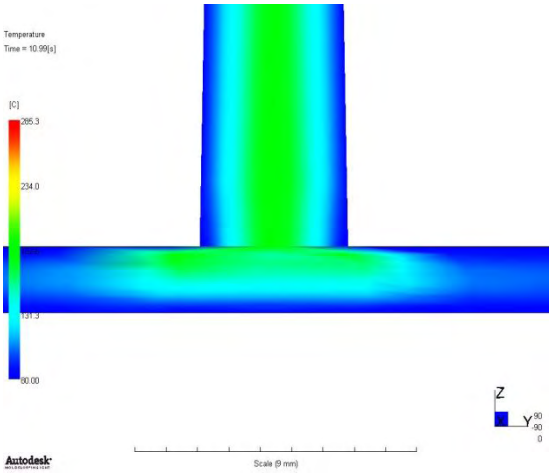

Figure 6.28: Temperature at 11 sec.
(Scale range: 80 – 285.3 ^{o}C).

Weld lines:

A *weld line* is formed when separate melt fronts traveling in opposite directions meet. A *meld line* occurs if two emerging melt fronts flow parallel to each other and create a bond between them. Weld and meld lines can be caused by holes or inserts in the part, multiple gates, or variable wall thickness where hesitation occurs.

The 'weld lines' result displays the angle of convergence as two flow fronts meet. The presence of weld lines may indicate a structural weakness and/or a surface blemish. The term "weld line" is often used to mean both weld and meld lines. The only difference between them is the angle at which they are formed; weld lines form at lower angles than meld lines. Weld lines can cause structural problems and make the part visually unacceptable, but they are unavoidable when the flow front splits and comes together around a hole, or if the part has multiple gates.

Weld and meld lines should be avoided, particularly weld lines in areas that require strength or a smooth appearance.

According to figure 6.29, no weld lines appear on the part.

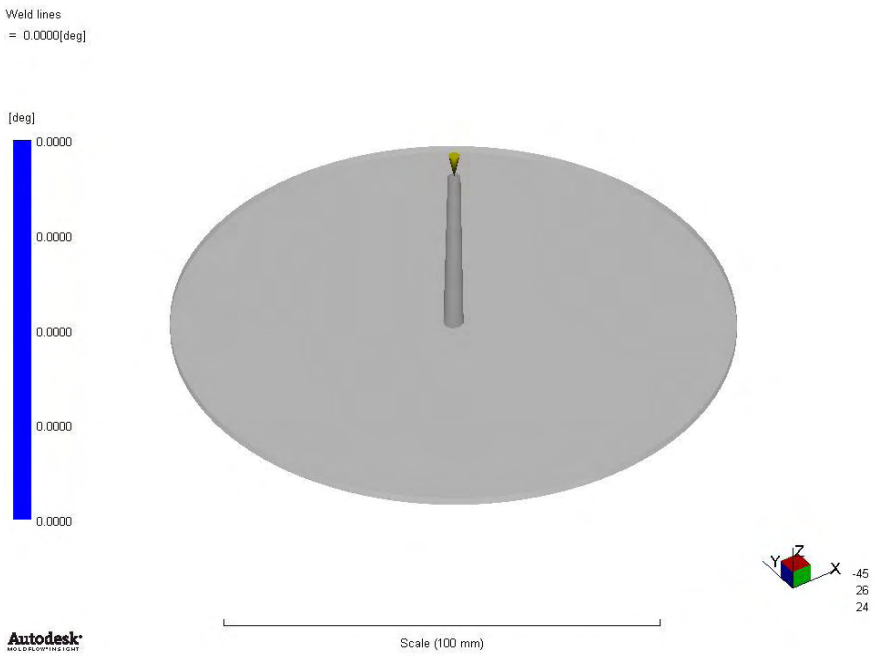

Figure 6.29:

The weld lines result.

Pressure (3D):

The ‘pressure’ result shows the pressure distribution through the flow path inside the mold at the time the result was written. At the very beginning of filling, the pressure is zero throughout the mold. The pressure at a specific location starts to increase, only after the melt front reaches that location. The pressure continues to increase as the melt front moves past, due to the increasing flow length between this specific location and the melt front. The pressure difference from one location to another is the force that pushes the polymer melt to flow, during filling. The pressure gradient is the pressure difference divided by the distance between two locations.

A polymer always moves in the direction of the negative pressure gradient, i.e. from higher pressure to lower pressure. Therefore, the maximum pressure occurs at the polymer injection locations and the minimum pressure occurs at the melt front, during the filling stage.

Through the ‘Clamp force: XY Plot’ result described earlier, the pressure inside the cavity could also be examined. However, the goal here is to check how the cavity pressure changes over time, when a very low and very high mold temperature is used. Moreover, a series of plots will be presented, depicting the pressure as a function of distance from the gate in the radius direction, i.e. P(r). In total 10 random points were selected across the radius, with the node right at the center of the disk (R = 0) as the starting point and with the node at the end (R = 65 mm) as the ending point.

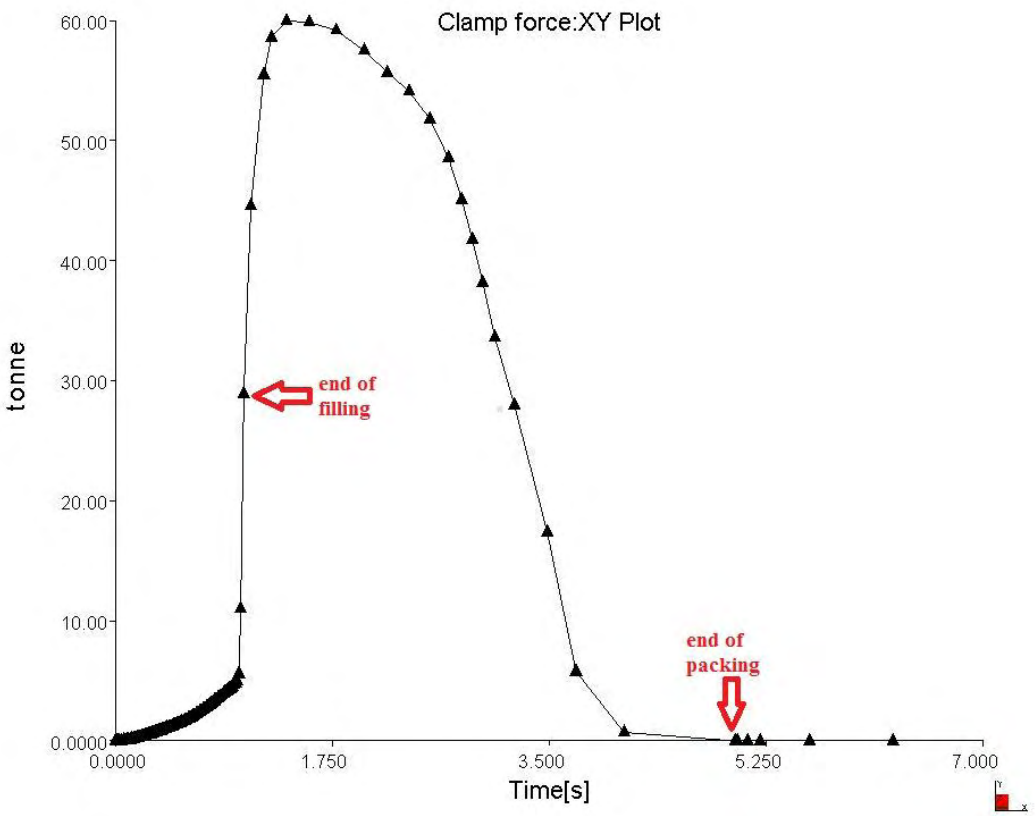

Figure 6.30: Clamping force (tonnes) vs. time (sec), for T_{mold} = 40 ^{o}C.

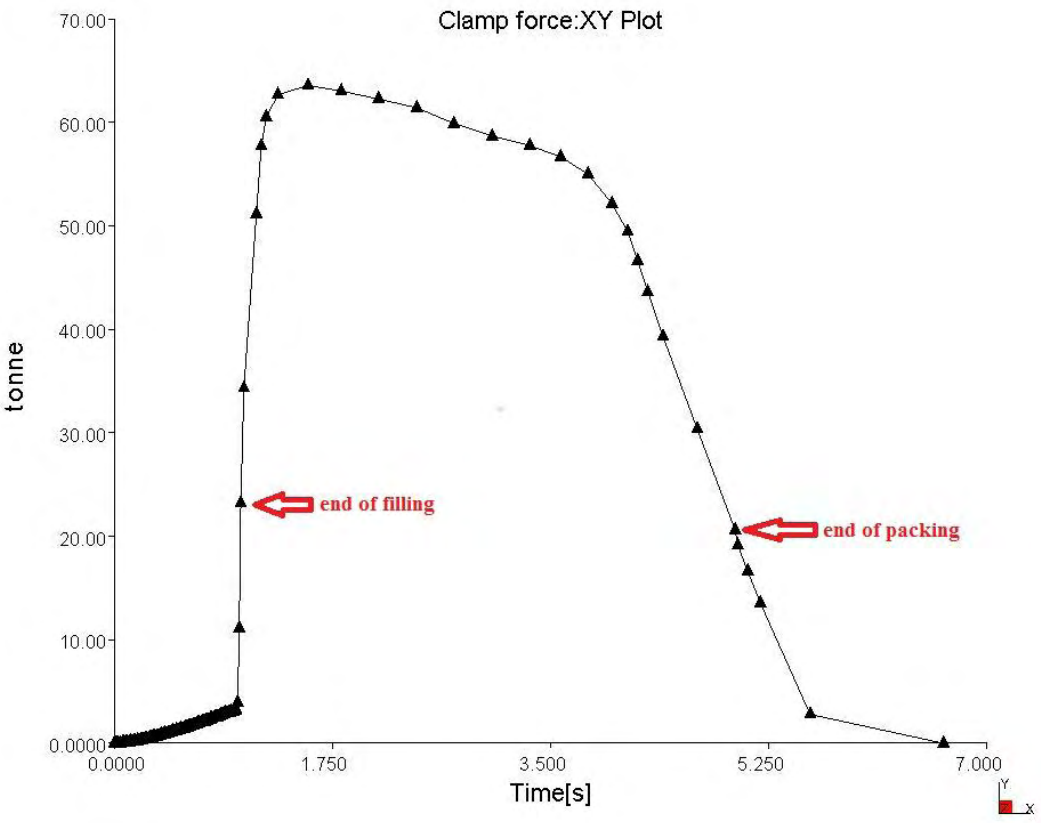

Figure 6.31: Clamping force (tonnes) vs. time (sec), for T_{mold} = 120 ^{o}C.

According to AMI logs, using the 40 ^{o}C as a constant mold temperature, gives a total cycle time of 8.72 sec, while using the 120 ^{o}C gives a cycle time of 15.31 sec. Therefore, a lower mold temperature decreases the cooling phase time, while a higher mold temperature makes the cooling slower, i.e. cooling phase lasts longer.

As far as cavity pressure is concerned, it almost becomes zero at 4.1 sec (figure 6.30), while 2 more seconds are needed in the second case (figure 6.31). Thus, a lower mold temperature forces the pressure to drop to zero much faster. Also, notice the difference at the filling phase. A more sudden increase takes place in the first case, while in the second case filling seems to have a more linear form. Colder molds are more difficult to fill, necessitating higher injection pressure (41 MPa vs. 34 MPa). Because of the very low mold temperature, material has cooled faster; viscosity is higher, so the pressure requirements are higher, too.

Moreover, one can tell that after t = 1.5 sec, the curve is much steeper in figure 6.30. Something that does not happen in the other case. The reason is that a high mold temperature causes the frozen volume to develop much slower. For example, at t = 3 sec, the frozen volume for T_{mold} = 40 ^{o}C is about 98%, while for T_{mold} = 120 ^{o}C it is only 54%.

Lastly, figures 6.32-6.35 show the cavity pressure behavior as the flow front moves further from the sprue gate. During the filling phase, the further from the gate – the lower the pressure. It is also observed that average pressure increases during the packing phase (figure 6.33), as expected. Towards the end of packing (figure 6.34), average pressure inside the cavity has dropped, as the frozen volume has taken up most of the space (~ 99%). At the end of packing and till the cycle time ends, cavity pressure has dropped to zero and remains zero, as shown in figure 6.35.

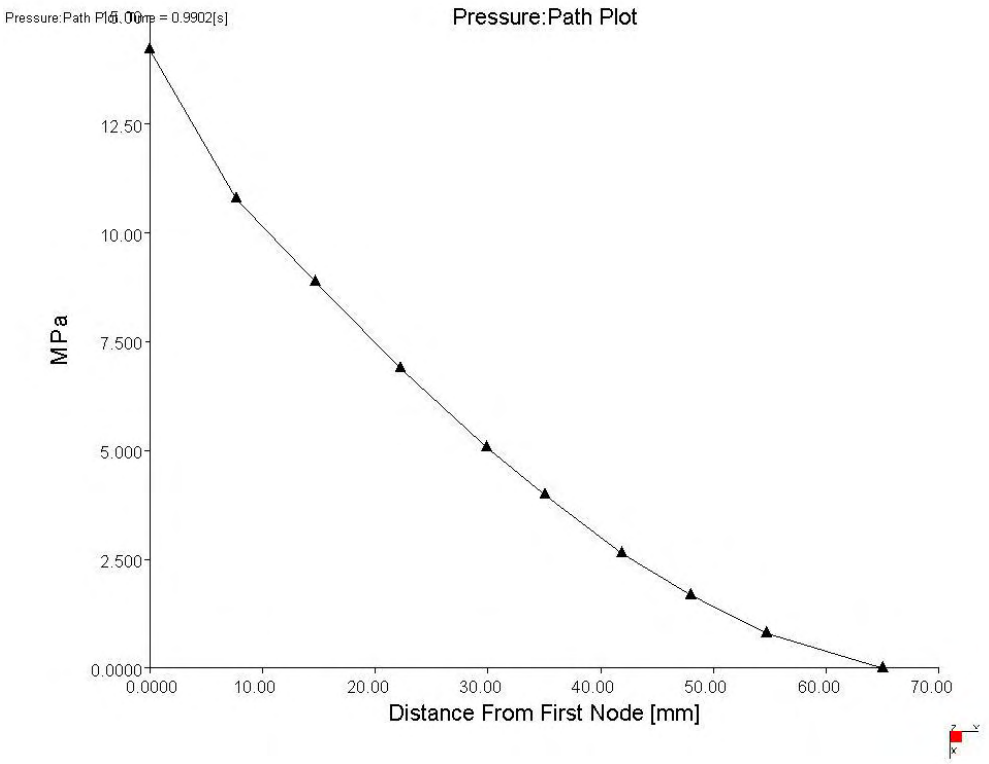

Figure 6.32: Pressure (MPa) vs. distance from the gate (mm), at t = 1 sec.

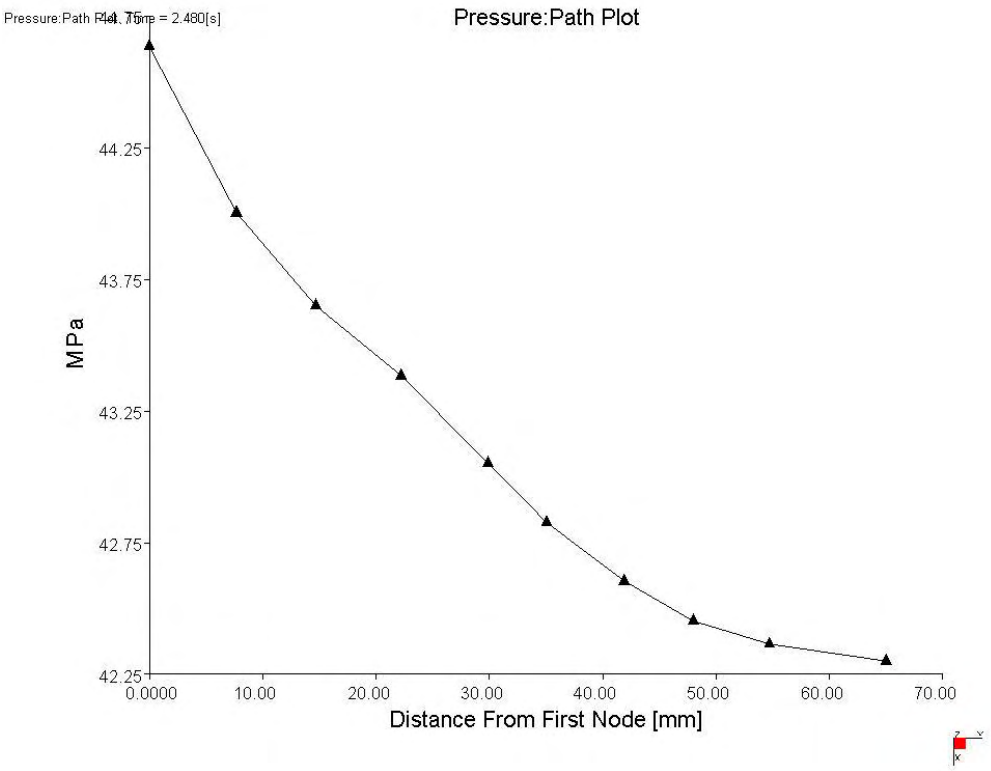

Figure 6.33: Pressure (MPa) vs. distance from the gate (mm), at t = 2.5 sec.

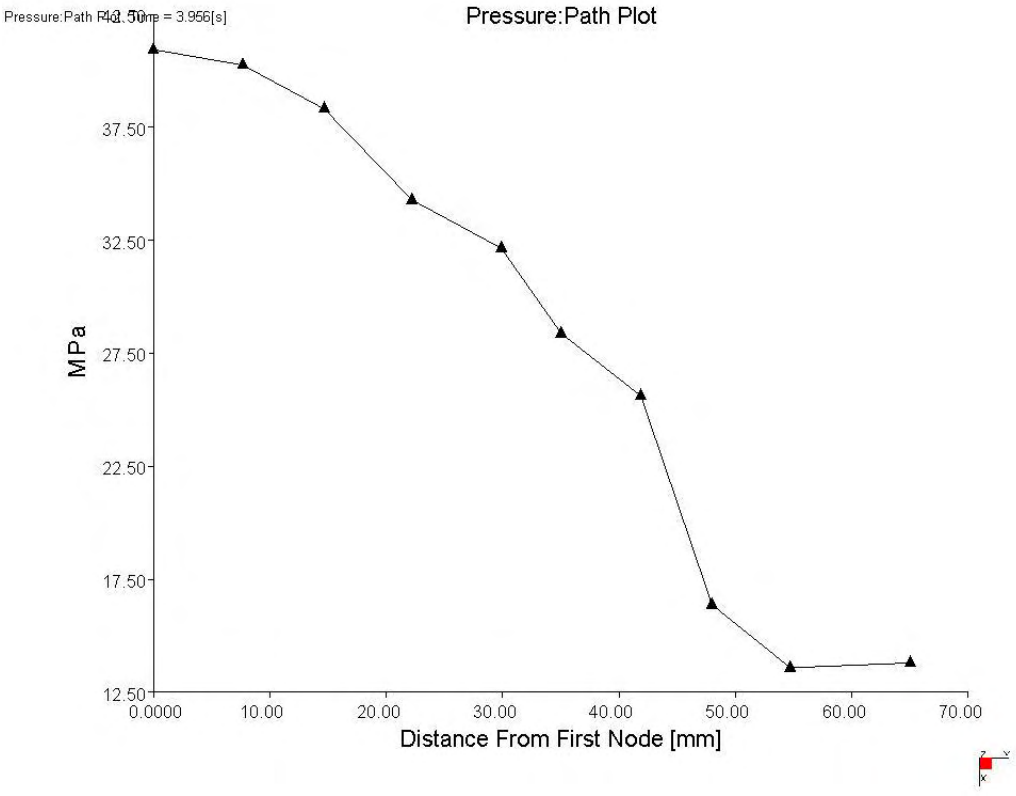

Figure 6.34: Pressure (MPa) vs. distance from the gate (mm), at t = 4 sec.

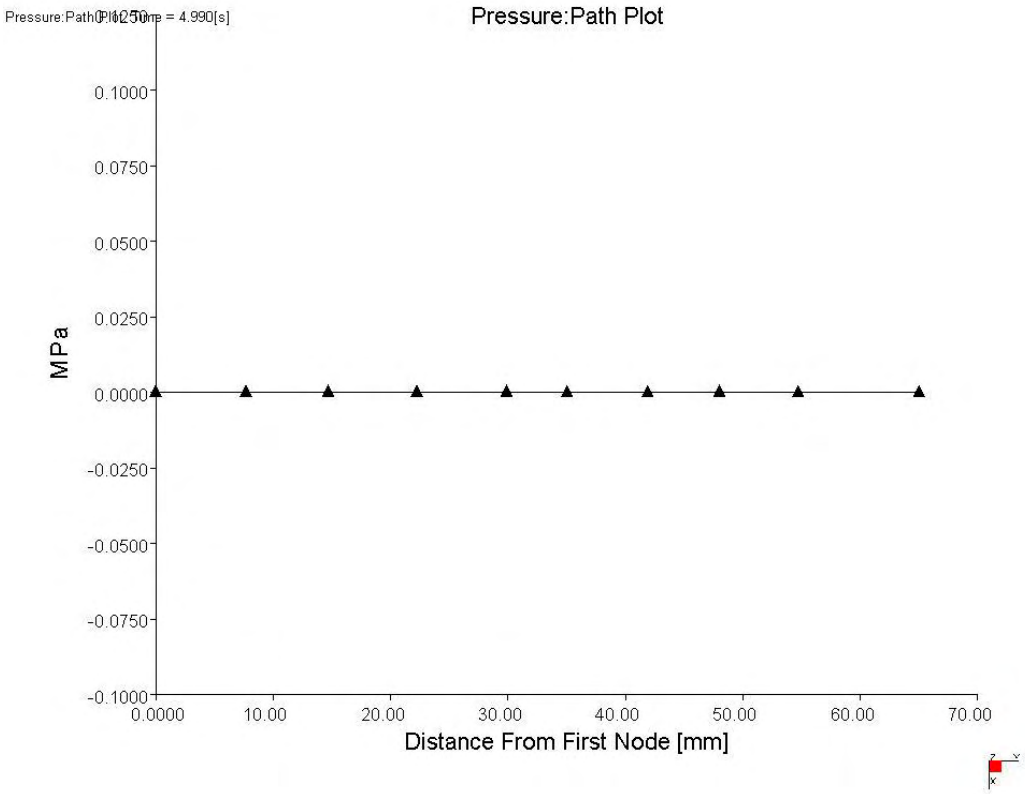

Figure 6.35: Pressure (MPa) vs. distance from the gate (mm), at t = 5 sec.

Pressure at end of fill & Pressure at V/P switchover (3D):

- The 'pressure at end of fill' result shows the pressure distribution in the cavity at the instant, when the cavity is completely filled with polymer.

As one can notice from figure 6.36 below, the pressure distribution is uniform. The maximum pressure (37 MPa) is located at the top of the sprue, where the hot material is directly injected into the sprue and the lowest pressure is observed at the disk walls (18-19 MPa).

- The 'pressure at V/P switchover' result shows the pressure distribution through the flow path inside the mold at the switchover point from velocity to pressure control.

Remember that the switch-over from velocity to pressure control was set to happen, when 98% of the cavity was filled. According to AMI logs, this happened exactly when 98.1% of the disk was filled. At that moment, the time was 0.99 sec and the injection pressure at 33.7 MPa. The red circle, on figure 6.37, simply indicates the 2% of cavity's volume that was unfilled.

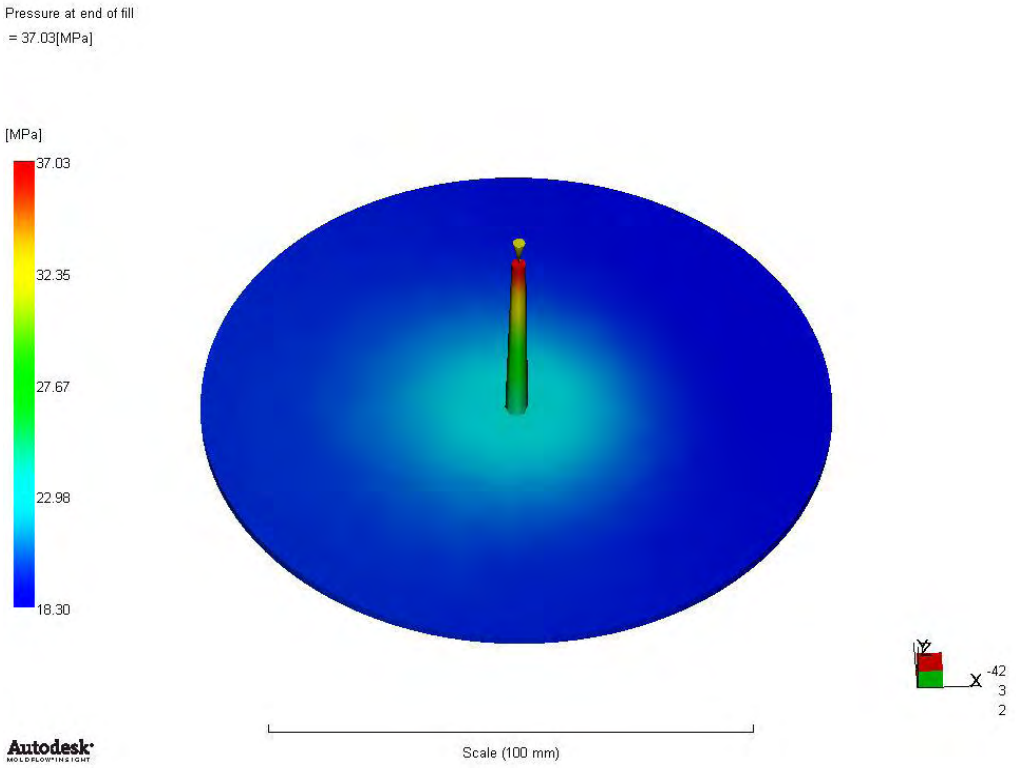

Figure 6.36: Pressure at the end of fill (t = 1 sec). (Scale range: 18.30 – 37.03 MPa).

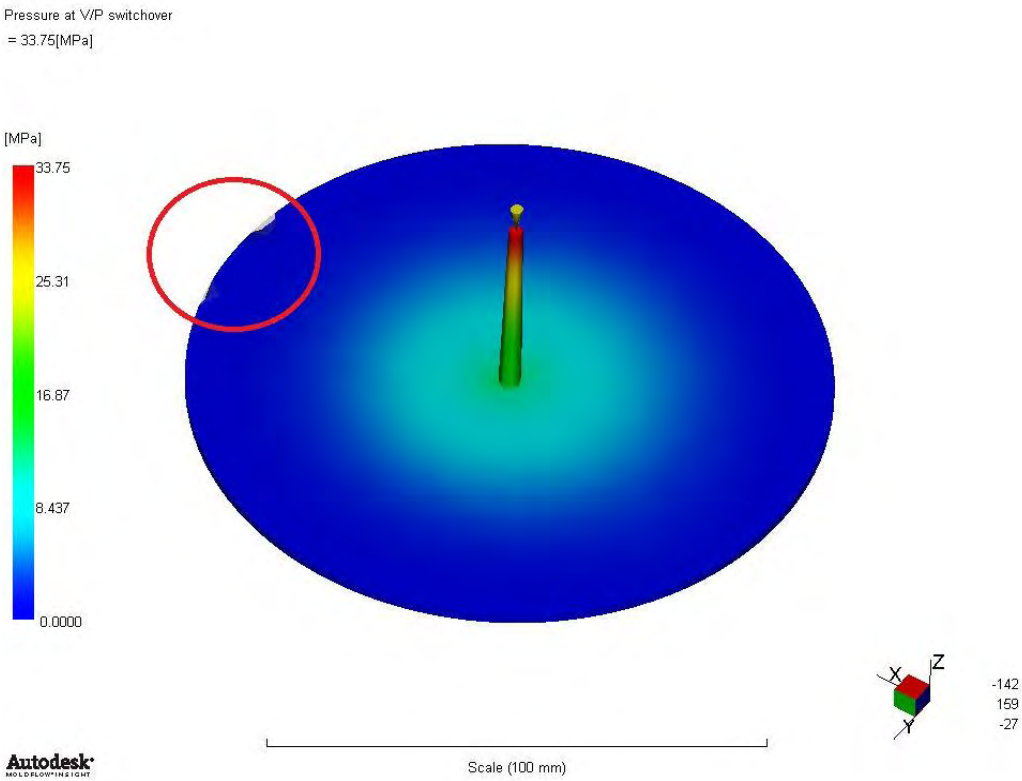

Figure 6.37: Pressure at the V/P switchover. (Scale range: 0 – 33.75 MPa).

Temperature at flow front (Dual domain & 3D):

The 'temperature at flow front' result shows the temperature of the polymer, when the flow front reaches a specified point in the center of the plastic cross-section. The flow front temperatures should not drop more than 2-5 ^{o}C, during the filling phase.

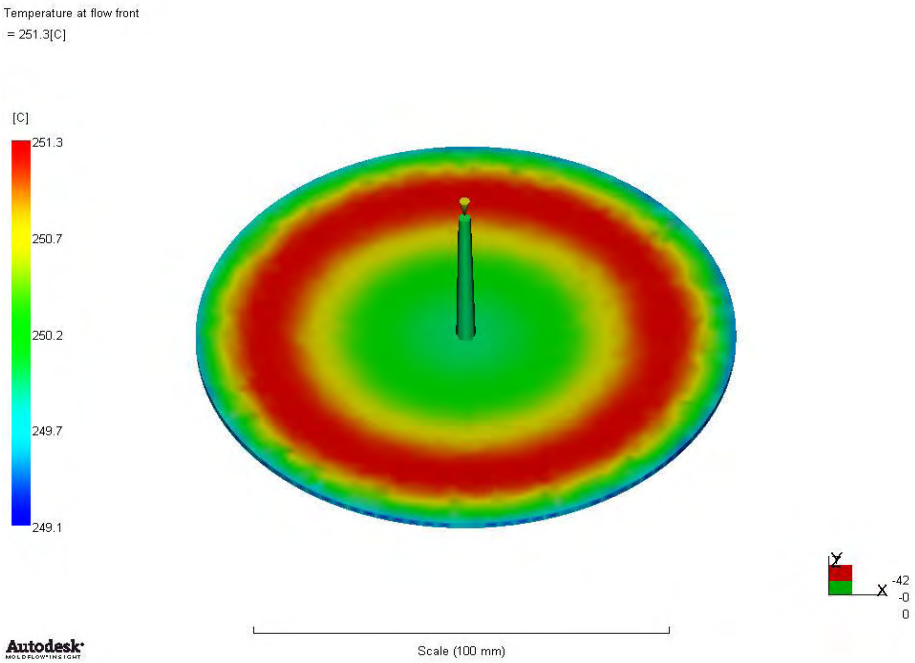

Figure 6.38: Temperature at flow front (Dual Domain).
(Scale range: 249.1 – 251.3 ^{o}C).

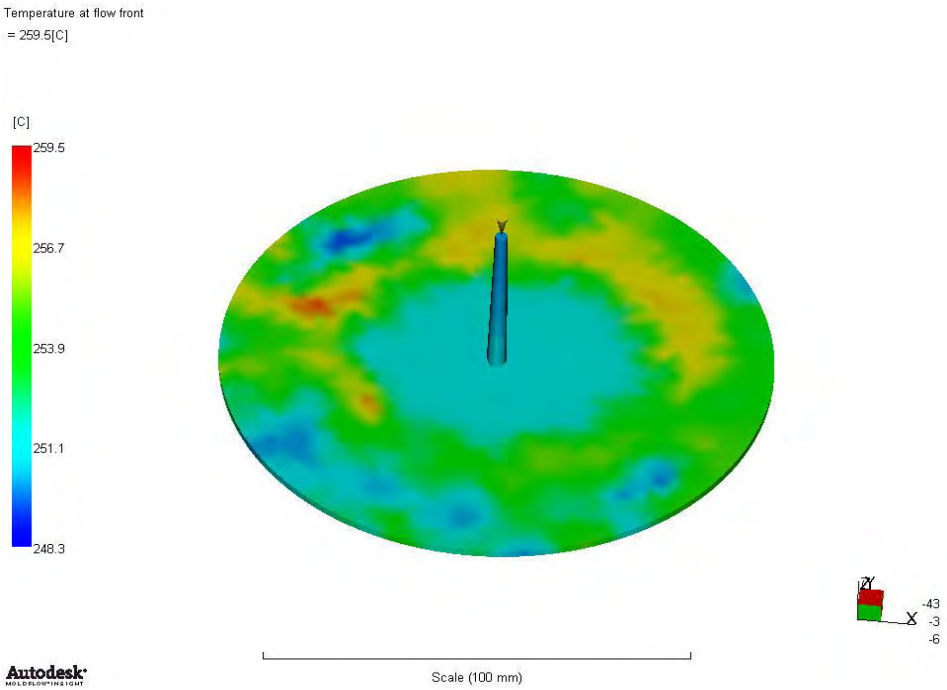

Figure 6.39: Temperature at flow front (3D).
(Scale range: 248.3 – 259.5 ^{o}C).

A rise in the melt front temperature is observed, as the melt front travels away from the gate. This appears counter-intuitive, but can only be explained as a result of viscous dissipation within the still molten material. This heat is transferred through conduction to the mold walls and convected with the melt. However, conduction is known to be very low in polymers, due to their poor thermal conductivity. As a result, viscous heat produced is convected downstream with the melt and results in the melt front having a slightly increasing temperature, as it travels downstream into the cavity. According to figure 6.38, no temperature variations > 2 ^{o}C exist. However, what is interesting enough here, is the fact that the 3D result (figure 6.39) gives a 10 ^{o}C temperature variation for the disk.

Density (3D):

The 'density' result shows the density of the tetrahedral elements before shrinkage occurs, at the time the result file was written. The program measures the density of the material at this time and uses it as the starting point for calculation of the volumetric shrinkage and warpage of the part. The figures below show the material's density through the part thickness at specified times and for this reason the YZ cutting plane has been selected. The times are: 1 sec (end of filling), 2.5 sec (packing phase), 5 sec (end of packing) and 11 sec (end of cycle).

This result determines whether the part was uniformly packed with polymer, during the packing phase. Variations in polymer density can indicate problems with the part. Once the material has filled the mold cavity and the packing phase has begun, material flow is driven by the variation of density across the part. If one region of a part is less densely packed than an adjacent region, then polymer will flow into the less dense region, until equilibrium is reached.

Figures 6.40-6.43 have something in common. Notice that every time the density near the mold walls is much higher than that in the midplane of the cavity. It has been already mentioned that the polymer's density behavior is described through the pvT model, where density is dependent both on pressure and temperature ($\rho(T,P)$). As pressure increases, so does the density. Also, the more temperature decreases - the more density increases. So which of those two variants affects the density result more?

Having tested manually the effect of both parameters into equations 4.1.4.1 and 4.1.4.2, i.e. the 0-50 MPa pressure range and the 80-250 ^{o}C temperature range, it was eventually concluded that *temperature* has the biggest impact on density. This is possibly explained by the fact that the material is semi-crystalline.

At the end of filling (figure 6.40), the density of the polymer in the midplane is 1.29 g/cm^3. The closer to the surface - the higher the density. At t = 2.5 sec (packing phase), the cavity pressure has already begun to drop. Thus, one would expect for the density to drop, as well. According to figure 6.41, this is not true. And the reason is temperature. At this point, temperature at the cavity walls has dropped down to almost 80 ^{o}C. Therefore, it is expected for the density to have nearly reached its max value. Indeed, at the wall surface a value of 1.48 g/cm^3 is observed, while in the midplane this value is much smaller, at 1.31 g/cm^3.

The more we reach the end of cycle, the more temperature is decreased. Therefore, it is expected for the density in the midplane to increase more and more. Indeed, notice how the light blue color has vanished in the cavity (figure 6.42). It is also obvious that the disk has been uniformly packed with polymer and no variations exist. At the cavity walls, density has already reached its max value (1.484 g/cm^3) and in the midplane its value is 1.37 g/cm^3, at the end of packing phase (figure 6.42) and 1.42 g/cm^3, when the molding cycle has ended (figure 6.43).

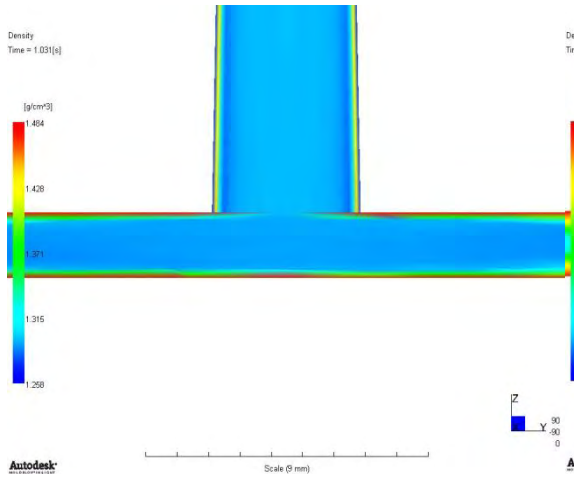

Figure 6.40: Density at t = 1 sec.
(Scale range: 1.258 – 1.484 g/cm^3).

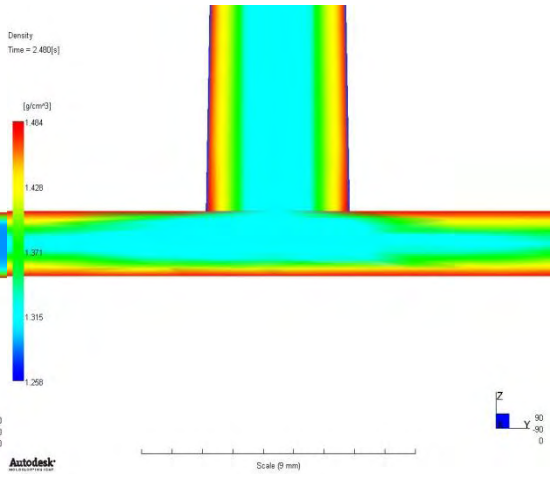

Figure 6.41: Density at t = 2.5 sec.
(Scale range: 1.258 – 1.484 g/cm^3).

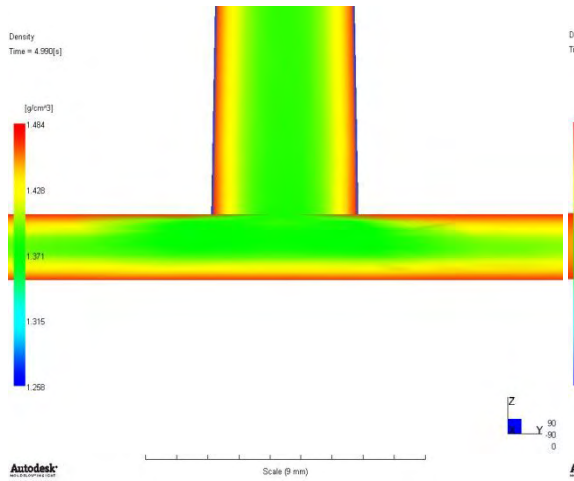

Figure 6.42: Density at t = 5 sec.
(Scale range: 1.258 – 1.484 g/cm^3).

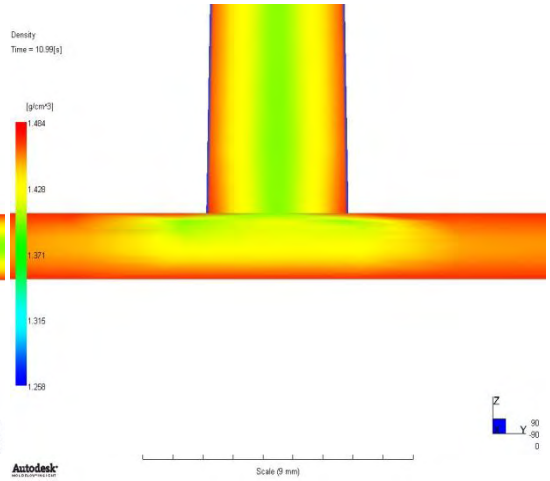

Figure 6.43: Density at t = 11 sec.
(Scale range: 1.258 – 1.484 g/cm^3).

Average volumetric shrinkage (3D):

The 'Average volumetric shrinkage' result shows the average value of volumetric shrinkage over the half-gap thickness for 3D models.

Volumetric shrinkage is the percentage increase in local density from the end of the filling-packing phase to when the part has cooled to the ambient temperature (23°C). The calculations begin once the cavity is filled, based on the difference between the current pvT state and the reference state:

$$VS(t) = \frac{AD(t)}{D(T_{ambient}, \rho_{atm})}$$

where:

- *VS* is the volumetric shrinkage,
- *AD* is the average density,
- *D* is the density, and
- the pressure p is zero and temperature T is the specified ambient temperature.

As the mass of an element changes (for example, with polymer flow during packing), shrinkage continues to change with each change in the element's pvT state. Once the mass stops changing, the element's current pvT state is fixed in the shrinkage calculation, as the reference state. The average volumetric shrinkage of the part is depicted below, at four different times: t = 1.5 sec (slightly after filling has ended), t = 2.7 sec & t = 3.5 sec (packing phase) and t = 5 sec (end of packing).

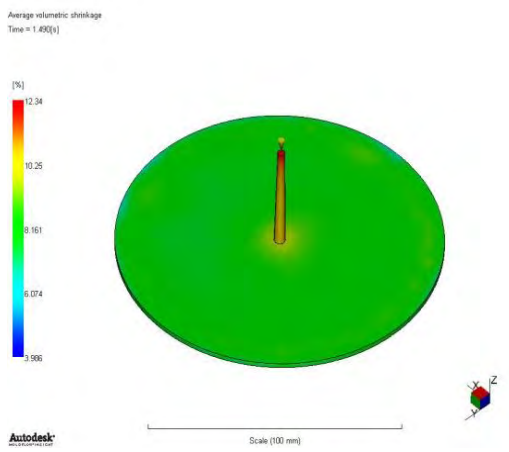

Figure 6.44: Average shrinkage at 1.5 sec. (Scale range: 3.986 – 12.34%).

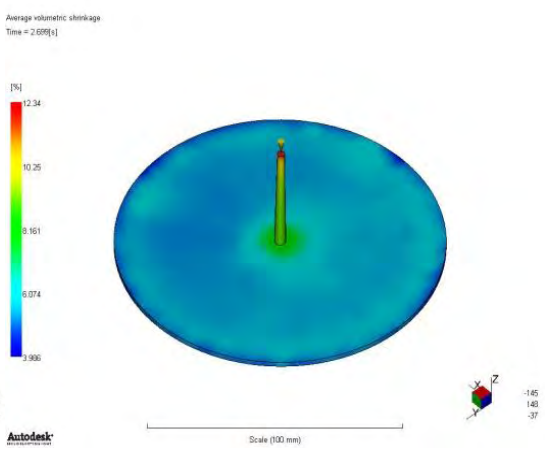

Figure 6.45: Average shrinkage at 2.7 sec. (Scale range: 3.986 – 12.34%).

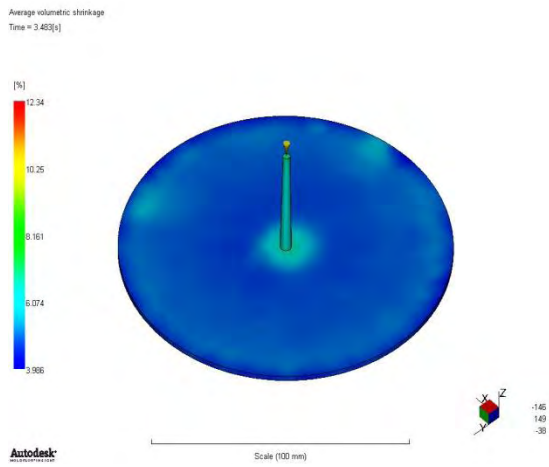

Figure 6.46: Average shrinkage at 3.5 sec. (Scale range: 3.986 – 12.34%).

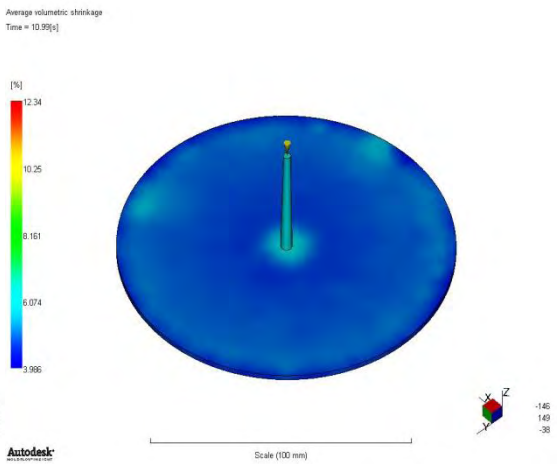

Figure 6.47: Average shrinkage at 5 sec. (Scale range: 3.986 – 12.34%).

According to logs, at t = 1.5 sec the maximum clamp force is observed, thus the maximum cavity pressure. At this point, the frozen volume (~ 40%) is the minimum it will be at this highest pressure (since most of the material is still molten) and the shrinkage is 7.7-8.5% (figure 6.44).

At t = 2.7 sec (figure 6.45), the solidified material's volume has increased to 65% and pressure has dropped only a little. Shrinkage has also dropped to 5.3-6%, but very close to the gate, shrinkage remains high. This is expected, because at this point hot molten material is still injected through the sprue.

At t = 3.5 sec (figure 6.46), frozen volume has taken up most of the cavity space (~97%) and shrinkage is now in the range of 4.7-5.2%, which practically is the lowest value achieved. When the packing phase is over (figure 6.47), no important changes on the volumetric shrinkage of the part are observed. However, notice that shrinkage around the small area of the gate has decreased from 6.1-6.5% (at t = 3.5 sec) down to 5.7-6%.

Note: The average volumetric shrinkage at the end of packing is the same with that at the end of cycle. This is reason that the shrinkage at t = 11 sec is not shown here. This means that packing indeed worked in ensuring that enough material was packed into the cavity, so that the final shrinkage will be minimized.

But are there ways to affect the average volumetric shrinkage on the part even more ? Having run a few simulations, with different parameters each time, the conclusions are as:

Note: All the figures below are accompanied by figure 6.47, so as to give a better presentation of the comparison that follows. Scale range used is the same for all. Remember again that shrinkage values were in the range of 4.7-5.2%, with most of the disk's area close to 4.9-5.1%.

a) The higher the pressure used in the packing/holding profile – the more shrinkage is reduced. Pressure affects directly the density (or specific volume), therefore the shrinkage. However, don't forget that there is always the clamping force limitation of the IMM. Increasing the packing pressure by 20 MPa drops the shrinkage down to 4.1-4.7%. Most of the disk's area has a shrinkage close to 4.2-4.3% (figure 6.49).

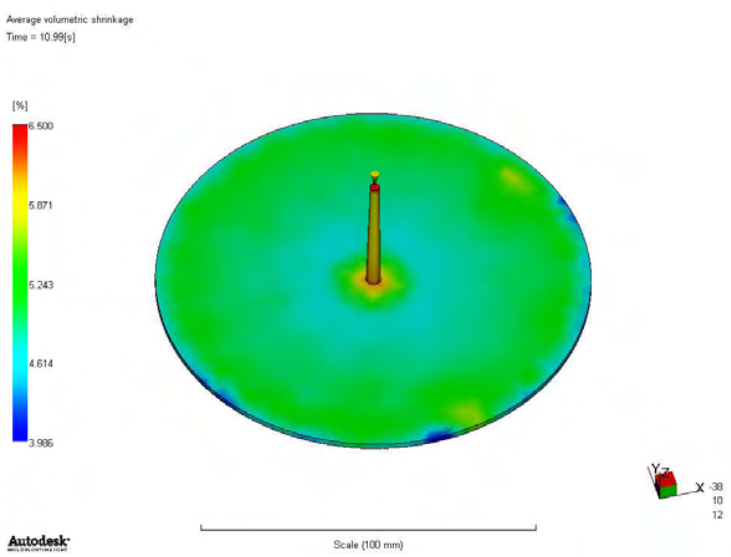

Figure 6.48: Average volumetric shrinkage at the end of cycle.
(Scale range: 3.986 – 6.5%).

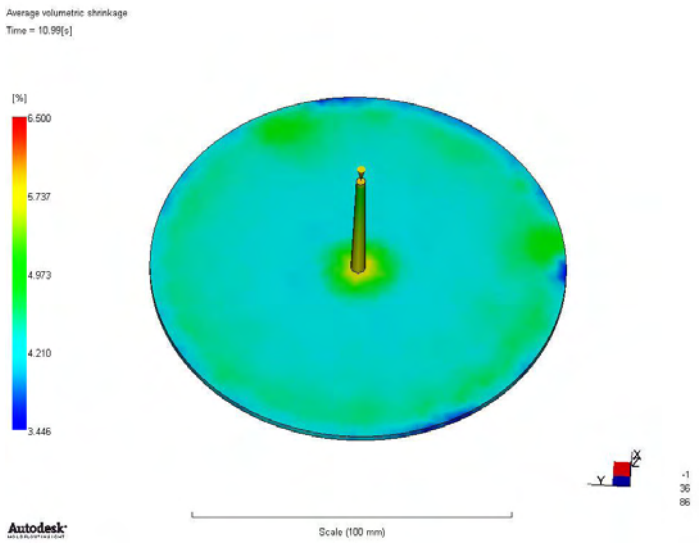

Figure 6.49: Average volumetric shrinkage at the end of cycle, for $P_{packing}$ = 70 MPa.
(Scale range: 3.446 – 6.5%).

b) The lower the mold temperature – the lower the volumetric shrinkage. Using a mold temperature of 60 ^{o}C drops the shrinkage down to 4.2-4.8%. Most of the disk's area has a shrinkage close to 4.6-4.8% (figure 6.51). Injecting the semi-crystalline PBT into a colder mould, causes a more rapid cooling, which slows down the formation of crystalline areas, resulting in a lower shrinkage.

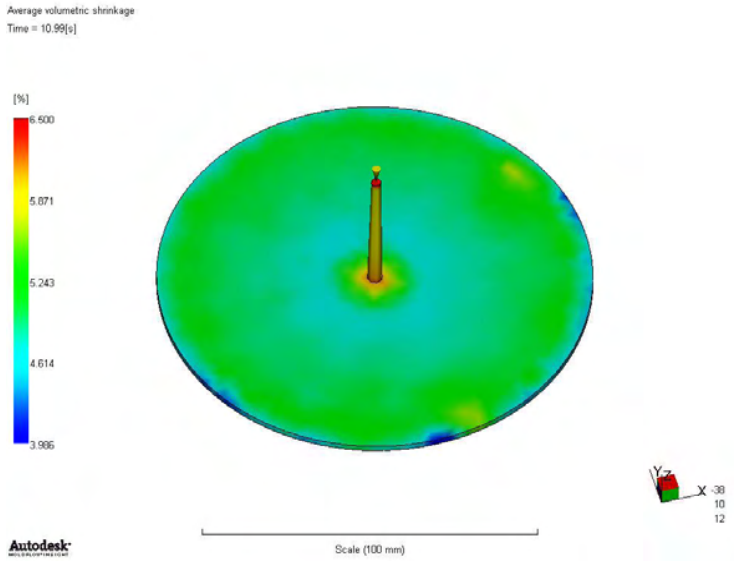

Figure 6.50: Average volumetric shrinkage at the end of cycle.
(Scale range: 3.986 – 6.5%).

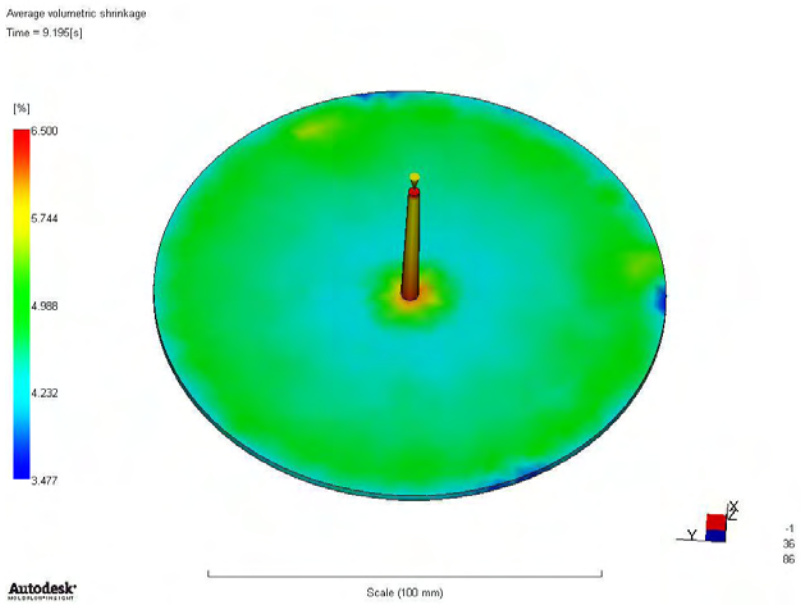

Figure 6.51: Average volumetric shrinkage at the end of cycle, for T_{mold} = 60 ^{o}C.
(Scale range: 3.477 – 6.5%).

c) The slower the cavity fills – the lower the volumetric shrinkage. Setting a flow rate of 11.5 cm^3/sec, increases the filling time to 2.55 sec. At the start of packing phase, a larger percent of the material has solidified, namely 43% (figure 6.53) vs. 26% (figure 6.52). A slower filling causes the frozen layers to become thicker. As a result, the actual flow channel for the material gets smaller. Therefore, more pressure is required to fill the mold and the in-cavity pressure values will be higher, resulting in a lower shrinkage. It is obvious how the blue color is dominating in figure 6.53. The range of shrinkage values is 4.5-5.1%, with most of the disk's area around 4.6-4.8%.

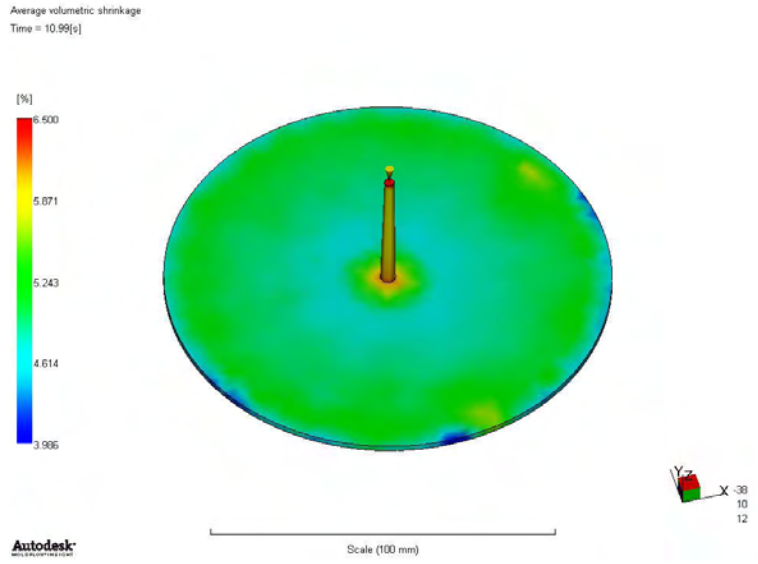

Figure 6.52: Average volumetric shrinkage at the end of cycle. (Scale range: 3.986 – 6.5%).

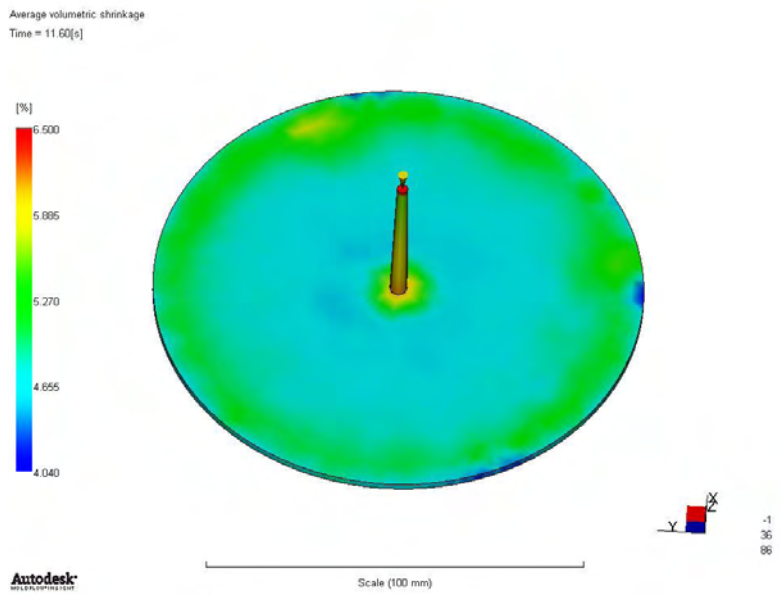

Figure 6.53: Average volumetric shrinkage at the end of cycle, for an injection time of 2.5 sec. (Scale range: 4.04 – 6.5%).

d) Using very small heat transfer coefficients (HTC) seems to have a big impact on shrinkage, too. However, volumetric shrinkage is not reduced, but increased to 8.1-8.3%. This is expected, as in this case cooling is very slow; namely, ~ 25% frozen volume (figure 6.55) vs. 99% (figure 6.54), at t = 4.5 sec. The scale here was set to 9%, as the minimum shrinkage value was 6.5% (figure 6.55). A very slow cooling means that it will take longer for the part to freeze, which makes the crystalline content increase. Therefore, the resulting shrinkage is much higher.

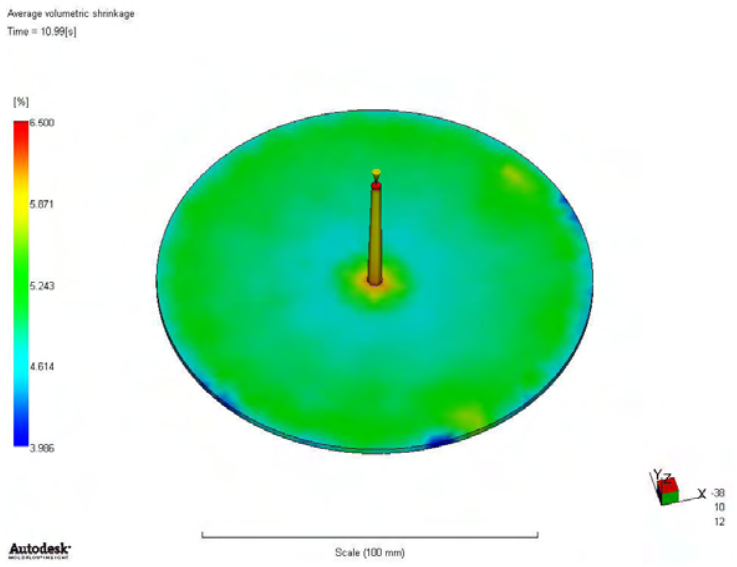

Figure 6.54: Average volumetric shrinkage at the end of cycle. (Scale range: 3.986 – 6.5%).

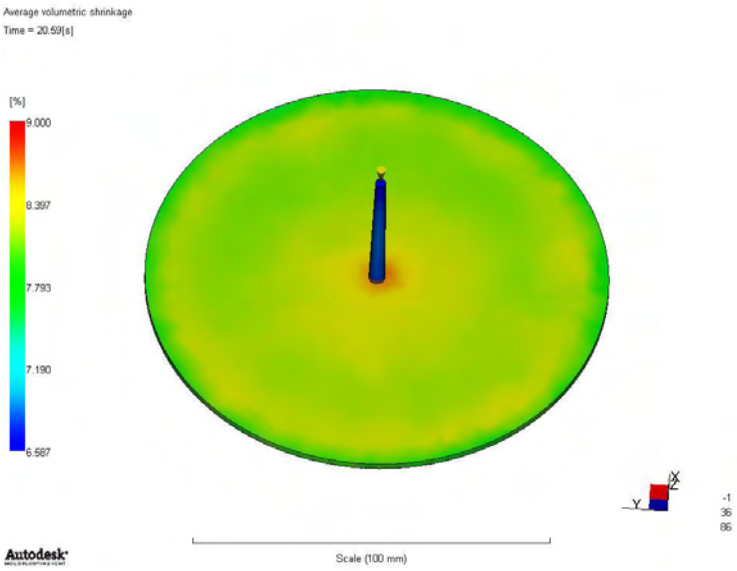

Figure 6.55: Average volumetric shrinkage at the end of cycle, using the 'HTC' option with: $h_{filling}$ = 500 W/m$^2 \cdot$ °C, $h_{packing}$ = 250 W/m$^2 \cdot$ °C and $h_{detached}$ = 125 W/m$^2 \cdot$ °C. (Scale range: 6.587 – 9%).

e) Increasing the melt temperature may increase or decrease shrinkage. Typically, very low melt temperatures lead to relatively high shrinkage, because the part cannot be adequately packed out. Increasing the temperature, up to a certain point, decreases the shrinkage because viscosity is reduced and so packing pressure can be better distributed through the cavity. For a given packing pressure and time, further increase in melt temperature leads to higher shrinkages, as the cavity is then filled with material of relatively low density (Shoemaker J., 2006). The main difference, between figures 6.56 and 6.57, is the area around the gate.

Using hotter material causes the shrinkage near the sprue to increase from about 5.9% to 6.4%. Volumetric shrinkage in the rest of the disk remains pretty much the same (4.8-5.2%).

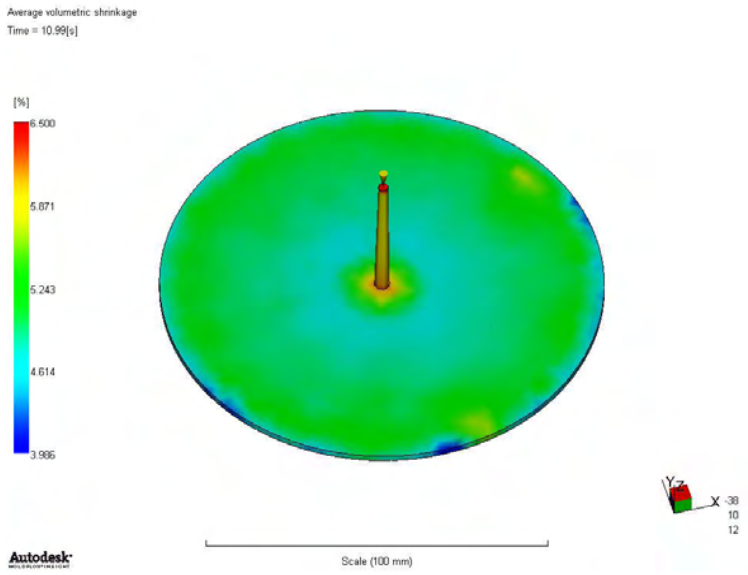

Figure 6.56: Average volumetric shrinkage at the end of cycle.
(Scale range: 3.986 – 6.5%).

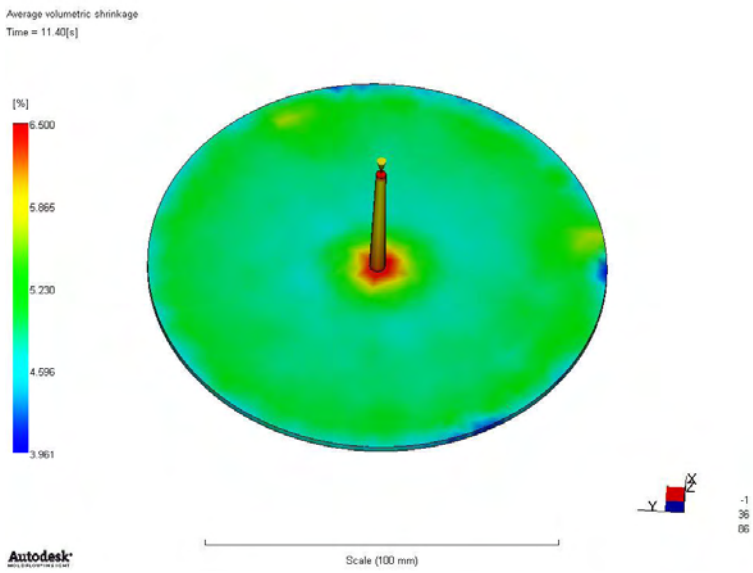

Figure 6.57: Volumetric shrinkage at the end of cycle, for T_{melt} = 270 ^{o}C.
(Scale range: 3.961 – 6.5%).

Note: Another parameter that can affect volumetric shrinkage is the gate diameter. The shrinkage of a moulding can be reduced by enlarging the gate, so as to increase feeding (Mills N., 2005).

Volumetric Shrinkage (3D) & Density (3D) results comparison:

The 'Volumetric shrinkage' result shows the volumetric shrinkage for each node, as a percentage of the original volume. Here, five figures of density and shrinkage behavior will be presented at different times of the molding cycle, right at the *center-plane* of the disk, i.e. (x, y, z) = (0, 0, 1).

Volumetric shrinkage calculations begin once the cavity is filled, based on the difference between the current pvT state and the reference state (where the pressure p is zero and temperature T is the specified ambient temperature):

$$S(t) = \frac{\rho(t)}{\rho_{amb}}$$

As the mass of an element changes (for example, with polymer flow during packing), shrinkage continues to change with each change in the element's pvT state. Once the mass stops changing, the element's current pvT state is fixed in the shrinkage calculation as the reference state.

The mass of an element stops changing, when the cavity pressure has decayed to zero. *After this, the volumetric shrinkage becomes a constant* (∗). However, if the holding pressure is removed before the material is frozen or while the pressure in the cavity is still non-zero, the volumetric shrinkage may rebound due to possible backflow into the nozzle or other warmer areas of the part.

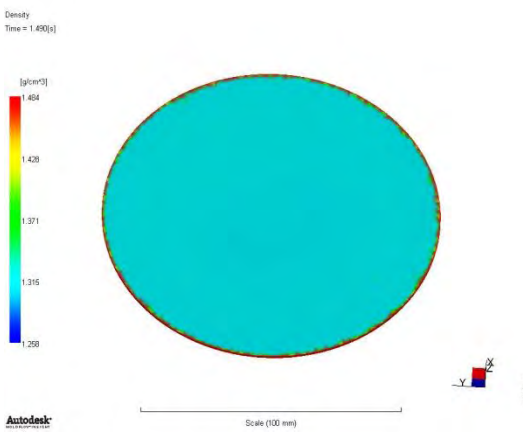

Figure 6.58: Density at t = 1.5 sec. (Scale range: 1.258 – 1.484 g/cm^3).

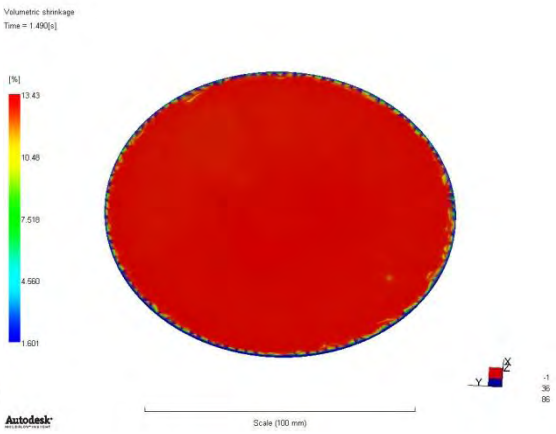

Figure 6.59: Shrinkage at t = 1.5 sec. (Scale range: 1.601 – 13.43%).

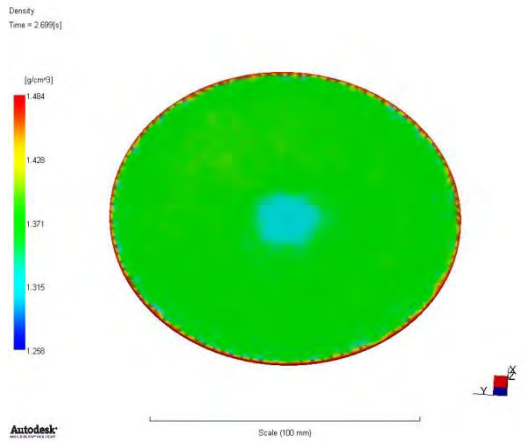

Figure 6.60: Density at t = 2.7 sec. (Scale range: 1.258 – 1.484 g/cm^3).

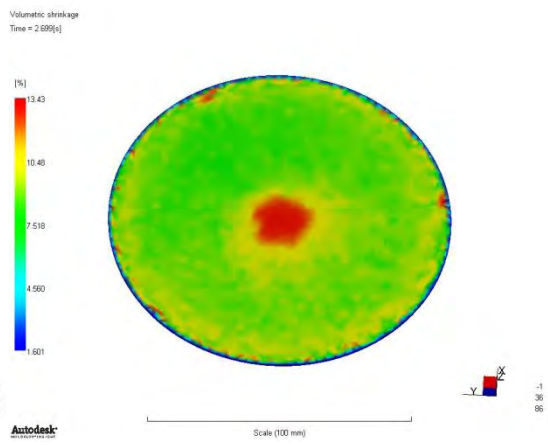

Figure 6.61: Shrinkage at t = 2.7 sec. (Scale range: 1.601 – 13.43%).

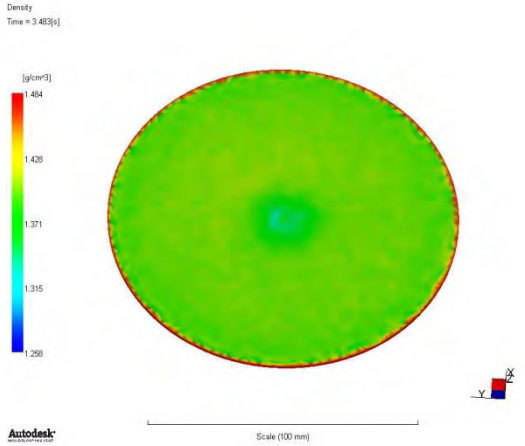

Figure 6.62: Density at t = 3.5 sec. (Scale range: 1.258 – 1.484 g/cm^3).

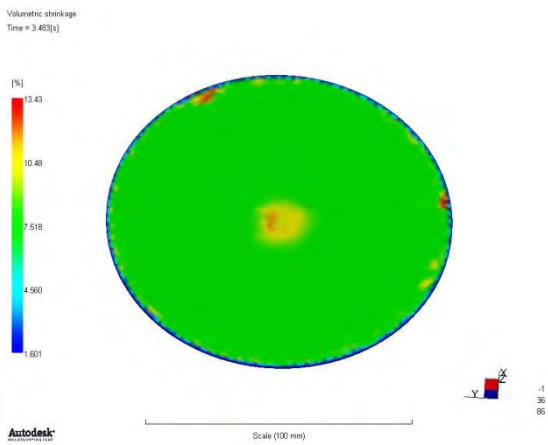

Figure 6.63: Shrinkage at t = 3.5 sec. (Scale range: 1.601 – 13.43%).

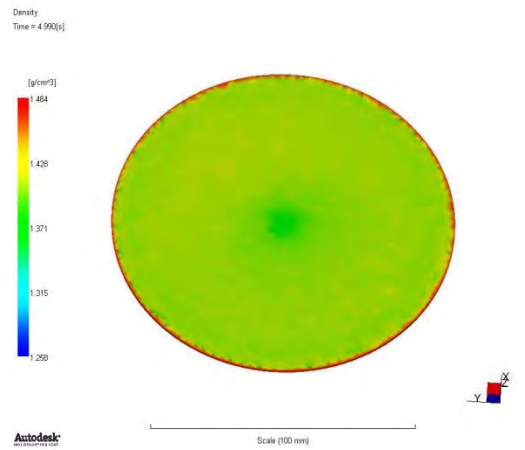

Figure 6.64: Density at t = 5 sec. (Scale range: 1.258 – 1.484 g/cm^3).

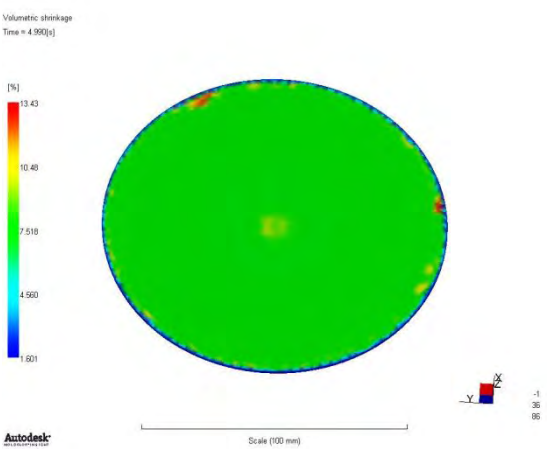

Figure 6.65: Shrinkage at t = 5 sec. (Scale range: 1.601 – 13.43%).

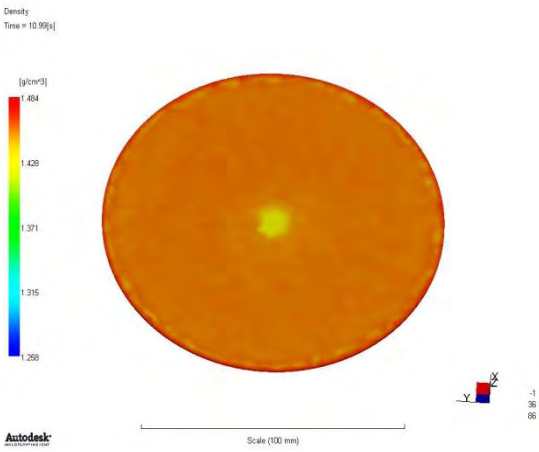

Figure 6.66: Density at t = 11 sec. (Scale range: 1.258 – 1.484 g/cm^3).

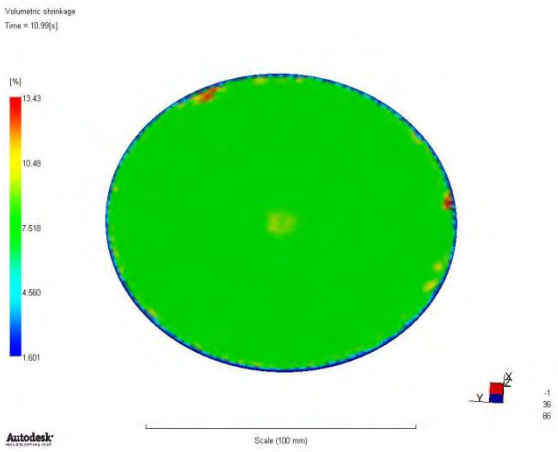

Figure 6.67: Shrinkage at t = 11 sec. (Scale range: 1.601 – 13.43%).

At t = 1.5 sec, the maximum clamp has been observed, thus, the cavity pressure has reached the maximum value (~ 46 MPa). Also, at this point, temperature is at about 254 ^{o}C. Density is at 1.31 g/cm^3 (higher than that at t = 1 sec (1.28 g/cm^3), as pressure has increased; figure not presented here) and shrinkage measures at about 13%, i.e. almost the maximum value it can have (figure 6.59).

As we move into the packing phase, at t = 2.7 sec, pressure has slightly dropped, but temperature has been reduced to 220 ^{o}C. Therefore, it is expected for the density to have increased (1.37 g/cm^3). Some spatial shrinkage variations appear on figure 6.61, however, on average the shrinkage has dropped to about 8.6 - 9.2%.

At t = 3.5 sec, pressure is around 38 MPa near the center of the disk, while far from it, it does not exceed 28 MPa. Also, temperature is at about 205 ^{o}C. Testing the effect of the two parameters into equations 4.1.4.1 and 4.1.4.2, proves again that temperature is much more effective in increasing the density. Density has now increased to 1.39 g/cm^3 and shrinkage has dropped to 7.3% (figures 6.62 and 6.63). Notice the high shrinkage near the sprue (10.7-11.5%).
At the end of packing period (t = 5 sec), as we have already seen, shrinkage remains more or less the same, and only near the sprue area a reduction is observed (8.8-9.4%). Pressure has become zero (ambient) and temperature has reached 175 ^{o}C. Density is increased a little, at 1.41 g/cm^3. The shrinkage observed at t = 5 sec is also the one observed in the final product.

At the end of cycle (t = 11 sec), density has increased even more (1.45 g/cm^3). However, from figure 6.67 it is clear that shrinkage has not changed at all. Normally, a small shrinkage decrease would be expected near the sprue. The most possible reason for this may be the fact that a packing time of 4 sec was used in the analysis. *This caused the cavity pressure to decay to zero, just at the end of packing period, i.e. after this, shrinkage remains the same* (∗). Remember that the part weight remained constant after t = 3.5 sec. So now the time has been extended for 0.5 sec. This reminds once again the importance of the time factor in injection molding.

The following figures (6.68 – 6.71) show the density and shrinkage results at the end of packing/holding period and at the end of cycle, using $t_{packing}$ = 3.5 sec. Indeed, volumetric shrinkage is decreased at the center (close to the sprue) and covers a smaller area. This probably reflects the fact that there is still a small flow of material in that area.

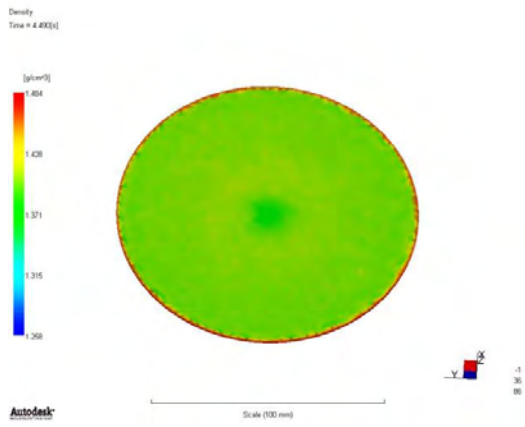

Figure 6.68: Density at end of packing.

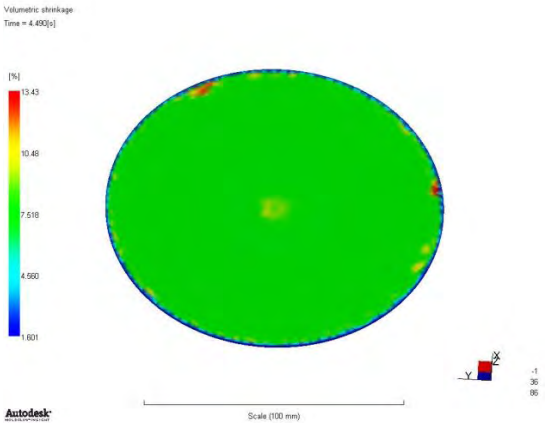

Figure 6.69: Shrinkage at end of packing.

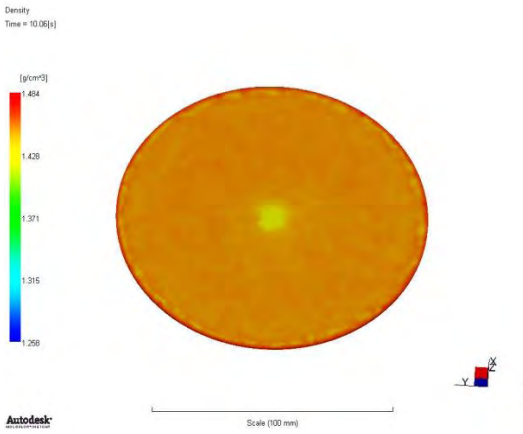

Figure 6.70: Density at end of cycle.

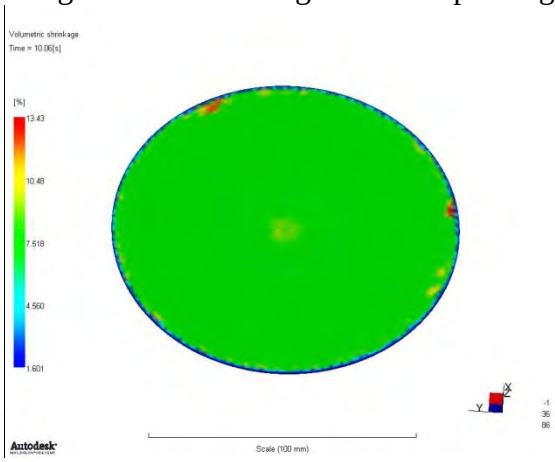

Figure 6.71: Shrinkage at end of cycle.

Lastly, the following figures (6.72 - 6.76) show the volumetric shrinkage at the end of cycle, for five different points in the thickness direction. Of course, the closer to the surface - the lower the volumetric shrinkage.

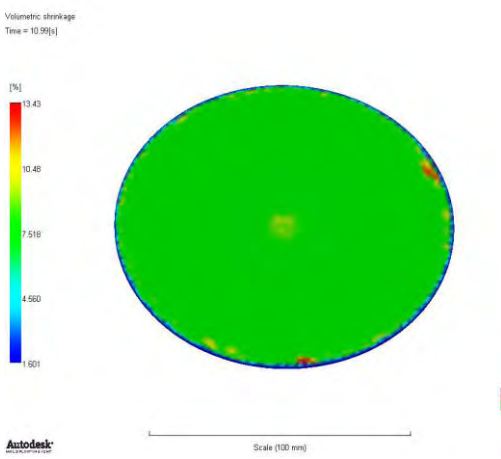

Figure 6.72: Shrinkage at (x, y, z) = (0, 0, 1). Values: 7.2 - 7.5%.

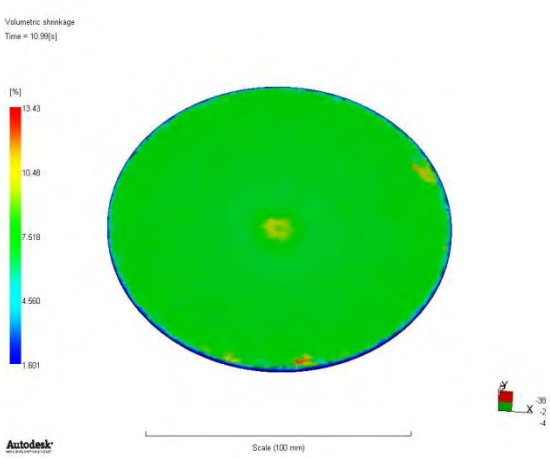

Figure 6.73: Shrinkage at (x, y, z) = (0, 0, 1.25). Values: 6.7 - 7%.

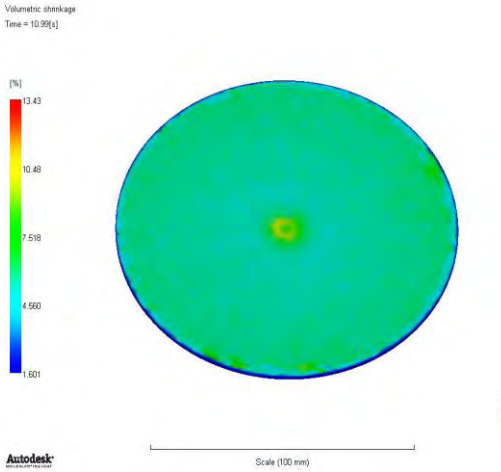

Figure 6.74: Shrinkage at (x, y, z) = (0, 0, 1.5). Values: 5.4 - 5.8%.

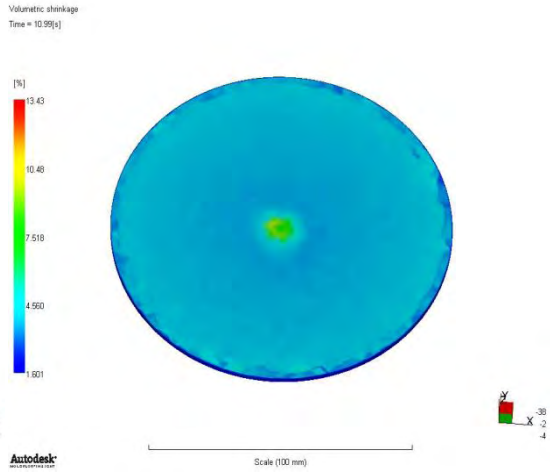

Figure 6.75: Shrinkage at (x, y, z) = (0, 0, 1.75). Values: 3.6 - 4%.

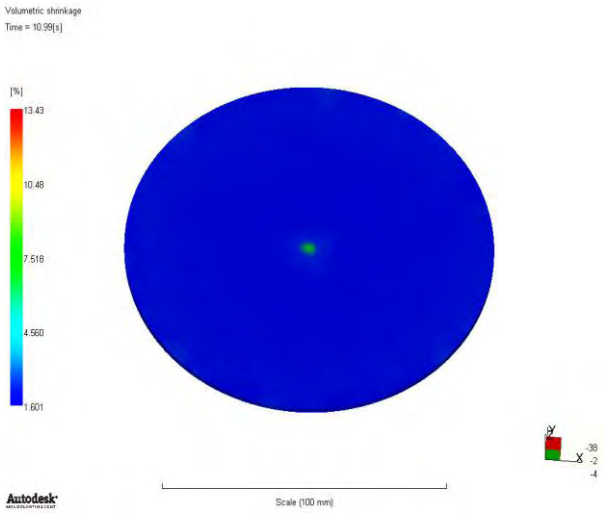

Figure 6.76: Shrinkage at (x, y, z) = (0, 0, 2). Values: 1.8 - 2%.

Suggestions for future studies

- Effect of viscous heating on 3D temperature profiles.
- Study of the fiber orientation tensor, using the Folgar-Tucker and the RSC model.
- Focus on the kinetics of crystallization and its effect on volumetric shrinkage.
- Examine the volumetric shrinkage, of fiber-filled TPs, in the flow direction and perpendicular to the flow direction.

REFERENCES

- Baldwin J.D., Altan M.C. and Rajamani K. Structural Analysis of an Injection Molded Short-Fiber-Reinforced Disk. Journal of Materials Processing & Manufacturing Science, vol. 6, USA, October 1997.

- Bay R.S. & Tucker III C.L. Fiber Orientation in Simple Injection Moldings. Part I: Theory and Numerical Methods. Polymer Composites, vol. 13, p. 317-331, Illinois, August 1992.

- BASF Corporation Engineering Plastics. Estimating Cooling Times in Injection Molding (2007).

- Benretem A., Benidir M. and Chaib R. Factors Influencing Slurry Rheology. WorldPumps, p. 30-31, July 2010.

- Dantzig J.A. & Tucker III C.L. Modeling in Materials Processing (p. 218). Cambridge University Press, 2001.

- DSM Engineering Plastics. Performance and Value with Engineering Plastics – Design Guide, USA, 2005.

- DuPont Performance Polymers. Thermoplastic Polyester Resin - Crastin® HR5330HF NC010, Product Information, 2013.

- DuPont™ Delrin acetal resin – Molding Guide (Technical Information), USA, 2006.

- Engelmann Paul & Dealey Bob. Injection Molding Design Guidelines – Maximizing Performance Using Copper Alloys. For the Mold Marketing Task Group of the Copper Development Association, May, 1999.

- Groover Mikell P. Fundamentals of Modern Manufacturing Materials, Processes, and Systems (4th edition). John Wiley & Sons, Inc. USA, 2010.

- Islam A., Hansen H.N., Gasparin S. and Bondo M. Effects of Glass Fibers on the Properties of Micro Molded Plastic Parts. Department of Mechanical Engineering, Technical University of Denmark, 2011.

- Jian Wang. PVT Properties of Polymers for Injection Molding - Some Critical Issues for Injection Molding. School of Chemical Engineering and Environment, Beijing Institute of Technology, China, 2012.

- Kunc Vlastimil, Frame Barbara, Nguyen Ba Nghiep, Tucker III Charles L. and Vélez-García Gregorio. Fiber Length Distribution Measurement for Long Glass and Carbon Fiber Reinforced Injection Molded Thermoplastics (2007).

- Mills Nigel. Plastics: Microstructure and Engineering Applications (Third edition), p. 186. Butterworth-Heinemann, October 15, 2005.

- Nguyen Quoc-Hung & Nguyen Ngoc-Diep. Incompressible Non-Newtonian Fluid Flows, Continuum Mechanics - Progress in Fundamentals and Engineering Applications, Dr. Yong Gan (Ed.), 2012.

- O'Gara J. F., Wyzgoski M. G. and G. E. Novak. Development of an ISO Standard for determining Anisotropic Properties of Glass-Filled Thermoplastics. Proceedings of the 61th Annual Technical Conference and Exhibition, May 4-8, 2003, Nashville, Tennessee, U.S.A.

- Pontes A.J., Neves N.M. and Pouzada A.S. The role of the interaction coefficient in the prediction of the fiber orientation in planar injection moldings. Polymer Composites, vol. 24, p. 358-366. Department of Polymer Engineering, Portugal, June 2003.

- Rännar Lars-Erik. On optimization of Injection Molding Cooling. Norwegian University of Science and Technology - Faculty of Engineering Science and Technology. Department of Engineering Design and Materials. Trondheim, April 2008.

- Rosato Dominick V., Rosato Donald V. and Rosato Marlene G. Injection Molding Handbook (3rd edition). Kluwer Academic Publishers, USA, 2000.

- Shoemaker Jay. Moldflow Design guide – A Resource for Plastics Engineers (1st edition). Moldflow Corporation, Framingham, Massachusetts, USA, 2006.

- Somjate Patcharaphun. Characterization and Simulation of Material Distribution and Fiber Orientation in Sandwich Injection Molded Parts Faculty of Mechanical Engineering, Institute of Mechanical and Plastics Engineering, Chemnitz University of Technology, 2006.

- Strong A. Brent. Plastics: Materials and Processing. Prentice Hall Inc., New Jersey, 1996.

- Tadmor Z. Molecular Orientation in Injection Molding. Journal of Applied Polymer Science, vol. 18, p. 1753-1772, 1974.

- Tadmor Z. & Gogos C. Principles of Polymer Processing, Wiley 1979. Injection Molding of Polymers (14.1), p. 584 – 610.

- Vélez-García Gregorio Manuel. Experimental Evaluation and Simulations of Fiber Orientation in Injection Molding of Polymers Containing Short Glass Fibers. Department of Macromolecular Science & Engineering, Virginia Polytechnic Institute and State University, Blacksburg, USA, January 31, 2012.

- Wang Jin & Jin Xiaoshi. Comparison of Recent Fiber Orientation Models in AMI Simulations with Measured Fiber Orientation Data. Proceedings of the polymer processing society 26th annual meeting, Banff, Canada, July 4-8, 2010.

- Wilkinson Arthur N. & Ryan Anthony J. Polymer Processing and Structure Development (p. 233-234). Kluwer Academic Publishers, 1998.

ADDITIONAL LINKS

[Autodesk Moldflow Insight Help]:
http://wikihelp.autodesk.com/Simulation_Moldflow/enu/2013/Help/2.0Insight

[1]:
http://www.dc.engr.scu.edu/cmdoc/dg_doc/develop/material/overview/a3000001.htm

[2]: http://www.custompartnet.com/wu/InjectionMolding

[3]:
http://www.dc.engr.scu.edu/cmdoc/dg_doc/develop/process/physics/b3200002.htm

[4]:
http://megamould.com/TechBlog/Mold-Design/Construction%20Injection%20Molds%20Classification.html

[5]: http://www.vnmold.com/2012/06/gate-designing-in-injection-mold-p1.html

[6]:
http://www.de.kuas.edu.tw/backup/laboratory/%E9%AB%98%E5%88%86%E5%AD%90%E5%8A%A0%E5%B7%A5%E7%A0%94%E7%A9%B6%E5%AE%A4-pplab/download/%E5%A1%91%E8%86%A0%E5%8A%A0%E5%B7%A5%E7%89%B9%E8%AB%96-Chapter%202.4.4.pdf *(page 52)*

[7]: http://www.dc.engr.scu.edu/cmdoc/rm_doc/02_Material_props.html

[8]:
http://www.dc.engr.scu.edu/cmdoc/dg_doc/develop/process/control/b1000005.htm#216586

[9]: http://www.plastictroubleshooter.com/ThePlasticTroubleshooter/sink_marks.htm

[10]: http://www.dc.engr.scu.edu/cmdoc/rm_doc/04_Process_modeling.html